



**HAL**  
open science

# Search of new physics through flavor physics observables

Olcyr Sumensari

► **To cite this version:**

Olcyr Sumensari. Search of new physics through flavor physics observables. High Energy Physics - Phenomenology [hep-ph]. Université Paris Saclay (COmUE), 2017. English. NNT : 2017SACLS315 . tel-01739406

**HAL Id: tel-01739406**

**<https://theses.hal.science/tel-01739406>**

Submitted on 21 Mar 2018

**HAL** is a multi-disciplinary open access archive for the deposit and dissemination of scientific research documents, whether they are published or not. The documents may come from teaching and research institutions in France or abroad, or from public or private research centers.

L'archive ouverte pluridisciplinaire **HAL**, est destinée au dépôt et à la diffusion de documents scientifiques de niveau recherche, publiés ou non, émanant des établissements d'enseignement et de recherche français ou étrangers, des laboratoires publics ou privés.

# Search of new physics through flavor physics observables

Thèse de doctorat de l'Université Paris-Saclay  
préparée à l'Université Paris-Sud

École doctorale n°564 Physique en Ile de France (EDPIF)  
Spécialité de doctorat : Physique

Thèse présentée et soutenue à Orsay, le 27 septembre 2017, par

**M. Olcyr Sumensari**

## Composition du Jury :

Mme Asmaa Abada Professeur, Université Paris-Sud (UMR 8627)	Présidente
M. Antonio Pich Professeur, Université de Valencia	Rapporteur
M. Gino Isidori Professeur, Université de Zurich	Rapporteur
M. Diego Guadagnoli Chargé de recherche, LAPTh (UMR 5108)	Examineur
Mme Justine Serrano Chargée de recherche, CPPM (UMR 7346)	Examinatrice
Mme Renata Zukanovich Funchal Professeur, Université de São Paulo	Examinatrice
M. Damir Bečirević Directeur de recherche, Université Paris-Sud (UMR 8627)	Directeur de thèse

**Titre :** Recherche de la nouvelle physique à travers les observables de la physique de la saveur

**Mots clés :** changement de la saveur, B meson, désintégration semileptonique, théorie effective des champs, Higgs, leptoquark.

**Résumé :** La recherche indirecte des effets de la physique au-delà du Modèle Standard à travers les processus de la saveur est complémentaire aux efforts au LHC pour observer directement la nouvelle physique. Dans cette thèse nous discutons plusieurs scénarios au-delà du Modèle Standard (a) en utilisant une approche basée sur les théories de champs effective et (b) en considérant des extensions explicites du Modèle Standard, à savoir les modèles à deux doublets de Higgs et les scénarios postulant l'existence des bosons leptoquarks scalaires à basse énergie.

En particulier, nous discutons le phénomène de la brisure de l'universalité des couplages leptoniques dans les désintégrations basées sur les transitions  $b \rightarrow s\mu\mu$  and  $b \rightarrow c\tau\nu$ , et la possibilité de chercher les signatures de la violation de la saveur leptonique à travers les modes de désintégration similaires. Une proposition pour tester la présence d'un boson pseudoscalaire léger à travers les désintégrations des quarkonia est aussi présentée.

**Title :** Search of new physics through flavor physics observables

**Keywords :** flavor changing, B meson, semileptonic decay, effective field theory, Higgs particle, leptoquark.

**Abstract :** Indirect searches of physics beyond the Standard Model through flavor physics processes at low energies are complementary to the ongoing efforts at the LHC to observe the New Physics phenomena directly. In this thesis we discuss several scenarios of physics beyond the Standard Model by (a) reusing the effective field theory approach and (b) by considering explicit extensions of the Standard Model, namely the two-Higgs doublet models and the scenarios involving the low energy scalar leptoquark states.

Particular emphasis is devoted to the issue of the lepton flavor universality violation in the exclusive decays based on  $b \rightarrow s\mu\mu$  and  $b \rightarrow c\tau\nu$ , and to the possibility of searching for signs of lepton flavor violation through similar decay modes. A proposal for testing the presence of the light CP-odd Higgs through quarkonia decays is also made.



*To the memory of my father.*

*“Doubt is one of the names of intelligence.”*

J. L. BORGES

# Contents

<b>Remerciements</b>	<b>4</b>
<b>Introduction</b>	<b>6</b>
<b>1 The Standard Model</b>	<b>9</b>
<b>The Standard Model</b>	<b>9</b>
1.1 The Standard Model Lagrangian . . . . .	9
1.2 Why do we need to go beyond? . . . . .	14
1.2.1 Neutrino masses . . . . .	14
1.2.2 The SM flavor problem . . . . .	16
1.2.3 The hierarchy problem . . . . .	18
<b>2 Flavor observables as a probe of New Physics</b>	<b>20</b>
<b>Flavor observables as a probe of New Physics</b>	<b>20</b>
2.1 Effective field theories . . . . .	21
2.2 Tree-level electroweak decays of mesons . . . . .	21
2.2.1 Leptonic decays of mesons . . . . .	23
2.2.2 Semileptonic $P \rightarrow P'$ decays . . . . .	24
2.2.3 Brief discussion of $P \rightarrow V$ semileptonic decays . . . . .	30
2.2.4 Phenomenological analysis . . . . .	31
2.3 FCNC processes . . . . .	38
2.3.1 $B_s \rightarrow \ell^+\ell^-$ . . . . .	39
2.3.2 $B \rightarrow K\ell^+\ell^-$ . . . . .	40
2.3.3 $B \rightarrow K^*\ell^+\ell^-$ and $B_s \rightarrow \phi\ell^+\ell^-$ . . . . .	41
2.4 Lepton flavor violation in lepton decays . . . . .	43
2.4.1 $\ell \rightarrow \ell'\gamma$ and neutrino masses . . . . .	43
2.4.2 Status of current LFV searches . . . . .	45
2.4.3 Sterile neutrinos and LFV . . . . .	46
2.5 LFV in $b \rightarrow s$ exclusive decays . . . . .	51
2.5.1 $B_s \rightarrow l_1 l_2$ . . . . .	52
2.5.2 $B \rightarrow K l_1 l_2$ . . . . .	53
2.5.3 $B \rightarrow K^* l_1 l_2$ and $B_s \rightarrow \phi l_1 l_2$ . . . . .	54
2.5.4 Numerical significance . . . . .	59
<b>3 Scrutinizing Two-Higgs doublet models</b>	<b>62</b>

<b>Scrutinizing Two-Higgs doublet models</b>	<b>62</b>
3.1 General aspects of 2HDM	63
3.1.1 The extended scalar sector	63
3.1.2 Including fermions	65
3.1.3 Model spectrum and theory constraints	67
3.2 Phenomenology of heavy scalars	70
3.3 Leptonic and semileptonic decays of mesons	72
3.4 Wilson coefficients for the $b \rightarrow s\ell\ell$ transition	74
3.5 Lessons from $b \rightarrow s$ exclusive observables	83
3.6 The light CP-odd Higgs window	88
3.6.1 General scan for a light CP-odd	88
3.7 Seeking the CP-odd Higgs via $h \rightarrow P\ell\ell$	90
3.8 Probing a light CP-odd Higgs through quarkonia decays	97
<b>4 Leptoquarks at low and high energies</b>	<b>103</b>
<b>Leptoquarks at low and high energies</b>	<b>103</b>
4.1 Introduction	103
4.1.1 $SU(5)$ unification and light leptoquarks	104
4.1.2 Proton stability	106
4.2 A concrete $SU(5)$ realization with light leptoquarks	108
4.2.1 Model setup	109
4.2.2 RGE equations	110
4.2.3 Scan of parameters	111
4.2.4 Unification scale and proton decay	112
4.3 Specific leptoquark states	115
4.4 Direct searches at the LHC	121
<b>5 Lepton flavor (universality) violation</b>	<b>124</b>
<b>Lepton flavor (universality) violation</b>	<b>124</b>
5.1 Introduction	124
5.2 Lepton flavor (universality) violation in $b \rightarrow s\ell_1\ell_2$	127
5.2.1 Effective description of the deviations	127
5.2.2 Proposed explanations of $R_K$ and $R_{K^*}$	133
5.2.3 Tree-level leptoquark models for $R_{K^{(*)}}$	135
5.2.4 Loop induced leptoquark models: A first attempt	136
5.2.5 A viable leptoquark explanation of $R_{K^{(*)}} < 1$ through loops	140
5.3 Lepton flavor universality violation in $b \rightarrow c\ell\nu$	149
5.3.1 Standard Model predictions for $R_D$ and $R_{D^*}$	150
5.3.2 Simultaneous explanations of $R_{K^{(*)}}$ and $R_{D^{(*)}}$	153
5.3.3 $(3, 2)_{1/6}$ and light right-handed neutrinos	155
<b>Conclusion</b>	<b>167</b>
<b>Publication List</b>	<b>170</b>
<b>A Useful identities</b>	<b>172</b>
A.1 Fierz identities	172
A.2 Passarino-Veltman Functions	172

---

<b>B 2HDM</b>	<b>174</b>
B.1 Feynman rules for 2HDM . . . . .	174
B.2 Auxiliary functions . . . . .	175
B.2.1 Wilson Coefficients for the Derivative Operators . . . . .	176
B.2.2 Wilson Coefficients Suppressed by $m_\ell$ . . . . .	177
<b>Résumé en Français</b>	<b>197</b>

## Remerciements

Je voudrais tout d'abord remercier Sébastien Descotes-Genon, le directeur du Laboratoire de Physique Théorique d'Orsay, pour son accueil au sein du laboratoire et pour tout son soutien au cours de ces trois années. Je remercie aussi les autres membres administratifs et scientifiques du laboratoire, toujours très attentifs et disponibles pour m'aider. Je garderai de très bons souvenirs de l'ambiance agréable mais sérieuse de notre laboratoire. Je pense surtout à Asmaa Abada, toujours très gentille, qui m'a permis de participer à plusieurs événements du réseau Invisibles/Elusives et avec qui j'ai pu aussi collaborer. Merci également pour la recette d'infusion à gingembre qui a sauvé un vulnérable brésilien pendant les saisons froides à Orsay.

Je tiens à remercier tout particulièrement les membres de mon jury de thèse qui ont gentiment accepté notre invitation et qui ont fait l'effort de se déplacer pour la soutenance de thèse. Je remercie tout d'abord Asmaa Abada d'avoir présidé le jury. Merci à Antonio Pich et Gino Isidori d'avoir accepté d'être rapporteurs et d'avoir lu mon manuscrit dans un court délai. Merci à Diego Guadagnoli et Justine Serrano pour leur présence et pour les discussions lors de la soutenance. C'était un grand plaisir et honneur de vous avoir tous dans mon jury de thèse.

Je suis pleinement conscient que j'étais un doctorant (doublement) privilégié. Damir Bećirević était un brillant directeur de thèse. Toujours très attentif, je tiens à remercier pour son immense générosité et pour avoir toujours veillé à ma croissance. C'était un énorme plaisir de partager mon temps avec une personne si gentille, si lucide, avec une si vaste connaissance en physique. Cette page est certainement trop courte pour décrire tout ce que j'ai appris de lui, sur la physique surtout, mais pas seulement. Je remercie également Renata Zukanovich Funchal, quelqu'un que je connais depuis plus de huit ans. Merci de m'avoir ouvert sa porte à l'Université de São Paulo, ma première maison. Merci pour tous les conseils, pour les nombreuses discussions et pour le constant partage de ta passion pour la science. Ton enthousiasme pour la physique est toujours pour moi une source d'inspiration. J'espère que les travaux que nous (trois) avons fait ensemble ne seront que le début d'enrichissantes collaborations.

Je tiens à remercier Pierre Fayet, mon professeur à l'École polytechnique et au M2 de physique théorique, pour ses cours passionnants et pour son orientation qui m'a acheminé vers la physique des particules et, plus particulièrement, vers le LPT d'Orsay. Je remercie aussi Adel Bilal, coordinateur au M2 de physique théorique à l'ENS, pour ses excellents cours de QFT et pour ses recommandations lors de la candidature pour la thèse.

Pendant ces trois années, j'ai pu aussi travailler avec des physiciens exceptionnels. Merci à Federico Mescia pour avoir partagé ses astuces (analytiques et numériques) et pour les blagues inoubliables, bien que parfois difficiles à comprendre. Merci à Nejc Kosnik pour les nombreuses discussions à propos des leptosquarks (et les signes dans les formules !). Un grand merci à Svjetlana Fajfer pour toute sa gentillesse et pour les très plaisantes et fructueuses discussions/collaborations qui ne font que commencer. Je remercie aussi mes autres collaborateurs au Brésil, en Croatie et au Japon.

Je remercie tous les doctorants et stagiaires avec qui j'ai pu partager ces trois années : Andrei, Antoine, Florent, Florian, Gabriel, Hermès, Luca, Lucho, Maíra, Matias, Math-

ias, Michele, Renaud, Timothé... Je garderai de très bons souvenirs de cette période (on s'est bien amusés !). Je remercie également mes amis dans le cercle polytechnicien qui ont contribué à ce que ces années en France soient si agréables : André, Anne-Sophie, Arthur, Daniel, Hudson, Juan, Laís, Lucas, Marlen, Nicolas, Noémie, Pedro, Rafael, Ricardo, Thiago, Victor... Je pars de Paris avec une "tristeza distraída". Un grand merci aussi à mes amis qui se trouvent de l'autre côté de l'Atlantique : Bruno, Eduardo, Guilherme, Leonardo, Nathália et Ricardo.

Por fim, não posso deixar de agradecer aos meus pais por todo o suporte e carinho. Mais que isso, sou eternamente grato por terem sempre me deixado traçar os meus próprios caminhos – sem imposições, talvez com uma dolorosa lucidez. Tudo o que eu conquisei, não somente durante o meu doutorado, começa em vocês. Também agradeço ao meu irmão, Caio, por ter sido sempre um bom companheiro e por ter zelado por nossa mãe quando a distância era grande demais.

# Introduction

The Standard Model (SM) of particle physics is a quantum gauge theory which describes with elegance and precision the interactions of sub-atomic particles. The phenomenological successes of the SM are numerous, including extensive tests at accelerator facilities performed at low and high energies which agree very well with the SM predictions. The discovery of its last missing piece at the Large Hadron Collider (LHC), the Higgs boson, represents one of its greatest achievements and corroborates six decades of persistent phenomenological success [1, 2].

However, it is well known that the SM cannot be the ultimate theory of nature. Firstly, it does not incorporate the gravitational interaction, even though the quantum effects from gravity become significant only at inaccessibly high energies near the Planck scale. Furthermore, neutrinos are massless in the SM, in disagreement with the well established experimental observations that neutrinos are massive and oscillate among different flavors. There is also a growing number of astrophysical and cosmological evidences, based on the standard model of cosmology and on general relativity, which suggest that a substantial part of the matter in the universe is neither baryonic nor luminous. If one assumes the validity of those theories at large scales, then particle physics should be able to propose a new particle, which might interact by means not described by the SM of particle physics.

In addition to the experimental observations described above, which cannot be accounted for by the SM, there are also several conceptual problems which cannot be fully understood without introducing physics beyond the SM. While the gauge sector of the SM is surprisingly simple and predictive, our current understanding of flavor is highly unsatisfactory. Fermions appear in three similar copies which are only distinguished by the Yukawa interactions. Contrary to the gauge sector, the Yukawa sector is poorly constrained by symmetry. As a consequence, many parameters (fermion masses and mixing) must be fixed by confronting theory and experiment. Measurements have revealed a strong hierarchy for fermion masses and a strikingly hierarchical structure of the Cabibbo-Kobayashi-Maskawa (CKM) matrix elements, suggesting the existence of unknown underlying symmetry still to be unveiled. The lack of understanding of the SM flavor structure is known as the flavor problem. Furthermore, quantum corrections to the Higgs boson mass are quadratically divergent, thus “unnaturally” sensitive to the ultraviolet (UV) completion of the theory. This issue is known as the hierarchy problem and it is the main motivation to searching the New Physics (NP) effects at the TeV scale.

All of the above problems call for physics beyond the SM, and many proposals have been made over the past several decades to address each of the above-mentioned issues. Simplicity and beauty have been the main guidelines in the quest for NP. However, despite the intense theoretical effort, there is no strong theoretical preference for a specific scenario of physics beyond the SM. The community of theoretical physicists has found itself at a crossroad, and it becomes necessary to use the modern day high energy experiments to select among the various options for a NP scenario. The search of NP effects can proceed via two complementary approaches: the direct searches of new particles at high energy

facilities, and the indirect searches for NP effects in low energy observables, which will be the main focus of this thesis.

The indirect searches, and most particularly flavor physics, have been extensively used in the past to probe the high energy scales through low energy experiments. A notable example was the first observation of  $B^0 - \bar{B}^0$  mixing [3], which indicated that the top quark is much heavier than any other SM fermion years before its discovery at Tevatron [4,5]. Furthermore, the flavor physics observables provide very useful information about physics beyond the SM. A remarkable example is the  $K^0 - \bar{K}^0$  mixing parameter  $\epsilon_K$  which, after comparing the SM prediction with its measured values, sets a lower bound of about  $10^8$  GeV for the scale of NP under the assumptions of  $\mathcal{O}(1)$  flavor-universal couplings [6]. In particular, this means that NP models with particles in the TeV range, as suggested by the hierarchy problem, must have a non-trivial flavor structure to comply with the stringent limits from flavor changing processes. In what concerns the indirect searches of NP, one should rely on generic approaches with the least number of assumptions as possible. Effective field theories (EFT) are the most efficient approach in that respect, since they provide a general description of low energy physics without having to postulate what happens at arbitrarily high energy scales. Another complementary approach is to consider minimal and pragmatic extensions of the SM, preferably generic, which allow us to use the information from flavor observables to guide the direct searches for new resonances at high energies. Such an example is of two-Higgs doublet model (2HDM), also embedded in various supersymmetric (or not) extensions of the SM [7]. Another possibility that became popular in recent years is to consider the various leptoquark (LQ) states, which can arise in grand unification scenarios and composite Higgs models, among other NP scenarios [8].

In this thesis we will extract the information on NP from the flavor physics observables. Current experiments at NA62, BES-III and LHCb provide us with a rich set of data for testing the various NP scenarios and to guide the theoretical effort towards a flavor theory beyond the SM. The information extracted from this data will be further corroborated/complemented by the future experiments at Belle-II, KOTO, TREK,  $(g-2)_\mu$  and Mu2E, producing a prolific scenario for flavor physics. To interpret these results, we will formulate effective theories which will be matched onto minimal models of NP motivated by the recent experimental findings. The first part of this thesis is devoted to the Higgs boson, which was the last ingredient of the SM observed in experiments. While the Higgs boson couplings measured at the LHC still allow for large deviations from the SM predictions, the direct searches have not ruled out the possibility of other light scalar particles in the spectrum. In this first part of the thesis, we will focus on the 2HDM, and explore the lessons on their spectrum that can be learned by using the general theoretical and phenomenological constraints. The scalar masses and couplings allowed by our analysis will then be confronted with the flavor physics observables. To that purpose we will compute the full set of Wilson coefficients contributing to the relevant tree-level and loop induced meson decays and confront these results with recent data. Particular emphasis will be devoted to the exclusive  $b \rightarrow s\ell^+\ell^-$  decay modes due to the increasing experimental effort to measure the corresponding observables at LHCb. Among the scenarios we consider, the intriguing possibility that a light CP-odd Higgs ( $m_A \lesssim 125$  GeV) is present in the spectrum will be explored. Such a particle would be most welcome as a mediator between the SM and the dark sector because the so-called pseudoscalar portal can evade the strong constraints coming from the null results in dark matter direct detection experiments [9,10]. We will show that this scenario is perfectly plausible in light of current theoretical and experimental constraints, and we will discuss the opportunities to look for this particle in Higgs exclusive decays and in the decay modes of quarkonia.

The second part of this thesis is devoted to the hints of lepton flavor universality (LFU) violation in semileptonic  $B$  meson decays. More specifically, the LHCb measurement of  $R_K = \mathcal{B}(B \rightarrow K\mu^+\mu^-)/\mathcal{B}(B \rightarrow Ke^+e^-)$  [11] and  $R_{K^*} = \mathcal{B}(B \rightarrow K^*\mu^+\mu^-)/\mathcal{B}(B \rightarrow K^*e^+e^-)$  [12] in different bins of dilepton squared momentum  $q^2$  were shown to be significantly lower than predicted [13]. These observables are almost free of theoretical uncertainties since the hadronic uncertainties cancel out to a large extension in the ratio. While these results still need to be confirmed by an independent experiment (Belle-II), they triggered an intense theoretical activity to understand the source of these discrepancies. Within the 2HDM scenarios discussed above, the violation of LFU is found to be negligibly small, suggesting that other bosonic contributions are needed to accommodate these discrepancies. To this purpose, we consider the scenarios containing various LQ states. While these particles are often considered to be exotic in the direct searches at the LHC, they offer one of the prominent candidates to explain the effects of LFU violation. In this thesis, we will scrutinize the proposed LQ explanations of  $R_{K^{(*)}}^{\text{exp}} < R_{K^{(*)}}^{\text{SM}}$  and discuss the implications for the current and future experiments. In particular, we will show that a popular scenario in the literature is not viable, and we will propose a new LQ mechanism to explain  $R_{K^{(*)}}^{\text{exp}} < R_{K^{(*)}}^{\text{SM}}$  through loops. Among the predictions of these models, we will emphasize the importance of lepton flavor violating (LFV) decays, since they offer a very clean alternative allowing to test most of the proposed New Physics scenarios. Another intriguing evidence of LFU violation was unveiled in the processes mediated by the charged current [14], where it was found that  $R_{D^{(*)}} = \mathcal{B}(B \rightarrow D^{(*)}\tau\nu)/\mathcal{B}(B \rightarrow D^{(*)}l\nu)$ , with  $l = e, \mu$ , are larger than predicted in the SM [15–17]. The possibility that the  $b \rightarrow s$  and  $b \rightarrow c$  anomalies are generated by the same mechanism, possibly related to flavor breaking effects beyond the SM, triggered a lot of interest in the theory community. One should, however, be cautious because the prediction of  $R_{D^*}$  requires the assessment of the  $B \rightarrow D^*$  form factors which are still not available from first principle computations. In this thesis, after critically reviewing the status of the SM predictions of  $R_{D^{(*)}}$ , we will discuss the models that have been proposed to simultaneously explain the ensemble of LFU violating observables. In particular, we will discuss a minimal LQ model that we proposed to explain some of these deviations.

The outline of this thesis is as follows. In Chapter 1, we briefly introduce the SM to fix our notation and we discuss some of the SM problems which suggest the existence of NP. In Chapter 2, we present the flavor observables that will be discussed in the subsequent chapters. In particular, we will overview the assessment of hadronic uncertainties entering these quantities and give the general expressions for the relevant observables in terms of an effective field theory. In Chapter 3, we present the general features of two-Higgs doublet models and discuss the most relevant probes of the additional scalar particles at low energies. In Chapter 4, we introduce the main generalities of leptoquark models and discuss how these particle can arise from grand unification models. In Chapter 5, we discuss the tantalizing hints of NP in lepton flavor universality ratios of  $B$ -meson decays. We attempt to overview the viable NP explanations to these puzzles which have been proposed in the literature. In particular, we will focus our discussion on the leptoquark models introduced in Chapter 4. Finally, we summarize our results and conclude.

# Chapter 1

## The Standard Model

The Standard Model (SM) of particle physics is one of the most successful physical theories ever conceived. Its predictions have been experimentally tested in a wide range of energy scales and they agree very well with the data. Furthermore, the Higgs boson found at the LHC in 2012 is the last missing piece of the SM which corroborated more than five decades of phenomenological success [1, 2]. Nonetheless, there are several phenomenological and aesthetic reasons which indicate that the SM cannot be the ultimate fundamental theory.

The purpose of this Section is to fix our notation by introducing the SM Lagrangian and to briefly discuss the limitations of the SM which motivate the quest for physics beyond the SM.

### 1.1 The Standard Model Lagrangian

The SM is a quantum field theory that describes the fundamental electromagnetic, weak and strong interactions based on the gauge principle. The building blocks of the SM are fermions (leptons and quarks), which appear in three copies of chiral multiplets. The interactions in the SM are introduced by the gauge group

$$\mathcal{G}_{\text{SM}} = SU(3)_c \times SU(2)_L \times U(1)_Y, \quad (1.1)$$

where  $SU(3)_c$  is the group associated to the Quantum Chromodynamics (QCD),  $SU(2)_L$  to the weak isospin, and  $U(1)_Y$  the hypercharge. To give masses to the SM particles, a scalar field belonging to a  $SU(2)_L$  doublet ( $\Phi$ ) is also introduced. This doublet is responsible for the spontaneous symmetry breaking  $\mathcal{G}_{\text{SM}} \rightarrow SU(3)_c \times U(1)_{\text{em}}$  via the so-called Higgs-Brout-Englert mechanism [18–21].

The quantum numbers of the SM fields are summarized in Table 1.1. By imposing the requirements of renormalizability and gauge invariance, one can write the most general Lagrangian for the SM in the following form

$$\mathcal{L}_{\text{SM}} = \mathcal{L}_{\text{gauge}} + \mathcal{L}_{\text{matter}} + \mathcal{L}_{\text{Higgs}} + \mathcal{L}_{\text{Yukawa}}. \quad (1.2)$$

The expressions for each piece in  $\mathcal{L}_{\text{SM}}$  will be described below.

#### The gauge sector

The SM gauge sector contains eight gluons  $G_\mu^a$  ( $a = 1, \dots, 8$ ), three electroweak gauge bosons  $W_\mu^a$  ( $a = 1, 2, 3$ ) associated with  $SU(2)_L$ , and the  $U(1)_Y$  vector boson  $B_\mu$ . These

	$SU(3)$	$SU(2)$	$U(1)_Y$
$L_i$	<b>1</b>	<b>2</b>	1/2
$Q_i$	<b>3</b>	<b>2</b>	1/6
$\ell_R$	<b>1</b>	<b>1</b>	-1
$u_R$	<b>3</b>	<b>1</b>	2/3
$d_R$	<b>3</b>	<b>1</b>	-1/3
$\Phi$	<b>1</b>	<b>2</b>	1/2

**Table 1.1:** Representations under which the SM fermion and scalar fields transform. For the non-Abelian groups, the representation is denoted by its dimension.

fields transform under the adjoint representation of the corresponding gauge groups. The gauge Lagrangian is then described by

$$\mathcal{L}_{\text{gauge}} = -\frac{1}{4}G_{\mu\nu}^a G^{\mu\nu,a} - \frac{1}{4}W_{\mu\nu}^a W^{\mu\nu,a} - \frac{1}{4}B_{\mu\nu}B^{\mu\nu}, \quad (1.3)$$

where the summation over the  $SU(N)$  indices is implicit,  $a = 1, \dots, (N^2 - 1)$ . The field strength tensors are defined by

$$G_{\mu\nu}^a = \partial_\mu G_\nu^a - \partial_\nu G_\mu^a + g_s f^{abc} G_\mu^b G_\nu^c, \quad (1.4)$$

$$W_{\mu\nu}^a = \partial_\mu W_\nu^a - \partial_\nu W_\mu^a + g \varepsilon^{abc} W_\mu^b W_\nu^c, \quad (1.5)$$

$$B_{\mu\nu} = \partial_\mu B_\nu - \partial_\nu B_\mu, \quad (1.6)$$

where  $\varepsilon^{abc}$  and  $f^{abc}$  are the structure constants of the  $SU(2)_L$  and  $SU(3)_c$  groups, respectively. Moreover,  $g$  and  $g_s$  are the couplings of  $SU(3)_c$  and  $SU(2)_L$ , respectively. For completeness, we also define the coupling  $g'$  of the Abelian group  $U(1)_Y$ . The mass terms in  $\mathcal{L}_{\text{gauge}}$  are forbidden by the gauge symmetry. For the electroweak gauge bosons  $W^\pm$  and  $Z$ , this mass is generated by the Higgs-Brout-Englert mechanism, which will be briefly described below.

### The scalar sector

To generate the masses of the gauge bosons, the gauge symmetry must be broken. The main idea of the Brout-Englert-Higgs mechanism is that the dynamics of the theory can be such that a symmetry of the Lagrangian is not necessarily respected by its ground state [18–21]. In this case, the choice among one of the possible degenerate vacuum states spontaneously breaks the symmetry.

In the SM, the most general Lagrangian in the scalar sector reads

$$\mathcal{L}_{\text{Higgs}} = (D^\mu \Phi)^\dagger (D_\mu \Phi) + m^2 \Phi^\dagger \Phi - \lambda (\Phi^\dagger \Phi)^2, \quad (1.7)$$

where  $m^2$  and  $\lambda$  are free parameters. The quartic coupling  $\lambda$  is positive, since the scalar potential must be bounded from below. The covariant derivative of the Higgs doublet is

defined by

$$D_\mu \Phi = \left[ \partial_\mu - ig \frac{\sigma^a}{2} W_\mu^a - i \frac{g'}{2} B_\mu \right] \Phi, \quad (1.8)$$

where  $\sigma^a$  ( $a = 1, 2, 3$ ) are the Pauli matrices. In the case  $m^2 < 0$ , the minimization of the scalar potential leads to the ground state  $\langle \Phi^\dagger \Phi \rangle = 0$ , which is a singlet of the SM gauge symmetry. To implement the Brout-Englert-Higgs mechanism, one must assume  $m^2 > 0$ , in which case the minimization of the Higgs potential leads to a non-trivial vacuum,

$$\langle \Phi^\dagger \Phi \rangle = \frac{v^2}{2}, \quad (1.9)$$

where  $v = m/\sqrt{\lambda}$  is the vacuum expectation value (vev), which induces the spontaneous breaking of the SM symmetry  $SU(3)_c \times SU(2) \times U(1)_Y$  into  $SU(3)_c \times U(1)_{\text{em}}$ . Among the possible vacuum states, we can choose

$$\langle \Phi \rangle = \frac{1}{\sqrt{2}} \begin{pmatrix} 0 \\ v \end{pmatrix}. \quad (1.10)$$

The scalar doublet  $\Phi$  had four degrees of freedom, three of which are the Goldstone bosons eaten up to give mass to the electroweak bosons. The remaining scalar particle is the so-called Higgs boson  $h$ , which was discovered in 2012 at the LHC [1, 2]. In the unitary gauge, the scalar doublet  $\Phi$  can be parameterized as

$$\Phi = \frac{1}{\sqrt{2}} \begin{pmatrix} 0 \\ v + h \end{pmatrix}. \quad (1.11)$$

By inserting Eq. (1.11) in Eq. (1.7), one can then recognize three massive gauge bosons  $W^\pm$  and  $Z^0$ , defined by

$$W_\mu^\pm = \frac{W_\mu^1 \mp iW_\mu^2}{\sqrt{2}}, \quad (1.12)$$

and

$$\begin{cases} Z_\mu = W_\mu^3 \cos \theta_W + B_\mu \sin \theta_W, \\ A_\mu = -W_\mu^3 \sin \theta_W + B_\mu \cos \theta_W, \end{cases} \quad (1.13)$$

with masses

$$m_W = \frac{gv}{2}, \quad \text{and} \quad m_Z = \frac{gv}{2 \cos \theta_W}. \quad (1.14)$$

In addition to the  $W^\pm$  and  $Z^0$ , there is one massless vector field  $A_\mu$  which is related to the photon. The fact that the photon is massless is a manifestation of the residual symmetry  $U(1)_{\text{em}}$  of the theory. The Weinberg angle  $\theta_W$  is defined by

$$\tan \theta_W = \frac{g'}{g}, \quad (1.15)$$

which is related to the electric charge via the relation

$$e = g \sin \theta_W = g' \cos \theta_W. \quad (1.16)$$

On the phenomenological level, the electroweak vev can be determined from the muon lifetime, which is related to the Fermi constant  $G_F = 1.1663787(6) \times 10^{-5} \text{ GeV}^{-2}$  [22] via the relation

$$v^2 = \frac{1}{\sqrt{2}G_F}. \quad (1.17)$$

This fixes the vev to be  $v \approx 246 \text{ GeV}$ . The other parameters in the scalar sector are fixed by the Higgs boson mass  $m_h = \sqrt{2m^2} = 125.09(24) \text{ GeV}$  [22]. This value for  $m_h$  is in good agreement with the indirect bounds<sup>1</sup> from the LEP data [24] and implies that  $\lambda = m_h^2/(2v^2) \approx 0.13$  for the quartic coupling, which is therefore perturbative. Furthermore, the relations between the different couplings and masses of the electroweak bosons are one of the main predictions of the SM, which have been thoroughly verified at different experiments, including LEP, Tevatron and the LHC. The current experimental averages for the  $W^\pm$  and  $Z^0$  masses are given by [22]

$$\begin{aligned} m_W &= 80.385(15) \text{ GeV}, \\ m_Z &= 91.1876(21) \text{ GeV}. \end{aligned} \quad (1.18)$$

These values are found to be consistent with the global fit to the electroweak observables, to which the radiative corrections must be included. The assessment of the validity of the SM at electroweak scale via electroweak precision tests, including the parameters  $S$ ,  $T$  and  $U$  which permit to test it at the loop-level, is one of the most important achievements of the SM [23].

### Fermionic sector

The kinetic and gauge interactions of fermions are given by

$$\mathcal{L}_{\text{matter}} = \sum_{i=e,\mu,\tau} i\bar{L}_i \not{D} L_i + \sum_{i=e,\mu,\tau} i\bar{\ell}_{Ri} \not{D} \ell_{Ri} + \sum_{\text{quarks}} i\bar{Q}_i \not{D} Q_i + \sum_{\text{quarks}} i\bar{q}_{Ri} \not{D} q_{Ri}, \quad (1.19)$$

where the summations extend over the different fermions appearing in Table 1.1 and over family indices. Fermion masses are forbidden at this level, arising only in the Yukawa sector via the Higgs mechanism, as it will be discussed in the following. The covariant derivatives for the weak doublets are defined by

$$D_\mu \psi_L = \left[ \partial_\mu - \frac{ig}{\sqrt{2}} (\tau^+ W_\mu^+ + \tau^- W_\mu^-) + ieQA_\mu - \frac{ig}{2 \cos \theta_W} (\tau_3 - 2Q \sin^2 \theta_W) Z_\mu \right] \psi_L, \quad (1.20)$$

where we have used Eqs. (1.12) and (1.13) to make explicit the physical gauge bosons. In this expression,  $Y$  is the hypercharge of the fermion multiplet and the charge operator is defined as  $Q = Y + T_3$ . Moreover, we defined  $\tau^\pm = (\tau_1 \pm i\tau_2)/2$ , as usual. For RH fermions, which are  $SU(2)_L$  singlets, the covariant derivative takes a simpler form, namely,

$$D_\mu \psi_R = \left[ \partial_\mu + ieQA_\mu + \frac{ig}{\cos \theta_W} Q \sin^2 \theta_W Z_\mu \right] \psi_R. \quad (1.21)$$

From the expressions given above, one can derive the form of charged and neutral current interaction in the flavor basis.

---

<sup>1</sup>The SM fit to electroweak data predicts  $m_h = 94_{-22}^{+25} \text{ GeV}$  [23], which agrees within  $1.3\sigma$  with the value measured at the LHC.

## Yukawa sector

In the SM, the only source of flavor violation are the Yukawa couplings between fermions and the Higgs field, defined by

$$\mathcal{L}_{\text{Yukawa}} = -(Y_\ell)_{ij} \bar{L}_i \Phi \ell_{Rj} - (Y_d)_{ij} \bar{Q}_i \Phi d_{Rj} - (Y_u)_{ij} \bar{Q}_i \tilde{\Phi} u_{Rj} + \text{h.c.}, \quad (1.22)$$

where  $\tilde{\Phi} = i\sigma_2 \Phi^*$  is the conjugate  $SU(2)_L$  doublet and  $Y_{u,d,\ell}$  are  $3 \times 3$  complex matrices in flavor space. After spontaneous symmetry breaking, the Yukawa Lagrangian in the unitary gauge becomes

$$\mathcal{L}_{\text{Yukawa}} = -\frac{h+v}{\sqrt{2}} \left[ (Y_\ell)_{ij} \bar{\ell}_{Li} \ell_{Rj} + (Y_d)_{ij} \bar{d}_{Ri} d_{Rj} + (Y_u)_{ij} \bar{u}_{Li} u_{Rj} \right] + \text{h.c.}, \quad (1.23)$$

from which one can read the interactions of the Higgs boson to fermions and the charged fermion masses, namely,

$$M_f = \frac{Y_f v}{\sqrt{2}}, \quad (1.24)$$

where  $f = u, d, \ell$ . These fermion mass matrices are non-diagonal and can then be diagonalized by biunitary transformations,

$$M_f = V_L^{f\dagger} M_f^{\text{diag}} V_R^f. \quad (1.25)$$

The unitary matrices  $V_L^f$  and  $V_R^f$  can be absorbed by a redefinition of the LH and RH fermion fields,

$$\Psi_{f,L} \rightarrow V_L^{f\dagger} \Psi_{f,L}, \quad \Psi_{f,R} \rightarrow V_R^{f\dagger} \Psi_{f,R}. \quad (1.26)$$

The neutral currents remain flavor diagonal under this transformation, while the charged ones become flavor violating,

$$\mathcal{L}_{cc} = -\frac{g}{\sqrt{2}} \sum_{i,j} (V_{\text{CKM}})_{ij} \bar{u}_i \gamma^\mu P_L d_j W_\mu^+ + \text{h.c.}, \quad (1.27)$$

where  $V_{\text{CKM}} = V_L^u V_L^{d\dagger}$  is the Cabibbo–Kobayashi–Maskawa (CKM) matrix. The CKM matrix is unitary and it can be fully parameterized by three angles and one complex phase, which must be extracted from experiment, similarly to the fermion masses. To see that, note that any  $n \times n$  unitary matrix has  $n^2$  parameters, from which  $n(n-1)/2$  are real and  $n(n+1)/2$  are complex. Some of the complex parameters can be reabsorbed by rephasing the quark fields. More specifically, by redefining the  $n$  down-type quarks and the  $n$  up-type quarks, while imposing baryon number conservation, one can eliminate  $2n-1$  phases (the relative phases of the quark fields). Therefore, by taking  $n=3$  we obtain that the CKM matrix has  $n(n-1)/2 = 3$  angles, and  $(n-1)(n-2)/2 = 1$  phase. The observation that a third generation is needed in order to have  $CP$  violation in the SM is known as the Kobayashi–Maskawa mechanism [25].

One of the main peculiarities of the SM is that flavor changing neutral currents (FCNC) are absent at tree-level. These processes are only generated at loop-level, as illustrated in Fig. 1.1. Since these phenomena are loop-induced, they are rare in the SM, which is why they provide very useful tests of the validity of the SM and a probe of physics beyond

the SM, as we will discuss in Chapter 2. Furthermore, it should be stressed that FCNC processes are directly related to fermion masses and mixing because the Yukawa couplings are the only sources of flavor violation in the SM.

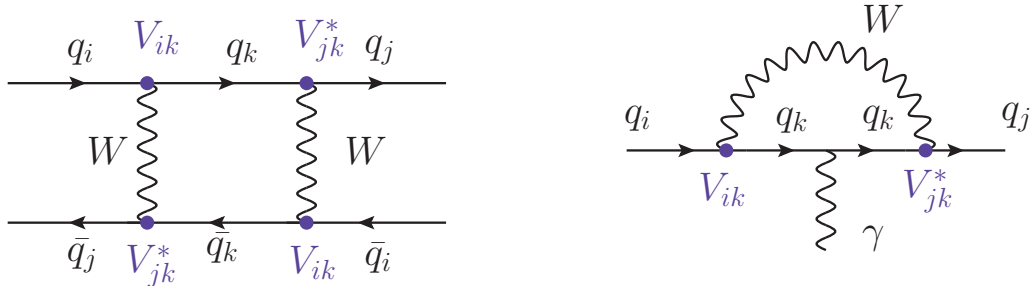


**Figure 1.1:** Examples of loop diagrams contributing to  $\Delta F = 2$  (left) and  $\Delta F = 1$  (right) FCNC processes in the SM. For simplicity, we wrote  $V \equiv V^{\text{CKM}}$ .

As a final remark, note that neutrinos are massless in the SM. These particles do not acquire a mass through the Higgs mechanism since this would require the presence of gauge singlets  $\nu_R$ , which are absent by construction. Furthermore, a Majorana mass term for  $\nu_L$  is forbidden at the renormalizable level by the gauge symmetry.

## 1.2 Why do we need to go beyond?

Despite its remarkable phenomenological success, the SM cannot be a final theory of fundamental interactions. Firstly, it does not incorporate gravitational interactions, which should become important at energy scales near the Planck scale. The solution to this long standing problem is one of the great open questions in theoretical physics and the lack of experimental signals to guide us makes this task particularly difficult. In addition to the lack of a quantum theory of gravity, the SM cannot accommodate some experimental observations, such as neutrino masses and the observation of dark matter. While there is no doubt that neutrinos are massive particles, the conclusion that dark matter must manifest itself as new particles interacting weakly with the SM depends on the validity of the Standard Model of cosmology. This inference must be corroborated by direct and indirect searches for dark matter particles, which have been inconclusive until the present moment. Moreover, in addition to neutrino masses, the SM also leaves many aesthetic questions unanswered, such as the hierarchy and flavor problems.

In the following, we will briefly overview some of the above mentioned problems which motivate physics beyond the SM.

### 1.2.1 Neutrino masses

One of the most compelling evidences of physics beyond the SM comes from the observation that neutrinos are massive particles that oscillate among different flavors. The picture of massive neutrinos has been corroborated by several experiments measuring atmospheric [26–31] and solar neutrinos [32, 33, 33–41], as well as neutrinos produced in accelerators [42–44] and nuclear reactors [45–48]. In 2012, the last missing angle in the lepton sector,  $\theta_{13} \approx 8^\circ$ , was measured by reactor experiments [49], which helped establishing that neutrinos are indeed massive and oscillate. In addition to the mixing angles, the oscillation experiments

can also measure the squared mass differences  $\Delta m_{ij}^2 = m_{\nu_i}^2 - m_{\nu_j}^2$  ( $i, j = 1, 2, 3$ ) of the neutrinos mass eigenstates  $\nu_i$ , which satisfy [50]

$$\Delta m_{21}^2 \approx 7.5 \times 10^{-5} \text{ eV}^2, \quad \text{and} \quad \left| \Delta m_{3\ell}^2 \right| \approx 2.5 \times 10^{-3} \text{ eV}^2. \quad (1.28)$$

The ordering of neutrino masses is still unknown, which can be normal  $m_{\nu_1} < m_{\nu_2} < m_{\nu_3}$ , or inverted  $m_{\nu_3} < m_{\nu_1} < m_{\nu_2}$ . For that reason, we define in the above equation  $\Delta m_{3\ell}^2 = \Delta m_{31}^2 > 0$  for the normal ordering, and  $\Delta m_{3\ell}^2 = \Delta m_{32}^2 < 0$  for the inverted one.

The absolute mass scale of neutrinos remains unconstrained, since the oscillation probabilities are only sensitive to the squared mass differences. Limits on  $m_{\nu_i}$  can be obtained by studying the kinematics of tritium beta decay, which sets limits of the order  $m_{\nu_i} \lesssim 1 \text{ eV}$  [51]. Stronger limits on the sum of neutrino masses can be obtained from cosmology, but these require further assumptions about the cosmological model. For this reason, those bounds are less compelling. Based on the discussion above, it becomes clear that neutrinos are not only massive fermions, but also that they are several orders of magnitude lighter than the other SM particles. This mass gap is often considered as an indication that neutrino masses might be generated by a different mechanism than the one inducing the charged fermion masses.

On theory side, the SM is constructed in such a way that neutrinos are massless, as discussed Sec. 1.1. Therefore, a mechanism beyond the SM is needed to generate neutrino masses. It is beyond the scope of this thesis to review the plethora of scenarios proposed to generate neutrino masses and to explain their smallness. Nonetheless, it is fair to say that the minimal scenarios predict the existence of particles well beyond the reach of current and future experiments, see for example the original proposal of the type I seesaw mechanism [52–55]. To lower these energy scales, it is usually necessary to introduce new degrees of freedom, at the price of increasing the complexity of the models, as in the so-called Inverse seesaw scenario [56–58]. Other possibility is to fine tune the couplings. Finally, in terms of an effective theory, the lowest-dimension operator capable of generating neutrino masses is the Weinberg operator [59],

$$\mathcal{O}_5 = \frac{f_{ij}}{2\Lambda} \left( \overline{L_i^C} \widetilde{\Phi}^* \right) \left( \widetilde{\Phi}^\dagger L_j \right) + \text{h.c.}, \quad (1.29)$$

which is the only dimension-5 allowed by the SM gauge symmetry. In this equation,  $f_{ij}$  are complex numbers satisfying  $f_{ij} = f_{ji}$  and  $\Lambda$  is an energy scale associated to the mechanism behind neutrino masses. Moreover, the fermion conjugation of a generic fermion field  $\Psi$  is defined by  $\Psi^C = \gamma_0 C \Psi^*$ , where  $C = i\gamma^2 \gamma^0$ . The Weinberg operator violates lepton number  $L$  by two units and gives the following Majorana mass term

$$\mathcal{L} \supset \frac{f_{ij} v^2}{4\Lambda} \nu_{Li}^C \nu_{Lj} + \text{h.c.} \quad (1.30)$$

It should be stressed that any scenario of NP generating Majorana neutrino masses can be matched onto an effective theory containing  $\mathcal{O}_5$  once the heavy degrees of freedom have been integrated out.

The mechanism just described can generate neutrino masses if the lepton number symmetry  $L$  is violated, i.e. if neutrinos are Majorana particles. Until now, the violation of  $L$  has still not been observed in experiments, which have been mostly focused on the search of the neutrinoless double beta decay  $nn \rightarrow ppe^-e^-$  [60–62]. Therefore, despite the strong theoretical preference for Majorana neutrinos, the hypothesis of Dirac neutrinos remains equally plausible. If neutrinos are Dirac particles then the generation of their masses would

proceed through the Yukawa interactions with the introduction of right-handed neutrinos, in a similar way to the mechanism for charged fermions.

### 1.2.2 The SM flavor problem

The origin of the flavor of quarks and leptons remains one of great open questions in theoretical physics. The only source of flavor violation in the SM comes from the Yukawa interactions, which break the global flavor symmetry of the SM

$$\mathcal{G}_G = U(3)_L \times U(3)_{\ell_R} \times U(3)_Q \times U(3)_{u_R} \times U(3)_{d_R}, \quad (1.31)$$

where each  $U(3)$  transformation acts in flavor space for a fermion field in Table 1.1. The description of flavor in terms of the Higgs mechanism is highly unsatisfactory since the Yukawa interactions are not controlled by any symmetry principle, contrary to the SM gauge sector, resulting in a large number of parameters that must be extracted from experiment. In other words, the SM Higgs sector can only *accommodate* fermion masses and mixing, but it does not constraint the size or pattern of Yukawa couplings.

The flavor problem arises when one inspects the very hierarchical pattern taken by the flavor violating parameters, namely fermion masses and CKM entries. The observed pattern does not look accidental and it is expected to be explained by a symmetry argument or a flavor theory based on that symmetry. If for the moment we put aside  $\theta_{\text{QCD}}$ , in the SM there are 13 free parameters in the SM flavor sector, which comprise masses, mixing angles and one complex phase. Charged fermion masses span six orders of magnitude, going from the very light electron with mass  $m_e = 0.5110$  MeV to the top quark mass  $m_t^{\text{pole}} = 173.3 \pm 0.8$  GeV [63], which is the heaviest particle of the SM. This hierarchy becomes even more pronounced when one considers neutrino masses, which are known to be  $m_{\nu_i} \lesssim \mathcal{O}(1 \text{ eV})$ , as depicted in Fig. 1.2. Up to now, there is no convincing explanation of that hierarchy.

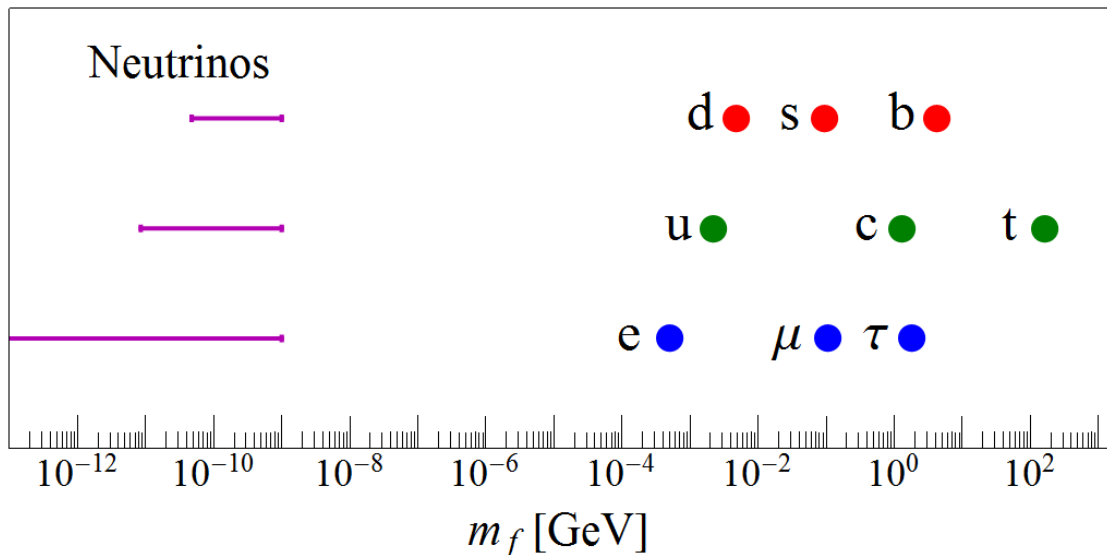


**Figure 1.2:** Fermion masses in the SM amended with neutrino masses. We consider the  $\overline{\text{MS}}$  quark masses from Ref. [22] at the scale  $\mu = 2$  GeV for light quarks, and at  $\mu = m_q$  for  $q = c, b, t$ .

Another facet of the flavor problem comes from the mixing parameters. CKM and PMNS matrices have very different structures: while CKM is hierarchical, PMNS is not.

The CKM matrix can be generically parameterized by three angles  $\theta_{12}$ ,  $\theta_{13}$  and  $\theta_{23}$ , and one phase  $\delta_{13}$  [22],

$$V_{\text{CKM}} = \begin{pmatrix} c_{12}c_{13} & s_{12}c_{13} & s_{13}e^{-i\delta_{13}} \\ -s_{12}c_{23} - c_{12}s_{23}s_{13}e^{i\delta_{13}} & c_{12}c_{23} - s_{12}s_{23}s_{13}e^{i\delta_{13}} & s_{23}c_{13} \\ s_{12}s_{23} - c_{12}c_{23}s_{13}e^{i\delta_{13}} & -c_{12}s_{23} - s_{12}c_{23}s_{13}e^{i\delta_{13}} & c_{23}c_{13} \end{pmatrix}, \quad (1.32)$$

where  $s_{ij} \equiv \sin \theta_{ij}$  and  $c_{ij} \equiv \cos \theta_{ij}$  ( $i, j = 1, 2, 3$ ). The off-diagonal elements of the CKM matrix are found to satisfy a strong hierarchical pattern:  $|V_{us}|$  and  $|V_{cd}|$  are of order  $\approx 0.22$ ,  $|V_{cb}|$  and  $|V_{ts}|$  are of order  $\approx 4 \times 10^{-2}$ , whereas the elements  $|V_{ub}|$  and  $|V_{td}|$  are of order  $\approx 5 \times 10^{-3}$  [64, 65]. This hierarchical pattern becomes even more explicit in the so-called Wolfenstein parameterization, which makes manifest the fact that  $s_{12} \gg s_{23} \gg s_{13}$  [66]. This parameterization is obtained by expanding the CKM matrix is expanded in powers of the small parameter  $\lambda \equiv |V_{us}| \approx 0.22 \ll 1$ ,

$$V_{\text{CKM}} = \begin{pmatrix} 1 - \frac{\lambda^2}{2} & \lambda & A\lambda^3(\rho - i\eta) \\ -\lambda & 1 - \frac{\lambda^2}{2} & A\lambda^2 \\ A\lambda^3(1 - \rho - i\eta) & -A\lambda^2 & 1 \end{pmatrix} + \mathcal{O}(\lambda^4), \quad (1.33)$$

where  $A$ ,  $\rho$  and  $\eta$  are  $\mathcal{O}(1)$  real numbers.<sup>2</sup> The present fits to the ensemble of flavor changing processes result in the precise values  $\rho = 0.157(14)$ ,  $\eta = 0.352(11)$ ,  $A = 0.833(12)$  and  $\lambda = 0.22497(69)$  [64]. On the other hand, the leptonic mixing matrix, also called Pontecorvo-Maki-Nakagawa-Sakata (PMNS) matrix, shows a completely different pattern with very large mixing angles. The most recent fits to neutrino data give, to  $1\sigma$  accuracy [50],

$$\theta_{23}^{\text{PMNS}} = (41.6_{-1.2}^{+1.5})^\circ, \quad (1.34)$$

$$\theta_{12}^{\text{PMNS}} = (33.56_{-0.75}^{+0.77})^\circ, \quad (1.35)$$

$$\theta_{13}^{\text{PMNS}} = (8.46 \pm 0.15)^\circ, \quad (1.36)$$

where we have used the same parameterization of Eq. (1.32) and taken the results for the normal ordering for illustration. For comparison, the largest angle in the CKM matrix is given by the Cabibbo angle,  $\theta_{12}^{\text{CKM}} = (13.00 \pm 0.04)^\circ$ , which is of the same order as the smallest mixing angle in the lepton sector,  $\theta_{13}^{\text{PMNS}} = (8.46 \pm 0.15)^\circ$ . Why are the CKM parameters so hierarchical? Why are the mixing parameters so large in the leptonic sector? These questions call for physics beyond the SM.

The ensemble of striking observations described above is called the flavor problem, which requires physics beyond the SM. The fact that there is no theoretical hint for the scale of NP responsible for the flavor breaking mechanism beyond the SM makes the flavor problem particularly difficult to solve. Therefore, experimental hints are more than needed to guide the theoretical efforts towards a flavor theory that could give an explanation for the observed patterns of flavor parameters by using symmetry principles.

<sup>2</sup>The inclusion of terms  $\mathcal{O}(\lambda^4)$  and  $\mathcal{O}(\lambda^5)$  is mandatory for phenomenological applications. The expansion at higher orders can be obtained by adopting the convention  $\lambda \equiv s_{12}$ ,  $A\lambda^2 \equiv s_{23}$  and  $A\lambda^3(\rho - i\eta) \equiv s_{13}e^{-i\delta}$ .

### 1.2.3 The hierarchy problem

The Higgs sector is the least constrained piece of the SM Lagrangian by symmetries, being for that reason the source of many of its puzzles. We have already discussed the SM flavor problem, which is related to the lack of a flavor symmetry in the Yukawa sector (Higgs couplings to fermions). The hierarchy problem is related to the fact that the SM contains a fundamental scalar with a mass term unconstrained by symmetries, which receives then large radiative corrections from the UV completion of the theory.

In the SM, the masses of fermions and vector bosons are forbidden by the  $SU(2)_L \times U(1)_Y$  gauge symmetry. In this case, it can be shown that any loop correction to these parameters will be proportional to the tree-level masses, which means that they are *multiplicatively* renormalized. This property holds for fermions even in the absence of the gauge symmetry, because the chiral symmetry also protects fermion masses. For the Higgs boson, the situation is different since the limit  $m_h \rightarrow 0$  does not enhance the SM symmetries. In this case, we say that the parameters  $m_h^2$  is *additively* renormalized since it receives corrections proportional to the masses of the particles running in the loops. As a consequence of that, the SM Higgs sector becomes highly sensitive to quantum corrections and to the cutoff of the theory.

To illustrate the above-mentioned issue, one can compute the one loop-corrections to the Higgs mass in the SM, which are illustrated in Fig. 1.3. By regularizing the integral with a hard cutoff  $\Lambda$ , one obtains

$$\delta m_h^2 = \frac{3\Lambda^2}{8\pi^2 v^2} \left[ 4m_t^2 - 2m_W^2 - m_Z^2 - m_h^2 + \mathcal{O}\left(\log \frac{\Lambda}{\mu}\right) \right], \quad (1.37)$$

where we recognize contribution from top quark which is proportional to  $m_t^2/v^2$ , and that gives the most significant radiative correction to the Higgs mass in the SM. From this expression we see that the Higgs mass is quadratically sensitive to the cutoff of the theory. Since the only available cutoff is the Planck scale,  $M_{\text{Pl}} \approx 1.22 \times 10^{19}$  GeV, which is much larger than the Higgs mass  $m_h = 125.09(24)$  GeV [22], we observe that the bare Higgs mass and its counter term must be fine tuned to an enormous accuracy to reproduce a light Higgs mass. This statement is precisely the hierarchy problem, which arises in theories with fundamental scalars where a hierarchy of scales  $m_h \ll \Lambda$  is present. In particular, the hierarchy problem is an indication that the NP scale cannot be too large. More precisely, for the Higgs mass observed at the LHC, the requirement of fine tuning in  $m_h$  of less than 1 part in 10 implies that the scale of NP should be below a few TeV [67].

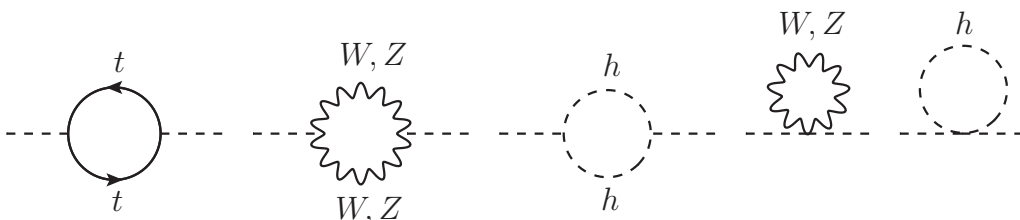


**Figure 1.3:** One loop corrections to the Higgs self-energy in the SM.

We have not yet enough information to unambiguously determine how the SM should be extended to address the hierarchy problem. Most concrete proposals point at the existence of new degrees of freedom in the TeV range, possibly accessible at the LHC. This observation is in apparent contradiction with the information extracted from the flavor experiments, which set stringent bounds on the NP scale  $\Lambda_{\text{NP}}$ . More specifically, FCNC processes in

the SM are suppressed by (i) the loop factors, (ii) by the GIM mechanism [68] and (iii) by the hierarchy of the CKM matrix,  $|V_{td}| \ll |V_{ts}| \ll |V_{tb}| \approx 1$ . Hence, the precise study of these processes and the comparison with the experimental results allows us to impose severe constraints on  $\Lambda_{\text{NP}}$ . For instance, the  $K^0 - \overline{K}^0$  mixing parameter  $\epsilon_K$  sets an lower bound of about  $\Lambda_{\text{NP}} \gtrsim 10^8$  GeV if  $\mathcal{O}(1)$  NP couplings are assumed [6]. This apparent contradiction between bounds on NP stemming from flavor experiments and the prejudice that NP should emerge at the TeV scale is often called the NP flavor puzzle, and it implies that NP should have a non-trivial flavor structure. The most popular solution to this problem goes under the name of Minimal Flavor Violation (MFV) [69,70]. In this approach, the Yukawa interactions are identified as the only source of flavor violation, reproducing the SM flavor structure also beyond the SM. In this case, the bounds from flavor changing observables are lowered to the TeV range at which we expect that the solution to the hierarchy will emerge. Nonetheless, it is worth stressing that the MFV hypothesis is not a theory of flavor, since it does allow us to determine the pattern of Yukawa couplings in terms of a small number of parameters of a more fundamental theory. Therefore, the ultimate solution to the hierarchy and flavor problems remains an open question. Experimental hints from indirect and/or direct searches are in that respect most welcome guides of the theoretical effort to the solution of these problems.

# Chapter 2

## Flavor observables as a probe of New Physics

The current situation of direct searches of New Physics is that no particle beyond the SM has been found at the LHC at energies  $\lesssim 1$  TeV, and that most theoretical speculations about the possible scale/nature of New Physics seem to be unsound. In such a situation, flavor physics can be very useful, since it can probe scales well above the ones attained by the direct experimental searches. Furthermore, the constraints coming from indirect searches can be complementary in guiding the direct searches, pointing to the observables where New Physics could be effectively seen.

The main difficulty in the comparison between the SM predictions and the experimental results lies in the fact that non-perturbative QCD remains not under full theoretical control. While an analytic solution to non-perturbative QCD is still lacking, in some situations the hadronic uncertainties can be controlled by means of numerical simulations of QCD on the Lattice (LQCD). Over the past decades we witnessed a huge progress of LQCD simulations which nowadays allows us to attain a precision at the percent level for certain hadronic quantities. At the same time, the experimental precision for many observables will be substantially improved by the new generations of flavor experiments. For these reasons, indirect searches and in particular those involving flavor physics are a very promising route to seek the effects of physics beyond the SM.

The goal of this chapter is to review the flavor physics results after the first run of LHC, and the results from meson factories (CLEO-c, BES, BaBar and Belle, among others), which experimentally established the unitarity of the CKM matrix with great precision. In this Chapter, our approach will rely on Effective Field Theories (EFT), since they provide the most general description of low-energy physics in the absence of new light degrees of freedom. Particular emphasis of this Chapter will be given to the assessment of theoretical uncertainties (mainly those of non-perturbative QCD) entering the SM predictions for the flavor physics observables.

The chapter is organized as follows: In Sec. 2.1, we briefly introduce the concept of EFT. In Sec. 2.2, we discuss tree-level electroweak decays of mesons and how those can be used to search the effects of New Physics. In Sec. 2.3, we extend our discussion to the FCNC processes, and most particularly to the transition  $b \rightarrow s\ell^+\ell^-$ . Lastly, we conclude the Chapter in Sec. 2.4 with a discussion of lepton flavor violation in decays of both leptons and hadrons.

## 2.1 Effective field theories

Effective field theories (EFT) are nowadays widely used in all branches of theoretical physics. The basic principle which warrants the validity of EFT method is that one can isolate sets of phenomena with different energy/length scales and then find a suitable description for each class of physical problems. This property is greatly responsible for the gradual progress in physics, where one could for instance formulate the Newtonian mechanics well before the discovery of special relativity, or understand quantum mechanics without having to deal with the uneasy subtleties of QFT.

In the context of QFT, the relevant parameter is the distance scale. Short distance contributions are replaced by local operators, which are obtained by integrating out the irrelevant degrees of freedom, and by expanding in a suitable chosen expansion parameter. The small finite size effects are then treated as perturbations. In particular, this approach is useful for studying the effects of physics beyond the SM in a model independent manner. More precisely, in the so-called bottom up approach, one can write the most general effective Lagrangian consistent with the symmetries of the low energy theory which contains only the light degrees of freedom, i.e.

$$\mathcal{L}_{\text{eff}} = \mathcal{L}_{d=4} + \sum_i \frac{C_i(\mu)}{\Lambda^{d_i-4}} \mathcal{O}_i(\mu), \quad (2.1)$$

where  $\mathcal{O}_i$  are operators of dimension  $d_i > 4$ ,  $\mu$  is the renormalization scale, and  $C_i(\mu)$  are the so-called Wilson coefficients. The Lagrangian  $\mathcal{L}_{d=4}$  describes the (renormalizable) low energy theory, which is typically considered to be the SM. Even though  $\mathcal{L}_{\text{eff}}$  is non-renormalizable, the predictivity of the effective theory is guaranteed by the fact that the contributions of higher dimensional operators to the amplitudes are suppressed by powers of  $(p/\Lambda)^{d_i-4}$ , where  $p$  is the typical momentum of the low energy process. Henceforth, by working in the regime  $p \ll \Lambda$  and to a given experimental precision, one can renormalize the effective theory with a finite number of counter-terms. The effects of the (unknown) short distance physics are then encoded in the Wilson coefficients  $C_i(\mu)$ , which can be matched onto a full theory by requiring that the amplitudes computed in the full and effective theories coincide at large distances. The main advantage of this approach is that one can generically describe the low-energy physics without having to postulate what happens at arbitrarily high energy scales.

## 2.2 Tree-level electroweak decays of mesons

Tree-level electroweak decays of kaons, and  $D_{(s)}$  and  $B$  mesons are induced by a tree-level exchange of the  $W$  boson, as illustrated in the left panel of Fig. 2.1. These processes provide a straightforward way of extracting the moduli of several CKM matrix elements, such as  $|V_{ud}|$ ,  $|V_{us}|$ ,  $|V_{ub}|$ ,  $|V_{cd}|$ ,  $|V_{cs}|$  and  $|V_{cb}|$ , which can then be confronted with the CKM matrix  $V \equiv V_{\text{CKM}}$  unitarity,  $V^\dagger = V^{-1}$ . To do so, the determination of the hadronic matrix elements plays a crucial role. Nowadays, the level of maturity of Lattice QCD (LQCD) simulations and the developments on the experimental side allow us to go beyond the simple determination of CKM entries, and to use leptonic and semileptonic decays to probe scenarios of physics beyond the SM. For instance, in scenarios with two Higgs doublets, a charged Higgs  $H^\pm$  can generate a tree-level contribution to these decays, as depicted in Fig. 2.1. Therefore, the study of these decays offer a low-energy window to probe the bosonic sector beyond the SM.

Another motivation to search for NP effects in tree-level semi-leptonic decays comes from the discrepancies observed by the  $B$ -physics experiments in the lepton flavor universality ratios, namely

$$R_{D^{(*)}} = \frac{\mathcal{B}(B \rightarrow D^{(*)}\tau\nu)}{\mathcal{B}(B \rightarrow D^{(*)}l\nu)}, \quad (2.2)$$

where  $l = e, \mu$  are averaged in the denominator. The experimental value of  $R_D^{\text{exp}}$  determined by BaBar [71,72] and Belle [73] was found to be about  $2\sigma$  larger than the SM prediction [14]. This observation was further corroborated by the measurement of  $R_{D^{*}}^{\text{exp}}$  [71–76] which indicates a  $\approx 3.3\sigma$  excess with respect to the quoted SM prediction [17]. If these deviations are indeed generated by NP, it is likely that similar effects are present in other leptonic and semileptonic decays. The experimental and theoretical status of  $R_{D^{(*)}}$  will be discussed in Chapter 5, where we will also review some of the proposed NP explanations.

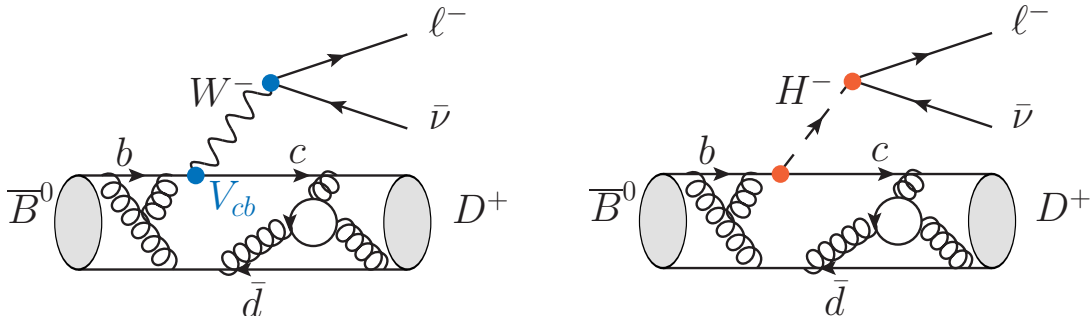


**Figure 2.1:** Contributions to the semi-leptonic decay  $\bar{B}^0 \rightarrow D^+ \ell \nu$  in the SM (left panel) and in 2HDM (right panel).

The dimension-6 effective Hamiltonian describing the transition  $u \rightarrow d \ell \nu$  can be generically parameterized as <sup>1</sup>

$$\begin{aligned} \mathcal{H}_{\text{eff}} = \sqrt{2}G_F V_{ud} & \left[ (1 + g_V)(\bar{u}\gamma_\mu d)(\bar{\ell}_L\gamma^\mu \nu_L) - (1 + g_A)(\bar{u}\gamma_\mu \gamma_5 d)(\bar{\ell}_L\gamma^\mu \nu_L) \right. \\ & \left. + g_S(\mu)(\bar{u}d)(\bar{\ell}_R\nu_L) + g_P(\mu)(\bar{u}\gamma_5 d)(\bar{\ell}_R\nu_L) + g_T(\mu)(\bar{u}\sigma_{\mu\nu}(1 - \gamma_5)d)(\bar{\ell}_R\sigma^{\mu\nu}\nu_L) \right] + \text{h.c.}, \end{aligned} \quad (2.3)$$

where  $u$  and  $d$  stand for generic up-type and down-type quarks, and  $\ell = e, \mu, \tau$ . The NP couplings  $g_{V,A,S,P,T}$  are defined relatively to the Fermi constant, namely,

$$\frac{G_F}{\sqrt{2}} = \frac{g^2}{8m_W^2}. \quad (2.4)$$

Note that the NP couplings can depend on the renormalization scale  $\mu$ , and that the SM corresponds to  $g_{V,A,S,P,T} \equiv 0$ .

The relevant decay channels can be separated into two classes of processes with different QCD content:

- Leptonic decays:  $K^- \rightarrow \ell \nu$ ,  $D_{(s)}^- \rightarrow \ell \nu$  and  $B \rightarrow \ell \nu$ ;
- Semileptonic decays:  $K_L \rightarrow \pi^\pm \ell \nu$ ,  $D \rightarrow K \ell \nu$  and  $B \rightarrow D \ell \nu$ , among others,

<sup>1</sup>We neglect the possibility of RH neutrinos in Eq. (2.3).

where  $\ell$  stands for a generic charged lepton. For leptonic decays, the non-perturbative content needed to compute the branching ratios amounts to a single quantity, which is the meson decay constant, computed in numerical simulations of QCD on the Lattice (LQCD). The situation of semileptonic modes is more elaborated, as it involves several  $q^2$  dependent form-factors where  $q^2$  stands for the dilepton mass squared.

In the following, we will discuss the peculiarities of each of these process, including the non-perturbative inputs needed to do phenomenology, and we will give the general expressions for the experimentally accessible observables in terms of the effective couplings defined in Eq. (2.3).

### 2.2.1 Leptonic decays of mesons

In this Section, we discuss the decay modes of the type  $P^- \rightarrow \ell \bar{\nu}$ , where  $P = K, D_{(s)}, B_{(c)}$  is a pseudoscalar meson ( $J^P = 0^-$ ). For simplicity, we will write the expressions for the decays of  $B$  mesons, but all the other modes can be obtained *mutatis mutandis*.

From Lorentz and parity symmetries, we know that only axial and pseudo-scalar hadron currents can contribute to a transition of the type  $P^- \rightarrow \ell \nu$ . The most general parameterization of the axial hadronic matrix element reads

$$\langle 0 | \bar{b} \gamma_\mu \gamma_5 u | B(p) \rangle = i p_\mu f_B, \quad (2.5)$$

where  $p^\mu$  is the 4-momentum of the  $B$  meson, and  $f_B$  is the so-called decay constant. By virtue of the axial Ward identity, the matrix element of the pseudoscalar density is given by

$$\langle 0 | \bar{b} \gamma_5 u | B(p) \rangle = -i \frac{m_B^2 f_B}{m_u + m_b}. \quad (2.6)$$

The decay constant  $f_B$  encapsulates the non-perturbative content of the transition and it has to be computed by numerical simulations of QCD on the lattice. The current values of the different decay constants obtained by LQCD simulations are summarized in Tab. 2.1, which show a degree of precision below the percent level [77].

Quantity	Value [MeV]
$f_K$	155.6(4)
$f_D$	212.2(15)
$f_{D_s}$	249.8(13)
$f_B$	186(4)
$f_{B_s}$	224(5)
$f_{B_c}$	434(15)

**Table 2.1:** Decay constants of pseudoscalar mesons computed by numerical simulations of QCD on the lattice. These values were extracted from Ref. [77] with the exception of  $f_{B_c}$ , which was computed in Ref. [78].

By using the Hamiltonian Eq. (2.3) and the hadronic matrix elements defined Eqs. (2.5) and (2.6), one can compute the amplitude for  $B^- \rightarrow \ell \bar{\nu}$ :

$$\mathcal{M} = -i\sqrt{2}V_{ub}(if_B)\bar{u}(k_1)\left[(1+g_A)\gamma^\mu P_L p_\mu + g_P(\mu)P_L\frac{m_B^2}{m_u+m_b}\right]v(k_2), \quad (2.7)$$

where the convention for the momenta of the particles are  $B^-(p) \rightarrow \ell(k_1)\bar{\nu}(k_2)$  and the couplings  $g_A$  and  $g_P$  parameterize the most general contributions from NP. Multiplying this amplitude by its conjugate and after summing over the spins we get

$$\sum_{\text{spins}}|\mathcal{A}|^2 = 2G_F^2|V_{ub}|^2f_B^2m_\ell^2(m_B^2 - m_\ell^2)\left|1 + g_A - g_P(\mu)\frac{m_B^2}{m_\ell(m_u+m_b)}\right|^2, \quad (2.8)$$

so that the final expression for the branching ratio reads

$$\mathcal{B}(B^- \rightarrow \ell \nu) = \frac{G_F^2 m_B m_\ell^2}{8\pi} \left(1 - \frac{m_\ell^2}{m_B^2}\right)^2 f_B^2 |V_{ub}|^2 \tau_{B^+} \left|1 + g_A - g_P(\mu)\frac{m_B^2}{m_\ell(m_u+m_b)}\right|^2. \quad (2.9)$$

We recall that the couplings  $g_V$ ,  $g_S$  and  $g_T$  do not contribute to this decay, because the corresponding hadronic matrix elements vanish due to parity and Lorentz invariance of QCD. We reiterate that leptonic decays are considered to be extremely clean, since the whole non-perturbative content of these processes are encoded in a single parameter, the decay constant.

### 2.2.2 Semileptonic $P \rightarrow P'$ decays

In this Section, we discuss the decays of the type  $P \rightarrow P'\ell\nu$ , where  $P, P' = K, D_{(s)}, B_{(s)}, B_c, \eta_c$  are pseudoscalar mesons. We focus on the processes involving pseudoscalar mesons since they require a minimal input from non-perturbative QCD. Electroweak processes with vector mesons or baryons depend on many more hadronic form factors which are more difficult to study in LQCD. For that reason, we will disregard the semileptonic decays to vector mesons and baryons.

In a similar way to the leptonic case, Lorentz invariance and parity guarantee that the transition  $P \rightarrow P'$  only depends on the coefficients  $g_{S,V,T}$ . The hadronic matrix element which appears in the SM amplitude is defined as

$$\langle D^+(k)|\bar{c}\gamma_\mu b|\bar{B}(p)\rangle = \left[(p+k)_\mu - \frac{m_B^2 - m_D^2}{q^2}q_\mu\right]f_+(q^2) + \frac{m_B^2 - m_D^2}{q^2}q_\mu f_0(q^2), \quad (2.10)$$

where  $q = p - k$  is the dilepton 4-momentum, and  $f_+(q^2)$  and  $f_0(q^2)$  are the so-called vector and scalar form factors. Here we focus on the transition  $\bar{B} \rightarrow D^+\ell\bar{\nu}$ , but our results can be easily translated to the other semileptonic modes. These form factors satisfy the constraint  $f_+(0) = f_0(0)$ , a condition which considerably simplifies the determination of these form-factors from LQCD simulations, as well as in the phenomenological analyses of these decays. To demonstrate this property, it is sufficient to parameterize the matrix element in a simplest different way,

$$\langle D^+(k)|\bar{c}\gamma_\mu b|\bar{B}(p)\rangle = (p+k)_\mu f_+(q^2) + (p-k)_\mu f_-(q^2), \quad (2.11)$$

where  $f_-(q^2)$  is related to  $f_{+,0}(q^2)$  by

$$q^2 f_-(q^2) = (m_B^2 - m_D^2) [f_0(q^2) - f_+(q^2)]. \quad (2.12)$$

Since  $f_-(q^2)$  is an analytic function in  $q^2 = 0$ , we directly obtain the desired relation  $f_0(0) = f_+(0)$ . The scalar matrix element is derived from Eq. (2.10) by applying the vector Ward identity, which amounts to <sup>2</sup>

$$\langle D^+(k) | \bar{c}b | \bar{B}(p) \rangle = f_0(q^2) \frac{m_B^2 - m_D^2}{m_b - m_c}. \quad (2.13)$$

In addition to the above-defined form factors, a third one is also needed when the tensor current is considered, namely,

$$\langle D^+(k) | \bar{c} \sigma_{\mu\nu} b | \bar{B}(p) \rangle = -i(p_\mu k_\nu - p_\nu k_\mu) \frac{2f_T(q^2, \mu)}{m_B + m_D}, \quad (2.14)$$

where  $f_T(q^2, \mu)$  is the so-called tensor form factor. An example of NP scenario where the tensor coupling  $g_T$  can be generated is the scenario with scalar leptoquark, which will be discussed in Chapter 4.

### LQCD determination of $P \rightarrow P'$ form factors

Regarding the current status of the LQCD determinations of  $P \rightarrow P'$  hadronic matrix elements, most lattice computations focus only on the normalization of the form factors,  $f_+(0) = f_0(0)$ . That results is then combined with the  $q^2$  spectrum of the differential decay rate,  $d\Gamma(P \rightarrow P'\ell\nu)/dq^2$ , with  $\ell = e, \mu$ , from which is extracted  $|V_{quqd}|f_+(0)$  and therefore  $V_{quqd}$ . That strategy assumes that NP does not contribute to these decays rates. However, in the presence of NP, the  $q^2$  spectrum of the differential decay can be modified and therefore in order to probe the NP scenarios from the semileptonic decays it is essential to compute the  $q^2$  dependence of the form factors on the lattice in a way very similar to the one used to compute  $f_+(0)$ . Currently, the most precisely determined  $P \rightarrow P'$  form factors are the ones for the transition  $K \rightarrow \pi$ , which have been recently updated in Ref. [79] with a precision better than the percent level for both the shape parameters and the normalization. Similarly, the  $D \rightarrow K$  form factors have computed in Ref. [80], which agree with the recent computations reported in Ref. [81]. The  $B \rightarrow \pi$  and  $B_s \rightarrow K$  form factors have also been determined in Ref. [82–84] and Ref. [84, 85], respectively. However, these results are available only computed for very large values of  $q^2$ , whereas the information experimental information is most precise for the low values of  $q^2$ . This fact already makes it difficult to extract the value of  $V_{ub}$  from the exclusive  $B \rightarrow \pi\ell\nu$  decay modes. For that reason, we will not attempt to constraint the NP effects from the exclusive decays based on the  $b \rightarrow u$  transition. Furthermore, the MILC and HPQCD collaborations have computed the  $B \rightarrow D$  form factors [15, 16], providing consistent results, which will be extremely relevant for the phenomenological discussion of Sec. 5.3. Interestingly, a first result for the  $B_c \rightarrow \eta_c$  form factors has been recently computed in Ref. [86]. The results quoted above will be considered in the phenomenological analysis in this thesis. See Ref. [77] for a complete overview of other form factor determinations.

<sup>2</sup>We have explicitly written the charges of the mesons since they can change the sign of this expression. More explicitly, one can show that  $\langle D^-(k) | \bar{b}c | B(p) \rangle = -f_0(q^2) \frac{m_B^2 - m_D^2}{m_b - m_c}$ . This sign difference does not appear in the final expression for the decay rates, since it is compensated by the lepton trace for conjugate mode, so that  $\mathcal{B}(\bar{B} \rightarrow D\ell\bar{\nu}) = \mathcal{B}(B \rightarrow D^-\ell\bar{\nu})$  if  $g_{S,V,T} \in \mathbb{R}$ .

### Computation of $P \rightarrow P' \ell \nu$

We emphasize once again that  $P \rightarrow P' \ell \bar{\nu}$  will be specifically replaced by the example  $\bar{B} \rightarrow D^+ \ell \bar{\nu}$ . In what follows, we assume the kinematics to be  $\bar{B}(p) \rightarrow D^+(k) \ell(p_\ell) \bar{\nu}(p_\nu)$ , with  $q = p - k = p_\ell + p_\nu$ . Although the semi-leptonic decays are more complicated than the leptonic ones from the point of view of QCD, they have a richer kinematic structure which opens the possibility more observables than just the total branching ratio. The full differential branching fractions for this decay is given by

$$\frac{d^2 \mathcal{B}(\bar{B} \rightarrow D^+ \ell \bar{\nu})}{dq^2 d \cos \theta_\ell} = a_\ell(q^2) + b_\ell(q^2) \cos \theta_\ell + c_\ell(q^2) \cos^2 \theta_\ell, \quad (2.15)$$

where  $\theta_\ell$  is the angle between the lepton  $\ell^-$  in the dilepton rest frame and the axis of flight of the  $D$  meson in the  $B$  rest frame, as depicted in Fig. 2.2. The angular coefficients  $a_\ell(q^2)$ ,  $b_\ell(q^2)$  and  $c_\ell(q^2)$  are functions of the effective coefficients  $g_{V,S,T}$ , the form factors and the kinematical variables.

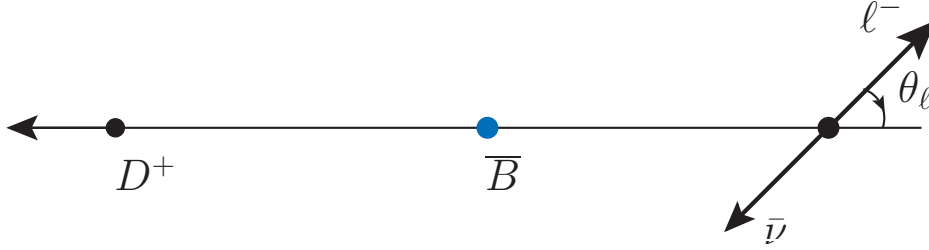


**Figure 2.2:** Angular conventions for the decay  $\bar{B}^0 \rightarrow D^+ \ell^- \bar{\nu}$ .

To compute  $a_\ell(q^2)$ ,  $b_\ell(q^2)$  and  $c_\ell(q^2)$ , it is convenient to use the helicity amplitude formalism. The idea is to decompose the decay as  $B(p) \rightarrow D(k) V^*(q)$ , where  $V^*$  is a virtual gauge boson with four-momentum  $q = p - k$ . This decomposition allows us to factorize the hadronic and leptonic tensors, simplifying the computation and providing more compact formulas for the decay rates. We define the helicity vectors of the virtual gauge boson  $V$  as,

$$\begin{aligned} \varepsilon_V^\mu(\pm) &= \frac{1}{\sqrt{2}}(0, \pm 1, i, 0), \\ \varepsilon_V^\mu(0) &= \frac{1}{\sqrt{q^2}}(q_z, 0, 0, q_0), \\ \varepsilon_V^\mu(t) &= \frac{1}{\sqrt{q^2}}(q_0, 0, 0, q_z), \end{aligned} \quad (2.16)$$

where  $q^\mu = (q_0, 0, 0, q_z)$  and

$$q_0 = \frac{m_B^2 - m_D^2 + q^2}{2m_B}, \quad q_z = \frac{\lambda^{1/2}(m_B, m_D, \sqrt{q^2})}{2m_B}. \quad (2.17)$$

The helicity vectors are orthonormal and satisfy the completeness relation

$$\sum_{n, n'} \varepsilon_V^{*\mu}(n) \varepsilon_V^\nu(n') g_{nn'} = g^{\mu\nu}, \quad (2.18)$$

where  $n, n' \in \{0, t, \pm\}$ , and  $g_{nn'} = \text{diag}(1, -1, -1, -1)$ . To define the helicity amplitudes, we decompose the Hamiltonian (2.3) as

$$\mathcal{H}_{\text{eff}} = \frac{G_F}{\sqrt{2}} V_{cb} \left( H_\mu L^\mu + H_{\mu\nu}^T L^{T\mu\nu} \right) + \text{h.c.}, \quad (2.19)$$

where the leptonic tensors are defined by

$$L^\mu = \bar{\ell} \gamma^\mu (1 - \gamma_5) \nu, \quad L^{T\mu\nu} = \bar{\ell} \sigma^{\mu\nu} (1 - \gamma_5) \nu. \quad (2.20)$$

The NP coefficients are incorporated in the hadronic tensors via the relations

$$\begin{aligned} H_\mu &= (1 + g_V) [\bar{c} \gamma_\mu b] + i \frac{g_S}{m_\ell} \partial_\mu [\bar{c} b], \\ H_{\mu\nu}^T &= g_T [\bar{c} \sigma_{\mu\nu} (1 - \gamma_5) b], \end{aligned} \quad (2.21)$$

where we used the Dirac equation to recast the scalar contribution as a derivative,  $\bar{\ell} P_L \nu = -i \partial^\mu [\bar{\ell} \gamma_\mu P_L \nu] / m_\ell$ , which is transferred to the hadronic current after integrating by parts. The helicity amplitudes are then defined by

$$\begin{aligned} h_m(q^2) &= \varepsilon_V^{\mu*}(m) \langle D | H_\mu | \bar{B} \rangle, \\ h_{mn}(q^2) &= \varepsilon_V^{\mu*}(m) \varepsilon_V^\nu(n) \langle D | H_{\mu\nu}^T | \bar{B} \rangle, \end{aligned} \quad (2.22)$$

where  $m, n \in \{0, t, \pm\}$ . By using Eq. (2.116), one can express the total amplitude in terms of the helicity amplitudes, namely,

$$\begin{aligned} \mathcal{M}(\bar{B} \rightarrow D \ell \bar{\nu}) &= -i \frac{G_F}{\sqrt{2}} V_{cb} \left[ \langle D | H_\mu | \bar{B} \rangle L^\mu + \langle D | H_{\mu\nu}^T | \bar{B} \rangle L^{T\mu\nu} \right] \\ &= -i \frac{G_F}{\sqrt{2}} V_{cb} \left[ \sum_m h_m(q^2) g_{mm} \varepsilon_V^\mu(m) L_\mu + \sum_{m,n} h_{m,n}(q^2) g_{mm} g_{nn} \varepsilon_V^\mu(m) \varepsilon_V^{\nu*}(n) L_{\mu\nu}^T \right], \end{aligned} \quad (2.23)$$

from which it is straightforward to compute the differential decay rate by contracting the leptonic traces with the polarization vectors in the dilepton rest frame ( $q_z = 0$ ). For completeness, we also give the expression of the three-body phase space,

$$\frac{d\mathcal{B}(\bar{B} \rightarrow D \ell \bar{\nu})}{dq^2 d \cos \theta_\ell} = \frac{\lambda_B^{1/2} \lambda_\ell^{1/2}}{512 \pi^3 m_B^3 q^2} \sum_\sigma \left| \mathcal{M}(\bar{B} \rightarrow D \ell \bar{\nu}) \right|^2, \quad (2.24)$$

where we sum over lepton spins. The kinematic functions are defined by  $\lambda_B = \lambda(m_B, m_D, \sqrt{q^2})$  and  $\lambda_\ell = \lambda(\sqrt{q^2}, m_\ell, 0)$ , with  $\lambda(a, b, c) \equiv (a^2 - (b - c)^2)(a^2 - (b + c)^2)$ .

For the Hamiltonian we consider [Eq. (2.3)], the only non-vanishing helicity amplitudes are given by

$$\begin{aligned} h_0(q^2) &= (1 + g_V) f_+(q^2) \frac{\lambda_B^{1/2}}{\sqrt{q^2}}, \\ h_t(q^2) &= \left( 1 + g_V + g_S \frac{q^2}{m_\ell(m_b - m_c)} \right) f_0(q^2) \frac{m_B^2 - m_D^2}{\sqrt{q^2}}, \\ h_{0t}(q^2) &= i g_T f_T(q^2) \frac{\sqrt{\lambda_B}}{m_B + m_D}. \end{aligned} \quad (2.25)$$

By using the approach described above, we obtained for the angular coefficients <sup>3</sup>

$$\begin{aligned}
 a_\ell(q^2) &= \frac{3}{4} \mathcal{B}_0 \lambda_B^{1/2} q^2 \left(1 - \frac{m_\ell^2}{q^2}\right)^2 \left[ |h_0(q^2)|^2 + \frac{m_\ell^2}{q^2} |h_t(q^2)|^2 + \frac{4m_\ell^2}{q^2} |h_{0t}(q^2)|^2 + \frac{4m_\ell}{\sqrt{q^2}} \text{Im} \left( h_{0t}(q^2) h_0^*(q^2) \right) \right], \\
 b_\ell(q^2) &= \frac{3}{2} \mathcal{B}_0 \lambda_B^{1/2} q^2 \left(1 - \frac{m_\ell^2}{q^2}\right)^2 \left[ \frac{m_\ell^2}{q^2} \text{Re} \left( h_0(q^2) h_t(q^2)^* \right) + \frac{2m_\ell}{\sqrt{q^2}} \text{Im} \left( h_{0t}(q^2) h_t^*(q^2) \right) \right], \\
 c_\ell(q^2) &= \frac{3}{4} \mathcal{B}_0 \lambda_B^{1/2} q^2 \left(1 - \frac{m_\ell^2}{q^2}\right)^3 \left[ 4|h_{0t}(q^2)|^2 - |h_0(q^2)|^2 \right],
 \end{aligned} \tag{2.26}$$

where the constant  $\mathcal{B}_0$  is defined by

$$\mathcal{B}_0 = \frac{\tau_B G_F^2 |V_{cb}|^2}{192 \pi^3 m_B^3}. \tag{2.27}$$

In the following, we will present the observables that can be constructed from the angular distributions given above.

### $P \rightarrow P' \ell \nu$ observables

Since there are three independent angular coefficients in Eq. (2.15), one can construct at most three independent angular observables. The most important observable is the total branching ratio, which is given by

$$\begin{aligned}
 \mathcal{B}_{\text{tot}} \equiv \mathcal{B}(B \rightarrow D \ell \nu) &= \int_{m_\ell^2}^{(m_B - m_D)^2} dq^2 \int_{-1}^1 d \cos \theta \frac{d^2 \mathcal{B}(B \rightarrow D \ell \nu)}{dq^2 d \cos \theta} \\
 &= 2 \left[ a(q^2) + \frac{1}{3} c(q^2) \right].
 \end{aligned} \tag{2.28}$$

This expression can be more compactly written in terms of the effective coefficients as

$$\begin{aligned}
 \frac{d\mathcal{B}}{dq^2}(B \rightarrow D \ell \nu) &= \mathcal{B}_0 |f_+(q^2)|^2 \left\{ \left| 1 + g_V |^2 c_+^\ell(q^2) + |g_T(\mu)|^2 c_T^\ell(q^2) \right| \left| \frac{f_T(q^2)}{f_+(q^2)} \right|^2 \right. \\
 &\quad \left. + c_{TV}^\ell(q^2) \text{Re} \left[ (1 + g_V) g_T^*(\mu) \right] \frac{f_T(q^2, \mu)}{f_+(q^2)} \right. \\
 &\quad \left. + c_0^\ell(q^2) \left| 1 + g_V + g_S(\mu) \frac{q^2}{m_\ell(m_b - m_c)} \right|^2 \left| \frac{f_0(q^2)}{f_+(q^2)} \right|^2 \right\},
 \end{aligned} \tag{2.29}$$

where the phase-space functions  $c_i^\ell(q^2)$  are given by

$$c_+^\ell(q^2) = \lambda_B^{3/2} \left[ 1 - \frac{3}{2} \frac{m_\ell^2}{q^2} + \frac{1}{2} \left( \frac{m_\ell^2}{q^2} \right)^3 \right], \tag{2.30}$$

$$c_0^\ell(q^2) = m_\ell^2 \lambda_B^{1/2} \frac{3}{2} \frac{m_B^4}{q^2} \left( 1 - \frac{m_\ell^2}{q^2} \right)^2 \left( 1 - \frac{m_D^2}{m_B^2} \right)^2, \tag{2.31}$$

<sup>3</sup>We have checked that our results agree with the ones given in Ref. [87, 88].

$$c_T^\ell(q^2) = \lambda^{3/2}(m_B, m_D, \sqrt{q^2}) \frac{2q^2}{(m_B + m_D)^2} \left[ 1 - 3 \left( \frac{m_\ell^2}{q^2} \right)^2 + 2 \left( \frac{m_\ell^2}{q^2} \right)^3 \right], \quad (2.32)$$

$$c_{TV}^\ell(q^2) = \frac{6m_\ell}{m_B + m_D} \lambda^{3/2}(m_B, m_D, \sqrt{q^2}) \left( 1 - \frac{m_\ell^2}{q^2} \right)^2. \quad (2.33)$$

A second observable commonly encountered in the literature is the forward-backward asymmetry, which is defined as

$$A_{\text{fb}}^\ell(q^2) = \frac{1}{\mathcal{B}_{\text{tot}}} \left[ \int_0^1 d \cos \theta \frac{d^2 \mathcal{B}(B \rightarrow D \ell \nu)}{dq^2 d \cos \theta} - \int_{-1}^0 d \cos \theta \frac{d^2 \mathcal{B}(B \rightarrow D \ell \nu)}{dq^2 d \cos \theta} \right] = \frac{b(q^2)}{\mathcal{B}_{\text{tot}}}. \quad (2.34)$$

This expression can be recast in terms of the effective coefficients in Eq. (2.3) as

$$\begin{aligned} A_{\text{fb}}^\ell(q^2) = & \frac{1}{\mathcal{B}_{\text{tot}}} \mathcal{B}_0 \lambda_B \left( 1 - \frac{m_\ell^2}{q^2} \right) \left\{ \frac{3}{2} |1 + g_V|^2 \frac{m_\ell^2 (m_B^2 - m_D^2)}{q^2} f_+(q^2) f_0(q^2) \right. \\ & + \frac{3}{2} \text{Re}[(1 + g_V) g_S^*] \frac{m_\ell (m_B^2 - m_D^2)}{m_b - m_c} + 3 \text{Re}[(1 + g_V) g_T^*] m_\ell (m_B - m_D) f_T(q^2) f_0(q^2) \\ & \left. + 3 \text{Re}[g_S g_T^*] q^2 \frac{m_B - m_D}{m_b - m_c} f_T(q^2) f_0(q^2) \right\}. \end{aligned} \quad (2.35)$$

Notice that the only contribution which is not helicity suppressed is the one proportional to  $\text{Re}[g_S g_T^*]$ . This contribution can be generated in several leptoquark scenarios, which will be discussed in Chapter 4. Finally, a third independent angular observable can be defined by taking another independent combination of the angular coefficients.

In addition to the angular observables, one can also employ the polarization of the charged lepton to construct a fourth experimentally accessible quantity. If we decompose the differential branching ratio as

$$\frac{d\mathcal{B}(B \rightarrow D \ell \nu)}{dq^2} = \frac{d\mathcal{B}_+(B \rightarrow D \ell \nu)}{dq^2} + \frac{d\mathcal{B}_-(B \rightarrow D \ell \nu)}{dq^2}, \quad (2.36)$$

where the subscripts  $\pm$  denote the polarizations of the charged lepton, then the lepton polarization asymmetry can be defined as

$$P_\ell(q^2) = \frac{1}{\mathcal{B}_{\text{tot}}} \left[ \frac{d\mathcal{B}_+(B \rightarrow D \ell \nu)}{dq^2} - \frac{d\mathcal{B}_-(B \rightarrow D \ell \nu)}{dq^2} \right]. \quad (2.37)$$

To compute these observables, we define the projectors  $P_\pm = (1 \pm \gamma_5 \not{s})/2$ , where the projection is made along the lepton polarization vector,

$$s = \left( \frac{|\vec{p}_\ell|}{m_\ell}, \frac{E_\ell}{m_\ell} \frac{\vec{p}_\ell}{|\vec{p}_\ell|} \right), \quad (2.38)$$

which satisfies  $s \cdot s = -1$  and  $s \cdot p_\ell = 0$ . By using these definitions, one can perform a similar computation as the one described above with a small difference in the leptonic traces due to the projectors, namely,

$$u_\ell(p) \bar{u}(p) = \frac{1}{2} (\not{p} + m) (1 \pm \gamma_5 \not{s}). \quad (2.39)$$

By using these definitions, we obtained

$$\begin{aligned}\frac{d\mathcal{B}_+}{dq^2} &= \mathcal{B}_0 \lambda_B^{1/2} q^2 \left(1 - \frac{m_\ell^2}{q^2}\right)^2 \left[ \frac{m_\ell^2}{2q^2} (|h_0(q^2)|^2 + 3|h_t(q^2)|^2) + 2|h_{0t}(q^2)|^2 + \frac{2m_\ell}{\sqrt{q^2}} \text{Im}(h_{0t}(q^2)h_0^*(q^2)) \right], \\ \frac{d\mathcal{B}_-}{dq^2} &= \mathcal{B}_0 \lambda_B^{1/2} q^2 \left(1 - \frac{m_\ell^2}{q^2}\right)^2 \left[ |h_0(q^2)|^2 + \frac{4m_\ell^2}{q^2} |h_{0t}(q^2)|^2 + \frac{4m_\ell}{\sqrt{q^2}} \text{Im}(h_{0t}(q^2)h_0^*(q^2)) \right].\end{aligned}\quad (2.40)$$

These expressions reproduced  $d\Gamma/dq^2 = d\Gamma_+/dq^2 + d\Gamma_-/dq^2$ , as expected, and give the following result for the lepton polarization asymmetry,

$$\begin{aligned}P_\ell(q^2) &= \frac{1}{\mathcal{B}_{\text{tot}}} \mathcal{B}_0 \lambda_B^{1/2} q^2 \left(1 - \frac{m_\ell^2}{q^2}\right)^2 \left[ \left(-1 + \frac{m_\ell^2}{2q^2}\right) |h_0(q^2)|^2 + \frac{3m_\ell^2}{2q^2} |h_t(q^2)|^2 \right. \\ &\quad \left. + 2 \left(1 - \frac{2m_\ell^2}{q^2}\right) |h_{0t}(q^2)|^2 - \frac{2m_\ell}{\sqrt{q^2}} \text{Im}(h_{0t}(q^2)h_0^*(q^2)) \right].\end{aligned}\quad (2.41)$$

Similarly to the observables discussed above, one can use Eq. (2.25) to rewrite this expression directly in terms of the NP couplings,

$$\begin{aligned}P_\ell(q^2) &= \frac{1}{\mathcal{B}_{\text{tot}}} \frac{1}{2} \mathcal{B}_0 \left\{ \left| 1 + g_V + g_S(\mu) \frac{q^2}{m_\ell(m_b - m_c)} \right|^2 \frac{3m_\ell^2}{q^4} (m_B^2 - m_D^2)^2 |f_0(q^2)|^2 \right. \\ &\quad + |1 + g_V|^2 \frac{\lambda_B}{q^2} \left(-2 + \frac{m_\ell^2}{q^2}\right) |f_+(q^2)|^2 + |g_T|^2 \frac{4\lambda_B}{(m_B + m_D)^2} \left(1 - \frac{2m_\ell^2}{q^2}\right) |f_T(q^2)|^2 \\ &\quad \left. - \text{Re}[(1 + g_V)g_T^*] \frac{4m_\ell \lambda_B}{q^2(m_B + m_D)} f_+(q^2) f_T(q^2) \right\}.\end{aligned}\quad (2.42)$$

In Sec. 2.2.4, we will confront the expressions presented above with current data and give predictions for the observables which are still to be studied experimentally.

### 2.2.3 Brief discussion of $P \rightarrow V$ semileptonic decays

In this section, we briefly comment on the decays  $P \rightarrow V \ell \nu$ , where  $P$  is a pseudoscalar meson ( $J^P = 0^-$ ) and  $V$  is a vector meson ( $J^P = 1^-$ ), such as  $D^*$  or  $J/\psi$ , for example. Even though LQCD computations still have an insufficient control of the hadronic matrix elements entering  $P \rightarrow V$  transitions, we will comment on their parameterization in terms of factors, and most particularly for  $B \rightarrow D^* \ell \nu$ , due to the increasing theoretical activity on this particular decay [87, 89, 90]. Part of this interest is motivated by the LFUV anomalies in  $B \rightarrow D^{(*)} \ell \bar{\nu}$  ( $\ell = e, \mu, \tau$ ), which will be discussed in Sec. 5.3. We stress once again that our formulas are general and can be easily translated to other decays of the type  $P \rightarrow V$ .

The vector/axial hadronic matrix elements for the  $B \rightarrow D^*$  transition can be generically parameterized as

$$\begin{aligned}\langle \bar{D}^*(k, \varepsilon) | \bar{c} \gamma^\mu b | \bar{B}(p) \rangle &= \varepsilon_{\mu\nu\rho\sigma} \varepsilon^{*\nu} p^\rho k^\sigma \frac{2V(q^2)}{m_B + m_{D^*}}, \\ \langle \bar{D}^*(k, \varepsilon) | \bar{c} \gamma^\mu \gamma_5 b | \bar{B}(p) \rangle &= i\varepsilon_\mu^* (m_B + m_{D^*}) A_1(q^2) - i(p+k)_\mu (\varepsilon^* \cdot q) \frac{A_2(q^2)}{m_B + m_{D^*}} \\ &\quad - iq_\mu (\varepsilon^* \cdot q) \frac{2m_{D^*}}{q^2} [A_3(q^2) - A_0(q^2)],\end{aligned}\quad (2.43)$$

where  $V(q^2)$  and  $A_{0-3}(q^2)$  are the relevant form factors and  $\varepsilon^\mu(0, \pm)$  denotes the polarization of the  $D^*$  meson.<sup>4</sup> The form factor  $A_3(q^2)$  is related to the others through the expression

$$A_3(q^2) = \frac{m_B + m_{D^*}}{2m_{D^*}} A_1(q^2) - \frac{m_B - m_{D^*}}{2m_{D^*}} A_2(q^2), \quad (2.44)$$

with  $A_3(0) = A_0(0)$ , which makes sure that the artificial pole at  $q^2$  does not appear. To predict the SM rate of  $B \rightarrow D^* \ell \nu$ , one must compute  $V(q^2)$  and  $A_{0-2}(q^2)$  via non-perturbative methods. It should also be noted that the contribution of the so-called pseudoscalar form factor  $A_0(q^2)$  to  $\mathcal{B}(B \rightarrow D^* \ell \nu)^{\text{SM}}$  is proportional to the charged lepton mass squared, which is why it is negligible for light leptons ( $\ell = e, \mu$ ). The matrix element of the scalar pseudoscalar densities can be obtained from Eq. (2.43) by applying the Ward identities, which give

$$\langle \bar{D}^*(k, \varepsilon) | \bar{c} b | \bar{B}(p) \rangle = 0, \quad (2.45)$$

$$\langle \bar{D}^*(k, \varepsilon) | \bar{c} \gamma_5 b | \bar{B}(p) \rangle = -i(\varepsilon \cdot q) \frac{2m_{D^*}}{m_b + m_c} A_0(q^2). \quad (2.46)$$

For the scalar current, it is easy to see that the matrix element vanishes since  $q = p - k$  and the tensor  $\varepsilon_{\mu\nu\rho\sigma}$  is fully anti-symmetric by definition.

For a scenario of NP contributing via tensor currents, another three form factors are needed to fully describe the hadronic matrix elements. These form factors, named  $T_1(q^2)$ ,  $T_2(q^2)$  and  $T_3(q^2)$ , are defined by

$$\begin{aligned} \langle \bar{D}^*(k, \varepsilon) | \bar{c} \sigma_{\mu\nu} q^\nu b | \bar{B}(p) \rangle &= 2i \varepsilon_{\mu\nu\rho\sigma} \varepsilon^{*\nu} p^\rho k^\sigma T_1(q^2), \\ \langle \bar{D}^*(k, \varepsilon) | \bar{c} \sigma_{\mu\nu} \gamma_5 q^\nu b | \bar{B}(p) \rangle &= [\varepsilon_\mu^* (m_B^2 - m_{D^*}^2) - (\varepsilon^* \cdot q)(2p - q)_\mu] T_2(q^2) \\ &\quad + (\varepsilon^* \cdot q) \left[ q_\mu - \frac{q^2}{m_B^2 - m_{D^*}^2} (p + k)_\mu \right] T_3(q^2). \end{aligned} \quad (2.47)$$

satisfying the relations  $T_1(0) = T_2(0)$  due to the formula that  $\sigma^{\mu\nu} = (i/2) \varepsilon^{\mu\nu\alpha\beta} \sigma_{\alpha\beta}$ . From the expressions given above, it becomes clear that the transitions  $P \rightarrow V$  depend on many more hadronic form factors than the semileptonic  $P \rightarrow P'$  transitions. In the latter case, only two form factors coinciding at  $q^2 = 0$  are needed to predict  $\mathcal{B}(B \rightarrow D \ell \nu)^{\text{SM}}$  and these have been computed by numerical simulations of LQCD. For the transition  $B \rightarrow D^*$ , only a few results concerning the normalization of the form factors have been computed on the lattice [91, 92]. The phenomenological studies of  $B \rightarrow D^* \ell \nu$  then require additional information, which is extracted from experimental data by using Heavy Quark Effective Theory (HQET) [93] or by means of QCD sum rules [94]. However, one should be careful in using HQET in dealing with the charm quark, since the neglected power corrections might be large. Moreover, the heavy quark symmetry fixes the form factors only at the zero-recoil point (up to calculable short distance perturbative corrections). For this reason, the use of  $B \rightarrow D^* \ell \nu$  as a laboratory to probe NP has often been controversial.

## 2.2.4 Phenomenological analysis

In this subsection, we derive constraints on  $g_P$ ,  $g_S$  and  $g_T$  defined in Eq. (2.3) by confronting the expressions derived above with the most recent experimental results for leptonic and

<sup>4</sup>In our convention,  $\varepsilon_{0123} = 1$ .

semileptonic meson decays, cf. Table 2.2. We will focus on the decay modes based on the transitions  $s \rightarrow u\mu\nu$ ,  $c \rightarrow d\mu\nu$ ,  $c \rightarrow s\mu\nu$ ,  $c \rightarrow s\tau\nu$ ,  $b \rightarrow u\tau\nu$  and  $b \rightarrow c\ell\nu$  ( $\ell = \mu, \tau$ ) for which we have a good control of hadronic uncertainties. In particular, we will not discuss the  $B \rightarrow \pi$  and  $B_s \rightarrow K$  semileptonic decays, since the form factors for these transitions are only available in the high  $q^2$  region.

### New Physics scenarios

We consider two different effective scenarios:

- In the first scenario, we assume that NP enters in a single coefficient  $g_{S,P,T}$ , which is generically taken to be a complex number.
- In the second one, we consider specific combinations of effective coefficients which are motivated by different NP scenarios. More precisely, we consider the cases where (i)  $(g_S, g_P) \in \mathbb{R}^2$ , and where (ii)  $g_S = -g_P \in \mathbb{R}$  and  $g_T \in \mathbb{R}$  are kept non-zero.

We do not consider modifications of the vector/axial couplings  $g_{V,A}$  since these are already tightly constrained by studies of the unitarity of the CKM matrix [95]. The case where both  $g_S$  and  $g_P$  are generated is motivated by models with an extended Higgs sector, which will be discussed in Chapter 3. The second choice of operators is motivated by different leptoquark scenarios, as we are going to discuss in Chapter 4, and can be understood by constructing the operators consistent with  $SU(2)_L \times U(1)_Y$  gauge invariance [96]. More precisely, the exchange of a particle transforming under the representation  $(\mathbf{3}, \mathbf{2})_{7/6}$  generates the gauge invariant operator

$$\begin{aligned} O^{(7/6)} &= \varepsilon_{\alpha\beta} (\bar{\ell}_R Q^\alpha) (\bar{u}_R L^\beta) \\ &= (\bar{\ell} P_L u) (\bar{u} P_L \ell) - (\bar{\ell} P_L d) (\bar{u} P_L \nu), \end{aligned} \quad (2.48)$$

where we omitted flavor indices for simplicity. Moreover, the  $SU(2)$  indices  $\alpha, \beta = 1, 2$  are explicitly written and  $\varepsilon_{\alpha\beta}$  denotes the total anti-symmetric tensor with convention  $\varepsilon_{12} = -\varepsilon_{21} = +1$ . By using the Fierz relation for anti-commuting fields, cf. Appendix A.1, we obtain for the second term

$$O^{(7/6)} \supset \frac{1}{2} \left[ (\bar{u} P_L d) (\bar{\ell} P_L \nu) + \frac{1}{4} (\bar{u} \sigma_{\mu\nu} P_L d) (\bar{\ell} \sigma_{\mu\nu} P_L \nu) \right], \quad (2.49)$$

from which one can easily recognize the combination of Wilson coefficients  $g_S = -g_P = g_T/4$  at the scale where the heavy state was integrated-out. Similarly, the exchange of a color triplet transforming as  $(\mathbf{3}, \mathbf{1})_{1/3}$  generates the operator

$$\begin{aligned} O^{(1/3)} &= \varepsilon^{\alpha\beta} (\bar{\ell}_R u_R^C) (\bar{Q}_{L\alpha}^C L_\beta) \\ &= (\bar{\ell} P_L u^C) (\bar{u}^C P_L \ell) - (\bar{\ell} P_L u^C) (\bar{d}^C P_L \nu). \end{aligned} \quad (2.50)$$

We will focus on the second term, which can be rearranged via the Fierz identity

$$\begin{aligned} O^{(1/3)} &\supset \frac{1}{2} \left[ (\bar{d}^C P_L u^C) (\bar{\ell} P_L \nu) + \frac{1}{4} (\bar{d}^C \sigma_{\mu\nu} P_L u^C) (\bar{\ell} \sigma_{\mu\nu} P_L \nu) \right] \\ &= \frac{1}{2} \left[ (\bar{u} P_L d) (\bar{\ell} P_L \nu) - \frac{1}{4} (\bar{u} \sigma_{\mu\nu} P_L d) (\bar{\ell} \sigma_{\mu\nu} P_L \nu) \right], \end{aligned} \quad (2.51)$$

where we can recognize the combination  $g_S = -g_P = g_T/4$ . The sign difference with respect to the previous scenario comes from the fermion conjugation, namely  $\bar{\psi}^C P_L \phi^C = \bar{\phi} P_L \psi$  and  $\bar{\psi}^C \sigma_{\mu\nu} P_L \phi^C = -\bar{\phi} \sigma_{\mu\nu} P_L \psi$ , where  $\psi \equiv \psi(x)$  and  $\phi \equiv \phi(x)$  stand for generic fermion fields.

## Experimental inputs

The experimental averages considered in our analysis are shown in Table 2.2, where we considered the results from PDG [22], unless stated otherwise. Note that we have also considered the ratio  $R_D$ , defined in Eq. 2.2, which appears to be  $\approx 2\sigma$  lower than the SM predictions. In particular, we will investigate some of the implications of this result which can be deduced by using a model independent approach.<sup>5</sup> To avoid an inconsistency in our approach due to the fact most of these decays are used to extract the moduli of CKM elements which are also theoretical inputs in our analysis, we conservatively vary the CKM parameters within the  $3\sigma$  ranges determined in Ref. [65,95]. We have checked that increasing this interval would not change significantly the constraints on the effective coefficients, which are therefore very robust. Furthermore, we include the decay modes with electrons in the fit, even though we disregard the NP couplings to electrons, so that these modes only help fixing the CKM matrix elements.

	Exp. average	Refs.
$\mathcal{B}(K^+ \rightarrow \mu^+ \nu)$	$2.488(9) \times 10^{-5}$	[22]
$\mathcal{B}(K^+ \rightarrow \pi^0 e^+ \nu)$	0.0494(5)	[22]
$\mathcal{B}(K_L \rightarrow \pi^- e^+ \nu)$	0.4047(28)	[22]
$\mathcal{B}(K^+ \rightarrow \pi^0 \mu^+ \nu)$	0.0324(4)	[22]
$\mathcal{B}(K_L \rightarrow \pi^- \mu^+ \nu)$	0.2700(8)	[22]
$\mathcal{B}(D \rightarrow \mu^+ \nu)$	3.74(17)	[97]
$\mathcal{B}(D_s \rightarrow \mu^+ \nu)$	$5.49(23) \times 10^{-3}$	[98–101]
$\mathcal{B}(D_s \rightarrow \tau^+ \nu)$	$5.51(25) \times 10^{-2}$	[98–103]
$\mathcal{B}(D^+ \rightarrow \bar{K}^0 e^+ \nu)$	$8.72(17) \times 10^{-2}$	[104, 105]
$\mathcal{B}(D^0 \rightarrow K^- e^+ \nu)$	$3.50(3) \times 10^{-2}$	[105–107]
$\mathcal{B}(D^+ \rightarrow \bar{K}^0 \mu^+ \nu)$	$8.72(19) \times 10^{-2}$	[108]
$\mathcal{B}(D^0 \rightarrow K^- \mu^+ \nu)$	$3.45(23) \times 10^{-2}$	[107]
$\mathcal{B}(B \rightarrow \tau \nu)$	$1.43(33) \times 10^{-4}$	[109, 110]
$\mathcal{B}(B \rightarrow D \mu \nu)$	$2.20(15) \times 10^{-2}$	[111, 112]
$R_D$	0.41(5)	[71, 73]

**Table 2.2:** Average of experimental results considered in our phenomenological analysis.

In the following, we will highlight some of the results from our fit. The results obtained by the one-dimensional fit of each coefficient will be summarized in Table 2.3 and 2.4.

<sup>5</sup>A full discussion of this observable as long as other lepton flavor universality tests will be made in Chapter 5.

## Fit results and predictions

We will now present our results for the NP fits to the different transitions. As mentioned above, we will only highlight the main results from our analysis. The full list of constraints for real and complex Wilson coefficients is given in Table 2.3 and 2.4. Furthermore, our notation will be such that  $(g_{S,P,T}^\ell)_{q_u q_d}$  denote the Wilson coefficients associated to the transition  $q_u \rightarrow q_d \ell \nu$ .

The constraints obtained from the kaon physics observables,  $\mathcal{B}(K \rightarrow \mu \nu)$  and  $\mathcal{B}(K \rightarrow \pi \mu \nu)$ , are shown in Fig. 2.3 at the scale  $\mu = 2$  GeV. From this plot, we see that the strongest constraint comes from the kaon leptonic decay, which sets limits on  $g_P$ . This can be understood by the helicity suppression which is lifted by this operator. The scalar and tensor coefficients are only constrained by the semileptonic decay modes, which allow for larger values of  $g_{S,T}$ . Notice, also, that these observables are consistent with the SM predictions to  $1\sigma$  accuracy. A similar result is obtained for the coefficients  $(g_i^\mu)_{cs}$ , with  $i = S, P, T$ , as shown in Fig. 2.4 at the scale  $\mu = 2$  GeV. These coefficients are constrained by the decay modes  $D_s \rightarrow \mu \nu$  and  $D \rightarrow K \mu \nu$ , which also have decay rates consistent with the SM predictions. Finally, we perform a fit to  $R_D$  by assuming that NP only contributes to the transition  $b \rightarrow c \tau \nu$ , i.e. we assume that the operators with muons have vanishing NP Wilson coefficients. In this case, the coefficient  $g_P$  is unconstrained because the corresponding leptonic decay mode,  $\mathcal{B}(B_c \rightarrow \tau \nu)$ , has not been studied experimentally yet. The results from our fit to the coefficients  $(g_S^\tau)_{cb}$  and  $(g_T^\tau)_{cb}$  is shown in Fig. 2.5 at the scale  $\mu = m_b$ . Note that the SM point  $(g_S, g_T) = (0, 0)$  is at the border of the  $2\sigma$  region due to the current disagreement between the SM prediction and  $R_D^{\text{exp}}$ . To study the implications of this deviation, we also show in the same plot the curves corresponding to the combination of Wilson coefficients

$$(g_S^\tau)_{cb} = - (g_P^\tau)_{cb} = \pm \frac{(g_T^\tau)_{cb}}{4}, \quad (2.52)$$

assumed to be valid at the scale  $\mu = 1$  TeV, which can appear in different scenarios with leptoquark bosons, as discussed above. To draw these curves, we considered the QCD running effect of the scalar and tensor density, which amount to  $g_T(\mu = 1 \text{ TeV}) \approx 1.3 \times g_T(\mu = m_b)$  and  $g_S(\mu = 1 \text{ TeV}) \approx 0.5 \times g_S(\mu = m_b)$ . The intersection between the red lines and the allowed region in Fig. 2.5 can now be used to predict the implications of  $R_D$  for other observables based on the same transition. We consider the ratio

$$R_{\eta_c} = \frac{\mathcal{B}(B_c \rightarrow \eta_c \tau \nu)}{\mathcal{B}(B_c \rightarrow \eta_c l \nu)} \quad (2.53)$$

where  $l = e, \mu$  are averaged in the denominator. This observable is particularly interesting since the relevant form factors have been recently computed in Ref. [86], offering a clean observable to test the discrepancy in  $R_D$ . This is shown in Fig. 2.6, where we see that the excess in  $R_D$  implies an enhancement of  $R_{\eta_c}/R_{\eta_c}^{\text{SM}}$  which can be as large as 50% in both scenarios, being possibly within reach at LHCb. This strategy can also be employed to other decays based on the same transition, such as  $B_c \rightarrow \eta_c \tau \nu$  or baryon decays. Finally, we have also checked that a similar enhancement can be found in scenarios where only  $g_S$  or  $g_T$  are assumed to be nonzero.

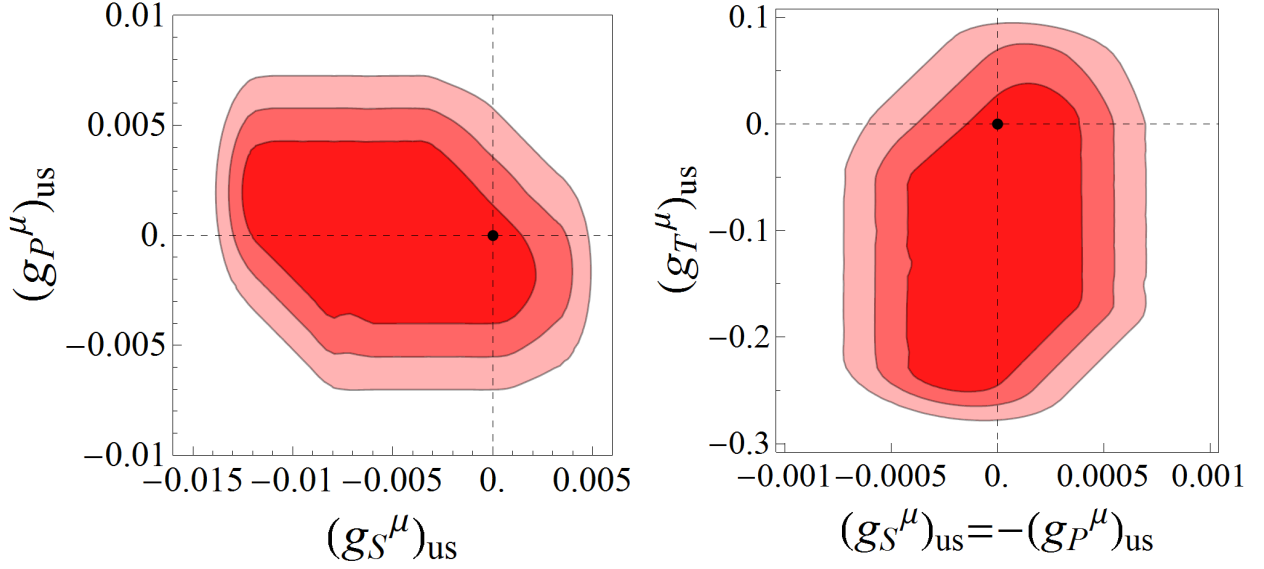


**Figure 2.3:** Regions of allowed values shown in the planes  $(g_S^\mu)_{us}$  vs  $(g_P^\mu)_{us}$  (left panel), and  $(g_S^\mu)_{us} = -(g_P^\mu)_{us}$  vs  $(g_T^\mu)_{us}$  at the scale  $\mu = 2$  GeV, compatible with experimentally measured kaon leptonic and semileptonic decays, cf. Table 2.2. The allowed regions are shown to 1, 2, 3 $\sigma$  accuracy (from dark red to light red). The black dot corresponds to the SM.

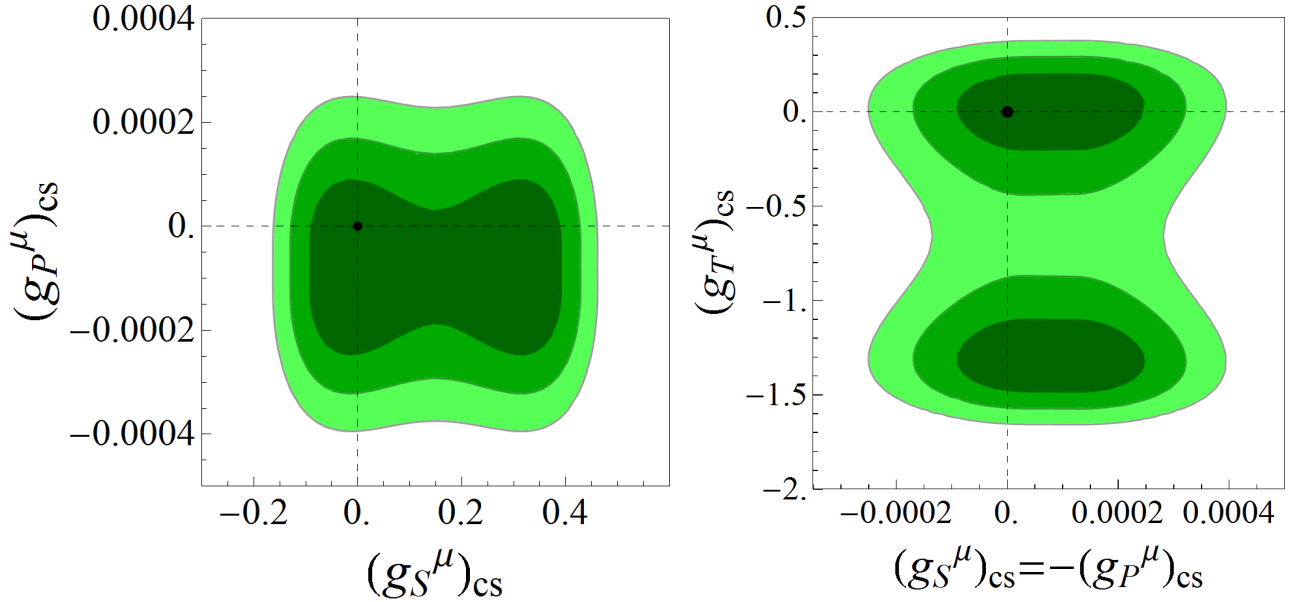


**Figure 2.4:** Regions of allowed values shown in the planes  $(g_S^\mu)_{cs}$  vs  $(g_P^\mu)_{cs}$  (left panel), and  $(g_S^\mu)_{cs} = -(g_P^\mu)_{cs}$  vs  $(g_T^\mu)_{cs}$  at the scale  $\mu = 2$  GeV, compatible with experimentally measured  $D$ -meson leptonic and semileptonic decays, cf. Table 2.2. The allowed regions are shown to 1, 2, 3 $\sigma$  accuracy (from dark green to light green). The black dot corresponds to the SM.

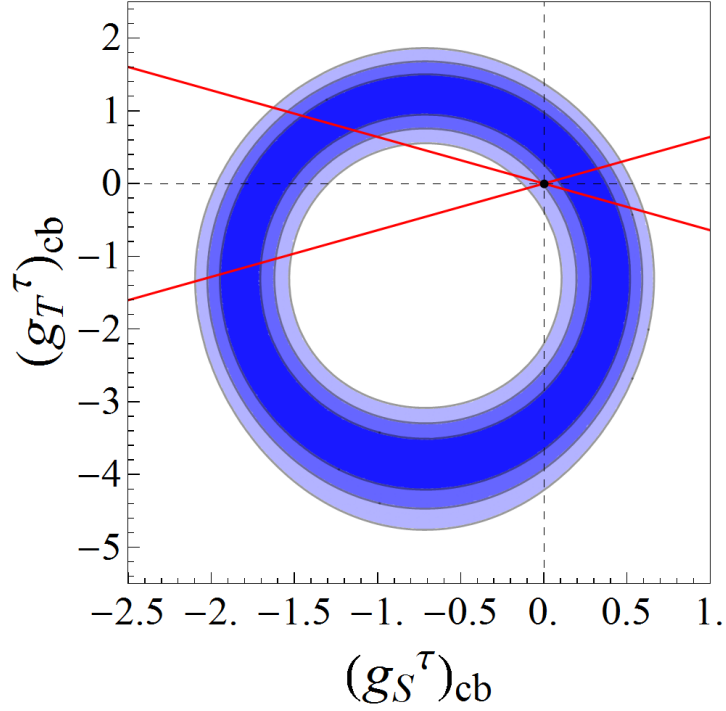


**Figure 2.5:** Regions of allowed values shown in the plane  $(g_S^\tau)_{cb}$  vs  $(g_T^\tau)_{cb}$  at the scale  $\mu = m_b$ , compatible with experimentally measured  $R_D$ , cf. Table 2.2. The allowed regions are shown to 1, 2, 3 $\sigma$  accuracy (from dark blue to light blue). The black dot corresponds to the SM. We show in the same plot the curves corresponding to the NP scenarios in which  $g_S(\mu) = -g_P(\mu) = \pm g_T(\mu)/4$  at the scale  $\mu = 1$  TeV, see text for details.

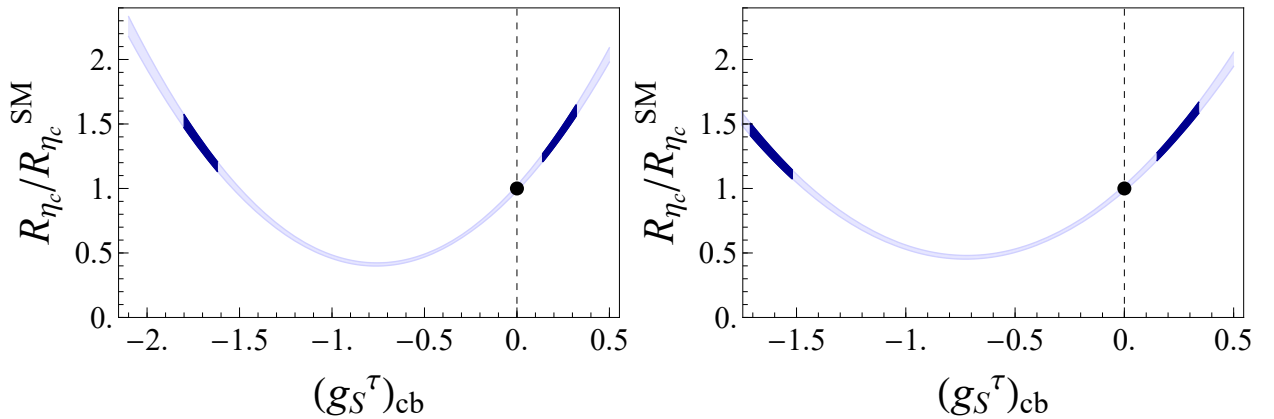


**Figure 2.6:** Predictions for  $R_{\eta_c}/R_{\eta_c}^{\text{SM}}$ , cf. Eq. (2.53), as a function of  $(g_S^\tau)_{cb}$  computed at  $\mu = m_b$ . We consider two scenarios in which we impose  $g_S(\mu) = -g_P(\mu) = g_T(\mu)/4$  (left panel) and  $g_S(\mu) = -g_P(\mu) = -g_T(\mu)/4$  (right panel) at the scale  $\mu = 1$  TeV. The dark blue regions are consistent with  $R_D^{\text{exp}}$  to 1 $\sigma$  accuracy, as shown in Fig. 2.5

$q_u q_d \ell \nu$	$\text{Re} [(g_P^\ell)_{quqd}]$	$\text{Re} [(g_S^\ell)_{quqd}]$	$\text{Re} [(g_T^\ell)_{quqd}]$
$us\mu\nu$	$(-5.0, 5.0) \times 10^{-4} \cup (8.4, 8.5) \times 10^{-2}$	$(-1.3, 0.3) \times 10^{-2} \cup (-2.9, -2.7) \times 10^{-1}$	$(-2.6, 0.6) \times 10^{-1}$
$cd\mu\nu$	$(-0.6, 3.6) \times 10^{-3} \cup (7.3, 7.8) \times 10^{-2}$	—	—
$cs\mu\nu$	$(-2.8, 1.3) \times 10^{-3} \cup (7.4, 7.7) \times 10^{-2}$	$(-1.1, 4.1) \times 10^{-1} \cup (-2.8, -2.7) \times 10^{-1}$	$(-1.5, -1.0) \cup (-3.0, 2.5) \times 10^{-1}$
$cs\tau\nu$	$(-5.5, 1.1) \times 10^{-2} \cup (1.24, 1.31)$	—	—
$ub\tau\nu$	$(-2.2, 0.4) \times 10^{-1} \cup (5.0, 7.5) \times 10^{-1}$	—	—
$cb\mu\nu$	—	$(-5.6, 4.3) \times 10^{-1}$	$(-1.6, 1.1)$
$cb\tau\nu$	—	$(0.4, 4.2) \times 10^{-1} \cup (-1.8, 1.5)$	$(0.1, 1.1) \times 10^{-1} \cup (-3.8, -2.7)$

**Table 2.3:** Constraints on the couplings  $(g_{P,S,T}^\ell)_{quqd}$  derived from leptonic and semileptonic decays to  $2\sigma$  accuracy, c.f Table 2.2. We assumed the NP couplings to be real in this Table. Moreover, the limits on  $(g_S)$  and  $(g_T)$  were derived at the scale where the form factors were computed, namely,  $\mu = 2$  GeV for the transitions  $K \rightarrow \pi$  and  $D \rightarrow K$ , and  $\mu = m_b$  for  $B \rightarrow D$ .

$q_u q_d \ell \nu$	$\text{Im} [(g_P^\ell)_{quqd}]$	$\text{Im} [(g_S^\ell)_{quqd}]$	$\text{Im} [(g_T^\ell)_{quqd}]$
$us\mu\nu$	$(-6.3, 6.3) \times 10^{-3}$	$(-3.0, 3.0) \times 10^{-2}$	$(-4.1, 4.1) \times 10^{-1}$
$cd\mu\nu$	$(-8.3, 8.3) \times 10^{-3}$	—	—
$cs\mu\nu$	$(-1.5, 1.5) \times 10^{-2}$	$(-2.1, 2.1) \times 10^{-1}$	$(-6.1, 6.1) \times 10^{-1}$
$cs\tau\nu$	$(-2.7, 2.7) \times 10^{-1}$	—	—
$ub\tau\nu$	$(-4.1, 4.1) \times 10^{-1}$	—	—
$cb\mu\nu$	—	$(-5.0, 5.0) \times 10^{-1}$	$(-1.3, 1.3)$
$cb\tau\nu$	—	$(-8.8, -2.6) \times 10^{-1} \cup (2.6, 8.8) \times 10^{-1}$	$(-2.0, -0.6) \cup (0.6, 2.0)$

**Table 2.4:** Constraints on the couplings  $(g_{P,S,T}^\ell)_{quqd}$  to  $2\sigma$  by assuming them to be imaginary. See caption of Fig. 2.3 for details.

## 2.3 FCNC processes

Physical processes driven by the flavor changing neutral currents (FCNC) are absent in the SM at tree level. Since they only occur through loops, their measurements offer a low energy window to the heavy particles (top quark or particles beyond the SM). In other words, they do not only represent a fine test of validity of the SM, but they also offer an opportunity to look for the effects of physics beyond the SM at low energies.

Historically, the study of FCNC processes has played a major role in the understanding of both the SM and NP. A first example was the prediction of the charm quark to explain the suppression of  $\mathcal{B}(K_L \rightarrow \mu^+ \mu^-)$  and of the  $K^0 - \bar{K}^0$  amplitude via the GIM mechanism [68] years before the discovery of  $J/\Psi$  at Brookhaven and SLAC [113, 114]. Another remarkable example was the first observation of  $B^0 - \bar{B}^0$  mixing, which gave the first indication that the top quark is much heavier than any other SM fermion [3]. In what concerns physics beyond the SM, the FCNC processes provide very useful tools to constraint the contributions from NP particles. An example comes from the  $K^0 - \bar{K}^0$  mixing parameter  $\varepsilon_K$ , which sets an lower bound on the scale of NP to  $10^8$  GeV if one assumes  $\mathcal{O}(1)$  NP couplings [6]. From this limit, we learn the general message that if NP emerges at the TeV scale, as suggested by the hierarchy problem, then its couplings should have a non-trivial flavor structure. A well-known solution to this paradox goes under the name of Minimal Flavor Violation (MFV) [69, 70], where the CKM matrix is identified as the only source of flavor violation, which can then lower the bound from FCNC processes to the TeV range too, as discussed in Sec. 1.2.

A considerable attention has been devoted in the past few years to the transition  $b \rightarrow s\ell^+\ell^-$ , which will be the focus of this Section. This interest comes mainly from the increasing experimental effort at the  $B$ -physics experiments at LHCb and at the  $B$ -factories, which allowed to measure several of these decays with a great precision. While the inclusive and exclusive processes based on the penguin-induced  $b \rightarrow s\gamma$  decay have been, and still are, a very significant constraint to the NP model building, the processes based on  $b \rightarrow s\ell^+\ell^-$  allow us to access other types of contributions. For instance, the process  $\mathcal{B}(B_s \rightarrow \mu^+\mu^-)$  was measured by the first time at the LHC and the result was found to be in agreement with the theoretical predictions [115], providing very useful constraints on physics beyond the SM. Moreover, several observables showed a consistent pattern of discrepancies with respect to the SM predictions. For instance, the spectrum of  $\mathcal{B}(B \rightarrow K\mu^+\mu^-)$  has been measured [116] and in the range of large  $q^2$ 's it appears to be smaller than predicted [117, 118]. A full angular analyses of  $\mathcal{B}(B \rightarrow K^*\mu^+\mu^-)$  [116, 119] and  $\mathcal{B}(B_s \rightarrow \phi\mu^+\mu^-)$  [120] revealed deviations in several observables [121], although there are several controversies about the reliability of some of the SM predictions [122]. Finally and most importantly, the measurement of  $R_K = \mathcal{B}(B \rightarrow K\mu^+\mu^-)/\mathcal{B}(B \rightarrow Ke^+e^-)$  [11] and  $R_{K^*} = \mathcal{B}(B \rightarrow K^*\mu^+\mu^-)/\mathcal{B}(B \rightarrow K^*e^+e^-)$  [12] in different bins of  $q^2$  were shown to be significantly lower than predicted [13]. Those new experimental data helped discarding several NP models and triggered an intense theoretical activity to understand the origin of these discrepancies, as we will discuss in Chapter 5.

The most general effective Hamiltonian describing the  $b \rightarrow s\ell\ell$  transitions, made of dimension six operators, is given by [123]

$$\mathcal{H}_{\text{eff}} = -\frac{4G_F}{\sqrt{2}}V_{tb}V_{ts}^* \sum_i \left( C_i(\mu)\mathcal{O}_i(\mu) + C'_i(\mu)\mathcal{O}'_i(\mu) \right) + \text{h.c.}, \quad (2.54)$$

where we have neglected the small contributions proportional to  $V_{ub}V_{us}^*$ . The operators which are relevant for our discussion are given by

$$\mathcal{O}_7 = \frac{e}{(4\pi)^2} m_b (\bar{s} \sigma_{\mu\nu} P_R b) F^{\mu\nu}, \quad \mathcal{O}_8 = \frac{g_s}{(4\pi)^2} m_b (\bar{s} \sigma_{\mu\nu} P_R b) G^{\mu\nu}, \quad (2.55)$$

$$\mathcal{O}_9 = \frac{e^2}{(4\pi)^2} (\bar{s} \gamma_\mu P_L b) (\bar{\ell} \gamma^\mu \ell), \quad \mathcal{O}_S = \frac{e^2}{(4\pi)^2} (\bar{s} \gamma_\mu P_L b) (\bar{\ell} \gamma^\mu \gamma_5 \ell), \quad (2.56)$$

$$\mathcal{O}_{10} = \frac{e^2}{(4\pi)^2} (\bar{s} P_R b) (\bar{\ell} \ell), \quad \mathcal{O}_P = \frac{e^2}{(4\pi)^2} (\bar{s} P_R b) (\bar{\ell} \gamma_5 \ell), \quad (2.57)$$

$$\mathcal{O}_T = \frac{e^2}{(4\pi)^2} (\bar{s} \sigma_{\mu\nu} b) (\bar{\ell} \sigma^{\mu\nu} \ell), \quad \mathcal{O}_{T5} = \frac{e^2}{(4\pi)^2} (\bar{s} \sigma_{\mu\nu} b) (\bar{\ell} \sigma^{\mu\nu} \gamma_5 \ell). \quad (2.58)$$

$\mathcal{O}_7$  and  $\mathcal{O}_8$  are the electromagnetic and chromomagnetic penguin operator. Moreover, the operators with a flipped chirality  $\mathcal{O}'$  are obtained from  $\mathcal{O}$  by replacing  $P_L \leftrightarrow P_R$  in the quark current. In addition to those, there are also the charged current operators  $\mathcal{O}_{1,2}$  and the ones associated to QCD penguins  $\mathcal{O}_{3,\dots,6}$ . It is customary to absorb the effect of the latter operators by redefining the Wilson coefficients as [124]

$$C_7^{\text{eff}}(\mu_b) = C_7 - \frac{1}{3}C_3 - \frac{4}{9}C_4 - \frac{20}{3}C_5 - \frac{80}{9}C_6, \quad (2.59)$$

$$C_9^{\text{eff}}(\mu_b) = C_9 + Y(q^2), \quad (2.60)$$

$$C_{10}^{\text{eff}}(\mu_b) = C_{10}, \quad (2.61)$$

while the other Wilson coefficients remain unchanged. The function  $Y(q^2)$  at next-to-leading logarithmic (NLL) accuracy can be found in Ref. [123], and the computation of the next-to-next-to-leading logarithmic (NNLL) corrections to the mixing of  $\mathcal{O}_1$  and  $\mathcal{O}_2$  into  $\mathcal{O}_7$  and  $\mathcal{O}_9$  can be found in Ref. [125]. The values of the SM Wilson coefficients at the scale  $\mu_b = 4.8$  GeV are then given by  $C_7^{\text{eff}}(\mu_b) = -0.304$ ,  $C_9^{\text{eff}}(\mu_b) = 4.211$  and  $C_{10}^{\text{eff}}(\mu_b) = -4.103$  [123–125]. In the presence of NP, the effective coefficients will receive corrections of the form

$$C_i^{\text{eff}} \rightarrow C_i^{\text{eff}} + \delta C_i, \quad (2.62)$$

where  $\delta C_i$  denotes the additional contribution coming from NP. To simplify our notation, we will drop the label “eff” in the Wilson coefficients by writing  $C_i^{\text{eff}} \equiv C_i$ . Furthermore, when discussing the phenomenology of NP models, if confusion can be avoided, we will write  $C_i$  instead of  $\delta C_i$ .

In the following, we will present the generic expression for the branching ratio of the exclusive  $b \rightarrow s \ell \ell$  decays. To simplify our discussion, we will neglect the tensor operators  $\mathcal{O}_{T(5)}$  since they will play no role in the phenomenological discussions of Chapter 3 and 4.<sup>6</sup>

### 2.3.1 $B_s \rightarrow \ell^+ \ell^-$

The decay rate  $\mathcal{B}(B_s \rightarrow \mu^+ \mu^-)$  is one of the most reliable quantities that can be studied theoretically and experimentally at LHCb [115]. The only hadronic quantity entering the  $B_s \rightarrow \mu^+ \mu^-$  decay amplitude is the decay constant,  $f_{B_s}$ , defined in Eq. (2.5). It has been

<sup>6</sup>Note that if the scale of NP  $\Lambda$  lies well above the electroweak scale, i.e.  $\Lambda \gg v$ , then the requirement of  $SU(2)_L \times U(1)_Y$  gauge invariance for dimension-six operators tells us that  $C_T = C_{T5} = 0$  [126].

abundantly computed by means of numerical simulations of QCD on the lattice (LQCD) and its value is nowadays one of the most accurately computed hadronic quantities involving heavy-light mesons [77].

By using the Hamiltonian from Eq. (2.54), one can show that [127]

$$\begin{aligned} \mathcal{B}(B_s \rightarrow \ell^+ \ell^-)^{\text{th}} = & \tau_{B_s} \frac{\alpha^2 G_F^2 m_{B_s} \beta_\ell}{16\pi^3} |V_{tb} V_{ts}^*|^2 f_{B_s}^2 m_\ell^2 \left[ \left| C_{10} - C'_{10} + (C_P - C'_P) \frac{m_{B_s}^2}{2m_\ell(m_b + m_s)} \right|^2 \right. \\ & \left. + |C_S - C'_S|^2 \frac{m_{B_s}^2 (m_{B_s}^2 - 4m_\ell^2)}{4m_\ell^2 (m_b + m_s)^2} \right], \end{aligned} \quad (2.63)$$

where  $\beta_\ell = \sqrt{1 - 4m_\ell^2/m_{B_s}^2}$ . To compare Eq. (2.63) with the available experimental value, one needs to take into account the effects of  $B_s - \bar{B}_s$  oscillations, which amounts to [128]

$$\mathcal{B}(B_s \rightarrow \ell^+ \ell^-)^{\text{exp}} = \frac{1 + \mathcal{A}_{\Delta\Gamma}^{\ell\ell} y_s}{1 - y_s^2} \mathcal{B}(B_s \rightarrow \ell^+ \ell^-)^{\text{th}}, \quad (2.64)$$

where  $y_s = \Delta\Gamma_{B_s}/(2\Gamma_{B_s}) = 0.061(9)$ , experimentally established by the LHCb Collaboration [129], and  $\mathcal{A}_{\Delta\Gamma}^{\ell\ell}$  is a time-dependent observable defined in Ref. [128]. Within the SM  $\mathcal{A}_{\Delta\Gamma}^{\ell\ell} = 1$ , so that the time integrated branching ratio can be compactly written as

$$\mathcal{B}(B_s \rightarrow \ell^+ \ell^-)^{\text{exp}} \approx \frac{1}{1 - y_s} \mathcal{B}(B_s \rightarrow \ell^+ \ell^-)^{\text{th}}. \quad (2.65)$$

The SM prediction for this observable to which electroweak corrections have been included is given by [115],

$$\mathcal{B}(B_s \rightarrow \mu^+ \mu^-)^{\text{SM}} = (3.65 \pm 0.23) \times 10^{-9}. \quad (2.66)$$

This value is found to be in very good agreement with the most recent LHCb determination [130],

$$\mathcal{B}(B_s \rightarrow \mu^+ \mu^-)^{\text{exp}} = (3.0 \pm 0.6_{-0.2}^{+0.3}) \times 10^{-9}, \quad (2.67)$$

which provides very useful constraints for model building. In particular, the scenarios beyond the SM generating the (pseudo)-scalar operators  $\mathcal{O}_{S,P}$  are tightly constrained by  $\mathcal{B}(B_s \rightarrow \mu^+ \mu^-)$  due to the helicity suppression which is lifted by these operators in Eq. (2.63).

### 2.3.2 $B \rightarrow K \ell^+ \ell^-$

The decay mode  $B \rightarrow K \ell^+ \ell^-$  has also been the subject of many theoretical and experimental studies since it provides complementary information to the  $\mathcal{B}(B_s \rightarrow \mu^+ \mu^-)^{\text{exp}}$ . More precisely, some operators such as  $\mathcal{O}_9^{(\prime)}$  do not contribute to the latter quantity, but they can induce potentially observable effects in  $\mathcal{B}(B \rightarrow K \ell^+ \ell^-)$ . This can be easily seen from the general expression for the decay rate, which takes the form [127]

$$\begin{aligned} \frac{d\mathcal{B}}{dq^2}(\bar{B} \rightarrow \bar{K} \ell^+ \ell^-) = & |\mathcal{N}_K(q^2)|^2 \times \left[ \frac{1}{3} |f_+(q^2)|^2 \lambda_B \beta_\ell^2 |C_{10} + C'_{10}|^2 \right. \\ & \left. + 2 |f_0(q^2)|^2 (m_B^2 - m_K^2)^2 \frac{m_\ell^2}{q^2} \left| C_{10} + C'_{10} + \frac{(C_P + C'_P) q^2}{2m_\ell(m_b - m_s)} \right|^2 \right] \end{aligned}$$

$$\begin{aligned}
& + \frac{\lambda_B}{2} \left(1 - \frac{\beta_\ell^2}{3}\right) \left| (C_9 + C_9') f_+(q^2) + (C_7 + C_7') \frac{2m_b}{m_B + m_K} f_T(q^2) \right|^2 \\
& + |f_0(q^2)|^2 \frac{q^2 (m_B^2 - m_K^2)^2 \beta_\ell^2}{2(m_b - m_s)^2} |C_S + C_S'|^2, \tag{2.68}
\end{aligned}$$

where the normalization factor reads

$$|\mathcal{N}_K(q^2)|^2 = \tau_{B_d} \frac{\alpha^2 G_F^2 |V_{tb} V_{ts}^*|^2}{512 \pi^5 m_B^3} \beta_\ell \lambda_B^{1/2}. \tag{2.69}$$

For shortness, in the above formulas, we again use  $\lambda_B = \lambda(m_B, m_K, \sqrt{q^2})$  with  $\lambda(a, b, c) = [a^2 - (b - c)^2][a^2 - (b + c)^2]$ .

The hadronic form factors entering the  $B \rightarrow K \mu^+ \mu^-$  decay amplitude have been directly computed in LQCD only in the region of large  $q^2$ 's [131, 132]. For this reason, we opt for using  $\mathcal{B}(B \rightarrow K \mu^+ \mu^-)_{q^2 \in [15, 22] \text{ GeV}^2}$  to do phenomenology. Furthermore, since the bin corresponding to  $q^2 \in [15, 22] \text{ GeV}^2$  is rather wide and away from the very narrow charmonium resonances, the assumption of quark-hadron duality is likely to be valid [133]. By using the recent LQCD results for the form factors provided by HPQCD [131] and MILC Collaborations [132], the SM results are

$$\mathcal{B}(B \rightarrow K \mu^+ \mu^-)_{\text{high } q^2} = \left\{ (10.0 \pm 0.5) \times 10^{-8} \Big|_{\text{HPQCD}}, (10.7 \pm 0.5) \times 10^{-8} \Big|_{\text{MILC}} \right\}, \tag{2.70}$$

both being about  $2\sigma$  larger than the experimental value measured at LHCb [116],

$$\mathcal{B}(B \rightarrow K \mu^+ \mu^-)_{q^2 \in [15, 22] \text{ GeV}^2}^{\text{exp}} = (8.5 \pm 0.3 \pm 0.4) \times 10^{-8}. \tag{2.71}$$

This discrepancy is still not significant, but it is interesting to note that it is consistent with the ones obtained in lepton flavor universality tests in  $B \rightarrow K^{(*)} \mu^+ \mu^-$ , as it will be discussed in Chapter 5.

### 2.3.3 $B \rightarrow K^* \ell^+ \ell^-$ and $B_s \rightarrow \phi \ell^+ \ell^-$

Finally, the decay modes  $B \rightarrow K^* \ell^+ \ell^-$  and  $B_s \rightarrow \phi \ell^+ \ell^-$  received a lot of attention in the last years due to their rich kinematical structures, which allows us to construct several independent observables that can be studied experimentally. We will focus on the mode  $B \rightarrow \bar{K}^* \ell^+ \ell^-$ , but the expressions for the analogous  $B_s \rightarrow \phi \ell^+ \ell^-$  can be obtained *mutatis mutandis*. The differential branching ratio of  $B \rightarrow \bar{K}^* \ell^+ \ell^-$  is then given by <sup>7</sup>

$$\frac{d\mathcal{B}}{dq^2}(B \rightarrow \bar{K}^*(\rightarrow K\pi) \ell^+ \ell^-) = \frac{1}{4} \left[ 3I_1^c(q^2) + 6I_1^s(q^2) - I_2^c(q^2) - 2I_2^s(q^2) \right], \tag{2.72}$$

where the relevant angular coefficients  $I_i(q^2)$  read

$$I_1^s(q^2) = \left[ |A_\perp^L|^2 + |A_\parallel|^2 + (L \rightarrow R) \right] \frac{2 + \beta_\ell^2}{4} + \frac{4m_\ell^2}{q^2} \text{Re} \left( A_\parallel^L A_\parallel^{R*} + A_\perp^L A_\perp^{R*} \right), \tag{2.73}$$

<sup>7</sup>We postpone the expressions for the complete angular distribution of this decay for the following Sec. 2.5, where the derivation of these formulas will be also discussed.

$$I_1^c(q^2) = [ |A_0^L|^2 + |A_0^R|^2 ] + \frac{4m_\ell^2}{q^2} [ |A_t|^2 + 2\text{Re}(A_0^L A_0^{R*}) ] + \beta_\ell^2 |A_S|^2, \quad (2.74)$$

$$I_2^s(q^2) = \frac{\beta_\ell^2}{4} [ |A_\perp^L|^2 + |A_\parallel|^2 + (L \rightarrow R) ], \quad (2.75)$$

$$I_2^c(q^2) = -\frac{\lambda_q}{q^4} ( |A_0^L|^2 + |A_0^R|^2 ), \quad (2.76)$$

where here  $\beta_\ell = \sqrt{1 - 4m_\ell^2/q^2}$ . The helicity amplitudes appearing in the coefficients given above are defined by

$$\begin{aligned} A_\perp^{L(R)} &= \mathcal{N}_{K^*} \sqrt{2} \lambda_B^{1/2} \left[ [(C_9 + C'_9) \mp (C_{10} + C'_{10})] \frac{V(q^2)}{m_B + m_{K^*}} + \frac{2m_b}{q^2} (C_7 + C'_7) T_1(q^2) \right], \\ A_\parallel^{L(R)} &= -\mathcal{N}_{K^*} \sqrt{2} (m_B^2 - m_{K^*}^2) \left[ [(C_9 - C'_9) \mp (C_{10} - C'_{10})] \frac{A_1(q^2)}{m_B - m_{K^*}} + \frac{2m_b}{q^2} (C_7 - C'_7) T_2(q^2) \right], \\ A_0^{L(R)} &= -\frac{\mathcal{N}_{K^*}}{2m_{K^*} \sqrt{q^2}} \left\{ 2m_b (C_7 - C'_7) \left[ (m_B^2 + 3m_{K^*}^2 - q^2) T_2(q^2) - \frac{\lambda_B T_3(q^2)}{m_B^2 - m_{K^*}^2} \right] \right. \\ &\quad \left. + [(C_9 - C'_9) \mp (C_{10} - C'_{10})] \cdot \left[ (m_B^2 - m_{K^*}^2 - q^2) (m_B + m_{K^*}) A_1(q^2) - \frac{\lambda_B A_2(q^2)}{m_B + m_{K^*}} \right] \right\}, \\ A_t &= \frac{\mathcal{N}_{K^*}}{q^2} \lambda_B^{1/2} \left[ 2(C_{10} - C'_{10}) + \frac{q^2}{m_\ell (m_b + m_s)} (C_P - C'_P) \right] A_0(q^2), \\ A_S &= -2\mathcal{N}_{K^*} \lambda_B^{1/2} (C_S - C'_S) A_0(q^2), \end{aligned} \quad (2.77)$$

$$(2.78)$$

with

$$\mathcal{N}_{K^*}(q^2) = V_{tb} V_{ts}^* \left[ \tau_{B_d} \frac{\alpha_{\text{em}}^2 G_F^2}{3 \times 2^{10} \pi^5 m_B^3} \lambda_B^{1/2} \lambda_q^{1/2} \right]^{1/2}, \quad (2.79)$$

where  $\lambda_q = \lambda(q^2, m_\ell^2, m_\ell^2) = q^4 \beta_\ell^2$ .

The amplitude of  $B \rightarrow K^* \mu^+ \mu^-$  depends on several hadronic quantities which have not been fully determined by means of numerical simulations of LQCD. As of now, there are very few LQCD results available, which were obtained only for very large values of  $q^2$ , and still with large errors [134, 135]. The usual strategy employed in phenomenological studies is to perform a combined fit of these form factors with light-cone sum rules (LCSR) determinations of the same form factors in the low  $q^2$  region [136]. It should be stressed that assessment of uncertainties in the LCSR results for the  $B \rightarrow K^* \ell^+ \ell^-$  form factors remains controversial. In other words, by using the form factors obtained in that way, one runs the risk of misinterpreting hadronic uncertainties as NP effects. A safer strategy is to focus the experimental effort on the the quantities which are only mildly dependent on hadronic uncertainties. There are only a few of such quantities in the case of  $B \rightarrow K^* \ell^+ \ell^-$ , which can be directly deduced from the full angular decay distribution [137].

## 2.4 Lepton flavor violation in lepton decays

Lepton flavor violating (LFV) decays are the last class of observables presented in this Chapter. Contrary from the electroweak decays discussed above, these processes are completely absent in the SM, as required by the accidental lepton flavor symmetry  $U(1)_L \equiv U(1)_e \times U(1)_\mu \times U(1)_\tau$ . Although this symmetry is known to be broken, since neutrinos are massive and oscillate between different flavors, the smallness of neutrino masses ensures that all processes with LFV remain highly suppressed and basically not observable. Therefore, these processes are very clean probes of physics beyond the SM.

In the following, we highlight the importance of experimental searches of LFV, the observable of which would be a clear signal of physics beyond the SM. The usefulness of LFV constraints as a probe of NP is illustrated by computing  $\ell \rightarrow \ell' \gamma$ , with  $\ell, \ell' = e, \mu, \tau$ , in the SM extended by heavy neutrinos.

### 2.4.1 $\ell \rightarrow \ell' \gamma$ and neutrino masses

To illustrate the generation of LFV by massive neutrinos and to prove its smallness in the SM amended with neutrino masses, we consider the process  $\ell \rightarrow \ell' \gamma$ , with  $\ell, \ell' = e, \mu, \tau$ . If non-vanishing neutrino masses are added to the SM, then LFV is generated at loop-level by the diagrams shown in Fig. 2.7, where  $\nu_i$  denotes a generic neutrino mass eigenstate. To compute the contribution from these diagrams, we consider the charged current Lagrangian modified by neutrino masses and mixing, namely,

$$\mathcal{L} \supset -\frac{g}{\sqrt{2}} \sum_{i=1}^{n_\nu} U_{\alpha i} \bar{\ell}_\alpha \gamma^\mu P_L \nu_i W_\mu^- + \text{h.c.}, \quad (2.80)$$

with  $U$  being the leptonic mixing matrix (or PMNS matrix),  $\alpha$  the flavor of the charged leptons, and  $i = 1, \dots, n_\nu$  denotes a physical neutrino state. The amplitude for  $\ell \rightarrow \ell' \gamma$  then becomes

$$\mathcal{M}(\ell \rightarrow \ell' \gamma) = \varepsilon_\mu^* \frac{eg^2}{32\pi^2} \frac{m_\ell}{m_W^2} \left[ \bar{u}_\ell(p_\ell) i\sigma^{\mu\nu} q_\nu P_R u_{\ell'}(p_{\ell'}) \right] \sum_{i=1}^{n_\nu} U_{\ell i} U_{\ell' i} G_\gamma(x_i), \quad (2.81)$$

where  $\varepsilon_\mu$  is the photon polarization and  $q = p_\ell - p_{\ell'}$ , and we assumed  $m_{\ell'} \ll m_\ell$  in deriving this formula. The loop-factor  $G_\gamma(x_i)$  is a finite function, since the ultraviolet divergences cancel-out among the diagrams in Fig. 2.7, and it reads <sup>8</sup>

$$G_\gamma(x) = -\frac{2x^3 + 5x^2 - x}{4(1-x)^3} - \frac{3x^3}{2(1-x)^4} \log x. \quad (2.82)$$

where, for shortness, we use  $x_i = m_{\nu_i}^2/m_W^2$ .

By using these expressions, one can easily compute the relevant branching ratio, which is given by [138]

$$\mathcal{B}(\ell \rightarrow \ell' \gamma) = \frac{\sqrt{2} G_F^3 \sin^2 \theta_W m_W^2}{128 \pi^5 \Gamma_\ell} m_\ell^5 \left| \sum_{i=1}^{n_\nu} U_{\ell i}^* U_{\ell' i} G_\gamma(x_i) \right|^2. \quad (2.83)$$

<sup>8</sup>The total ultraviolet divergences must vanish in this loop since there is no flavor violating counter-term in the SM which could absorb it. Notice also that the loop computation is independent of the nature of neutrinos, i.e. if they are Majorana or Dirac particles.

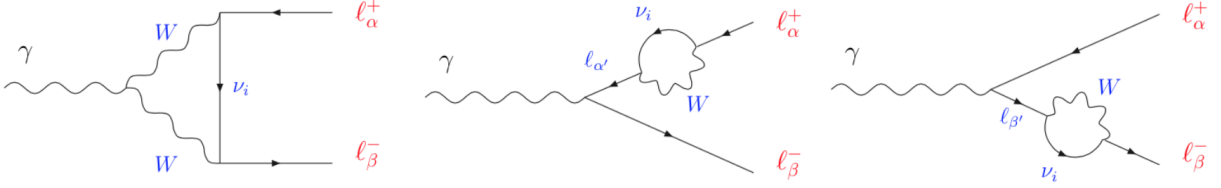


**Figure 2.7:** Diagrams for  $\ell \rightarrow \ell' \gamma$  at one-loop level.

From this expression, we observe the manifestation of a (leptonic) GIM mechanism similar to the one encountered in  $\Delta F = 1$  processes. From the unitarity of the PMNS matrix, we know that the branching ratio will depend only on the mass splitting of the neutrinos, which greatly suppresses the contribution of active neutrinos, since the corresponding mass differences satisfy

$$\Delta m_{ij}^2 \equiv m_{\nu_i}^2 - m_{\nu_j}^2 \leq \max(m_{\nu_i}^2; i = 1, 2, 3) \lesssim 1 \text{ eV}^2, \quad (2.84)$$

many orders of magnitude smaller than  $m_W^2$ . As an illustration of the result given above, we consider the most minimal neutrino mass model in which the SM is solely extended by the addition of three gauge singlets assumed to be Dirac particles, i.e. the conservation of lepton number is imposed. By Taylor expanding  $G_\gamma(x_i)$  and using the unitarity of the matrix  $U$ , one can show that

$$\sum_{i=1}^3 U_{\ell i}^* U_{\ell' i} G_\gamma(x_i) = \sum_{i=2}^3 U_{\ell i}^* U_{\ell' i} [G_\gamma(x_i) - G_\gamma(x_1)] \quad (2.85)$$

$$= \sum_{i=2}^3 U_{\ell i}^* U_{\ell' i} \left[ \frac{1}{8} \frac{\Delta m_{i1}^2}{m_W^2} \right] + \mathcal{O} \left( \frac{\Delta m_{i1}^4}{m_W^4} \right). \quad (2.86)$$

This expression can now be combined with the squared mass differences [50]

$$\Delta m_{21}^2 = (7.50_{-0.17}^{+0.19}) \times 10^{-5} \text{ eV}^2, \quad (2.87)$$

$$\Delta m_{31}^2 = (2.52 \pm 0.04) \times 10^{-3} \text{ eV}^2, \quad (2.88)$$

and the mixing angles determined by the neutrino oscillation experiments to predict<sup>9</sup>

$$\mathcal{B}(\mu \rightarrow e \gamma)^{\text{Dirac}} = 3.8(1.5) \times 10^{-55}, \quad (2.89)$$

which is well beyond reach of any current or future experiment. To quote the current limits, the most stringent upper bound is the one obtained by MEG (at 90% CL),

$$\mathcal{B}(\mu \rightarrow e \gamma)^{\text{exp}} < 4.2 \times 10^{-13}. \quad (2.90)$$

This limit will be improved in the future by the MEG-II upgrade which aims at a future sensitivity of  $6 \times 10^{-14}$  [139]. Notice that this value is still very far from the prediction given in Eq. (2.89).

<sup>9</sup>For simplicity we considered the results from the fit performed in Ref. [50] assuming the normal hierarchy. Since the value of the Dirac CP violating phase is still unknown, we scanned over the full range  $\delta \in [0, 2\pi)$ .

The purpose of the exercise described above was to demonstrate that LFV processes remain unobservable even if neutrino masses are included in the SM by hand, and therefore their detection would represent a clean signal of NP. In the following, we review the status of experimental searches for LFV and we discuss a scenario with heavy sterile neutrinos, which predicts sizable effects in LFV observables.

## 2.4.2 Status of current LFV searches

In this Section, we review the status of the experimental searches for LFV. The discussion given above can be extended to any type of LFV process, including leptonic three-body decays such as  $\mu \rightarrow 3e$ , hadronic LFV decays, or nuclear processes where  $\mu \rightarrow e$  conversion could take place, which are all predicted to be completely negligible in the SM amended with neutrino masses.

The current limits for purely leptonic LFV searches are listed in Table 2.5. One of the most promising opportunities for the future are the so-called  $\mu \rightarrow e$  conversion rates in nuclei, which will reach an impressive sensitivity in the years to come [140–143]. For LFV decays with hadrons in the initial and/or final state, the most constraining results are shown in Table 2.6. Even though the limits for those decays are orders of magnitude below the purely leptonic searches, it is important to emphasize that those searches are complementary to the latter, especially if the NP particles have sizable couplings to quarks. For instance, we will present in Sec. 5.3.3 a leptoquark scenario for which  $\mathcal{B}(B_s \rightarrow \ell\ell')$  is orders of magnitude larger than  $\mathcal{B}(\ell \rightarrow \ell'\gamma)$ . For hadronic decays, notice that we usually combine the rates with different lepton charges in the final state, e.g.  $\mathcal{B}(B_s \rightarrow \ell^\pm \ell'^\mp) = \mathcal{B}(B_s \rightarrow \ell^- \ell'^+) + \mathcal{B}(B_s \rightarrow \ell^+ \ell'^-)$  for  $\ell \neq \ell'$ .

Quantity	Exp. Bound
$\mathcal{B}(\mu \rightarrow e\gamma)$	$< 4.2 \times 10^{-13}$
$\mathcal{B}(\tau \rightarrow e\gamma)$	$< 3.3 \times 10^{-8}$
$\mathcal{B}(\tau \rightarrow \mu\gamma)$	$< 4.4 \times 10^{-8}$
$\mathcal{B}(\mu \rightarrow eee)$	$< 1.0 \times 10^{-12}$
$\mathcal{B}(\tau \rightarrow eee)$	$< 2.7 \times 10^{-8}$
$\mathcal{B}(\tau \rightarrow \mu\mu\mu)$	$< 2.1 \times 10^{-8}$
$\text{CR}(\mu - e, Ti)$	$< 4.3 \times 10^{-12}$
$\text{CR}(\mu - e, Au)$	$< 7 \times 10^{-13}$

**Table 2.5:** Current experimental bounds on the most relevant LFV leptonic decays at 90% CL. All limits are taken from Ref. [22], except for  $\mu \rightarrow e\gamma$  which was recently updated by the MEG Collaboration Ref. [144].

Before entering the discussion of hadronic LFV decays, which open a completely new window to the flavor structure beyond the SM, we will illustrate our discussion on a simple model where LFV can be generated at loop-level through heavy sterile neutrinos running in the loops.

Quantity	Exp. Bound
$\mathcal{B}(\tau \rightarrow eK_S)$	$< 2.6 \times 10^{-8}$
$\mathcal{B}(\tau \rightarrow \mu K_S)$	$< 2.3 \times 10^{-8}$
$\mathcal{B}(\tau \rightarrow \mu\phi)$	$< 8.4 \times 10^{-8}$
$\mathcal{B}(K_L \rightarrow e\mu)$	$< 4.7 \times 10^{-12}$
$\mathcal{B}(K_L \rightarrow \pi^0 e\mu)$	$< 7.6 \times 10^{-11}$
$\mathcal{B}(B_s \rightarrow e\mu)$	$< 1.1 \times 10^{-8}$
$\mathcal{B}(B^+ \rightarrow K^+ e\mu)$	$< 9.1 \times 10^{-8}$
$\mathcal{B}(B^+ \rightarrow K^+ e\tau)$	$< 3.0 \times 10^{-5}$
$\mathcal{B}(B^+ \rightarrow K^+ \mu\tau)$	$< 4.8 \times 10^{-5}$

**Table 2.6:** Current experimental bounds on the most relevant LFV decays containing hadrons at 90% CL [22].

### 2.4.3 Sterile neutrinos and LFV

One of the simplest extensions of the SM that can induce observable LFV rates are scenarios with heavy sterile neutrinos. These particles appear in many models aiming to explain the smallness of neutrino masses and they can enhance the loop function of  $\mu \rightarrow e\gamma$  and similar processes. If the scale of these particles is low enough, then the enhancement can be large enough to be detectable, as one can find for example in low scale realization of the seesaw mechanism, such as the inverse seesaw scenario [56, 57]. A similar enhancement can also be found in some models with Dirac neutrinos. For example, in the the so-called neutrinophilic two-Higgs doublet model, in which the charged Higgs contributions can play a similar role [145, 146].

#### Effective model setup

We consider an effective scenario where the only remnant at low energies of the neutrino mass generating mechanism is a sterile neutrino  $\nu_s$  which mixes with the active neutrinos through the leptonic mixing matrix  $U \in \mathbb{M}_{3 \times 4}(\mathbb{C})$ , generating three light neutrinos ( $\nu_1, \nu_2, \nu_3$ ) and one heavy neutrino ( $\nu_4$ ) defined as  $\nu_i = U_{\alpha i}^* \nu_\alpha$ . The leptonic mixing matrix can then be parameterized as,

$$U^T = R_{34}(\theta_{34}, \delta_{43}) \cdot R_{24}(\theta_{24}) \cdot R_{14}(\theta_{14}, \delta_{41}) \cdot \tilde{U} \cdot \text{diag}(\phi_{21}, \phi_{31}, \phi_{41}), \quad (2.91)$$

where  $R_{ij}$  is the rotation matrix between  $i$  and  $j$ , which includes the mixing angle  $\theta_{ij}$  and the Dirac CP-violating phase  $\delta_{ij}$ . The Majorana CP-violating phases are factorized in the last term of Eq. (2.91), where  $\phi_{ij} = \exp^{-i(\phi_i - \phi_j)}$ .  $\tilde{U}$  is the  $4 \times 3$  matrix which encodes the mixing among the active leptons as

$$\tilde{U} = \begin{pmatrix} U_{e1} & U_{e2} & U_{e3} \\ U_{\mu 1} & U_{\mu 2} & U_{\mu 3} \\ U_{\tau 1} & U_{\tau 2} & U_{\tau 3} \\ 0 & 0 & 0 \end{pmatrix}. \quad (2.92)$$

The upper  $3 \times 3$  submatrix of  $\tilde{U}$  is non-unitary due to the presence of a sterile neutrino and includes the usual Dirac CP phase actively searched for in neutrino oscillation facilities. In the case where the sterile neutrino decouples, this submatrix would correspond to the usual unitary PMNS lepton mixing matrix,  $U_{\text{PMNS}}$ . The active-sterile mixing is described by the rotation matrices  $R_{34}$ ,  $R_{24}$ ,  $R_{14}$  which are defined as

$$\begin{aligned}
 R_{34} &= \begin{pmatrix} 1 & 0 & 0 & 0 \\ 0 & 1 & 0 & 0 \\ 0 & 0 & \cos \theta_{34} & \sin \theta_{34} \cdot e^{-i\delta_{43}} \\ 0 & 0 & -\sin \theta_{34} \cdot e^{i\delta_{43}} & \cos \theta_{34} \end{pmatrix}, \\
 R_{24} &= \begin{pmatrix} 1 & 0 & 0 & 0 \\ 0 & \cos \theta_{24} & 0 & \sin \theta_{24} \\ 0 & 0 & 1 & 0 \\ 0 & -\sin \theta_{24} & 0 & \cos \theta_{24} \end{pmatrix}, \\
 R_{14} &= \begin{pmatrix} \cos \theta_{14} & 0 & 0 & \sin \theta_{14} \cdot e^{-i\delta_{41}} \\ 0 & 1 & 0 & 0 \\ 0 & 0 & 1 & 0 \\ -\sin \theta_{14} \cdot e^{i\delta_{41}} & 0 & 0 & \cos \theta_{14} \end{pmatrix}. \tag{2.93}
 \end{aligned}$$

The  $3 \times 3$  sub-matrix of  $U$  identified as the PMNS matrix is non-unitary and the deviation from unitarity is a function of the mixing angles between the active and the sterile neutrinos.

One can already see from Eq. (2.83) that the sterile neutrino can produce sizable effects in  $\mathcal{B}(\mu \rightarrow e\gamma)$  if it is sufficiently heavy to increase the loop factor  $G_\gamma(x)$ , which is plotted in Fig. 2.8. Note, however, that there is a competition between the mass enhancement of the loop function and the condition of perturbativity, which we choose to be <sup>10</sup>

$$\frac{\Gamma_{\nu_4}}{m_{\nu_4}} < \frac{1}{2}. \tag{2.94}$$

This result gives the limit

$$\frac{G_F m_{\nu_4}^4}{\sqrt{2}\pi} \sum_{\ell=e,\mu,\tau} |U_{\ell 4}|^2 < 1, \tag{2.95}$$

which ensures that  $|U_{\ell 4}|^2$ , with  $\ell = e, \mu, \tau$ , are small for large values of  $m_{\nu_4}$ . Therefore, there is an intermediate region where  $\mathcal{B}(\mu \rightarrow e\gamma)$  and other LFV processes can attain their maximal values. We will now perform a scan of parameters to quantify how large these observables can be in this effective scenario.

<sup>10</sup>In a concrete scenario, the perturbativity condition would be encoded in the fact that large active-sterile mass splittings imply small active-sterile mixing angles.

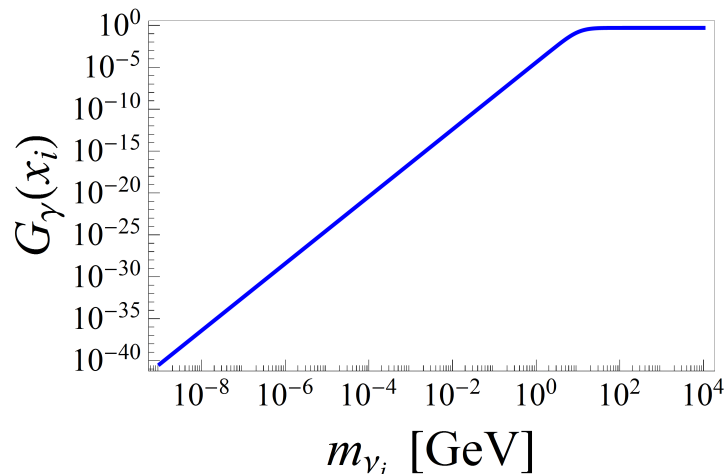


**Figure 2.8:** Loop factor  $G_\gamma(x_i)$  (with  $x_i = m_{\nu_i}^2/m_W^2$ ) plotted against  $m_{\nu_i}$ .

### Constraints and scan of parameters

To estimate the maximal value of  $\mathcal{B}(\mu \rightarrow e\gamma)$  in this model, we perform a scan of parameters in the range,

$$m_{\nu_4} \in [10^{-6}, 10^8] \text{ GeV}, \quad \theta_{i4} \in [0, 2\pi), \quad \delta_{ij} \in [0, 2\pi), \quad (2.96)$$

while keeping the active neutrino mass and mixing consistent with the global fits of neutrino oscillation data [50]. Before we list the observables used to constraint the parameter space, we need to emphasize that a price to pay for adding massive sterile neutrinos is that the Fermi constant, extracted from the muon decay, should be redefined according to  $G_F = G_\mu / \sqrt{\sum_{i,j} |U_{ei}|^2 |U_{\mu j}|^2}$ , where the sum runs over kinematically accessible neutrinos. We checked, however, that for the model we consider  $G_F = G_\mu$  remains an excellent approximation and thus it will be used in the following.

The randomly generated points are then confronted with several constraints listed below, which are imposed to  $2\sigma$  accuracy, unless stated otherwise [147, 148]:

- $W \rightarrow \ell\nu$ : We combine the measured  $\mathcal{B}(W \rightarrow e\nu) = 0.1071(16)$  and  $\mathcal{B}(W \rightarrow \mu\nu) = 0.1063(15)$  [22], with the expression

$$\mathcal{B}(W \rightarrow \ell\nu) = \frac{\sqrt{2}G_F m_W}{24\pi\Gamma_W} \sum_{i=1}^4 \lambda^{1/2}(m_\ell^2, m_{\nu_i}^2, m_W^2) \left[ 2 - \frac{m_\ell^2 + m_{\nu_i}^2}{m_W^2} - \frac{(m_\ell^2 - m_{\nu_i}^2)^2}{m_W^4} \right] |U_{\ell i}^2|, \quad (2.97)$$

where  $\lambda(a^2, b^2, c^2) = [a^2 - (b+c)^2][a^2 - (b-c)^2]$ . Since we do not include the electroweak radiative corrections to this formula we will use in our scan the experimental results with  $3\sigma$  uncertainties. Notice also that unlike  $\mathcal{B}(W \rightarrow e\nu)$  and  $\mathcal{B}(W \rightarrow \mu\nu)$ , which have also been recently measured at the LHC [149], the LEP result for  $\mathcal{B}(W \rightarrow \tau\nu)$  has not been measured at the LHC. For that reason, and despite the fact that the LEP result for  $\mathcal{B}(W \rightarrow \tau\nu)$  differs from the SM value at the  $2.3\sigma$  level, we prefer not to include  $\mathcal{B}(W \rightarrow \tau\nu)$  in our scan.

- $Z \rightarrow \nu\nu$ : In addition to the active neutrinos, the sterile ones can be used to saturate the experimental  $Z$  invisible decay width,  $\Gamma(Z \rightarrow \text{invisible}) = 0.503(16)$  GeV [22]. The

corresponding expression, which we compute by assuming that neutrinos are Majorana fermions is given by <sup>11</sup>

$$\Gamma(Z \rightarrow \nu\nu) = \sum_{\substack{i,j=1 \\ i \leq j}}^4 \left(1 - \frac{\delta_{ij}}{2}\right) \frac{\sqrt{2}G_F}{24\pi} m_Z \lambda^{1/2}(m_Z^2, m_{\nu_i}^2, m_{\nu_j}^2) \\ \times \left[ |C_{ij}|^2 \left(2 - \frac{m_{\nu_i}^2 + m_{\nu_j}^2}{m_Z^2} - \frac{(m_{\nu_i}^2 - m_{\nu_j}^2)^2}{m_Z^4}\right) - \text{Re}(C_{ij}^2) \frac{6m_{\nu_i}m_{\nu_j}}{m_Z^2} \right], \quad (2.98)$$

where

$$C_{ij} = \sum_{\alpha \in \{e, \mu, \tau\}} U_{\alpha i}^* U_{\alpha j}. \quad (2.99)$$

•  $\tau \rightarrow \ell\nu\nu$ : The leptonic decays  $\tau \rightarrow \ell\nu\nu$  ( $\ell = e, \mu$ ) represent very useful constraints as well. We derived the relevant expression for this process and found,

$$\frac{d\mathcal{B}(\tau \rightarrow \ell\nu\nu)}{dq^2} = \sum_{\substack{i,j=1 \\ i \leq j}}^4 \left(1 - \frac{\delta_{ij}}{2}\right) \frac{G_F^2 \tau_\tau}{192\pi^3 m_\tau^3 q^6} \lambda^{1/2}(m_\tau^2, m_\mu^2, q^2) \lambda^{1/2}(q^2 m_{\nu_i}^2, m_{\nu_j}^2) \left\{ (|U_{\tau i} U_{\ell j}^*|^2 + |U_{\tau j} U_{\ell i}^*|^2) \right. \\ \times \left[ 3 \left( q^4 - (m_{\nu_i}^2 - m_{\nu_j}^2)^2 \right) \left( (m_\tau^2 - m_\ell^2)^2 - q^4 \right) - \lambda(m_\tau^2, m_\mu^2, q^2) \lambda(q^2 m_{\nu_i}^2, m_{\nu_j}^2) \right] \\ \left. - 24 \text{Re}(U_{\tau i}^* U_{\ell j} U_{\tau j} U_{\ell i}^*) m_{\nu_i} m_{\nu_j} q^4 (m_\tau^2 + m_\ell^2 - q^2) \right\}. \quad (2.100)$$

The above formula is then combined with the average of experimental results, summarized in Ref. [22], namely  $\mathcal{B}(\tau \rightarrow \mu\nu\nu) = 17.33(5)\%$ , and  $\mathcal{B}(\tau \rightarrow e\nu\nu) = 17.82(5)\%$ .

•  $\Delta r_P = r_P^{\text{exp}}/r_P^{\text{SM}} - 1$ : The ratios  $r_P = \Gamma(P \rightarrow e\nu)/\Gamma(P \rightarrow \mu\nu)$  ( $P = \pi^+, K^+$ ) provide an efficient constraint, as recently argued in Ref. [150]. To that end, we combine the SM expression for the decay rate with the experimental values to obtain  $\Delta r_\pi = -0.004(3)$  and  $\Delta r_K = 0.004(4)$ , the result which is then compared with the formula,

$$\Delta r_P = -1 + \frac{m_\mu^2 (m_P^2 - m_\mu^2)^2 \sum_{i=1}^4 |U_{ei}|^2 \left[ m_P^2 (m_{\nu_i}^2 + m_e^2) - (m_{\nu_i}^2 - m_e^2)^2 \right] \lambda^{1/2}(m_P^2, m_{\nu_i}^2, m_e^2)}{m_e^2 (m_P^2 - m_e^2)^2 \sum_{i=1}^4 |U_{\mu i}|^2 \left[ m_\pi^2 (m_{\nu_i}^2 + m_\mu^2) - (m_{\nu_i}^2 - m_\mu^2)^2 \right] \lambda^{1/2}(m_\pi^2, m_{\nu_i}^2, m_\mu^2)}. \quad (2.101)$$

The constraints listed above are combined with the perturbativity condition Eq. (2.95) and with the limits from the direct searches of heavy sterile neutrinos [151]. The allowed regions of parameter space are shown in Fig. 2.9 in the planes  $m_4$  vs  $|U_{\ell 4}|^2$ ,  $\ell = e, \mu, \tau$ . It is

<sup>11</sup>The expression for Dirac neutrinos can be found in Ref. [148], which coincides with Eq. (2.98) in the limit  $m_{\nu_i} \rightarrow 0 \forall i$ .

worth noticing that the bounds shown in Fig. 2.9 are in agreement with those provided in Ref. [151], although slightly improved as some of the constraints discussed above have been updated. Since our goal is to predict the LFV rates, we did not impose these observables as constraints at this stage. Note, however, that the bounds shown in Fig. 2.9 in the plane  $m_4$  vs  $|U_{\ell 4}|^2$  remain the same after imposing the LFV constraints, since these observables are only sensitive to products of the type  $U_{\ell 4}U_{\ell' 4}^*$ , with  $\ell \neq \ell'$ .

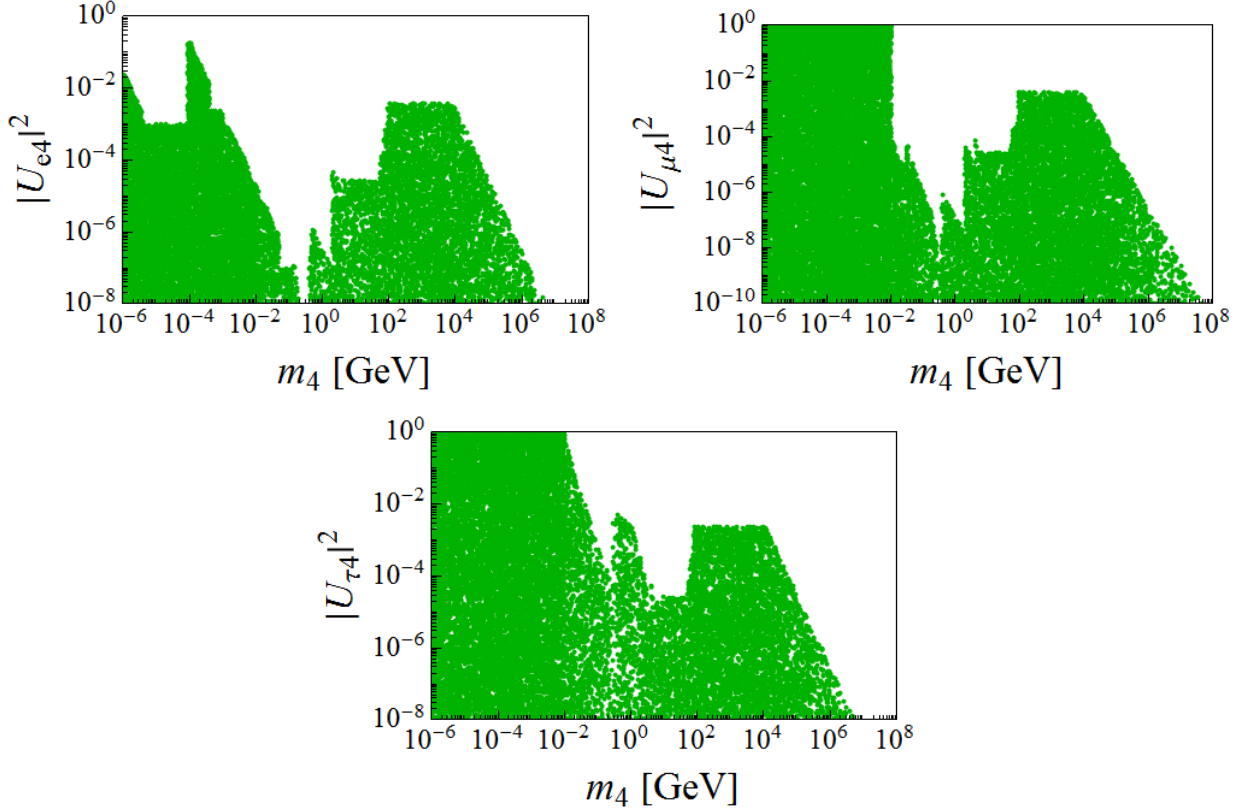


**Figure 2.9:** Result of the scan in the scenario of three active and one (effective) sterile neutrino, displayed in the planes  $m_4$  vs  $|U_{\ell 4}|^2$ . The green points agree with all constraints. Perturbative unitarity cuts the parameter space for large  $m_4$ .

We are now in position to use the allowed points in parameter space to predict the rates for  $\mathcal{B}(\ell \rightarrow \ell' \gamma)$  and  $\mathcal{B}(\ell \rightarrow 3\ell')$  and compare them with the experimental limits shown in Table 2.5. To that end, we consider the expression (2.83) for  $\mathcal{B}(\ell \rightarrow \ell' \gamma)$  and the expressions given in Ref. [138] for the three-body LFV decays. We will focus mostly on the observable  $\mathcal{B}(\mu \rightarrow e \gamma) < 4.2 \times 10^{-13}$ , since this is the most stringent LFV limit available thus far.

### Predictions for LFV

Our results are shown in Fig. 2.10, where  $\mathcal{B}(\mu \rightarrow e \gamma)$  is plotted as a function of  $m_{\nu_4}$  for the points allowed by our scan. The limits on  $\mathcal{B}(\mu \rightarrow e \gamma)$  and  $\mathcal{B}(\mu \rightarrow eee)$  are only applied *a posteriori* and shown with a different color, since we want to illustrate the sensitivity of those observables to sterile neutrinos. From this plot, we learn that  $\mathcal{B}(\mu \rightarrow e \gamma)$  can be as large as  $5 \times 10^{-9}$  for sterile fermions in the TeV mass range. A similar conclusion holds for the decay mode  $\mathcal{B}(\mu \rightarrow eee)$ , which is equally sensitive to this type of NP. Notice that the dips in the region  $m_{\nu_4} \in (10^{-2}, 10^2)$  in Fig. 2.10 come from the direct search limits on heavy neutrinos, which constrain the elements  $|U_{\ell 4}|^2$  with  $\ell = e, \mu, \tau$  for neutrinos with masses in the range  $m_{\nu_4} \lesssim 100$  GeV [151]. Moreover, the decrease of the LFV rate for large masses is

associated to the perturbativity limit Eq. (2.95) which constraints the active-sterile mixing for large sterile masses, as explained above.

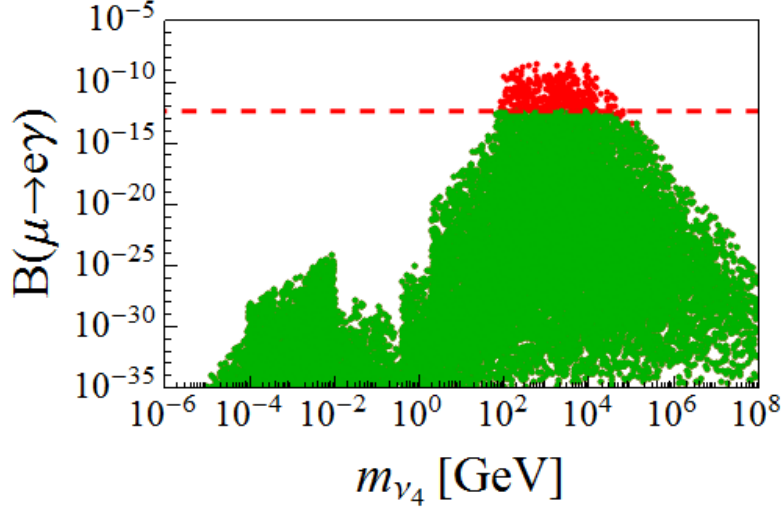


**Figure 2.10:** Result of the scan in the scenario of three active and one (effective) sterile neutrino in the plane  $(m_{\nu_4}, \mathcal{B}(\mu \rightarrow e\gamma))$ . The green points agree with all constraints, while the red ones are excluded by the limits  $\mathcal{B}(\mu \rightarrow e\gamma) < 4.2 \times 10^{-13}$  [144] and  $\mathcal{B}(\mu \rightarrow eee) < 10^{-12}$  [152].

The conclusion of this exercise is that the current limits on LFV decays can set useful limits on the parameters of sterile fermions, namely, their masses and/or couplings. These results can be particularly useful if the masses of sterile neutrinos lie at the TeV range, as it can be seen in Fig. 2.10. In the next Section, we will discuss LFV decays of mesons, which are complementary to the observables reported above, being mostly sensitive to other types of NP scenarios.

## 2.5 LFV in $b \rightarrow s$ exclusive decays

In this Section, we discuss the exclusive decays of the type  $b \rightarrow s\ell_1\ell_2$ , with  $\ell_1, \ell_2 = e, \mu, \tau$ , using a general EFT approach. The LFV decays of hadrons are complementary to the purely leptonic modes because they probe different LFV effective operators. Moreover, they offer a different environment to test the result of the above-mentioned leptonic modes. The interest on the transition  $b \rightarrow s$  is partially motivated by the recent observation of lepton flavor universality in the transition  $b \rightarrow s\ell\ell$ , with  $\ell = e, \mu$ , which will be discussed in Sec. 5.2. Interestingly, most of the concrete models aiming to explain this anomaly can induce LFV in  $B$  decays at experimentally accessible rates [153–155].

To describe the transition  $b \rightarrow s\ell_1\ell_2$  in a model independent way, we extend the Hamiltonian (2.54) to account for operators with different leptons,

$$\begin{aligned} \mathcal{H}_{\text{eff}} = & -\frac{4G_F}{\sqrt{2}}V_{tb}V_{ts}^* \left\{ \sum_{i=1}^6 C_i(\mu)\mathcal{O}_i(\mu) + \sum_{i=7,8} \left[ C_i(\mu)\mathcal{O}_i(\mu) + (C_i(\mu))'(\mathcal{O}_i(\mu))' \right] \right. \\ & \left. + \sum_{\ell_1, \ell_2} \sum_{i=9,10,S,P} \left[ C_i^{\ell_1\ell_2}(\mu)\mathcal{O}_i^{\ell_1\ell_2}(\mu) + (C_i^{\ell_1\ell_2}(\mu))'(\mathcal{O}_i^{\ell_1\ell_2}(\mu))' \right] \right\} + \text{h.c.}, \end{aligned}$$

where

$$\mathcal{O}_9^{\ell_1 \ell_2} = \frac{e^2}{(4\pi)^2} (\bar{s} \gamma_\mu P_L b) (\bar{\ell}_1 \gamma^\mu \ell_2), \quad \mathcal{O}_S^{\ell_1 \ell_2} = \frac{e^2}{(4\pi)^2} (\bar{s} P_R b) (\bar{\ell}_1 \ell_2), \quad (2.102)$$

$$\mathcal{O}_{10}^{\ell_1 \ell_2} = \frac{e^2}{(4\pi)^2} (\bar{s} \gamma_\mu P_L b) (\bar{\ell}_1 \gamma^\mu \gamma_5 \ell_2), \quad \mathcal{O}_P^{\ell_1 \ell_2} = \frac{e^2}{(4\pi)^2} (\bar{s} P_R b) (\bar{\ell}_1 \gamma_5 \ell_2). \quad (2.103)$$

Similarly to Sec. 2.3, we neglect the tensor operators  $O_{T(5)}$  since they are not generated by dimension-six operators consistent with  $SU(2)_L \times U(1)_Y$  gauge invariance [126]. Of course, the Wilson coefficient  $C_i^{\ell_1 \ell_2}$  are zero in the SM for  $\ell_1 \neq \ell_2$ . Furthermore, note that

- (i) in general, for  $\ell_1 \neq \ell_2$ ,  $C_i^{\ell_1 \ell_2} \neq C_i^{\ell_2 \ell_1}$ , which is particularly the case in the LQ models in which LFV occurs through tree-level diagrams;
- (ii) in some situations, even if  $C_i^{\ell_1 \ell_2} = (C_i^{\ell_2 \ell_1})^* \forall i$ , one can still generate an asymmetry between LFV modes with different lepton charges, e.g.  $\mathcal{B}(B_s \rightarrow \mu^- \tau^+) \neq \mathcal{B}(B_s \rightarrow \mu^+ \tau^-)$ .

Before discussing the issue of lepton charge asymmetry one must first observe LFV, that is why we will here combine the two charged modes, namely,  $\mathcal{B}(B_s \rightarrow \ell_1 \ell_2) \equiv \mathcal{B}(B_s \rightarrow \ell_1^- \ell_2^+) + \mathcal{B}(B_s \rightarrow \ell_1^+ \ell_2^-)$ , and  $\mathcal{B}(B \rightarrow K^{(*)} \ell_1 \ell_2) \equiv \mathcal{B}(B \rightarrow K^{(*)} \ell_1^- \ell_2^+) + \mathcal{B}(B \rightarrow K^{(*)} \ell_1^+ \ell_2^-)$ .

In the following, we will use the Hamiltonian defined above to derive the general expressions for the decay rates and angular distributions (when possible) of the exclusive  $b \rightarrow s$  decay modes. To simplify our notation, we will write  $C_i \equiv C_i^{\ell_1 \ell_2}$  ( $\ell_1 \neq \ell_2$ ) when confusion can be avoided. These expressions will then be used in Sec. 2.5.4 to discuss some generalities of LFV in the the transition  $b \rightarrow s \ell_1 \ell_2$ .

### 2.5.1 $B_s \rightarrow \ell_1 \ell_2$

We first focus on the simplest exclusive  $b \rightarrow s \ell_1 \ell_2$  mode,  $B_s \rightarrow \ell_1 \ell_2$ , which is also instructive as far as the operators contributing to the process are concerned. Of course, and after the trivial replacements, the same expressions will be valid for  $B_d \rightarrow \ell_1 \ell_2$ . The general expression for this decay is then given by

$$\begin{aligned} \mathcal{B}(B_s \rightarrow \ell_1^- \ell_2^+)^{\text{th}} &= \frac{\tau_{B_s}}{64\pi^3} \frac{\alpha^2 G_F^2}{m_{B_s}^3} f_{B_s}^2 |V_{tb} V_{ts}^*|^2 \lambda^{1/2}(m_{B_s}, m_1, m_2) \\ &\times \left\{ [m_{B_s}^2 - (m_1 + m_2)^2] \cdot \left| (C_9 - C'_9)(m_1 - m_2) + (C_S - C'_S) \frac{m_{B_s}^2}{m_b + m_s} \right|^2 \right. \\ &\quad \left. + [m_{B_s}^2 - (m_1 - m_2)^2] \cdot \left| (C_{10} - C'_{10})(m_1 + m_2) + (C_P - C'_P) \frac{m_{B_s}^2}{m_b + m_s} \right|^2 \right\}, \quad (2.104) \end{aligned}$$

where  $m_1$  and  $m_2$  are the lepton masses. What immediately becomes evident from Eq. (2.104) is that in the LFV channel the lepton vector current is not conserved,

$$i\partial_\mu (\bar{\ell}_1 \gamma^\mu \ell_2) = (m_2 - m_1) \bar{\ell}_1 \ell_2 \neq 0, \quad (2.105)$$

and the contribution of  $C_9^{(\prime)}$  cannot be neglected. Quite obviously, in the limit  $m_1 = m_2$  one finds the usual expression for  $\mathcal{B}(B_s \rightarrow \ell^+ \ell^-)$ , cf. Eq. (2.63). Finally, when confronting theory

with the experimental measurements one needs to account for the effect of oscillations in the  $B_s - \bar{B}_s$  system because the time dependence of the  $B_s$ -decay rate has been integrated in experiment, as derived in Eq. (2.65) to a good approximation.

### 2.5.2 $B \rightarrow K \ell_1 \ell_2$

The kinematics of the decay  $B \rightarrow K \ell_1^- \ell_2^+$  is defined in such a way that the main decay axis  $z$  is defined in the rest frame of  $B$ , so that  $K$  and the lepton pair travel in the opposite directions. The angle between the negatively charged lepton and the decay axis (opposite to the direction of flight of the kaon) is denoted by  $\theta_\ell$  and is defined in the lepton-pair rest frame. We can then write the differential decay rate in the following form,

$$\begin{aligned} \frac{d\mathcal{B}}{dq^2}(\bar{B} \rightarrow \bar{K} \ell_1^- \ell_2^+) &= |\mathcal{N}_K(q^2)|^2 \times \left\{ \varphi_9(q^2) |C_9 + C'_9|^2 + \varphi_{10}(q^2) |C_{10} + C'_{10}|^2 + \varphi_S(q^2) |C_S + C'_S|^2 \right. \\ &\quad + \varphi_P(q^2) |C_P + C'_P|^2 + \delta_{\ell_1 \ell_2} \varphi_7(q^2) |C_7 + C'_7|^2 + \varphi_{9S}(q^2) \text{Re}[(C_9 + C'_9)(C_S + C'_S)^*] \\ &\quad \left. + \delta_{\ell_1 \ell_2} \varphi_{79}(q^2) \text{Re}[(C_7 + C'_7)(C_9 + C'_9)^*] + \varphi_{10P}(q^2) \text{Re}[(C_{10} + C'_{10})(C_P + C'_P)^*] \right\}, \end{aligned} \quad (2.106)$$

where the Kronecker delta  $\delta_{\ell_1 \ell_2}$  accounts for the fact that the photon penguin only contributes to lepton flavor conserving decays. The functions  $\varphi_i(q^2)$  depend on kinematical quantities and on the form factors, as explicitly given below:<sup>12</sup>

$$\begin{aligned} \varphi_7(q^2) &= \frac{2m_b^2 |f_T(q^2)|^2}{(m_B + m_K)^2} \lambda(m_B, m_K, \sqrt{q^2}) \left[ 1 - \frac{(m_1 - m_2)^2}{q^2} - \frac{\lambda(\sqrt{q^2}, m_1, m_2)}{3q^4} \right], \\ \varphi_{9(10)}(q^2) &= \frac{1}{2} |f_0(q^2)|^2 (m_1 \mp m_2)^2 \frac{(m_B^2 - m_K^2)^2}{q^2} \left[ 1 - \frac{(m_1 \pm m_2)^2}{q^2} \right] \\ &\quad + \frac{1}{2} |f_+(q^2)|^2 \lambda(m_B, m_K, \sqrt{q^2}) \left[ 1 - \frac{(m_1 \mp m_2)^2}{q^2} - \frac{\lambda(\sqrt{q^2}, m_1, m_2)}{3q^4} \right], \\ \varphi_{79}(q^2) &= \frac{2m_b f_+(q^2) f_T(q^2)}{m_B + m_K} \lambda(m_B, m_K, \sqrt{q^2}) \left[ 1 - \frac{(m_1 - m_2)^2}{q^2} - \frac{\lambda(\sqrt{q^2}, m_1, m_2)}{3q^4} \right], \\ \varphi_{S(P)}(q^2) &= \frac{q^2 |f_0(q^2)|^2}{2(m_b - m_s)^2} (m_B^2 - m_K^2)^2 \left[ 1 - \frac{(m_1 \pm m_2)^2}{q^2} \right], \\ \varphi_{10P(9S)}(q^2) &= \frac{|f_0(q^2)|^2}{m_b - m_s} (m_1 \pm m_2) (m_B^2 - m_K^2)^2 \left[ 1 - \frac{(m_1 \mp m_2)^2}{q^2} \right]. \end{aligned} \quad (2.107)$$

Finally, the normalization factor in eq. (2.68) reads

$$|\mathcal{N}_K(q^2)|^2 = \tau_{B_d} \frac{\alpha^2 G_F^2 |V_{tb} V_{ts}^*|^2}{512 \pi^5 m_B^3} \frac{\lambda^{1/2}(\sqrt{q^2}, m_1, m_2)}{q^2} \lambda^{1/2}(\sqrt{q^2}, m_B, m_K). \quad (2.108)$$

Like in the previous subsection we see that due to the non-conservation of the leptonic vector current, the new pieces emerge in the functions  $\varphi_i(q^2)$ . By taking the limit  $m_1 = m_2$  in eq. (2.107) we retrieve the known expressions for the lepton flavor conserving case, cf. Eq. (2.68). We should also emphasize that the interference term  $\varphi_{9S}(q^2)$  changes the

<sup>12</sup>In the notation used to write the formulas for  $\varphi_{a(b)}(q^2)$  the upper signs correspond to  $\varphi_a(q^2)$  and lower to  $\varphi_b(q^2)$ .

sign depending on the charge of the heavier lepton. In other words, if one assumes that the Wilson coefficients  $(C_i)_{12} = (C_i)_{21}$ , then the difference between  $\mathcal{B}(B \rightarrow K \ell_1^- \ell_2^+)$  and  $\mathcal{B}(B \rightarrow K \ell_2^- \ell_1^+)$  will be a measure of the interference term proportional to  $\text{Re}[C_9 C_S^*]$ .

### 2.5.3 $B \rightarrow K^* \ell_1 \ell_2$ and $B_s \rightarrow \phi \ell_1 \ell_2$

These processes proceed via  $B \rightarrow K^*(\rightarrow K\pi)\ell_1^- \ell_2^+$  and  $B_s \rightarrow \phi(\rightarrow K\bar{K})\ell_1^- \ell_2^+$ . Since the expression for the angular distribution of the latter decay can be obtained by the trivial replacements in the ones for  $\bar{B} \rightarrow \bar{K}^*(\rightarrow K^-\pi^+)\ell_1^- \ell_2^+$ , we will focus on the  $B \rightarrow K^*$  transition. In this Section, we will present the full computation in detail, since there were several inconsistencies in the literature of  $B \rightarrow K^* \mu^+ \mu^-$  regarding the definition of the helicity amplitudes and the choice of angular conventions, which have been only recently clarified in Ref. [127, 156]. In these papers, we decided to adopt the same conventions of LHCb [157].<sup>13</sup> Furthermore, we will present in detail a non-ambiguous method to incorporate the (pseudo)-scalar operators in the helicity amplitude method which can also be applied to the lepton flavor conserving case.

#### Angular conventions and kinematics

We adopt the kinematics of Ref. [127, 156], which are fixed in such a way that they coincide with the conventions adopted in experiments at the LHC [157]. In particular, we denote the four-vectors by  $B(p_B) \rightarrow K^*(k)V^*(q) \rightarrow K(p_K)\pi(p_\pi)\ell_1^-(p_1)\ell_2^+(p_2)$ , where  $V$  is a virtual gauge boson. Moreover, our angular conventions are summarized in Fig. 2.11.

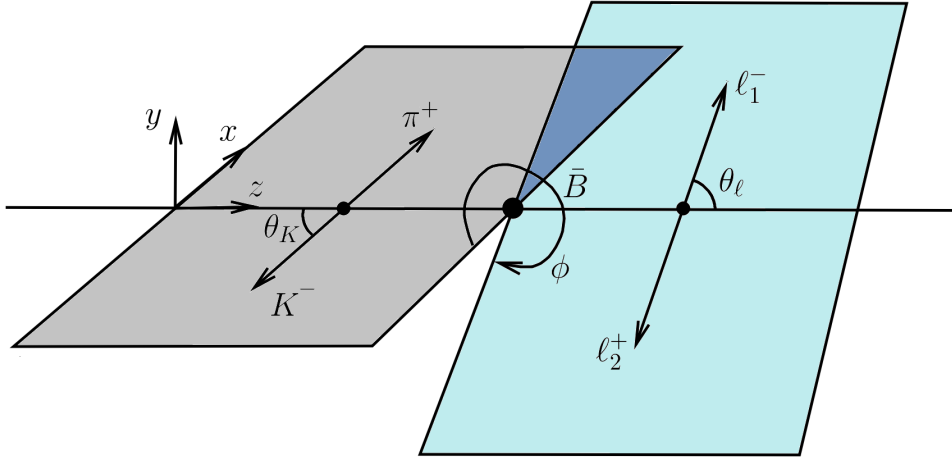


**Figure 2.11:** Angular conventions for the decay  $\bar{B} \rightarrow \bar{K}^* \ell_1^- \ell_2^+$ .

In the  $B$  rest frame, the leptonic and hadronic four-vectors are defined by  $q^\mu = (q_0, 0, 0, q_z)$  and  $k^\mu = (k_0, 0, 0, -q_z)$ , where

$$q_0 = \frac{m_B^2 + q^2 - m_{K^*}^2}{2m_B}, \quad k_0 = \frac{m_B^2 + m_{K^*}^2 - q^2}{2m_B}, \quad \text{and} \quad q_z = \frac{\lambda^{1/2}(m_B, m_{K^*}, \sqrt{q^2})}{2m_B}, \quad (2.109)$$

<sup>13</sup>We would like to thank Roman Zwicky for correspondence which helped to clarify the inconsistencies in the literature.

In the dilepton rest frame, the leptonic four-vectors read

$$p_1^\mu = (E_\alpha, |p_\ell| \sin \theta_\ell \cos \phi, -|p_\ell| \sin \theta_\ell \sin \phi, |p_\ell| \cos \theta_\ell), \quad (2.110)$$

$$p_2^\mu = (E_\beta, -|p_\ell| \sin \theta_\ell \cos \phi, |p_\ell| \sin \theta_\ell \sin \phi, -|p_\ell| \cos \theta_\ell), \quad (2.111)$$

where

$$E_1 = \frac{q^2 + m_1^2 - m_2^2}{2\sqrt{q^2}}, \quad E_2 = \frac{q^2 - m_1^2 + m_2^2}{2\sqrt{q^2}}, \quad \text{and} \quad |p_\ell| = \frac{\lambda^{1/2}(q^2, m_1^2, m_2^2)}{2m_B}. \quad (2.112)$$

In the same way, one can write in the  $K^*$  rest frame

$$p_K^\mu = (E_K, -|p_K| \sin \theta_K, 0, -|p_K| \cos \theta_K), \quad (2.113)$$

$$p_\pi^\mu = (E_\pi, +|p_K| \sin \theta_K, 0, +|p_K| \cos \theta_K), \quad (2.114)$$

where  $E_K$ ,  $E_\pi$  and  $|p_K|$  are given by the similar expressions.

### Polarization vectors

In the  $B$  rest frame, we choose the polarization vectors to be:

$$\begin{aligned} \varepsilon_V^\mu(\pm) &= \frac{1}{\sqrt{2}}(0, \pm 1, i, 0), & \varepsilon_{K^*}^\mu(\pm) &= \frac{1}{\sqrt{2}}(0, \mp 1, i, 0), \\ \varepsilon_V^\mu(0) &= \frac{1}{\sqrt{q^2}}(q_z, 0, 0, q_0), & \varepsilon_{K^*}^\mu(0) &= \frac{-1}{\sqrt{k^2}}(k_z, 0, 0, k_0), \\ \varepsilon_V^\mu(t) &= \frac{1}{\sqrt{q^2}}(q_0, 0, 0, q_z), \end{aligned} \quad (2.115)$$

where  $V$  stands for a virtual gauge boson, as we shall describe below. These four-vectors are orthonormal and satisfy the completeness relations

$$\begin{aligned} \sum_{n, n'} \varepsilon_V^{*\mu}(n) \varepsilon_V^\nu(n') g_{nn'} &= g^{\mu\nu}, \\ \sum_{m, m'} \varepsilon_{K^*}^{*\mu}(m) \varepsilon_{K^*}^\nu(m') \delta_{mm'} &= -g^{\mu\nu} + \frac{k^\mu k^\nu}{m_{K^*}^2}, \end{aligned} \quad (2.116)$$

where  $m \in \{0, \pm\}$ ,  $n, n' \in \{0, t, \pm\}$ , and  $g_{nn'} = \text{diag}(1, -1, -1, -1)$ .

### Computation of the decay amplitude

After fixing our convention for the kinematics of this decay and making it coincide with the one used at the LHCb experiment, we are in position to compute the  $B \rightarrow K^*(\rightarrow K^- \pi^+) \ell_1^- \ell_2^+$  decay amplitude by relying on the Hamiltonian (2.102). The first step is to assume that the  $K^*$  is decaying resonantly. Then, one can use the narrow-width approximation in the  $K^*$  propagator, namely,

$$\frac{1}{(k^2 - m_{K^*}^2)^2 + (m_{K^*} \Gamma_{K^*})^2} \rightarrow \frac{\pi}{m_{K^*} \Gamma_{K^*}} \delta(k^2 - m_{K^*}^2). \quad (2.117)$$

We write now the  $B \rightarrow K^*$  hadronic matrix element as

$$\langle \bar{K}^*(k) | J_\mu | \bar{B}(p) \rangle = \varepsilon_{K^*}^{\nu} A_{\nu\mu}, \quad (2.118)$$

where  $J^\mu$  is a generic current and  $A_{\nu\mu}$  contains the  $B \rightarrow K^*$  form factors. Then, one can show that the corresponding  $B \rightarrow K\pi$  matrix can be expressed as [158],

$$\langle \bar{K}(p_K)\pi(p_\pi) | J_\mu | \bar{B}(p) \rangle = -D_{K^*}(k^2)W^\nu A_{\nu\mu}, \quad (2.119)$$

with

$$|D_{K^*}(k^2)|^2 = \frac{48\pi^2 m_{K^*}^4}{\lambda_B^{3/2}} \delta(k^2 - m_{K^*}^2), \quad (2.120)$$

$$W^\mu = (p_K - p_\pi)^\mu - \frac{m_K^2 - m_\pi^2}{k^2} k^\mu, \quad (2.121)$$

where we write for shortness again  $\lambda_B = \lambda(m_B, m_{K^*}, \sqrt{q^2})$ .

To write the  $B \rightarrow K^*(\rightarrow K^-\pi^+)\ell_1^-\ell_2^+$  decay amplitude in a compact form, it is convenient to use the formalism of helicity amplitudes. In the absence of the (pseudo-)scalar operators, the total amplitude can be schematically written as

$$\mathcal{M}(B \rightarrow K^*\ell_1^-\ell_2^+) = W^\sigma \left[ \mathcal{M}_{\sigma\mu}^L \bar{\ell}_1 \gamma^\mu P_L \ell_2 + \mathcal{M}_{\sigma\mu}^R \bar{\ell}_1 \gamma^\mu P_R \ell_2 \right], \quad (2.122)$$

where  $\mathcal{M}_{\sigma\mu}^{L(R)}$  encapsulate the dependence on the effective coefficients and on the hadronic parameters via Eq. (2.119). By describing the decay mode as  $B \rightarrow K^*V^* \rightarrow K^*\ell_1^+\ell_2^-$ , where  $V^*$  is a virtual vector boson, one can decompose the total decay amplitude in terms of the helicity amplitudes,

$$H_{mn}^{L(R)} \equiv -\mathcal{M}_{\mu\nu}^{L(R)} \varepsilon_V^{\nu*}(m) \varepsilon_V^{\mu*}(n), \quad (2.123)$$

where  $\varepsilon_V^\mu(m)$  (with  $m, n = 0, t, \pm$ ) are the  $V^*$ -boson polarization vectors, explicitly defined in Eq. (2.115). We repeat that the above decomposition is valid as long as the scalar and the pseudoscalar operators are not present. To incorporate those contributions one can then apply the Dirac equation,

$$\bar{\ell}_1 \gamma_5 \ell_2 = \frac{q^\mu}{m_{\ell_1} + m_{\ell_2}} \bar{\ell}_1 \gamma_\mu \gamma_5 \ell_2, \quad \bar{\ell}_1 \ell_2 = \frac{q^\mu}{m_{\ell_1} - m_{\ell_2}} \bar{\ell}_1 \gamma_\mu \ell_2, \quad (2.124)$$

and absorb the (pseudo-)scalar terms in the time-like coefficients  $A_t^{L(R)}$ . It should be stressed that a similar decomposition for the scalar current cannot be made for the lepton flavor conserving decay ( $\ell_1 = \ell_2$ ). In that case, to unambiguously incorporate the  $C_S^{(\prime)}$  contribution in the helicity amplitudes formalism, it is necessary to perform the computation with different lepton masses and to take the limit  $m_{\ell_1} = m_{\ell_2}$  only in the final expression [127]. By using this approach, one can then obtain the desired helicity amplitudes and the total decay amplitude for the lepton flavor conserving decay  $B \rightarrow K^*\ell^+\ell^-$ .

The total amplitude (2.122) can be expressed in terms of the helicity amplitudes (2.123) by using the completeness relations (2.116), which allow us to factorize the amplitude into leptonic and hadronic tensors,

$$\mathcal{M}(B \rightarrow K^* \ell_1^- \ell_2^+) = \sum_{mn} [W \cdot \varepsilon_{K^*}(m)] \left[ \varepsilon_V^\mu(n) \left( H_{mn}^L \bar{\ell}_1 \gamma_\mu P_L \ell_2 + H_{mn}^R \bar{\ell}_1 \gamma_\mu P_R \ell_2 \right) \right], \quad (2.125)$$

where we have used  $W \cdot k = 0$  in writing this equation. The contraction with the  $K^*$  polarization vector is most easily computed in the  $K^*$ -meson rest frame, while the leptonic contractions can be computed in the dilepton rest frame after summing over the non-observed polarizations and computing the traces. For completeness, we give the expression for the 4-body phase space,

$$\frac{d\Gamma(B \rightarrow K^* \ell_1^- \ell_2^+)}{dq^2 dk^2 d \cos \theta_\ell d \cos \theta_K d\phi} = \frac{\lambda_B^{1/2} \lambda_q^{1/2} \lambda_{K^*}^{1/2}}{m_B^3 q^2 k^2} \frac{1}{8(4\pi)^6} \sum |\mathcal{M}(B \rightarrow K^* \ell_1^- \ell_2^+)|^2, \quad (2.126)$$

from which the decay rates can be easily computed. As before and for shortness, we write  $\lambda_B = \lambda(m_B, m_{K^*}, \sqrt{q^2})$ ,  $\lambda_{K^*} = \lambda(m_{K^*}, m_K, m_\pi)$  and  $\lambda_q = \lambda(\sqrt{q^2}, m_1, m_2)$ .

### Full angular distribution

The full angular distribution of the above decay reads <sup>14</sup>

$$\frac{d^4 \mathcal{B}(B \rightarrow \bar{K}^* \rightarrow (K\pi) \ell_1^- \ell_2^+)}{dq^2 d \cos \theta_\ell d \cos \theta_K d\phi} = \frac{9}{32\pi} I(q^2, \theta_\ell, \theta_K, \phi), \quad (2.127)$$

with

$$\begin{aligned} I(q^2, \theta_\ell, \theta_K, \phi) = & I_1^s(q^2) \sin^2 \theta_K + I_1^c(q^2) \cos^2 \theta_K + [I_2^s(q^2) \sin^2 \theta_K + I_2^c(q^2) \cos^2 \theta_K] \cos 2\theta_\ell \\ & + I_3(q^2) \sin^2 \theta_K \sin^2 \theta_\ell \cos 2\phi + I_4(q^2) \sin 2\theta_K \sin 2\theta_\ell \cos \phi \\ & + I_5(q^2) \sin 2\theta_K \sin \theta_\ell \cos \phi + [I_6^s(q^2) \sin^2 \theta_K + I_6^c(q^2) \cos^2 \theta_K] \cos \theta_\ell \\ & + I_7(q^2) \sin 2\theta_K \sin \theta_\ell \sin \phi + I_8(q^2) \sin 2\theta_K \sin 2\theta_\ell \sin \phi \\ & + I_9(q^2) \sin^2 \theta_K \sin^2 \theta_\ell \sin 2\phi, \end{aligned} \quad (2.128)$$

After integrating over angles the differential decay rate is simply

$$\frac{d\mathcal{B}}{dq^2} = \frac{1}{4} \left[ 3I_1^c(q^2) + 6I_1^s(q^2) - I_2^c(q^2) - 2I_2^s(q^2) \right]. \quad (2.129)$$

By using Eq. (2.123), one can compute the helicity amplitudes in the  $B$ -meson rest frame. The only ones which are non-zero read

$$\begin{aligned} A_\perp^{L(R)} &= \frac{H_{++}^{L(R)} - H_{--}^{L(R)}}{\sqrt{2}}, & A_0^{L(R)} &= H_{00}^{L(R)}, \\ A_\parallel^{L(R)} &= \frac{H_{++}^{L(R)} + H_{--}^{L(R)}}{\sqrt{2}}, & A_t^{L(R)} &= H_{0t}^{L(R)}, \end{aligned} \quad (2.130)$$

<sup>14</sup>Please notice that the convention used in eq. (2.43) is such that  $\varepsilon_{0123} = +1$ .

which can be compactly written as

$$A_{\perp}^{L(R)} = \mathcal{N}_{K^*} \sqrt{2} \lambda_B^{1/2} \left[ [(C_9 + C'_9) \mp (C_{10} + C'_{10})] \frac{V(q^2)}{m_B + m_{K^*}} + \delta_{\ell_1 \ell_2} \frac{2m_b}{q^2} (C_7 + C'_7) T_1(q^2) \right], \quad (2.131)$$

$$A_{\parallel}^{L(R)} = -\mathcal{N}_{K^*} \sqrt{2} (m_B^2 - m_{K^*}^2) \left[ [(C_9 - C'_9) \mp (C_{10} - C'_{10})] \frac{A_1(q^2)}{m_B - m_{K^*}} + \delta_{\ell_1 \ell_2} \frac{2m_b}{q^2} (C_7 - C'_7) T_2(q^2) \right],$$

$$A_0^{L(R)} = -\frac{\mathcal{N}_{K^*}}{2m_{K^*} \sqrt{q^2}} \left\{ \delta_{\ell_1 \ell_2} 2m_b (C_7 - C'_7) \left[ (m_B^2 + 3m_{K^*}^2 - q^2) T_2(q^2) - \frac{\lambda_B T_3(q^2)}{m_B^2 - m_{K^*}^2} \right] \right. \\ \left. + [(C_9 - C'_9) \mp (C_{10} - C'_{10})] \cdot \left[ (m_B^2 - m_{K^*}^2 - q^2) (m_B + m_{K^*}) A_1(q^2) - \frac{\lambda_B A_2(q^2)}{m_B + m_{K^*}} \right] \right\},$$

$$A_t^{L(R)} = -\mathcal{N}_{K^*} \frac{\lambda_B^{1/2}}{\sqrt{q^2}} \left[ (C_9 - C'_9) \mp (C_{10} - C'_{10}) + \frac{q^2}{m_b + m_s} \left( \frac{C_S - C'_S}{m_1 - m_2} \mp \frac{C_P - C'_P}{m_1 + m_2} \right) \right] A_0(q^2).$$

Notice that the first three expressions are the same than Eq. (2.77). In terms of the transversity amplitudes given above, the angular coefficients  $I_{1-9}(q^2)$  are given by

$$I_1^s(q^2) = \left[ |A_{\perp}^L|^2 + |A_{\parallel}^L|^2 + (L \rightarrow R) \right] \frac{\lambda_q + 2[q^4 - (m_1^2 - m_2^2)^2]}{4q^4} + \frac{4m_1 m_2}{q^2} \text{Re} \left( A_{\parallel}^L A_{\parallel}^{R*} + A_{\perp}^L A_{\perp}^{R*} \right), \quad (2.132)$$

$$I_1^c(q^2) = \left[ |A_0^L|^2 + |A_0^R|^2 \right] \frac{q^4 - (m_1^2 - m_2^2)^2}{q^4} + \frac{8m_1 m_2}{q^2} \text{Re} (A_0^L A_0^{R*} - A_t^L A_t^{R*}) \\ - 2 \frac{(m_1^2 - m_2^2)^2 - q^2 (m_1^2 + m_2^2)}{q^4} (|A_t^L|^2 + |A_t^R|^2), \quad (2.133)$$

$$I_2^s(q^2) = \frac{\lambda_q}{4q^4} \left[ |A_{\perp}^L|^2 + |A_{\parallel}^L|^2 + (L \rightarrow R) \right], \quad (2.134)$$

$$I_2^c(q^2) = -\frac{\lambda_q}{q^4} (|A_0^L|^2 + |A_0^R|^2), \quad (2.135)$$

$$I_3(q^2) = \frac{\lambda_q}{2q^4} \left[ |A_{\perp}^L|^2 - |A_{\parallel}^L|^2 + (L \rightarrow R) \right], \quad (2.136)$$

$$I_4(q^2) = -\frac{\lambda_q}{\sqrt{2} q^4} \text{Re} (A_{\parallel}^L A_0^{L*} + (L \rightarrow R)), \quad (2.137)$$

$$I_5(q^2) = \frac{\sqrt{2} \lambda_q^{1/2}}{q^2} \left[ \text{Re} (A_0^L A_{\perp}^{L*} - (L \rightarrow R)) - \frac{m_1^2 - m_2^2}{q^2} \text{Re} (A_t^L A_{\parallel}^{L*} + (L \rightarrow R)) \right], \quad (2.138)$$

$$I_6^s(q^2) = -\frac{2\lambda_q^{1/2}}{q^2} [\text{Re} (A_{\parallel}^L A_{\perp}^{L*} - (L \rightarrow R))], \quad (2.139)$$

$$I_6^c(q^2) = -\frac{4\lambda_q^{1/2}}{q^2} \frac{m_1^2 - m_2^2}{q^2} \text{Re} (A_0^L A_t^{L*} + (L \rightarrow R)), \quad (2.140)$$

$$I_7(q^2) = -\frac{\sqrt{2} \lambda_q^{1/2}}{q^2} \left[ \text{Im} (A_0^L A_{\parallel}^{L*} - (L \rightarrow R)) + \frac{m_1^2 - m_2^2}{q^2} \text{Im} (A_{\perp}^L A_t^{L*} + (L \rightarrow R)) \right], \quad (2.141)$$

$$I_8(q^2) = \frac{\lambda_q}{\sqrt{2}q^4} \text{Im}(A_0^L A_{\perp}^{L*} + (L \rightarrow R)), \quad (2.142)$$

$$I_9(q^2) = -\frac{\lambda_q}{q^4} \text{Im}(A_{\perp}^L A_{\parallel}^{L*} + A_{\perp}^R A_{\parallel}^{R*}), \quad (2.143)$$

Once again, by taking the limit  $m_1 \rightarrow m_2$ , one retrieves the usual expressions for the coefficients of the angular distribution of  $\bar{B} \rightarrow \bar{K}^* \ell^+ \ell^-$ . Our expressions agree with those recently presented in Ref. [156], and are related to those given in Ref. [123] via  $I_{4,6,7,9} \rightarrow -I_{4,6,7,9}$ .<sup>15</sup> In order to compare with usual expressions for  $A_t$  and  $A_S$ , as defined in Sec. 2.3, one needs to identify

$$A_t = \lim_{m_1 \rightarrow m_2} (A_t^L - A_t^R), \quad A_S = \lim_{m_1 \rightarrow m_2} \left[ \frac{m_1 - m_2}{\sqrt{q^2}} (A_t^L + A_t^R) \right]. \quad (2.144)$$

### 2.5.4 Numerical significance

To illustrate numerically the significance of the factors multiplying the Wilson coefficients, we use the form factors of Ref. [159] and distinguish the case of LFV arising from the vector operators, i.e.

$$\begin{aligned} \mathcal{B}(\bar{B} \rightarrow \bar{K}^{(*)} \ell_1 \ell_2) = 10^{-9} & \left( a_{K^{(*)}}^{12} |C_9 + C'_9|^2 + b_{K^{(*)}}^{12} |C_{10} + C'_{10}|^2 \right. \\ & \left. + c_{K^{(*)}}^{12} |C_9 - C'_9|^2 + d_{K^{(*)}}^{12} |C_{10} - C'_{10}|^2 \right), \end{aligned} \quad (2.145)$$

from the case in which the LFV comes from the scalar operators,

$$\begin{aligned} \mathcal{B}(\bar{B} \rightarrow \bar{K}^{(*)} \ell_1 \ell_2) = 10^{-9} & \left( e_{K^{(*)}}^{12} |C_S + C'_S|^2 + f_{K^{(*)}}^{12} |C_P + C'_P|^2 \right. \\ & \left. + g_{K^{(*)}}^{12} |C_S - C'_S|^2 + h_{K^{(*)}}^{12} |C_P - C'_P|^2 \right), \end{aligned} \quad (2.146)$$

The values of the factors multiplying the Wilson coefficients are obtained after integrating over all available  $q^2$ 's and are listed in Table 2.7 and Table 2.8.

$\ell_1 \ell_2$	$a_{K^*}^{12}$	$b_{K^*}^{12}$	$c_{K^*}^{12}$	$d_{K^*}^{12}$	$a_K^{12}$	$b_K^{12}$	$c_K^{12}$	$d_K^{12}$
$e\mu$	7.8(9)	7.8(9)	34(6)	34(6)	20(2)	20(2)	0	0
$e\tau$	3.8(4)	3.9(4)	18(2)	18(2)	12.7(9)	12.7(9)	0	0
$\mu\tau$	4.1(5)	3.6(4)	18(2)	17(2)	12.5(1.0)	12.9(9)	0	0

**Table 2.7:** Values for the multiplicative factors defined in eq. (2.145). The quoted uncertainties are at the  $1\sigma$  level.

Notice also that the functions which are being integrated to obtain those factors have a peculiar feature: those which multiply  $|C_{9,10} \pm C'_{9,10}|^2$  are more pronounced in the intermediate  $q^2$  region, whereas those multiplying  $|C_{S,P} \pm C'_{S,P}|^2$  are mostly receiving contributions

$\ell_1 \ell_2$	$e_{K^*}^{12}$	$f_{K^*}^{12}$	$g_{K^*}^{12}$	$h_{K^*}^{12}$	$e_K^{12}$	$f_K^{12}$	$g_K^{12}$	$h_K^{12}$
$e\mu$	0	0	12(1)	12(1)	26.2(4)	26.2(4)	0	0
$e\tau$	0	0	5.5(6)	5.5(6)	15.0(2)	15.0(2)	0	0
$\mu\tau$	0	0	5.2(6)	5.8(7)	14.4(2)	15.5(2)	0	0

**Table 2.8:** Values for the multiplicative factors defined in eq. (2.146) to  $1\sigma$  accuracy.

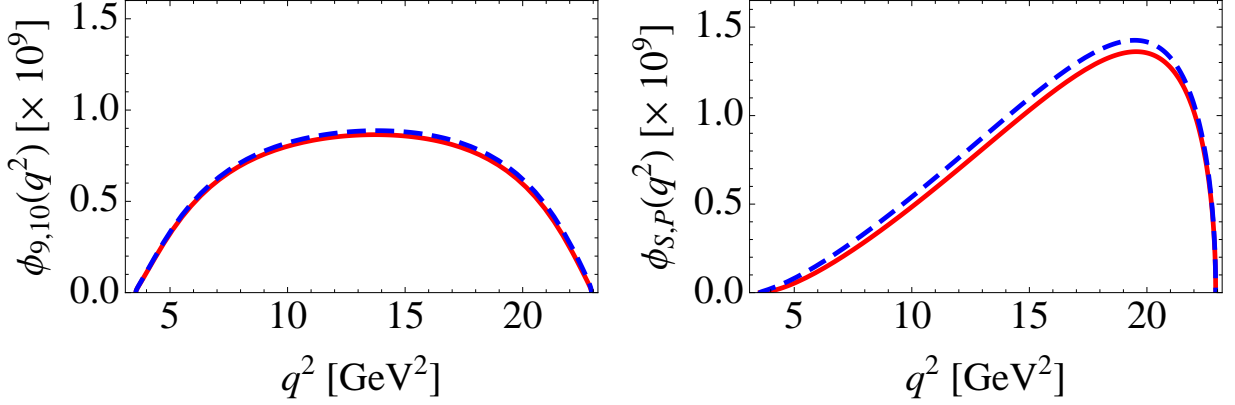


**Figure 2.12:** Coefficient functions  $\phi_{9,10}(q^2) = |\mathcal{N}_K(q^2)|^2 \varphi_{9,10}(q^2)$  and  $\phi_{S,P}(q^2) = |\mathcal{N}_K(q^2)|^2 \varphi_{S,P}(q^2)$  appearing in eq. (2.107), which after integration over  $q^2$  give the factors  $a_K^{\mu\tau}$ ,  $b_K^{\mu\tau}$ ,  $e_K^{\mu\tau}$  and  $f_K^{\mu\tau}$  in eqs. (2.145, 2.146). Full curves correspond to  $\phi_9(q^2)$  and  $\phi_S(q^2)$ , while the dashed ones to  $\phi_{10}(q^2)$  and  $\phi_P(q^2)$ .

from the large  $q^2$  region. To illustrate this feature, we show in Fig. 2.12 the coefficient functions  $\varphi_{9,10}(q^2)$  [ $\varphi_{S,P}(q^2)$ ], which upon integration amount to  $a_K^{\mu\tau}$  and  $b_K^{\mu\tau}$  [ $e_K^{\mu\tau}$  and  $f_K^{\mu\tau}$ ].<sup>16</sup>

Furthermore in the case of LFV generated by the scalar operators the lifted helicity suppression of the leptonic decay (2.104) leads to the following hierarchy among different modes:

$$C_{S,P}^{(\prime)} \neq 0, C_{9,10}^{(\prime)} = 0: \quad \mathcal{B}(B_s \rightarrow \ell_1 \ell_2) > \mathcal{B}(B \rightarrow K \ell_1 \ell_2) > \mathcal{B}(B \rightarrow K^* \ell_1 \ell_2). \quad (2.147)$$

That hierarchy is inverted for the LFV processes generated by the vector operators, namely

$$C_{S,P}^{(\prime)} = 0, C_{9,10}^{(\prime)} \neq 0: \quad \mathcal{B}(B_s \rightarrow \ell_1 \ell_2) < \mathcal{B}(B \rightarrow K \ell_1 \ell_2) < \mathcal{B}(B \rightarrow K^* \ell_1 \ell_2). \quad (2.148)$$

Of course the above discussion is valid as long as we do not consider the case of LFV generated by both the scalar and vector operators, which we will not discuss in what follows anyway.

Finally, the scenarios which satisfy  $C_9^{(\prime)} = -C_{10}^{(\prime)}$  will be extensively discussed in Chapter 4, since they are motivated by the anomalies in the  $b \rightarrow s\mu\mu$  transitions. In this case,

<sup>15</sup>Notice that in Ref. [123] the convention for the helicity vectors is inconsistent with the expressions given for the helicity amplitudes.

<sup>16</sup>The purpose of the plots shown in Fig. 2.12 is to illustrate the shapes of  $\phi_i(q^2) = |\mathcal{N}_K(q^2)|^2 \varphi_i(q^2)$  and the uncertainties on hadronic form factors were omitted in the plots. Those uncertainties, instead, have been properly accounted for when computing the factors listed in Tab. 2.8.

it is straightforward to verify from the expressions given above that the ratios between different modes are constant and given by

$$\frac{\mathcal{B}(B_s \rightarrow \mu\tau)}{\mathcal{B}(B \rightarrow K\mu\tau)} \approx 0.9 \quad \text{and} \quad \frac{\mathcal{B}(B \rightarrow K^*\mu\tau)}{\mathcal{B}(B \rightarrow K\mu\tau)} \approx 1.8, \quad (2.149)$$

where we considered the central values for the hadronic parameters. Therefore, experimental limits can be translated from one mode to another in these specific scenarios.

# Chapter 3

## Scrutinizing Two-Higgs doublet models

After decades of restless experimental effort, a scalar particle with SM-like properties was found at the LHC in 2012 [1, 2]. Nonetheless, the nature of NP has not been unveiled in the first runs of the LHC, leaving the hierarchy and flavor problems unsolved. One of the minimal extensions of the SM consists in enlarging the Higgs sector and, instead of one doublet of scalar fields, introducing an additional Higgs doublet, which comes under the generic name of Two Higgs Doublet Model (2HDM) [7]. With a peculiar choice of Yukawa couplings, 2HDM is embedded in the minimal supersymmetric extension of the Standard Model (MSSM) which made it particularly popular in phenomenological applications of low energy supersymmetry. The fact that the mass of observed Higgs boson was found to be consistent with the SM expectations made MSSM less compelling but the 2HDM remains a convenient framework to study the extensions of the Higgs sector in view of the current experimental searches.

In this Chapter we will discuss the theory and phenomenology of 2HDM, focusing on two main questions: (i) Which lessons on their spectrum can be learned by applying the general theory and phenomenological constraints? (ii) Which are the most sensitive low energy probes of the additional scalars in modern day experiments? To that purpose, we will compute the complete set of Wilson coefficients to the relevant processes, which include in particular the  $b \rightarrow s\ell^+\ell^-$  transition, and confront these results with the current experimental results.

The Chapter is organized as follows: in Sec. 3.1 we discuss the general features of 2HDM, and the general theory constraints on their scalar spectrum. In Sec. 3.2, we perform a scan of parameters by assuming that the additional scalars lie above the EW scale, as motivated by the lack of direct search signals at LHC. In Sec. 3.3, we derive the relevant constraints on the charged Higgs contributions which can be derived from tree-level meson decays. In Sec. 3.4, we derive the complete set of Wilson coefficients for the transition  $b \rightarrow s\ell^+\ell^-$  and discuss the subtleties in the matching between full and effective theories when the external momenta of fermions is kept nonzero. These results are then used in Sec. 3.5 to derive constraints on the model parameters by relying on the exclusive  $b \rightarrow s\ell^+\ell^-$  decays. Finally, the intriguing possibility of having a light CP-odd Higgs which escaped observation so far is discussed on Sec. 3.6. Our proposals to indirectly probe a scenario with a light CP-odd Higgs in modern day experiments are discussed in Sec. 3.7 and Sec. 3.8.

## 3.1 General aspects of 2HDM

In this Section we introduce our notation, remind the reader of the basic ingredients of 2HDM and list the main general constraints which will be used to perform a scan of the allowed parameters of the model in the following Sections.

### 3.1.1 The extended scalar sector

We consider a general CP-conserving 2HDM with a softly broken  $\mathbb{Z}_2$  symmetry. As we will discuss in the following, the  $\mathbb{Z}_2$  symmetry is imposed to prevent Higgs mediated FCNC from appearing at tree-level. The most general scalar potential consistent with these conditions is given by

$$V(\Phi_1, \Phi_2) = m_{11}^2 \Phi_1^\dagger \Phi_1 + m_{22}^2 \Phi_2^\dagger \Phi_2 + m_{12}^2 (\Phi_1^\dagger \Phi_2 + \Phi_2^\dagger \Phi_1) + \frac{\lambda_1}{2} (\Phi_1^\dagger \Phi_1)^2 + \frac{\lambda_2}{2} (\Phi_2^\dagger \Phi_2)^2 + \lambda_3 \Phi_1^\dagger \Phi_1 \Phi_2^\dagger \Phi_2 + \lambda_4 \Phi_1^\dagger \Phi_2 \Phi_2^\dagger \Phi_1 + \frac{\lambda_5}{2} [(\Phi_1^\dagger \Phi_2)^2 + (\Phi_2^\dagger \Phi_1)^2], \quad (3.1)$$

where  $\Phi_a$  ( $a = 1, 2$ ) are the two scalar doublets and  $\lambda_i \in \mathbb{R}$  are quartic couplings. The quadratic term  $m_{12}^2$  is responsible for the soft breaking of the  $\mathbb{Z}_2$  symmetry, and it is needed to produce a realistic spectrum of scalars and ensure the decoupling limit.<sup>1</sup> The weak doublets can be parameterized as

$$\Phi_a = \begin{pmatrix} \phi_a^+ \\ \frac{1}{\sqrt{2}}(v_a + \rho_a + i\eta_a) \end{pmatrix}, \quad a = 1, 2, \quad (3.2)$$

where  $v_{1,2} > 0$  are the two vacuum expectation values (vev) satisfying  $v^{\text{SM}} = \sqrt{v_1^2 + v_2^2} \approx 246.22$  GeV.<sup>2</sup> Three out of the eight degrees of freedom are eaten up by the gauge bosons, while the remaining fields are two CP-even scalars  $h$  and  $H$ , one CP-odd  $A$ , and one charged Higgs  $H^\pm$ . These fields can be expressed as

$$\begin{pmatrix} \phi_1^+ \\ \phi_2^+ \end{pmatrix} = \begin{pmatrix} \cos \beta & -\sin \beta \\ \sin \beta & \cos \beta \end{pmatrix} \begin{pmatrix} G^+ \\ H^+ \end{pmatrix}, \quad \begin{pmatrix} \eta_1 \\ \eta_2 \end{pmatrix} = \begin{pmatrix} \cos \beta & -\sin \beta \\ \sin \beta & \cos \beta \end{pmatrix} \begin{pmatrix} G^0 \\ A^0 \end{pmatrix}, \quad (3.3)$$

and

$$\begin{pmatrix} \rho_1 \\ \rho_2 \end{pmatrix} = \begin{pmatrix} \cos \alpha & -\sin \alpha \\ \sin \alpha & \cos \alpha \end{pmatrix} \begin{pmatrix} H \\ h \end{pmatrix}, \quad (3.4)$$

where the rotation angles  $\alpha$  and  $\beta$  satisfy

<sup>1</sup> We remind the reader that the  $\mathbb{Z}_2$  symmetry ( $\Phi_1 \rightarrow \pm \Phi_1, \Phi_2 \rightarrow \mp \Phi_2$ ) of the Lagrangian forbids transitions  $\Phi_1 \leftrightarrow \Phi_2$ . Soft breaking of  $\mathbb{Z}_2$  means that such transitions may occur only due to dimension-2 operators (terms proportional to  $m_{12}^2$  in Eq. (3.1)) so that  $\mathbb{Z}_2$  remains preserved at very short distances, cf. discussion in Ref. [160].

<sup>2</sup>The case where one of the vevs vanishes is called the inert 2HDM. Although this possibility is considered in many studies of dark matter [161, 162], we will discard it in the following since it is evasive from flavor physics constraints, i.e. the additional scalars have no couplings to fermions.

$$\tan \beta = \frac{v_2}{v_1}, \quad \tan 2\alpha = \frac{2(-m_{12}^2 + \lambda_{345}v_1v_2)}{m_{12}^2(v_2/v_1 - v_1/v_2) + \lambda_1v_1^2 - \lambda_2v_2^2}. \quad (3.5)$$

The tree-level expressions for the scalar masses are given by

$$m_H^2 = M^2 \sin^2(\alpha - \beta) + \left( \lambda_1 \cos^2 \alpha \cos^2 \beta + \lambda_2 \sin^2 \alpha \sin^2 \beta + \frac{\lambda_{345}}{2} \sin 2\alpha \sin 2\beta \right) v^2 \quad (3.6)$$

$$m_h^2 = M^2 \cos^2(\alpha - \beta) + \left( \lambda_1 \sin^2 \alpha \cos^2 \beta + \lambda_2 \cos^2 \alpha \sin^2 \beta - \frac{\lambda_{345}}{2} \sin 2\alpha \sin 2\beta \right) v^2 \quad (3.7)$$

$$m_A^2 = M^2 - \lambda_5 v^2, \quad (3.8)$$

$$m_{H^\pm}^2 = M^2 - \frac{\lambda_4 + \lambda_5}{2} v^2, \quad (3.9)$$

where the  $\mathbb{Z}_2$  breaking is parameterized by  $M^2 \equiv m_{12}^2/(\sin \beta \cos \beta)$  and we write for shortness  $\lambda_{345} \equiv \lambda_3 + \lambda_4 + \lambda_5$ .

### Decoupling limit and alignment

Several messages can be already learned from the equations given above. Since the quartic couplings are bounded by the perturbative requirement,  $|\lambda_i| < \sqrt{4\pi}$ , it is clear from Eqs. (3.6)–(3.9) that the decoupling limit must be driven by the soft-breaking parameter  $M^2$ . To quantify this statement, let us evaluate  $\cos^2(\beta - \alpha)$  in the large  $M^2$  limit. By using the relations given above, one can write

$$\sin(2\alpha) = \frac{2\mathcal{M}_{12}^2}{\sqrt{(\mathcal{M}_{11}^2 - \mathcal{M}_{22}^2)^2 + 4\mathcal{M}_{12}^2}}, \quad \cos(2\alpha) = \frac{\mathcal{M}_{11}^2 - \mathcal{M}_{22}^2}{\sqrt{(\mathcal{M}_{11}^2 - \mathcal{M}_{22}^2)^2 + 4\mathcal{M}_{12}^2}}, \quad (3.10)$$

where  $\mathcal{M}_{ij} \equiv (\mathcal{M})_{ij}$  are the elements of the CP-even mass matrix,

$$\mathcal{M} = \begin{pmatrix} \lambda_1 v^2 \cos^2 \beta + M^2 \sin^2 \beta & (\lambda_{345} v^2 - M^2) \sin \beta \cos \beta \\ (\lambda_{345} v^2 - M^2) \sin \beta \cos \beta & \lambda_2 v^2 \sin^2 \beta + M^2 \cos^2 \beta \end{pmatrix}. \quad (3.11)$$

By combining Eq. (3.10) and Eq. (3.11), we obtain after Taylor expanding in  $1/M^2$ ,

$$\begin{aligned} \cos^2(\beta - \alpha) &= \frac{1 + \cos(2\beta) \cos(2\alpha) - \sin(2\beta) \sin(2\alpha)}{2} \\ &= \frac{v^4 \sin^2(2\beta)}{16M^4} \left[ \lambda_1 - \lambda_2 + \cos(2\beta)(\lambda_1 + \lambda_2 - 2\lambda_{345}) \right] + \mathcal{O}(v^6/M^6), \end{aligned} \quad (3.12)$$

which can be rewritten by using the equations given above as

$$\cos^2(\beta - \alpha) = \frac{(m_H^2 - m_h^2)^2}{2M^4} \sin^2(2(\beta - \alpha)) + \mathcal{O}(v^6/M^6). \quad (3.13)$$

Therefore, the alignment limit,  $\cos(\beta - \alpha) \rightarrow 0$ , is retrieved in the decoupling limit,  $M^2 \rightarrow +\infty$ . Furthermore, the replacement of this identity in Eqs. (3.6)–(3.9) gives precisely the decoupling limit in the large  $M^2$  limit,

$$\begin{aligned} m_h^2 &= \lambda_1 v^2 + \mathcal{O}(v^4/M^2), \\ m_H^2, m_A^2, m_{H^\pm}^2 &= M^2 + \mathcal{O}(v^4/M^2), \end{aligned} \quad (3.14)$$

where  $h$  is identified as the SM Higgs, while the other scalars are heavy and approximately mass degenerate. Furthermore, one can show that the alignment condition,  $\cos(\beta - \alpha) \approx 0$ , ensures that  $h$  has SM-like couplings to  $V = W, Z$ , while the couplings of  $H$  with gauge bosons vanish in the same limit. It is worth stressing that these conclusions are completely independent on the values of  $\tan \beta$ .

### 3.1.2 Including fermions

In the fermionic sector, the second scalar doublet can spoil the suppression of FCNC processes, one of the main properties of the SM, which has been extensively tested at low-energies. To illustrate this issue, we consider the Yukawa Lagrangian terms which give mass to down-type quarks,

$$\mathcal{L}_{\text{Yuk}}^d = -Y_{ij}^{(1)} \bar{Q}_i \Phi_1 d_{Rj} - Y_{ij}^{(2)} \bar{Q}_i \Phi_2 d_{Rj} + \text{h.c.}, \quad (3.15)$$

where  $i, j$  are fermion generation indices, and  $Y^{(1)}$  and  $Y^{(2)}$  are the Yukawa matrices. In terms of the physical scalars, the neutral terms in the Yukawa Lagrangian can be written as

$$\mathcal{L}_{\text{Yuk}}^d \supset -\mathcal{M}_{ij}^d \bar{d}_{Li} d_{Rj} - \sum_{\varphi_k^0 = h, H, A} y_{ij}^{\varphi_k^0} \bar{d}_{Li} d_{Rj} \varphi_k^0 + \text{h.c.}, \quad (3.16)$$

where the fermion mass matrix reads,

$$\mathcal{M}_{ij}^d = \frac{v}{\sqrt{2}} \left( Y_{ij}^{(1)} \cos \beta + Y_{ij}^{(2)} \sin \beta \right), \quad (3.17)$$

while the interactions of down-type quarks depend on a different combination of the Yukawa matrices,

$$\begin{aligned} y_{ij}^A &= \frac{i}{\sqrt{2}} \left( -Y_{ij}^{(1)} \sin \beta + Y_{ij}^{(2)} \cos \beta \right), \\ y_{ij}^h &= \frac{i}{\sqrt{2}} \left( -Y_{ij}^{(1)} \sin \alpha + Y_{ij}^{(2)} \cos \alpha \right), \\ y_{ij}^H &= \frac{i}{\sqrt{2}} \left( Y_{ij}^{(1)} \cos \alpha + Y_{ij}^{(2)} \sin \alpha \right). \end{aligned} \quad (3.18)$$

Since the matrices  $Y^{(i)}$  are not necessarily simultaneously diagonalizable, tree-level interactions of the type  $\bar{d}_i d_j \varphi_k^0$  (with  $i \neq j$ ) can appear after the diagonalization of the fermion masses  $\mathcal{M}_{ij}^d$ . Therefore, a mechanism is needed to suppress these dangerous couplings, which are otherwise constrained by experimental data of decays of Kaons,  $D$  and  $B_{(s)}$  mesons, as already discussed in Sec. 2.3.

The simplest possibility to suppress the tree-level FCNC in 2HDMs is to invoke a  $\mathbb{Z}_2$  symmetry, which enforces that each quark doublet couples to a single scalar doublet [163,

164]. Four models are then possible, which are called of type I, II, X (lepton specific) and Z (flipped) [7]. In the type I 2HDM, all fermions couples only to the Higgs doublet  $\Phi_2$ . In the type II 2HDM,  $u_R$  couples to  $\Phi_2$ , while  $d_R$  and  $\ell_R$  couple to  $\Phi_1$ . The models type X and Z are then obtained by changing the lepton interactions in the models type I and type II, respectively, as shown in Table 3.1. As an illustration of the assignment of the  $\mathbb{Z}_2$  symmetry charges, the type I model can be obtained simply by imposing  $\Phi_1 \rightarrow -\Phi_1$  along with positive  $\mathbb{Z}_2$  charges to the SM fermion. Similarly, the type II couplings are obtained by imposing  $\Phi_1 \rightarrow -\Phi_1$ ,  $\ell_{Ri} \rightarrow -\ell_{Ri}$  and  $d_{Ri} \rightarrow -d_{Ri}$ , while the other fermions are assigned to transform with a plus sign.

Model	$u_R$	$d_R$	$\ell_R$
Type I	$\Phi_2$	$\Phi_2$	$\Phi_2$
Type II	$\Phi_2$	$\Phi_1$	$\Phi_1$
Type X (lepton specific)	$\Phi_2$	$\Phi_2$	$\Phi_1$
Type Z (flipped)	$\Phi_2$	$\Phi_1$	$\Phi_2$

**Table 3.1:** Couplings of fermions to Higgs doublets in the 2HDM based on discrete symmetries. See text for details.

Another possibility to suppress FCNC rates is to enforce the two Yukawa matrices in Eq. (3.15) to be collinear and hence simultaneously diagonalizable by construction, as proposed in the so-called Aligned two-Higgs doublet model (A2HDM) [165]. Remarkably, the models with a  $\mathbb{Z}_2$  symmetry turn out to be an asymptotic limit of the aligned scenarios. It is important to note that the alignment of Yukawa matrices are in general broken by radiative corrections. The  $\mathbb{Z}_2$ -symmetry models represent the only scenarios in which the alignment is preserved at all scales [166].

Finally, the most general model is conventionally called type III 2HDM. In this case, no mechanism is used to protect from appearing at tree-level FCNC mediated by scalars. The FCNC Higgs couplings, which are present at tree-level, are then suppressed by *ad hoc* ansatz for the Yukawa matrices or by a tuning of the parameters. We will not consider this possibility in this thesis given the large number of couplings which undermine the predictivity of these scenarios. See Ref. [7] for an extensive discussion about this possibility.

In the following we will focus on the  $\mathbb{Z}_2$  symmetric models due to their simplicity. For these models, the Yukawa Lagrangian after the spontaneous symmetry breaking can be compactly written as

$$\begin{aligned} \mathcal{L}_Y = & -\frac{\sqrt{2}}{v} H^+ \left\{ \bar{u} [\zeta_d V m_d P_R - \zeta_u m_u V P_L] d + \zeta_\ell \bar{\nu} m_\ell P_R \ell \right\} \\ & -\frac{1}{v} \sum_{\varphi_i^0=h,H,A} \xi_f^{\varphi_i^0} \varphi_i^0 [\bar{f} m_f P_R f] + \text{h.c.}, \end{aligned} \quad (3.19)$$

where  $u$  and  $d$  stand for the up- and down-type quark,  $\ell$  is a lepton flavor,  $f$  stands for a generic fermion,  $V$  for the CKM matrix. A specific choice of parameters  $\zeta_f$  corresponds to the above mentioned types of 2HDM, which we also summarize in Table 3.2. Notice that the couplings  $\xi_f^{\varphi_i^0}$  appearing in the neutral Lagrangian part can be mapped onto the charged ones via

$$\xi_f^h = \sin(\beta - \alpha) + \cos(\beta - \alpha)\zeta_f \quad (3.20)$$

$$\xi_f^H = \cos(\beta - \alpha) - \sin(\beta - \alpha)\zeta_f, \quad (3.21)$$

$$\xi_{d,\ell}^A = i\zeta_{d,\ell}, \quad \xi_u^A = -i\zeta_u. \quad (3.22)$$

Model	$\zeta_u$	$\zeta_d$	$\zeta_\ell$
Type I	$\cot \beta$	$\cot \beta$	$\cot \beta$
Type II	$\cot \beta$	$-\tan \beta$	$-\tan \beta$
Type X (lepton specific)	$\cot \beta$	$\cot \beta$	$-\tan \beta$
Type Z (flipped)	$\cot \beta$	$-\tan \beta$	$\cot \beta$

**Table 3.2:** The expressions of the couplings  $\zeta_f$  for the 2HDM based on discrete symmetries.

In the next subsection we will discuss the general constraints on the spectrum of the general CP-conserving 2HDM models, and we will describe our methodology to scan their parameter space.

### 3.1.3 Model spectrum and theory constraints

The parameter space of the models we consider is composed of two angle parameters ( $\alpha$  and  $\beta$ ), and five mass parameters ( $m_h^2$ ,  $m_H^2$ ,  $m_{H^\pm}^2$ ,  $m_A^2$  and  $M^2$ ). From these, one can fully reconstruct the quartic couplings in the scalar potential (3.1) via the relations,

$$\lambda_1 = \frac{1}{v^2} \left( -\tan^2 \beta M^2 + \frac{\sin^2 \alpha}{\cos^2 \beta} m_h^2 + \frac{\cos^2 \alpha}{\cos^2 \beta} m_H^2 \right), \quad (3.23)$$

$$\lambda_2 = \frac{1}{v^2} \left( -\cot^2 \beta M^2 + \frac{\cos^2 \alpha}{\sin^2 \beta} m_h^2 + \frac{\sin^2 \alpha}{\sin^2 \beta} m_H^2 \right), \quad (3.24)$$

$$\lambda_3 = \frac{1}{v^2} \left( -M^2 + 2m_{H^\pm}^2 + \frac{\sin 2\alpha}{\sin 2\beta} (m_H^2 - m_h^2) \right), \quad (3.25)$$

$$\lambda_4 = \frac{1}{v^2} (M^2 + m_A^2 - 2m_{H^\pm}^2), \quad (3.26)$$

$$\lambda_5 = \frac{1}{v^2} (M^2 - m_A^2), \quad (3.27)$$

which are then subject to several theoretical constraints. Notice that Eq. (3.23)–(3.27) are equivalent to Eq. (3.5) and (3.6)–(3.9).

To scan over the allowed parameters of these models, we impose the following general constraints:

- Stability:

To ensure that the scalar potential is bounded from below, the quartic couplings should satisfy [167]

$$\lambda_{1,2} > 0, \quad \lambda_3 > -(\lambda_1\lambda_2)^{1/2}, \quad \text{and} \quad \lambda_3 + \lambda_4 - |\lambda_5| > -(\lambda_1\lambda_2)^{1/2}. \quad (3.28)$$

Moreover, the tree-level stability of the vacuum amounts to

$$m_{11}^2 + \frac{\lambda_1 v_1^2}{2} + \frac{\lambda_3 v_2^2}{2} = \frac{v_2}{v_1} \left[ m_{12}^2 - (\lambda_4 + \lambda_5) \frac{v_1 v_2}{2} \right], \quad (3.29)$$

$$m_{22}^2 + \frac{\lambda_2 v_2^2}{2} + \frac{\lambda_3 v_1^2}{2} = \frac{v_1}{v_2} \left[ m_{12}^2 - (\lambda_4 + \lambda_5) \frac{v_1 v_2}{2} \right], \quad (3.30)$$

which determines the parameters  $m_{11}^2$  and  $m_{22}^2$  in terms of  $\lambda_{1-5}$  and  $M^2$ . These relations should be combined with the necessary and sufficient condition to have a global minimum of  $(v_1, v_2)$ , which reads [168]

$$m_{12}^2 \left( m_{11}^2 - m_{22}^2 \sqrt{\lambda_1/\lambda_2} \right) \left( \tan \beta - \sqrt[4]{\lambda_1/\lambda_2} \right) > 0. \quad (3.31)$$

- **Perturbative Unitarity:**

Another important condition stems from the requirement of unitarity of the scalar scattering amplitudes [169]. More precisely, the  $J$ -th partial wave for a  $2 \rightarrow 2$  scattering process, with center of mass energy  $\sqrt{s}$ , is defined by

$$a_J(s) = \frac{1}{32\pi} \int d \cos \theta P_J(\cos \theta) \mathcal{M}(s, \theta), \quad (3.32)$$

where  $\theta$  is the diffusion angle,  $P_J(\cos \theta)$  is the  $J$ -th Legendre polynomial and  $\mathcal{M}(s, \theta)$  is the amplitude for this process. The unitarity requirement of the  $S$ -wave component of the partial wave decomposition implies that  $|a_0| < 1$ . By applying this bound to the eigenvalues of the scalar scattering matrix, one can obtain the following limits on the quartic couplings [170, 171]

$$|a_{\pm}|, |b_{\pm}|, |c_{\pm}|, |f_{\pm}|, |e_{1,2}|, |f_1|, |p_1| < 8\pi, \quad (3.33)$$

where the tree-level computation gives

$$\begin{aligned}
 a_{\pm} &= \frac{3}{2}(\lambda_1 + \lambda_2) \pm \sqrt{\frac{9}{4}(\lambda_1 - \lambda_2)^2 + (2\lambda_3 + \lambda_4)^2}, \\
 b_{\pm} &= \frac{1}{2}(\lambda_1 + \lambda_2) \pm \frac{1}{2}\sqrt{(\lambda_1 - \lambda_2)^2 + 4\lambda_4^2}, \\
 c_{\pm} &= \frac{1}{2}(\lambda_1 + \lambda_2) \pm \frac{1}{2}\sqrt{(\lambda_1 - \lambda_2)^2 + 4\lambda_5^2}, \\
 e_1 &= \lambda_3 + 2\lambda_4 - 3\lambda_5, \\
 f_+ &= \lambda_3 + 2\lambda_4 + 3\lambda_5, \\
 e_2 &= \lambda_3 - \lambda_5, \\
 f_- &= \lambda_3 + \lambda_5, \\
 f_1 &= \lambda_3 + \lambda_4, \\
 p_1 &= \lambda_3 - \lambda_4.
 \end{aligned} \tag{3.34}$$

Notice that the inequalities in Eq. (3.33) give more restrictive constraints than the naive perturbative conditions  $|\lambda_i| < \sqrt{4\pi}$ .

- **Higgs Gauge Couplings:**

The Higgs couplings to gauge bosons read

$$\mathcal{L}_{2\text{HDM}} \supset g m_W \lambda_{VV}^{\varphi_i^0} W_\mu W^\mu \varphi_i^0 + g m_W \lambda_{VV}^{\varphi_i^0} Z_\mu Z^\mu \varphi_i^0, \tag{3.35}$$

where  $\varphi_i^0 \in \{h, H, A\}$  and the couplings are given by

$$\lambda_{VV}^{\varphi_i^0} = \begin{cases} \sin(\beta - \alpha) & \text{if } \varphi_i^0 = h \\ \cos(\beta - \alpha) & \text{if } \varphi_i^0 = H \\ 0 & \text{if } \varphi_i^0 = A \end{cases}. \tag{3.36}$$

To ensure that the couplings of  $h \simeq h^{\text{SM}}$  to gauge bosons  $V = W, Z$  are consistent with the experimental results, which point at SM-like values with an accuracy of  $\approx \mathcal{O}(10\%)$  [172], we impose the alignment condition

$$|\cos(\alpha - \beta)| \lesssim 0.3. \tag{3.37}$$

- **Electroweak Precision Data:**

Lastly, the additional scalars contribute to the gauge boson vacuum polarization. As a result, the electroweak precision data provide additional constraints to the mass spectrum. Mostly important, the  $T$  parameter bounds the mass-splitting between  $H$  and  $H^\pm$  in the scenario in which  $h$  is identified as the SM-like Higgs, cf. Ref. [173], for example.<sup>3</sup> The general expressions for the parameters  $S$ ,  $T$  and  $U$  in 2HDM can

---

<sup>3</sup>Conversely, if  $H$  (with  $m_H > m_h$ ) is assumed to be the SM-like Higgs, then the  $T$  parameter will constraint the mass-splitting  $m_{H^\pm} - m_A$ .

be found in Ref. [174]. To derive the bounds on the scalar spectrum and mixing, we consider the following values and the corresponding correlation matrix [175],

$$\begin{aligned} \Delta S^{\text{SM}} &= 0.05 \pm 0.11, \\ \Delta T^{\text{SM}} &= 0.09 \pm 0.13, \\ \Delta U^{\text{SM}} &= 0.01 \pm 0.11, \end{aligned} \quad \text{corr} = \begin{pmatrix} 1 & 0.90 & -0.59 \\ 0.90 & 1 & -0.83 \\ -0.59 & -0.83 & 1 \end{pmatrix}. \quad (3.38)$$

The  $\chi^2$  function is then written as

$$\chi^2 = \sum_{i,j} (X_i - X_i^{\text{SM}})(\sigma^2)_{ij}^{-1}(X_j - X_j^{\text{SM}}), \quad (3.39)$$

where the vector of central values and uncertainties are denoted as  $X = (\Delta S, \Delta T, \Delta U)$  and  $\sigma = (0.11, 0.13, 0.11)$ , while the elements of the covariance matrix are obtained via  $\sigma_{ij}^2 \equiv \sigma_i \text{corr}_{ij} \sigma_j$ .

In the following, the lightest CP-even state  $h$  will be identified with the scalar observed at the LHC with mass  $m_h = 125.09(24)$  GeV. The masses of the additional scalars,  $m_A$ ,  $m_H$  or  $m_{H^\pm}$ , are correlated via Eqs. (3.6)–(3.9). Therefore, if one mass is known, then the others are fixed up to  $\mathcal{O}(v)$  corrections. Based on this argument, we will distinguish two different scenarios in Sec. 3.2 and Sec. 3.6 by fixing the pseudoscalar boson mass:

- (i) A heavy CP-odd state, with  $m_A > m_h$ .
- (ii) a light CP-odd Higgs, with  $m_A \leq m_h$ .

The first scenario is motivated by the lack of NP signals in the direct searches for heavy scalar resonances performed at the LHC, while the latter one corresponds to the intriguing possibility that the pseudoscalar boson escaped observation thus far. We will show that both possibilities remain viable and that they offer different opportunities for phenomenology.

## 3.2 Phenomenology of heavy scalars

The simplest explanation to the lack of signals in the direct search experiments is that the new particles are heavier than the current sensitivity at LHC. In this Section, we explore this possibility by making the assumption that  $m_A > m_h$ . The implications of these results for low and high-energy observables will be discussed in the following sections.

To fully explore the viable parameter space of the model, we performed a random scan with logarithmic priors in the following ranges <sup>4</sup>

$$\begin{aligned} \tan \beta &\in (0.2, 50], & \alpha &\in \left(-\frac{\pi}{2}, \frac{\pi}{2}\right), & |M^2| &\leq (1.2 \text{ TeV})^2, \\ m_{H^\pm} &\in (m_W, 1.2 \text{ TeV}), & m_H &\in (m_h, 1.2 \text{ TeV}), & m_A &\in (m_h, 1.2 \text{ TeV}), \end{aligned} \quad (3.40)$$

<sup>4</sup>Notice that the upper bound 1.2 TeV is arbitrary, since the additional particles decouple from the low-energy theory and have no phenomenological impact above a certain threshold.

where  $m_h = 125.09$  GeV is fixed, as explained above. A scan of parameters consistent with the constraints listed above favors the moderate and small values of  $\tan \beta \in (0.2, 15]$ . To see that the larger values of  $\tan \beta$  cannot be discarded it is sufficient to examine Eq. (3.6) in the alignment limit  $\cos(\beta - \alpha) = 0$ , which exactly gives

$$m_H^2 = M^2 + \frac{v^2(\lambda_1 + \lambda_2 - 2\lambda_{345})}{2} \frac{\tan \beta}{1 + \tan^2 \beta}. \quad (3.41)$$

For large values of  $\tan \beta$ , the second term becomes small, giving  $m_H \approx |M|$ . For that reason, and in addition to the free scan described above, we perform a second scan with  $m_H \approx |M|$ , which helps us probing higher values of  $\tan \beta$ . In the end, we combine the results of both scans, which are shown in Fig. 3.1 in two planes:  $(\tan \beta, m_{H^\pm})$  and  $(m_A, m_{H^\pm})$ . From the right panel of Fig. 3.1 we observe that the additional scalars become mass degenerate in the decoupling region ( $M^2 \gg v^2$ ), as it can be easily deduced from Eqs. (3.6)–(3.9). Conversely, the scalar masses are constrained to the region  $m_A, m_H, m_{H^\pm} \lesssim 700$  GeV for  $M^2 \ll v^2$ . The correlations on the planes  $(\cos(\beta - \alpha), \tan \beta)$  and  $(\cos(\beta - \alpha), m_{H^\pm})$  are also shown in Fig. 3.2, where we can see that the alignment limit,  $\cos(\beta - \alpha) = 0$ , is retrieved as the heavy particles decouple, in agreement with Eq.(3.13). Lastly, we should also emphasize that the results of our scans agree with what has been previously reported in the literature, cf. e.g. [176–179].

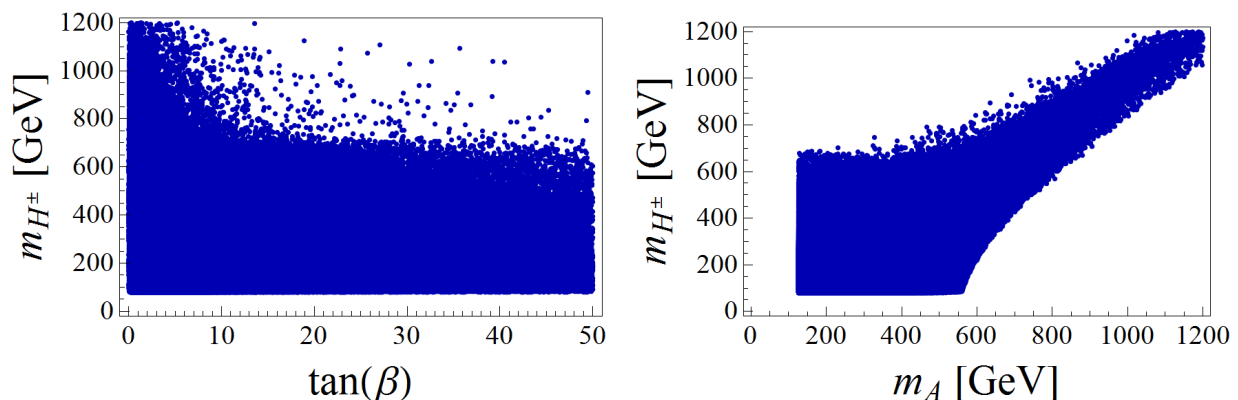


Figure 3.1: Results of the scan as described in the text.

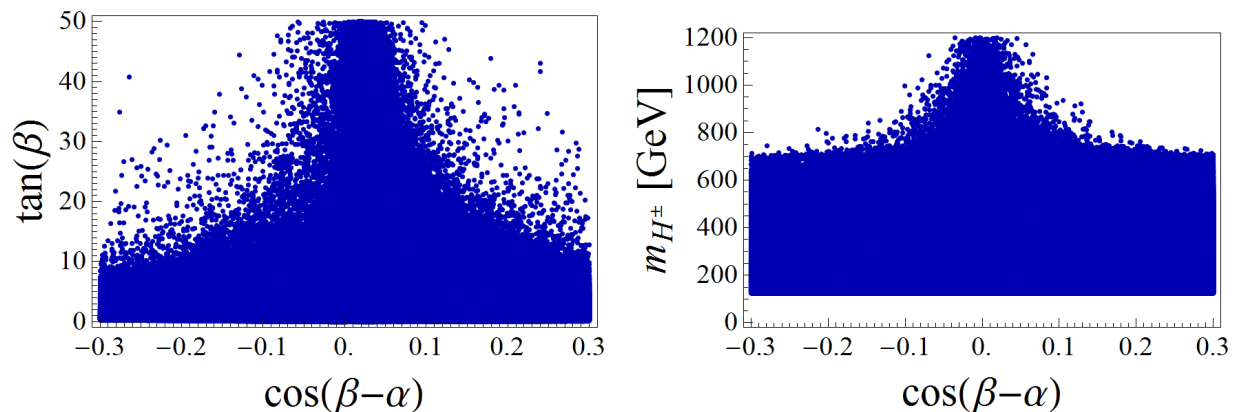


Figure 3.2: Results of the scan as described in the text.

In the following, we will discuss the phenomenology of the relevant flavor physics observables. In Sec. 3.3, we will discuss the constraints stemming from tree-level leptonic and semileptonic decays of mesons. The constraints from the loop induced processes relying on the transition  $b \rightarrow s\ell\ell$  will be discussed in Sec. 3.4 and 3.5, where we also present the computation of the relevant Wilson coefficients. In both cases, the established experimental results will provide useful limits on the charged Higgs mass and its couplings to fermions.

### 3.3 Leptonic and semileptonic decays of mesons

In this Section, we will present the impact of the leptonic and semileptonic decays, discussed in Sec. 2.2.4, on the parameter space of the different 2HDM scenarios. The charged Higgs can induce a tree-level contribution to these processes, as illustrated in Fig. 3.3 for the transition  $b \rightarrow c\ell\nu$ . Since the charged Higgs interactions are proportional to the fermion masses, we can anticipate that the stronger constraints will come from the processes with heavy leptons and quarks.

After integrating-out  $H^\pm$  in Eq. (3.19), the matching with the Hamiltonian (2.3) gives<sup>5</sup>

$$g_S = \frac{m_\ell \zeta_\ell^* (m_u \zeta_u - m_d \zeta_d)}{m_{H^\pm}^2}, \quad \text{and} \quad g_P = \frac{m_\ell \zeta_\ell^* (m_u \zeta_u + m_d \zeta_d)}{m_{H^\pm}^2}. \quad (3.42)$$

where  $u(d)$  stands for generic up(down)-quarks and  $\ell$  for a generic charged lepton. In the  $\mathbb{Z}_2$ -symmetric scenarios, the effective coefficients read

$$g_{S(P)}^I = \cot^2 \beta \frac{m_\ell (m_u \mp m_d)}{m_{H^\pm}^2}, \quad g_{S(P)}^X = -\frac{m_\ell (m_u \mp m_d)}{m_{H^\pm}^2}, \quad (3.43)$$

$$g_{S(P)}^{II} = -\frac{m_\ell (m_u \pm m_d \tan^2 \beta)}{m_{H^\pm}^2}, \quad g_{S(P)}^Z = \frac{m_\ell (m_u \cot^2 \beta \pm m_d)}{m_{H^\pm}^2}, \quad (3.44)$$

where we have replaced the values of  $\zeta_f$  given in Tab. 3.2.

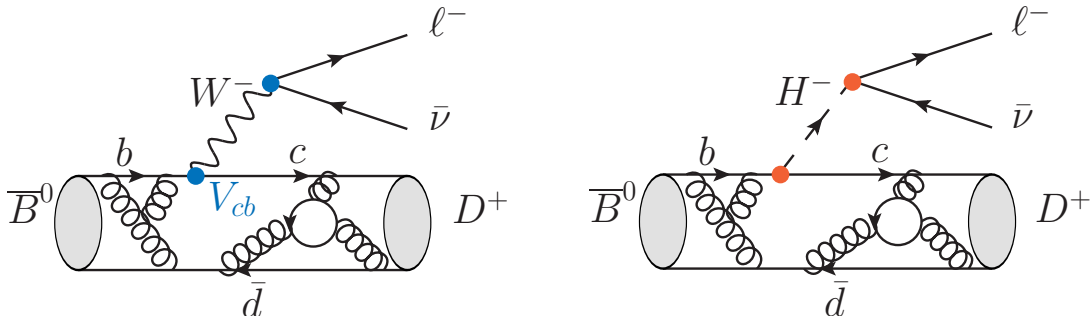


**Figure 3.3:** Contributions to the semi-leptonic decay  $\bar{B}^0 \rightarrow D^+ \ell \nu$  in the SM (left panel) and in 2HDMs (right panel).

By using the limits from Table 2.3, one can derive limits on the plane  $(m_{H^\pm}, \tan \beta)$  for each of the 2HDM scenarios. The only modes which will provide useful constraints are the ones with  $\tau$  leptons, since the coefficients  $g_{S,P}$  are proportional to the fermion masses, cf. Eq. (3.42). The scenario which receives the most significant constraints is the type

<sup>5</sup>We checked that our results agree with the ones presented in Ref. [180].

II model, since the couplings to the  $\tau$ -lepton and  $b$ -quark are both enhanced by  $\tan\beta$ , assuming  $\tan\beta > 1$ , as it can be seen from Tab. 3.2. The constraints coming from the leptonic models  $D_s \rightarrow \tau\nu$  and  $B \rightarrow \tau\nu$  are shown in Fig. 3.4, where we see that large values of  $\tan\beta$  are excluded. It is interesting to note that these limits are complementary, as it can be seen from the region with  $m_{H^\pm} < 200$  GeV, which is allowed by  $\mathcal{B}(B \rightarrow \tau\nu)$ , but excluded by  $\mathcal{B}(D_s \rightarrow \tau\nu)$ . Finally, we have checked that the limits derived for the other types of 2HDM, namely are not significant except for extreme values of  $\tan\beta$  and/or very low values of  $m_{H^\pm}$ .

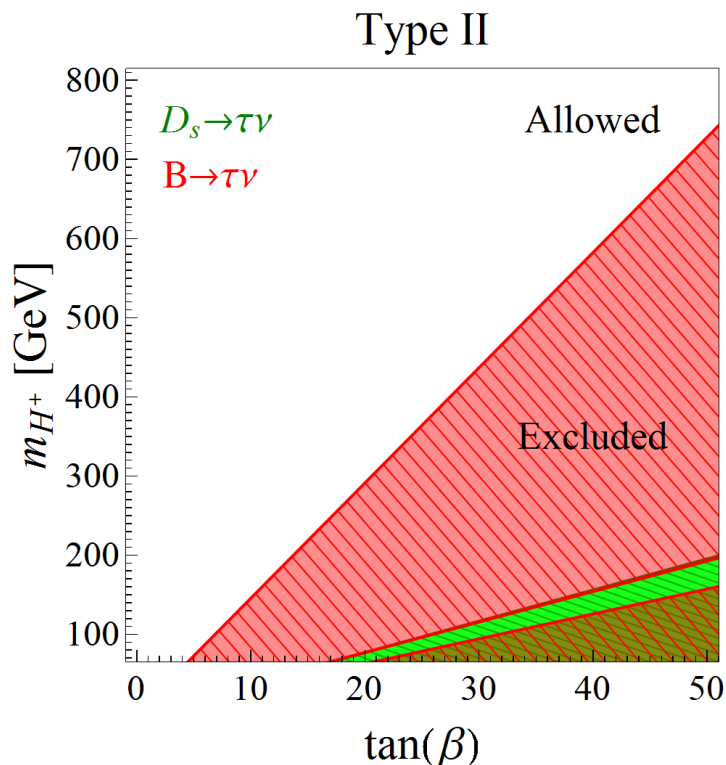


**Figure 3.4:** Exclusions on the plane  $(m_{H^\pm}, \tan\beta)$  for the type II 2HDM derived from  $\mathcal{B}(D_s \rightarrow \tau\nu)$  (green) and  $\mathcal{B}(B \rightarrow \tau\nu)$  (red) to  $2\sigma$  accuracy.

As a curiosity, we also confront the different 2HDM scenarios with the value of  $R_D = \mathcal{B}(B \rightarrow D\tau\nu)/\mathcal{B}(B \rightarrow Dl\nu)$ , which was found to be about  $2\sigma$  larger than the SM value.<sup>6</sup> From the discussion above, we know that the only scenario which can contribute significantly to this observable is the type II. The allowed region in the plane  $(\tan\beta, m_{H^\pm})$  is shown in Fig. 3.5 to  $1\sigma$  and  $2\sigma$  accuracy, from which it becomes clear that an explanation of  $R_D$  would require a very light charged Higgs, already in disagreement with the constraints from leptonic modes, cf. Fig. 3.4.<sup>7</sup> A similar conclusion holds true for  $R_{D^*}$ . The main reason for this incompatibility between the 2HDM of type II and  $R_D^{\text{exp}}$  is that  $g_S < 0$  in the type II scenario (cf. Eq. 3.43), while an explanation of  $R_D^{\text{SM}} < R_D^{\text{exp}}$  would require  $g_S > 0$ , except for the tuned region where where the interference term is compensated by a large value of  $|g_S| = -g_S$ , (cf. Table 2.3). Hence, the 2HDM with natural flavor conservation do not provide a viable explanation to the  $R_{D^{(*)}}$  puzzles. However, it is worth stressing that the

<sup>6</sup>The  $R_D$  anomaly will be discussed in detail in Sec. 5.3, along with the viable NP explanations proposed so far.

<sup>7</sup>Furthermore, the constraints from the FCNC processes  $\mathcal{B}(B \rightarrow X_s\gamma)$  that will be discussed in Sec. 3.5 also exclude masses of the charged Higgs below 439 GeV to  $2\sigma$  accuracy [181].

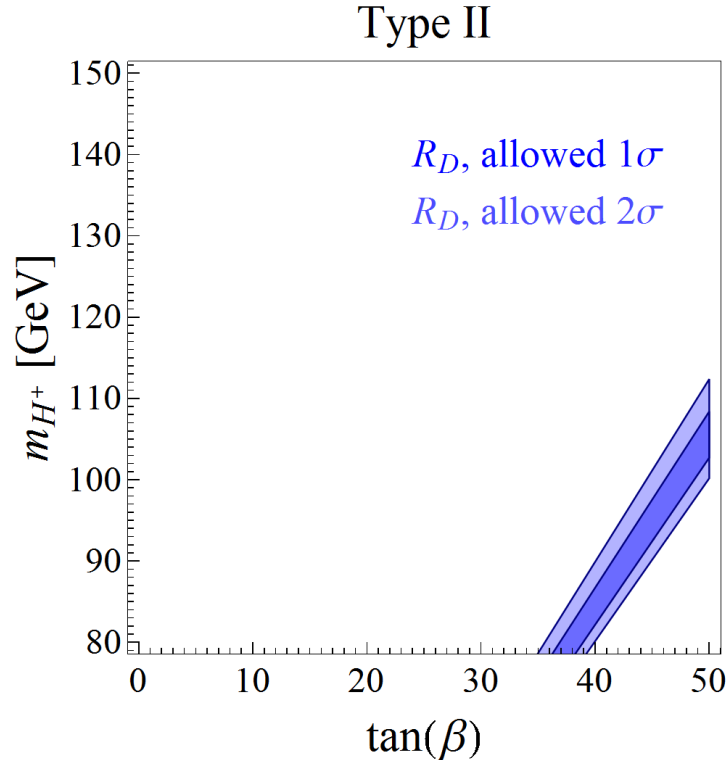


**Figure 3.5:** The allowed regions in the plane  $(m_{H^\pm}, \tan\beta)$  allowed by  $R_D = \mathcal{B}(B \rightarrow D\tau\nu)/\mathcal{B}(B \rightarrow Dl\nu)$  in the type II 2HDM to  $1\sigma$  (dark blue) and  $2\sigma$  accuracy (light blue). This region is, however, excluded by the constraints shown in Fig. 3.4

discrepancies in  $R_D$  and  $R_{D^*}$  are still experimental hints that need to be corroborated by more data, and by the study of similar processes. The  $2\sigma$  exclusions discussed above are a good indication, but not yet a clear signal that the 2HDM type II is ruled out.

### 3.4 Wilson coefficients for the $b \rightarrow sll$ transition

In this Section, we will present the general expressions for the  $b \rightarrow sll$  Wilson coefficients in a general 2HDM. These results will be compared to the ones available in the literature and we will propose a general framework for the appropriate matching between the full and effective theories in the case where it is necessary to keep the external momenta different from zero. The results derived in this Section will be used in Sec. 3.5 to investigate the phenomenological impact of the present exclusive  $b \rightarrow s$  data on the scan of parameters described above.

#### Expressions for the Wilson coefficients

The leading 2HDM contributions to  $b \rightarrow sll$  can be separated in four groups of one-loop diagrams which are illustrated in Figs. 3.6 to 3.9 and correspond to  $\gamma$ ,  $Z$  and scalar penguins, as well as box diagrams. Before presenting the results of our computation, let us briefly discuss the issues of the matching between the 2HDM amplitudes and Eq. (2.54).

The dimension six operators introduced in Eq. (2.54) are sufficient to match the one-loop 2HDM amplitude when the external fermion momenta are neglected. This, however, is not true if the computation is made with external momenta different from zero which is,

in general, *necessary* when dealing with (pseudo-)scalar operators. For example, in order to get a correct expression for the Wilson coefficient  $C_P$  one needs to consider the external momenta, which then can give rise to the contributions coming from the dimension-seven operators. One class of such terms can be related to the operators of basis (2.54) by equations of motion. For example,

$$\begin{aligned} \frac{\alpha}{4\pi} \frac{1}{m_W} (\bar{s} \not{q} P_L b) (\bar{\ell} \gamma_5 \ell) &= \frac{\alpha}{4\pi} \frac{m_b}{m_W} (\bar{s} P_R b) (\bar{\ell} \gamma_5 \ell) - \frac{\alpha}{4\pi} \frac{m_s}{m_W} (\bar{s} P_L b) (\bar{\ell} \gamma_5 \ell) \\ &= \frac{m_b}{m_W} \mathcal{O}_P - \frac{m_s}{m_W} \mathcal{O}'_P \simeq \frac{m_b}{m_W} \mathcal{O}_P. \end{aligned} \quad (3.45)$$

A complication arises when encountering the operators with insertion of  $\not{p}_b + \not{p}_s$  in the leptonic current, with the convention  $b(p_b) \rightarrow s(p_s) \ell^-(p_-) \ell^+(p_+)$ , where we also use  $q = p_b - p_s = p_+ + p_-$ . A way to deal with that, adopted in Ref. [182], consists in setting  $p_s = 0$ , so that  $\not{p}_b + \not{p}_s = \not{q} + 2\not{p}_s = \not{q} = \not{p}_+ + \not{p}_-$ , and in this way one can again, like in the previous example, use the equations of motion. That way to deal with the problem in hands, however, leads to a wrong expression for  $C_P$ , for example. If, instead, one keeps all the momenta nonzero, we get a correct result. At this point we just emphasize that the matching should be performed by keeping all the external momenta different from zero and the contributions stemming from dimension-seven operators can be neglected at the very end of computation. We further elucidate this problem in the end of this Section, where we also propose a general framework for the appropriate matching between the full and effective theories in a case in which the (pseudo-)scalar bosons are explicitly taken into account.

We are now in a position to present the effective coefficients in a general 2HDM. The contributions from the 2HDM scalars can be recast as,

$$C_7 = C_7^{\text{NP}, \gamma}, \quad (3.46)$$

$$C_9 = C_9^{\text{NP}, \gamma} + C_9^{\text{NP}, Z}, \quad (3.47)$$

$$C_{10} = C_{10}^{\text{NP}, Z}, \quad (3.48)$$

$$C_P = C_P^{\text{NP}, \text{box}} + C_P^{\text{NP}, Z} + C_P^{\text{NP}, A} \quad (3.49)$$

$$C_S = C_S^{\text{NP}, \text{box}} + C_S^{\text{NP}, h} + C_S^{\text{NP}, H}, \quad (3.50)$$

where the superscripts denote the types of diagrams that contributes to a given Wilson coefficient, namely, the box diagrams, the  $\gamma$ ,  $Z$ -penguins and the (pseudo-)scalar penguins. These coefficients should be added to the (effective) ones obtained in the SM:  $C_7 = -0.304$ ,  $C_9 = 4.211$ ,  $C_{10} = -4.103$ , and  $C_{S,P} \simeq 0$  [183].<sup>8</sup>

Henceforth, we neglect the  $s$ -quark mass and give all our results in the unitary gauge. To check the consistency of our formulas, we also performed the computation in the Feynman gauge. Furthermore, to simplify our computation, we expand the propagators before integration on the fermion external momenta [182],

$$\frac{1}{(k+p)^2 - M^2} = \frac{1}{k^2 - M^2} \left[ 1 - \frac{p^2 + 2k \cdot p}{k^2 - M^2} + \frac{4(k \cdot p)^2}{(k^2 - M^2)^2} \right] + \mathcal{O}(p^4/M^4), \quad (3.51)$$

<sup>8</sup>Special attention should be paid to the scalar penguin generated by the SM-like Higgs  $h$  to avoid the double counting, since it also appears in the 2HDM.

where  $k$  is the loop momentum,  $p$  is a generic external momenta and  $M$  is the mass of a particle running in the loop.<sup>9</sup> This expansion is justified, since the external momenta are much smaller than the masses of the particles running in the loops, namely, the top quark,  $W^\pm$  and  $H^\pm$ . In this way, we can directly use the analytical results for the Passarino-Veltman functions [184, 185] with zero external momenta, which are also given in Appendix A.2. In the remainder of this Section we present our resulting expressions for each of the coefficients appearing in Eqs. (3.46)–(3.50). We use the standard notation,

$$x_q = \frac{m_q^2}{m_W^2}, \quad x_{H^\pm} = \frac{m_{H^\pm}^2}{m_W^2}, \quad x_{\varphi_i^0} = \frac{m_{\varphi_i^0}^2}{m_W^2}, \quad (3.52)$$

where  $q \in \{b, t\}$ , and  $\varphi_i^0 \in \{h, H, A\}$ .

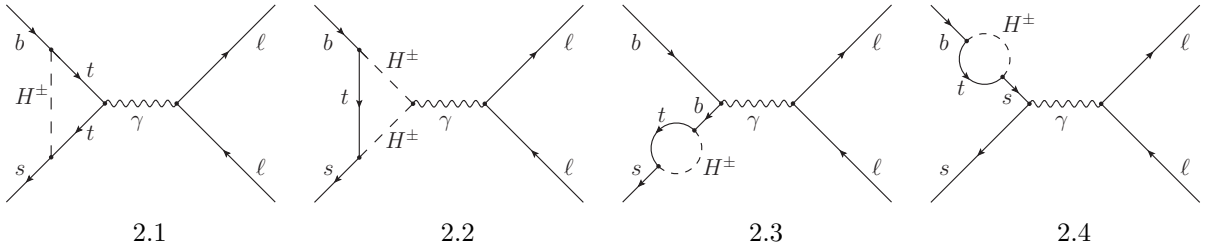


**Figure 3.6:** Photon penguin diagrams generated by the additional scalars.

- $\gamma$  penguins in 2HDM:

The  $\gamma$ -penguin diagrams induced by the charged Higgs are shown in Fig. 3.6. The off-shell and on-shell contributions can be matched onto the Wilson coefficients  $C_7$  and  $C_9$ , respectively, we obtained,

$$C_7^{\text{NP},\gamma} = -|\zeta_u|^2 \frac{x_t}{72} \left[ \frac{7x_{H^\pm}^2 - 5x_{H^\pm}x_t - 8x_t^2}{(x_{H^\pm} - x_t)^3} + \frac{6x_{H^\pm}x_t(3x_t - 2x_{H^\pm})}{(x_{H^\pm} - x_t)^4} \log\left(\frac{x_{H^\pm}}{x_t}\right) \right] - \zeta_u^* \zeta_d \frac{x_t}{12} \left[ \frac{3x_{H^\pm} - 5x_t}{(x_t - x_{H^\pm})^2} + \frac{2x_{H^\pm}(3x_t - 2x_{H^\pm})}{(x_t - x_{H^\pm})^3} \log\left(\frac{x_t}{x_{H^\pm}}\right) \right], \quad (3.53)$$

and

$$C_9^{\text{NP},\gamma} = |\zeta_u|^2 \frac{x_t}{108} \left[ \frac{38x_{H^\pm}^2 - 79x_{H^\pm}x_t + 47x_t^2}{(x_{H^\pm} - x_t)^3} - \frac{6(4x_{H^\pm}^3 - 6x_{H^\pm}^2x_t + 3x_t^3)}{(x_{H^\pm} - x_t)^4} \log\left(\frac{x_{H^\pm}}{x_t}\right) \right] + \zeta_u^* \zeta_d \frac{x_t x_b}{108} \left[ \frac{-37x_{H^\pm}^2 + 8x_{H^\pm}x_t + 53x_t^2}{(x_{H^\pm} - x_t)^4} + \frac{6(2x_{H^\pm}^3 + 6x_{H^\pm}^2x_t - 9x_{H^\pm}x_t^2 - 3x_t^3)}{(x_{H^\pm} - x_t)^5} \log\left(\frac{x_{H^\pm}}{x_t}\right) \right]. \quad (3.54)$$

The dominant terms in both  $C_7^{\text{NP},\gamma}$  and  $C_9^{\text{NP},\gamma}$  come from the top quark contribution and are proportional to  $|\zeta_u|^2$ . The terms proportional to  $\zeta_u^* \zeta_d$  are suppressed by  $m_b^2$ , thus indeed subdominant, but numerically not necessarily negligible.

<sup>9</sup>We stopped the expansion at order  $\mathcal{O}(p^4/M^4)$  for illustration purposes. In our computation, we include the higher order terms when needed to compute the sub-leading contributions.

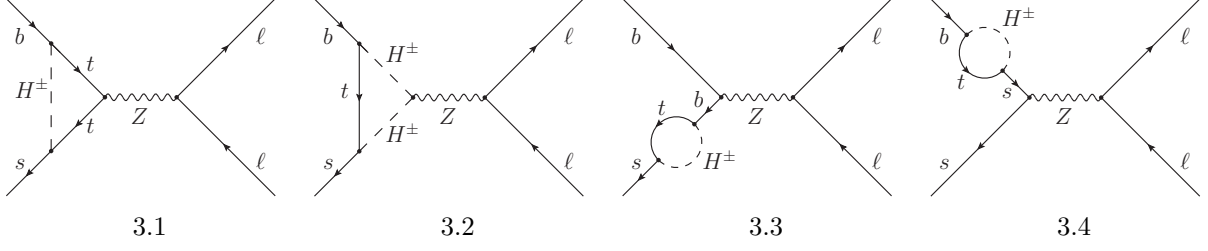


**Figure 3.7:**  $Z$  penguin diagrams generated by the additional scalars.

- **$Z$  penguins in 2HDM:**

The  $Z$ -penguin diagrams contribute significantly to the Wilson coefficients  $C_P$ ,  $C_9$  and  $C_{10}$  through the diagrams shown in Fig. 3.7. The leading order expressions for  $C_9$  and  $C_{10}$  read,

$$C_9^{\text{NP},Z} = C_{10}^{\text{NP},Z}(-1 + 4 \sin^2 \theta_W), \quad (3.55)$$

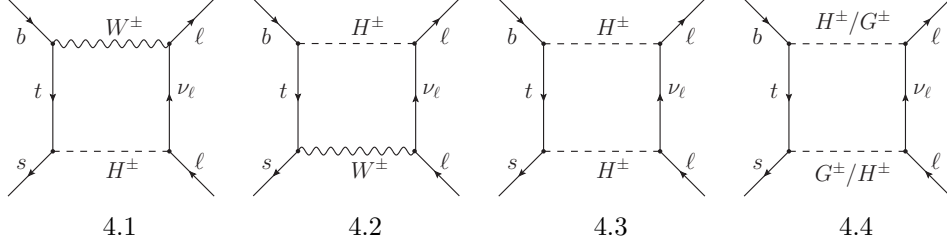
$$C_{10}^{\text{NP},Z} = |\zeta_u|^2 \frac{x_t^2}{8 \sin^2 \theta_W} \left[ \frac{1}{x_{H^\pm} - x_t} - \frac{x_{H^\pm}}{(x_{H^\pm} - x_t)^2} \log \left( \frac{x_{H^\pm}}{x_t} \right) \right] + \zeta_u^* \zeta_d \frac{x_t x_b}{16 \sin^2 \theta_W} \left[ \frac{x_{H^\pm} + x_t}{(x_{H^\pm} - x_t)^2} - \frac{2x_t x_{H^\pm}}{(x_{H^\pm} - x_t)^3} \log \left( \frac{x_{H^\pm}}{x_t} \right) \right]. \quad (3.56)$$

Similarly, for  $C_P$  we obtain

$$C_P^{\text{NP},Z} = \zeta_u^* \zeta_d \frac{\sqrt{x_b x_\ell} x_t}{16 \sin^2 \theta_W} \left[ \frac{x_t - 3x_{H^\pm}}{(x_{H^\pm} - x_t)^2} + \frac{2x_{H^\pm}^2}{(x_{H^\pm} - x_t)^3} \log \left( \frac{x_{H^\pm}}{x_t} \right) \right] + |\zeta_u|^2 \frac{\sqrt{x_b x_\ell} x_t}{216} \left\{ \frac{38x_{H^\pm}^2 + 54x_{H^\pm}^2 x_t - 79x_{H^\pm} x_t - 108x_{H^\pm} x_t^2 + 47x_t^2 + 54x_t^3}{(x_{H^\pm} - x_t)^3} - \frac{6(4x_{H^\pm}^3 + 9x_{H^\pm}^3 x_t - 6x_{H^\pm}^2 x_t - 18x_{H^\pm}^2 x_t^2 + 9x_{H^\pm} x_t^3 + 3x_t^3)}{(x_{H^\pm} - x_t)^4} \log \left( \frac{x_{H^\pm}}{x_t} \right) - \frac{3}{2 \sin^2 \theta_W} \left[ \frac{2x_{H^\pm}^2 + 36x_{H^\pm}^2 x_t - 7x_{H^\pm} x_t - 72x_{H^\pm} x_t^2 + 11x_t^2 + 36x_t^3}{(x_{H^\pm} - x_t)^3} - \frac{6x_t(6x_{H^\pm}^3 - 12x_{H^\pm}^2 x_t + 6x_{H^\pm} x_t^2 + x_t^2)}{(x_{H^\pm} - x_t)^4} \log \left( \frac{x_{H^\pm}}{x_t} \right) \right] \right\}. \quad (3.57)$$

- **Charged Higgs boxes in 2HDM:**

The box diagrams, peculiar for 2HDM, are drawn in Fig. 3.8. At low-energy they contribute to the Wilson coefficients  $C_S$  and  $C_P$  as,


**Figure 3.8:** Box diagrams generated by the additional scalars.

$$\begin{aligned}
 C_S^{\text{NP, box}} &= \frac{\sqrt{x_\ell x_b} x_t}{8(x_{H^\pm} - x_t) \sin^2 \theta_W} \left\{ \zeta_\ell \zeta_u^* \left( \frac{x_t}{x_t - 1} \log x_t - \frac{x_{H^\pm}}{x_{H^\pm} - 1} \log x_{H^\pm} \right) \right. \\
 &+ \zeta_u \zeta_\ell^* \left[ 1 - \frac{x_{H^\pm} - x_t^2}{(x_{H^\pm} - x_t)(x_t - 1)} \log x_t - \frac{x_{H^\pm}(x_t - 1)}{(x_{H^\pm} - x_t)(x_{H^\pm} - 1)} \log x_{H^\pm} \right] \\
 &\left. + 2\zeta_d \zeta_\ell^* \log \left( \frac{x_t}{x_{H^\pm}} \right) \right\}, \quad (3.58)
 \end{aligned}$$

and

$$\begin{aligned}
 C_P^{\text{NP, box}} &= \frac{\sqrt{x_\ell x_b} x_t}{8(x_{H^\pm} - x_t) \sin^2 \theta_W} \left\{ \zeta_\ell \zeta_u^* \left( \frac{x_t}{x_t - 1} \log x_t - \frac{x_{H^\pm}}{x_{H^\pm} - 1} \log x_{H^\pm} \right) \right. \\
 &- \zeta_u \zeta_\ell^* \left[ 1 - \frac{x_{H^\pm} - x_t^2}{(x_{H^\pm} - x_t)(x_t - 1)} \log x_t - \frac{x_{H^\pm}(x_t - 1)}{(x_{H^\pm} - x_t)(x_{H^\pm} - 1)} \log x_{H^\pm} \right] \\
 &\left. - 2\zeta_d \zeta_\ell^* \log \left( \frac{x_t}{x_{H^\pm}} \right) \right\}. \quad (3.59)
 \end{aligned}$$

In addition to  $C_{S,P}^{\text{NP, box}}$ , the tensor and (axial-)vector operators receive contributions, which are however suppressed by the charged lepton mass, i.e. by  $x_\ell = m_\ell^2/m_W^2$ . These coefficients are negligible even for decays with  $\tau$ 's in the final state as it can be verified by using the expressions provided in Ref. [186].

- **Scalar penguins in 2HDM:**

We now turn to the effective coefficients  $C_P^{\text{NP}, A}$ ,  $C_S^{\text{NP}, h}$  and  $C_S^{\text{NP}, H}$ , generated by the scalar penguin diagrams shown in Fig. 3.9. We recall that the total ultraviolet divergence coming from these diagrams is proportional to the factor  $(1 + \zeta_u \zeta_d)(\zeta_u - \zeta_d)$ , which vanishes due to the  $\mathbb{Z}_2$  symmetry, cf. Table 3.2.<sup>10</sup>

The penguins with the CP-odd Higgs give rise to,

<sup>10</sup>Notice that this is not true in general. For instance, in the A2HDM the divergences are canceled by contributions coming from the radiatively induced misalignment of the Yukawa matrices. The alignment is only preserved at all scales in the context of  $\mathbb{Z}_2$ -symmetric models [182].

$$\begin{aligned}
 C_P^{\text{NP},A} = & -\frac{\sqrt{x_\ell x_b} \zeta_\ell x_t}{\sin^2 \theta_W 2x_A} \left\{ \frac{\zeta_u^3 x_t}{2} \left[ \frac{1}{x_{H^\pm} - x_t} - \frac{x_{H^\pm}}{(x_{H^\pm} - x_t)^2} \log \left( \frac{x_{H^\pm}}{x_t} \right) \right] \right. \\
 & + \frac{\zeta_u}{4} \left[ -\frac{3x_{H^\pm} x_t - 6x_{H^\pm} - 2x_t^2 + 5x_t}{(x_t - 1)(x_{H^\pm} - x_t)} + \frac{x_{H^\pm}(x_{H^\pm}^2 - 7x_{H^\pm} + 6x_t)}{(x_{H^\pm} - x_t)^2(x_{H^\pm} - 1)} \log x_{H^\pm} \right. \\
 & \left. \left. - \frac{x_{H^\pm}^2(x_t^2 - 2x_t + 4) + 3x_t^2(2x_t - 2x_{H^\pm} - 1)}{(x_{H^\pm} - x_t)^2(x_t - 1)^2} \log x_t \right] \right\}, \quad (3.60)
 \end{aligned}$$

where we have used again the properties  $\zeta_f \in \mathbb{R}$  and  $(1 + \zeta_u \zeta_d)(\zeta_u - \zeta_d) = 0$  to simplify the expressions. Similarly, the penguins with the CP-even scalars lead to

$$\begin{aligned}
 C_S^{\text{NP},h} &= \frac{\sqrt{x_\ell x_b} x_t}{\sin^2 \theta_W 2x_h} [\sin(\beta - \alpha) + \cos(\beta - \alpha)\zeta_\ell] \\
 &\quad \times \left[ g_1 \sin(\beta - \alpha) + g_2 \cos(\beta - \alpha) - g_0 \frac{2v^2}{m_W^2} \lambda_{H^+H^-}^h \right], \\
 C_S^{\text{NP},H} &= \frac{\sqrt{x_\ell x_b} x_t}{\sin^2 \theta_W 2x_H} [\cos(\beta - \alpha) - \sin(\beta - \alpha)\zeta_\ell] \\
 &\quad \times \left[ g_1 \cos(\beta - \alpha) - g_2 \sin(\beta - \alpha) - g_0 \frac{2v^2}{m_W^2} \lambda_{H^+H^-}^H \right], \quad (3.61)
 \end{aligned}$$

where  $\lambda_{H^+H^-}^i$  are the trilinear couplings defined in Appendix B.1. The functions  $g_{0,1,2}$  are given in Appendix B.2.

### Comparison with other computations

We shall now compare our Wilson coefficients with the results obtained in previous studies. Before doing so we should emphasize the novelties of our computation:

- (i) The result for  $C_9$  in a general 2HDM with a  $\mathbb{Z}_2$  symmetry is new;
- (ii) The subleading terms  $\mathcal{O}(m_b)$  to  $C_{9,10}$  have been neglected in the previous computations, and they are included here;
- (iii) We provided an independent computation of the coefficients  $C_S$  and  $C_P$ , and elucidate inconsistencies present in Ref. [182], where we propose a general prescription for matching procedure when the external momenta are not neglected, as it will be discussed in the following.

$$C_P = -C_S \simeq \tan^2 \beta \frac{\sqrt{x_\ell x_b} x_t}{4 \sin^2 \theta_W x_{H^\pm} - x_t} \log \left( \frac{x_{H^\pm}}{x_t} \right). \quad (3.62)$$

Along the same lines, the leading order QCD corrections to the same coefficients were included in Ref. [187]. Recently, the computation of  $C_S$  and  $C_P$  was extended to the context of a general A2HDM, which comprises all four types of 2HDM with  $\mathbb{Z}_2$  symmetry

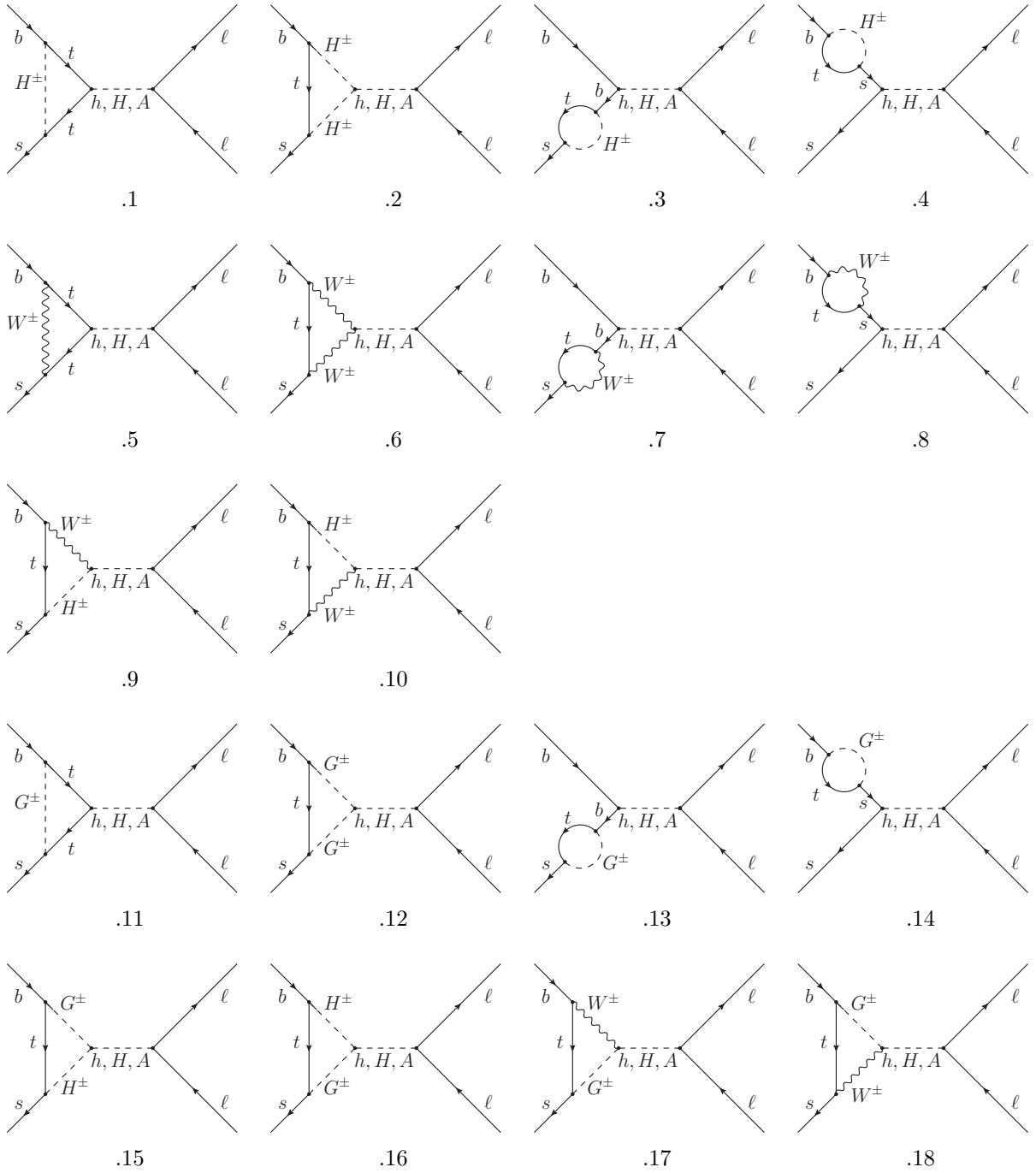


**Figure 3.9:** Higgs penguin diagrams generated by the additional scalars.

discussed here but without the usual assumption of large  $\tan\beta$  [182]. We agree with their general results, except for the expression for  $C_P^{\text{NP},Z}$  which differs from the one reported in this thesis. The disagreement comes from the fact that the authors of Ref. [182] worked with the assumption  $p_s = 0$ , which appears not to be fully appropriate.<sup>11</sup> By keeping  $p_s \neq 0$  one realizes that the computation of  $Z$ -penguin leads to two independent terms, one proportional to  $p_H = p_b + p_s$  and the other to  $q = p_b - p_s$ . By using equations of motion,  $C_{P,S}$  correctly receive contributions from the terms proportional to  $q$ , but not from those proportional to  $p_H$ . With  $p_s = 0$  only one invariant appears, because  $p_H \equiv q$ , and thus the resulting  $C_{P,S}$  also receive spurious contributions from  $p_H$ .

Regarding the other Wilson coefficients, the first computations of  $C_7$  for a general 2HDM have been performed in Ref. [188], then in Refs. [189, 190] and [191] where the leading and subleading QCD corrections were included too. Our results are consistent with those, as well as with the expression for  $C_{10}$  presented in Ref. [192] and more recently in Ref. [182]. The only difference with respect to those results is that we include the subleading terms in  $m_b$ .

### Matching procedure

In this section we discuss in more detail the matching of the one-loop amplitudes when the nonzero external momenta are considered. We stress once again that keeping external momenta nonzero is necessary to obtain the correct values for the Wilson coefficients  $C_{S,P}$ . As we mentioned above, the insertion of external momenta result in dimension-seven operators which can be simplified by using equations of motion, except in the cases when the lepton momenta are to be contracted with the quark current and/or the quark momenta to be contracted with the lepton current. The amplitudes which need a special treatment, to leading order in external momenta, are:

$$\begin{aligned} \mathcal{A}_{ij}^\ell &= \frac{\alpha}{4\pi m_W} (\bar{s}(\not{p}_- - \not{p}_+)P_i b)(\bar{\ell}P_j \ell), & \mathcal{A}_{ij}^q &= \frac{\alpha}{4\pi m_W} (\bar{s}P_i b)(\bar{\ell}(\not{p}_b + \not{p}_s)P_j \ell), \\ \mathcal{A}_{ij}^{V\ell} &= \frac{\alpha}{4\pi m_W} (\bar{s}(\not{p}_- - \not{p}_+)\gamma_\mu P_i b)(\bar{\ell}\gamma^\mu P_j \ell), & \mathcal{A}_{ij}^{Vq} &= \frac{\alpha}{4\pi m_W} (\bar{s}\gamma_\mu P_i b)(\bar{\ell}(\not{p}_b + \not{p}_s)\gamma^\mu P_j \ell), \end{aligned} \quad (3.63)$$

where  $i, j = L, R$  and  $s, b, \ell$  are the fermion spinors. Note again that our convention is  $b(p_b) \rightarrow s(p_s)\ell^-(p_-)\ell^+(p_+)$ , and  $q = p_b - p_s = p_+ + p_-$ . In order to keep our discussion general, we first extend the Hamiltonian (2.54) and include the following operators

$$\mathcal{H}'_{\text{eff}} = -\frac{4G_F}{\sqrt{2}} V_{tb}V_{ts}^* \sum_{i,j=L,R} \left( C_{ij}^{\mathcal{T}\ell}(\mu)\mathcal{O}_{ij}^{\mathcal{T}\ell}(\mu) + C_{ij}^{\mathcal{T}q}(\mu)\mathcal{O}_{ij}^{\mathcal{T}q}(\mu) \right) + \text{h.c.}, \quad (3.64)$$

where

$$\begin{aligned} \mathcal{O}_{ij}^{\mathcal{T}\ell} &= \frac{e^2}{(4\pi)^2 m_W} (\bar{s}\gamma^\mu P_i b)\partial^\nu (\bar{\ell}\sigma_{\mu\nu} P_j \ell), \\ \mathcal{O}_{ij}^{\mathcal{T}q} &= -\frac{e^2}{(4\pi)^2 m_W} \partial^\nu (\bar{s}\sigma_{\mu\nu} P_i b)(\bar{\ell}\gamma^\mu P_j \ell), \end{aligned} \quad (3.65)$$

<sup>11</sup>We should emphasize that we were able to reproduce the expression for  $C_P^{\text{NP},Z}$  reported in Ref. [182] by taking  $p_s = 0$ , which however is not an appropriate assumption as we argue in the text.

with  $i, j = L, R$ .<sup>12</sup> We reiterate that even though these operators are suppressed by  $1/m_W$ , they are necessary to unambiguously match the loop induced amplitudes with the effective field theory. The above choice of the basis of dimension-seven operators is convenient since they do not contribute to  $\mathcal{B}(B_s \rightarrow \mu^+\mu^-)$ , while for the other decays their hadronic matrix elements are easy to calculate.

By using the Fierz rearrangement and by applying the field equations, the amplitudes (3.63) are reduced to

$$\mathcal{A}_{LL}^\ell \leftrightarrow -\mathcal{O}_{LL}^{\mathcal{T}\ell} + \mathcal{O}_9 \frac{m_\ell}{m_W}, \quad (3.66)$$

$$\mathcal{A}_{LR}^\ell \leftrightarrow -\mathcal{O}_{LR}^{\mathcal{T}\ell} + \mathcal{O}_9 \frac{m_\ell}{m_W}, \quad (3.67)$$

$$\mathcal{A}_{LL}^{V\ell} \leftrightarrow -\mathcal{O}_{LL}^{\mathcal{T}q} + \left( \mathcal{O}'_S - \frac{\mathcal{O}_T - \mathcal{O}_{T5}}{4} \right) \frac{m_\ell}{m_W}, \quad (3.68)$$

$$\mathcal{A}_{LR}^{V\ell} \leftrightarrow \mathcal{O}_{LR}^{\mathcal{T}q} + \left( \mathcal{O}'_S + \frac{\mathcal{O}_T - \mathcal{O}_{T5}}{4} \right) \frac{m_\ell}{m_W}, \quad (3.69)$$

$$\mathcal{A}_{LL}^q \leftrightarrow \mathcal{O}_{LL}^{\mathcal{T}q} + \frac{\mathcal{O}'_9 - \mathcal{O}'_{10}}{2} \frac{m_b}{m_W} + \frac{\mathcal{O}_9 - \mathcal{O}_{10}}{2} \frac{m_s}{m_W}, \quad (3.70)$$

$$\mathcal{A}_{LR}^q \leftrightarrow \mathcal{O}_{LR}^{\mathcal{T}q} + \frac{\mathcal{O}'_9 + \mathcal{O}'_{10}}{2} \frac{m_b}{m_W} + \frac{\mathcal{O}_9 + \mathcal{O}_{10}}{2} \frac{m_s}{m_W}, \quad (3.71)$$

$$\mathcal{A}_{LL}^{Vq} \leftrightarrow \mathcal{O}_{LL}^{\mathcal{T}\ell} + \frac{\mathcal{O}_S - \mathcal{O}_P}{2} \frac{m_b}{m_W} + \left( \mathcal{O}'_S - \mathcal{O}'_P - \frac{\mathcal{O}_T - \mathcal{O}_{T5}}{2} \right) \frac{m_s}{2m_W}, \quad (3.72)$$

$$\mathcal{A}_{LR}^{Vq} \leftrightarrow -\mathcal{O}_{LR}^{\mathcal{T}\ell} + \frac{\mathcal{O}'_S + \mathcal{O}'_P}{2} \frac{m_s}{m_W} + \left( \mathcal{O}_S + \mathcal{O}_P + \frac{\mathcal{O}_T + \mathcal{O}_{T5}}{2} \right) \frac{m_b}{2m_W}. \quad (3.73)$$

To remain completely general, in the above equations we also kept the lepton mass and the mass of  $s$ -quark different from zero. As an example we show the validity of Eq. (3.68). To do so, it is useful to note that

$$\int d^4x \langle \ell^+(p_+) \ell^-(p_-) s(p_s) | \mathcal{O}_{LL}^{\mathcal{D}q}(x) | b(p_b) \rangle \rightarrow -\frac{\alpha}{4\pi} \frac{1}{m_W} \bar{u}_s(p_s) P_L u_b(p_b) \bar{u}_\ell(p_-) (\not{p}_b + \not{p}_s) P_L v_\ell(p_+). \quad (3.74)$$

Using  $p_- - p_+ = 2p_- - q$ , and by the multiple use of field equations, we can write:

$$\begin{aligned} \mathcal{A}_{LL}^{V\ell} &= \frac{\alpha}{4\pi} \frac{2}{m_W} (\bar{s} \not{p}_- \gamma_\mu P_L b) (\bar{\ell} \gamma^\mu P_L \ell) - \frac{\alpha}{4\pi} \frac{1}{m_W} (\bar{s} \not{q} \gamma_\mu P_L b) (\bar{\ell} \gamma^\mu P_L \ell) \\ &= \frac{\alpha}{4\pi} \frac{1}{m_W} \left[ 4(\bar{s} P_L b) (\bar{\ell} \not{p}_- P_L \ell) - 2(\bar{s} \gamma_\mu P_R \not{p}_- b) (\bar{\ell} \gamma^\mu P_L \ell) \right. \\ &\quad \left. + m_s (\bar{s} \gamma_\mu P_L b) (\bar{\ell} \gamma^\mu P_L \ell) + m_b (\bar{s} \gamma_\mu P_R b) (\bar{\ell} \gamma^\mu P_L \ell) - 2(\bar{s} P_L b) (\bar{\ell} \not{p}_b P_L \ell) \right] \\ &\stackrel{\text{Fierz}}{=} \frac{\alpha}{4\pi} \frac{1}{m_W} \left[ 4m_\ell (\bar{s} P_L b) (\bar{\ell} P_L \ell) - 4(\bar{s} P_L \ell) (\bar{\ell} P_R \not{p}_- b) + m_s (\bar{s} \gamma_\mu P_L b) (\bar{\ell} \gamma^\mu P_L \ell) \right. \\ &\quad \left. + m_b (\bar{s} \gamma_\mu P_R b) (\bar{\ell} \gamma^\mu P_L \ell) - (\bar{s} P_L b) (\bar{\ell} (\not{p}_b + \not{p}_s) P_L \ell) + m_\ell (\bar{s} P_L b) (\bar{\ell} \gamma_5 \ell) \right]. \quad (3.75) \end{aligned}$$

By applying the Fierz identity once again, we arrive at,

<sup>12</sup>Notice that we are not computing the QCD corrections to the Wilson coefficients and therefore, at this order, we do not make distinction between the ordinary and the covariant  $SU(3)_c$  derivative.

$$\mathcal{A}_{LL}^{V\ell} \xrightarrow{\text{Fierz}} \frac{m_\ell}{m_W} \left( \mathcal{O}'_S - \frac{\mathcal{O}_T - \mathcal{O}_{T5}}{4} \right) - \mathcal{O}_{LL}^{Tq}. \quad (3.76)$$

Clearly, for the appropriate matching of these amplitudes to the effective theory, the operators appearing in Eq. (2.54) are not enough and the extended basis given in Eq. (3.64) is necessary. Once the matching is performed, the operators from Eq. (3.64) could be neglected since they are  $1/m_W$  suppressed with respect to the dominant (dimension six) ones. This delicate point can then be verified explicitly by computing the Wilson coefficients  $C_{RL}^{Tq}$  and  $C_{RR}^{Tq}$  which come from the  $Z$ -penguin diagrams and the coefficients  $C_{LL}^{T\ell} = (C_{LR}^{T\ell})^*$  generated by the box diagrams. Their explicit expression is given in Appendix B.2.1.

We can now easily understand the source of our disagreement with Ref. [182]. If one sets  $p_s = 0$  in  $\mathcal{A}_{RR}^q$  of Eq. (3.63), then just like in Ref. [182] one could write  $\not{p}_b + \not{p}_s = \not{p}_b = \not{q}$  which, by means of equations of motion, yields

$$\mathcal{A}_{RR}^q = \frac{m_\ell}{m_W} \frac{\alpha}{4\pi} (\bar{s} P_R b) (\bar{\ell} (P_R - P_L) \ell) = \sqrt{x_\ell} \mathcal{O}_P, \quad (3.77)$$

which then in the actual computation gives a contribution to  $C_P$ . With our procedure, we understand that this contribution does not come from  $C_P$  but actually from  $\sqrt{x_\ell} C_{RL}^{Tq}$ . In other words, and by using our definition of operators and of the effective Hamiltonian, we find<sup>13</sup>

$$C_P^{\text{Li et al.}} = \left[ C_P + \frac{\sqrt{x_\ell}}{2 \sin^2 \theta_W} C_{RR}^{Tq} \right]^{\text{(this work)}}. \quad (3.78)$$

Therefore the Wilson coefficient  $C_P$  of Ref. [182] contains the Wilson coefficient of the operator  $\mathcal{O}_{RR}^{Tq}$ , the matrix element of which is not equal to the matrix element of the operator  $\mathcal{O}_P$  but is, instead, suppressed by  $m_W$  as we explicitly check in the next section. For that reason the Wilson coefficient of Ref. [182] is not correct, even though the phenomenological impact of the difference between our  $C_P$  and the results of Ref. [182] is numerically negligible.

### 3.5 Lessons from $b \rightarrow s$ exclusive observables

In this Section, we confront the scan of parameters performed in Sec. 3.2 with the experimentally established exclusive  $b \rightarrow s$  data. To that purpose, we will use the expressions for the effective coefficients derived in Sec. 3.5 for the various types of 2HDMs. We decided to focus on [130]

$$\mathcal{B}(B_s \rightarrow \mu^+ \mu^-)^{\text{exp}} = (3.0 \pm 0.6_{-0.2}^{+0.3}) \times 10^{-9}, \quad (3.79)$$

and [116]

$$\mathcal{B}(B \rightarrow K \mu^+ \mu^-)_{q^2 \in [15, 22]}^{\text{exp}} \text{ GeV}^2 = (8.5 \pm 0.3 \pm 0.4) \times 10^{-8}. \quad (3.80)$$

The reason for opting for these decay modes is that the relevant hadronic uncertainties are under good theoretical control, as discussed in Sec. 2.3.

<sup>13</sup> Notice also that the notation of Ref. [182] is such that their Wilson coefficient  $C_P$ , which we can call  $\tilde{C}_P$ , is related to ours via  $C_P = \sqrt{x_\ell x_b} \tilde{C}_P / \sin^2 \theta_W$ .

The hadronic quantity entering the  $B_s \rightarrow \mu^+ \mu^-$  decay amplitude is the decay constant,  $f_{B_s}$ . It has been abundantly computed by means of numerical simulations of QCD on the lattice (LQCD) and its value is nowadays one of the most accurately computed hadronic quantities as far as  $B_{(s)}$ -mesons are concerned [77]. The hadronic form factors entering the  $B \rightarrow K \mu^+ \mu^-$  decay amplitude have been directly computed in LQCD only in the region of large  $q^2$ 's [131, 132], which explains why we use  $\mathcal{B}(B \rightarrow K \mu^+ \mu^-)_{\text{high } q^2}^{\text{exp}}$  to do phenomenology. Furthermore, since the bin corresponding to  $q^2 \in [15, 22]$  GeV<sup>2</sup> is rather wide and away from the very narrow charmonium resonances, the assumption of quark-hadron duality is likely to be valid [133]. By using the recent LQCD results for the form factors provided by HPQCD [131] and MILC Collaborations [132], the SM results are

$$\mathcal{B}(B \rightarrow K \mu^+ \mu^-)_{\text{high } q^2} = \left\{ (10.0 \pm 0.5) \times 10^{-8} \Big|_{\text{HPQCD}}, (10.7 \pm 0.5) \times 10^{-8} \Big|_{\text{MILC}} \right\}, \quad (3.81)$$

both being about  $2\sigma$  larger than the experimental value measured at LHCb.<sup>14</sup> Since the current disagreement between theory and experiment needs to be corroborated by more data, we decided to impose all the constraints to  $3\sigma$  accuracy. We will then discuss the impact of  $\mathcal{B}(B \rightarrow K \mu^+ \mu^-)_{\text{high } q^2}^{\text{exp}}$  on 2HDM if the current discrepancy remains, i.e. by requiring the 2HDM to compensate the disagreement between theory (SM) and experiment at the level of  $2\sigma$  and more. Notice also that the measured  $\mathcal{B}(B_s \rightarrow \mu^+ \mu^-)^{\text{exp}}$  is slightly smaller than predicted,  $\mathcal{B}(B_s \rightarrow \mu^+ \mu^-)^{\text{SM}} = (3.65 \pm 0.23) \times 10^{-9}$  [115].

We now use the results of our scan from Sec. 3.2, require the  $3\sigma$  agreement between experiment and theory, which means that we add the generic 2HDM Wilson coefficients derived in the previous Section to the SM values. The result, in the plane  $(\tan \beta, m_{H^\pm})$ , is shown in Fig. 3.10 for each type of 2HDM we consider. We learn that both  $\mathcal{B}(B_s \rightarrow \mu^+ \mu^-)$  and  $\mathcal{B}(B \rightarrow K \mu^+ \mu^-)_{\text{high } q^2}$  exclude the low  $\tan \beta \lesssim 1$  region regardless of the type of 2HDM considered. The limit of exclusion of low  $\tan \beta$  coming from  $\mathcal{B}(B \rightarrow K \mu^+ \mu^-)_{\text{high } q^2}$  is slightly larger than the one arising from  $\mathcal{B}(B_s \rightarrow \mu^+ \mu^-)$ . The limit on low  $\tan \beta$  obtained in this way for each of our four models is given in Tab. 3.3.

Besides excluding  $\tan \beta \lesssim 1$ , it may appear as a surprise that the large  $\tan \beta$  are not excluded by these data. The reason for that is the fact that the (pseudo-)scalar Wilson coefficient, with respect to the dominant (axial-)vector one, comes with a term proportional to  $(m_{B_s}/m_W)^2$  which suppresses the large  $\tan \beta$  values. This feature can be easily verified in the Type II model for which the coefficients  $C_{S,P}$ , in the large  $\tan \beta$  limit, are given in Eq. (3.62). This is why only a small number of points have been eliminated from our scan of Type II model at large  $\tan \beta$  but relatively light  $m_{H^\pm}$ .

Model	Type I	Type II	Type X	Type Z
$\tan \beta$	$> 1.0$	$> 0.9$	$> 1.0$	$> 1.3$

**Table 3.3:** Allowed values of low  $\tan \beta$  (at 99% CL) for the different 2HDMs. See text for details.

Since the SM value is in slight tension with  $\mathcal{B}(B \rightarrow K \mu^+ \mu^-)_{\text{high } q^2}^{\text{exp}}$  at the  $2.1\sigma$  level, we can now check which of the models discussed in this paper can be made consistent with

<sup>14</sup>In the following we will average the results obtained by using the two sets of form factors obtained in LQCD.

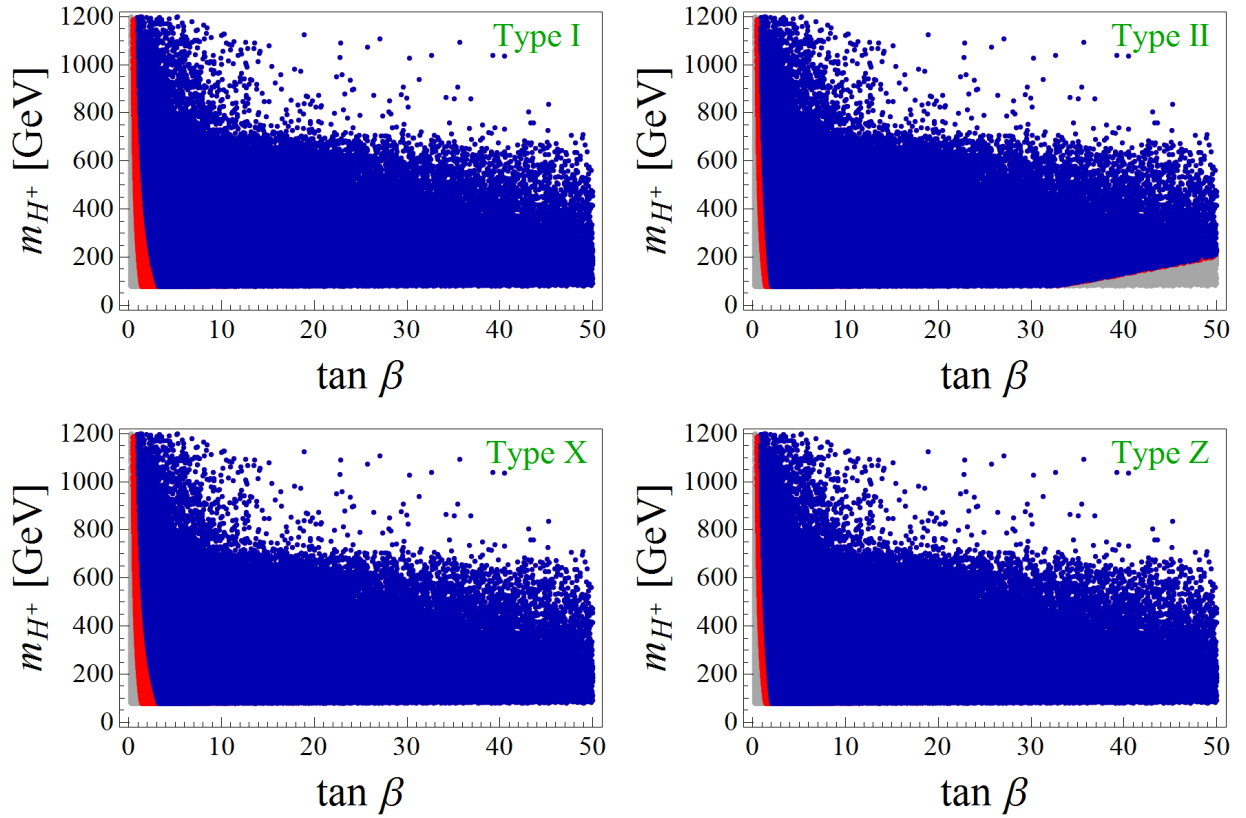


**Figure 3.10:** Results of the scan given in Fig. 4.4 after imposing the constraints coming from  $\mathcal{B}(B_s \rightarrow \mu^+ \mu^-)$  and  $\mathcal{B}(B \rightarrow K \mu^+ \mu^-)_{\text{high } q^2}$  to  $3\sigma$  accuracy. Blue points are allowed by all observables, while gray points are excluded by  $\mathcal{B}(B_s \rightarrow \mu^+ \mu^-)$ , and the red ones are excluded by  $\mathcal{B}(B \rightarrow K \mu^+ \mu^-)_{\text{high } q^2}$ .

the experimental data if any disagreement beyond  $2\sigma$  between theory (SM) and experiment is to be attributed to 2HDM. It turns out that two such models are Type II and Type Z 2HDM, which we illustrate in Fig. 3.11. For the other two scenarios (Type I and Type X) the NP contributions are either too small or already in conflict with  $\mathcal{B}(B_s \rightarrow \mu^+ \mu^-)^{\text{exp}}$ . From Figs. 3.11 and 3.12 we see that in order to explain the discrepancy one needs a relatively light charged scalar: (i)  $m_{H^\pm} \lesssim 735$  GeV and  $\tan \beta > 2.3$  in the Type II scenario, and (ii)  $m_{H^\pm} \lesssim 380$  GeV and  $\tan \beta > 3.5$  for the Type Z scenario. Since the masses of the additional scalars are correlated, we see that  $m_H$  and  $m_A$  become bounded as well, cf. Fig. 3.12. In the case of Type II and Type Z 2HDM an additional bound on the charged Higgs has been recently derived from the inclusive mode  $\mathcal{B}(B \rightarrow X_s \gamma)$ . After comparing the experimental spectra with theoretical expressions in which the higher order QCD corrections have been included, the lower bound  $m_{H^\pm} > 570$  GeV (95% CL) was obtained in Ref. [181] (c.f. also Ref. [193]). This bound is superposed on our results in Figs. 3.11 and 3.12, which then also eliminates Type Z 2HDM. Furthermore, we can say that the requirement of agreement between theory and experiment to  $2\sigma$ , for the quantities discussed in this Section, reduces the available space of parameters for Type II 2HDM to  $m_{H^\pm} \in (570, 735)$  GeV, and  $\tan \beta \in (16, 35)$ , while the available range of values for the mass of the CP-odd Higgs becomes  $m_A \in (145, 865)$  GeV.

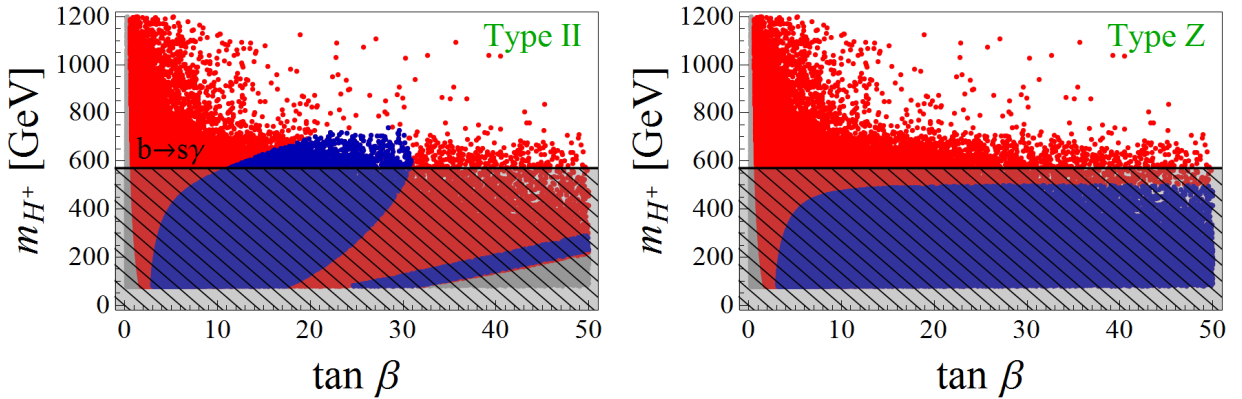


**Figure 3.11:** Results of the scan in Fig. 4.4 after imposing the  $b \rightarrow s$  constraints to  $2\sigma$  accuracy. The hatched area is excluded by  $\mathcal{B}(B \rightarrow X_s \gamma)$  at 95% [181]. See Fig. 3.10 for the color code.

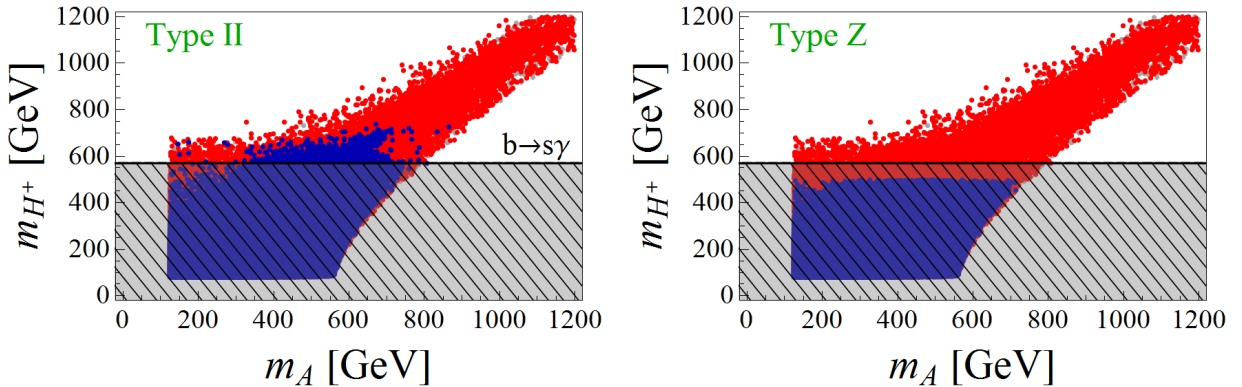


**Figure 3.12:** Same as in Fig. 3.11 but in the  $(m_A, m_{H^\pm})$  plane.

In what follows we will assume that the  $2\sigma$  disagreement of the measure  $\mathcal{B}(B \rightarrow K \mu^+ \mu^-)_{\text{high } q^2}^{\text{exp}}$  with respect to the SM prediction indeed remains as such in the future and

discuss the consequences on the decays  $\mathcal{B}(B_s \rightarrow \tau^+\tau^-)$  and  $\mathcal{B}(B \rightarrow K\tau^+\tau^-)_{\text{high } q^2}$  if the Type II 2HDM is used to explain the disagreement. From Eq. (2.63) we can see that

$$\frac{\mathcal{B}(B_s \rightarrow \tau^+\tau^-)}{\mathcal{B}(B_s \rightarrow \tau^+\tau^-)^{\text{SM}}} = \frac{\mathcal{B}(B_s \rightarrow \mu^+\mu^-)}{\mathcal{B}(B_s \rightarrow \mu^+\mu^-)^{\text{SM}}} - \frac{|C_S^{\tau\tau}|^2}{|C_{10}^{\text{SM}}|^2} \frac{m_{B_s}^2}{(m_b + m_s)^2}, \quad (3.82)$$

where the only remaining  $m_\ell$  dependence comes from the last numerator in the factor multiplying  $|C_S - C_S'|^2$  in Eq. (2.63). In Fig. 3.13 we illustrate the validity of the above equality. Notice that a tiny departure from equality comes from the large  $\tan \beta$  values which enhance the  $C_S$  contribution. In other words, the current experimental result  $\mathcal{B}(B_s \rightarrow \mu^+\mu^-)^{\text{exp}}$ , which is slightly lower than the one predicted in the SM, is expected to lead to  $\mathcal{B}(B_s \rightarrow \tau^+\tau^-)^{\text{exp}}$  compatible or slightly lower than predicted in the SM. The cancellation of the lepton mass in  $\mathcal{B}(B_s \rightarrow \ell^+\ell^-)^{2\text{HDM}}$ , discussed above, does not occur in  $\mathcal{B}(B \rightarrow K\ell^+\ell^-)_{\text{high-}q^2}^{2\text{HDM}}$ . As a result we obtain,

$$\frac{\mathcal{B}(B \rightarrow K\tau^+\tau^-)^{\text{Type II}}}{\mathcal{B}(B \rightarrow K\tau^+\tau^-)^{\text{SM}}} \lesssim \frac{\mathcal{B}(B \rightarrow K\mu^+\mu^-)^{\text{Type II}}}{\mathcal{B}(B \rightarrow K\mu^+\mu^-)^{\text{SM}}}, \quad (3.83)$$

where we omitted the subscript “high- $q^2$ ” to avoid too heavy a notation. Illustration is provided in Fig. 3.13. We can rephrase this observation with an equivalent statement:

$$\frac{\mathcal{B}(B \rightarrow K\tau^+\tau^-)^{\text{Type II}}}{\mathcal{B}(B \rightarrow K\mu^+\mu^-)^{\text{Type II}}} < \frac{\mathcal{B}(B \rightarrow K\tau^+\tau^-)^{\text{SM}}}{\mathcal{B}(B \rightarrow K\mu^+\mu^-)^{\text{SM}}}. \quad (3.84)$$

To be fully explicit, we obtain

$$\left. \frac{\mathcal{B}(B \rightarrow K\tau^+\tau^-)}{\mathcal{B}(B \rightarrow K\mu^+\mu^-)} \right|_{\text{high-}q^2} \in (1.12, 1.14)_{\text{SM}}, (1.0, 1.1)_{\text{Type II}}. \quad (3.85)$$

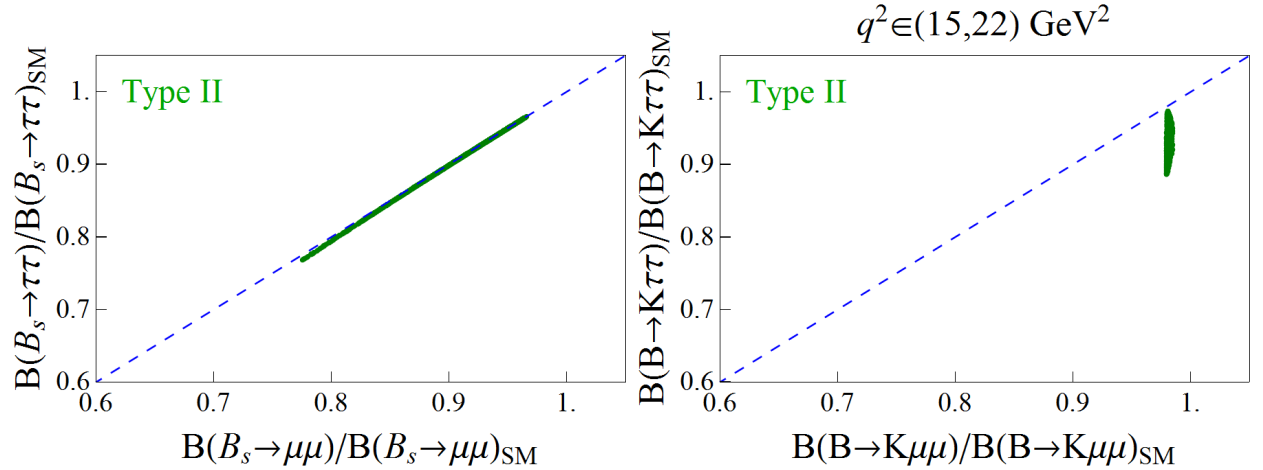


**Figure 3.13:** We show the branching fractions of the decay to  $\tau$ -leptons with respect to their SM predictions, as obtained in the Type II 2HDM, consistent with experimental results for the decays to muons in the final state.

## 3.6 The light CP-odd Higgs window

In this Section, we consider an alternative scenario to the usual belief that the additional scalars should be heavier than  $m_h^{\text{SM}} = 125$  GeV. By keeping the assumption that  $h \simeq h^{\text{SM}}$  is the scalar discovered at the LHC, we explore the possibility that a CP-odd Higgs  $A$  lighter than  $h$  was missed by the direct searches performed thus far.

The following questions will be addressed in this Section:

- (i) Is this scenario consistent with current theoretical and phenomenological constraints?
- (ii) Which are the most sensitive probes at low and high energies to a light CP-odd Higgs?

In the following, we will describe our scan of the parameter space and the main flavor constraints in Sec. 3.6.1. In Sec. 3.7, we investigate the possibility of probing a light CP-odd in exclusive decays of the Higgs to quarkonia. Finally, we propose in Sec. 3.8 some quarkonia decay which are highly sensitive to the light CP-odd contributions and can be studied at current (LHCb) and future (Belle-II) experiments.

### 3.6.1 General scan for a light CP-odd

To answer the above-asked questions, we perform a scan similar to the one presented in Sec. 3.2 but with a different range for the scalar masses:

$$\begin{aligned} \tan \beta &\in (0.2, 50], & \alpha &\in \left(-\frac{\pi}{2}, \frac{\pi}{2}\right), & |M^2| &\leq (1.2 \text{ TeV})^2, \\ m_{H^\pm} &\in (m_W, 1.2 \text{ TeV}), & m_H &\in (m_h, 1.2 \text{ TeV}), & m_A &\in (20 \text{ GeV}, m_h). \end{aligned} \quad (3.86)$$

where the lower limit  $m_A > 20$  GeV is chosen to avoid resonant contributions of the type  $\mathcal{B}(\Upsilon \rightarrow \gamma A)$  and  $\mathcal{B}(B \rightarrow KA)$ , which are constrained by limits reported by BaBar [194–196].

In addition to the general constraints presented in Sec. 3.1, the light CP-odd Higgs can contribute significantly to the SM-like Higgs total width  $\Gamma_h$ , which is indirectly constrained by LHC data. More precisely, although ATLAS and CMS do not have enough mass resolution to directly probe  $\Gamma_h$ , non-standard contributions to the tiny  $\Gamma_h^{\text{SM}} = 4.10(4)$  MeV [197] are constrained by the analysis of Higgs strength signals.<sup>15</sup> The most up-to-date analysis of Higgs data suggests that [198]

$$\frac{|\Gamma_h - \Gamma_{h^{\text{SM}}}|}{\Gamma_{h^{\text{SM}}}} \lesssim 0.3, \quad (3.87)$$

which will also be imposed as a constraint to our scan. For  $m_A < m_h/2$ , the most potentially dangerous contribution to  $\Gamma_h$  comes from  $h \rightarrow AA$ , which is generated via the trilinear scalar coupling<sup>16</sup>

$$\begin{aligned} \lambda_{hAA} = \frac{1}{2v^2 \sin 2\beta} &\left[ m_h^2 (\cos(\alpha - 3\beta) + 3 \cos(\alpha + \beta)) - 4m_A^2 \sin 2\beta \sin(\alpha - \beta) \right. \\ &\left. - 4M^2 \cos(\alpha + \beta) \right], \end{aligned} \quad (3.88)$$

<sup>15</sup>The term *invisible* width is sometimes used to describe this quantity, but it is misleading since the non-standard contributions to  $\Gamma_h$  can be potentially observable. The term *non-standard* decay width is more suitable.

<sup>16</sup>We agree with the expression derived in Ref. [199].

which enters the Lagrangian

$$\mathcal{L} \supset \frac{\lambda_{hAA}}{2!} hAA. \quad (3.89)$$

The total rate for this decay is given by

$$\Gamma(h \rightarrow AA) = \frac{|\lambda_{hAA}|^2 v^2}{32\pi m_h} \sqrt{1 - \frac{4m_A^2}{m_h^2}}. \quad (3.90)$$

To be consistent with current Higgs data, the coupling  $\lambda_{hAA}$  has to be sufficiently small in the region  $m_A < m_h/2$ . This constraint is particularly strong since bosonic interactions can be orders of magnitude stronger than the Yukawa interactions, which dominate the SM Higgs total width. Furthermore, the channel  $h \rightarrow ZA$  is also open for a very light CP-odd scalar, i.e. with  $m_A < m_h - m_Z$ . The expression for this decay rate is given by

$$\Gamma(h \rightarrow ZA) = \frac{1}{16\pi} \frac{\cos^2(\beta - \alpha)}{v^2} \frac{\lambda^{3/2}(m_h, m_Z, m_A)}{m_h^3}, \quad (3.91)$$

which vanishes identically in the alignment limit  $\cos(\beta - \alpha) = 0$ .

The constraints described above are combined with the ones presented in Sec. 3.2 to determine the allowed parameters. It is important to mention that a scan of parameters consistent with the constraints listed above favors the moderate and small values of  $\tan \beta \in (0.2, 15]$ . Larger values of  $\tan \beta$  can be probed around the alignment limit as it can be seen from Eq. (3.6). For that reason, in addition to the *free* scan, we also perform a *fine-tuned* scan, i.e. with  $m_H \approx |M|$ . We combine both results and show them in Fig. 3.14 for Type I and Type II models. Similar results are obtained for Type X and Type Z. The constraints coming from  $b \rightarrow s\gamma$  and exclusive  $b \rightarrow s\ell\ell$  are also superimposed on the same plot to  $3\sigma$  accuracy, giving the allowed points in blue [181, 186].<sup>17</sup> From this plot we observe that the charged Higgs cannot be infinitely heavy, since  $m_{H^\pm}$  is correlated with the light CP-odd mass  $m_A$  due to the theory constraints discussed above. The lower bound on the charged Higgs,  $m_{H^\pm} \geq 439$  GeV [181], eliminates many points in Type II and Type Z models. As it can be seen from Fig. 3.14, among the remaining points in the parameter space of the Type II model, the free scan prefers low  $\tan \beta \approx 2$  values, while the large  $\tan \beta$  values can only be accessed through the scan in the  $m_H \approx |M|$  direction. The same observation applies to the Type Z model.

Notice also from Fig. (3.14) that one cannot simultaneously access  $m_A < m_h/2$  and have large  $\tan \beta$ , except for the very tuned solutions. To see that we expand Eq. (3.88) around the alignment limit,  $\delta = \cos(\alpha - \beta) \approx 0$ , and obtain

$$\lambda_{hAA} = \frac{m_h^2 + 2m_A^2 - 2M^2}{v^2} + \frac{2(m_h^2 - m_H^2)}{v^2 \tan 2\beta} \delta + \mathcal{O}(\delta^2). \quad (3.92)$$

To suppress  $\Gamma(h \rightarrow AA)$  in the perfect alignment limit, one needs  $2M^2 = m_h^2 + 2m_A^2$ , which for the low  $m_A$  gives  $M^2 \leq 3m_h^2/4 \ll m_H^2$ . Therefore, in order to get a small width  $\Gamma(h \rightarrow AA)$  one needs  $M^2 \ll m_H^2$ , which cannot be simultaneously satisfied with the condition  $M \approx m_H$ , which is needed to find large values of  $\tan \beta$ .

<sup>17</sup>Notice that we consider bounds only to  $3\sigma$  accuracy, since the 2HDM contributions cannot explain the deficit in  $\mathcal{B}(B \rightarrow K\mu\mu)_{q^2 \in [15, 22]} \text{ GeV}^2$ , which is still not significant. In this case, the constraint from  $b \rightarrow s\gamma$  becomes  $m_{H^\pm} > 439$  GeV [181].

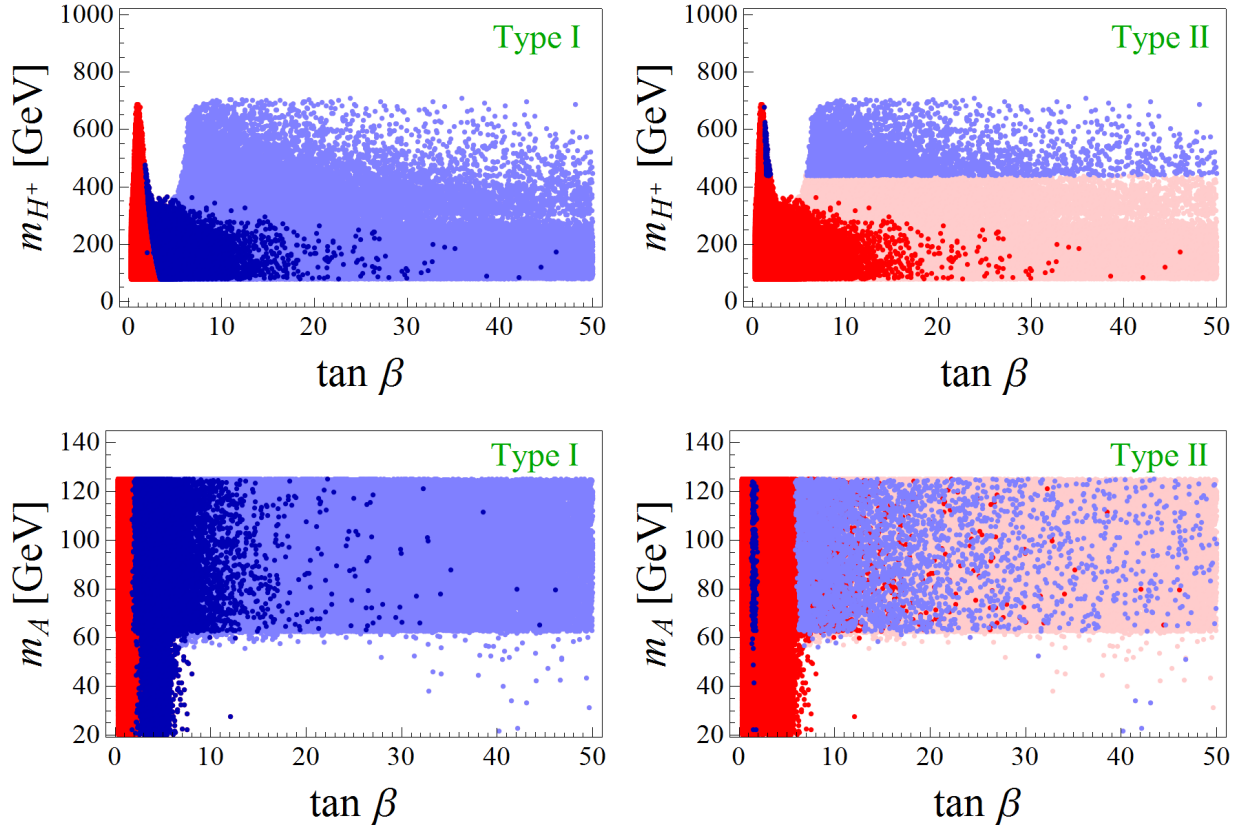


**Figure 3.14:** Results of the scan of parameters (3.86) after imposing constraints discussed in the text. Darker/lighter points correspond to the free/fine-tuned scan. Notice in particular that the red points are forbidden by the flavor bounds [181, 186]. The results for the models of Type X and Z are similar to the ones of type I and II, as described in the text.

The conclusion of the study performed in this Section is that a light CP-odd Higgs is perfectly consistent with current theory and phenomenology constraints in some regions of the parameter space. In the following we discuss the most sensitive indirect probes of a light CP-odd Higgs, which can help us to disentangle among the various 2HDM.

### 3.7 Seeking the CP-odd Higgs via $h \rightarrow P\ell\ell$

In this Section, we propose to study decays of Higgs to the pseudoscalar heavy quarkonia ( $P$ ),  $h \rightarrow P\ell^+\ell^-$ , ( $P \in \{\eta_c, \eta_b\}$ ) processes in which the CP-odd Higgs can contribute at the tree level and make a significant enhancement of various decay rates. The level of such an enhancement is related to the structure of the Yukawa couplings and to the mass of the  $A$ -state. As we shall see in the following, we find that  $\mathcal{B}(h \rightarrow \eta_{c,b}\tau^+\tau^-)$  can be enhanced by an order of magnitude with respect to its SM value, which is why we find it worth studying in experiments.

Studies of the Higgs boson to quarkonia attracted quite a bit of attention: Radiative decay  $h \rightarrow J/\psi\gamma$  could be used to probe the Yukawa coupling  $h\bar{c}c$ , a possibility which is compromised in the case of  $b$ -quark quarkonia ( $\Upsilon(nS)$ ) due to cancellation of two contributions to the decay amplitude [200]. A possibility to study  $h \rightarrow PZ$  and  $h \rightarrow VZ$  (where  $V$  and  $P$  stand for the vector and pseudoscalar quarkonium states, respectively) was elaborated in Refs. [201, 202]. Finally, a possibility to search for the effects of lepton flavour violation via  $h \rightarrow V\ell_1\ell_2$  has been proposed in Ref. [203].

In the following, we derive the general expressions for  $\mathcal{B}(h \rightarrow P\ell^+\ell^-)$  both in the SM and in 2HDM with a light CP-odd Higgs state. The results of the scan of parameters presented above is then used to test the sensitivity of  $\mathcal{B}(h \rightarrow \eta_{c,b}\ell^+\ell^-)$  on the presence of a light CP-odd Higgs state. We will not discuss the decays  $\mathcal{B}(h \rightarrow PZ)$  in this thesis, since the 2HDM contributions are expected to be much smaller in this case. We refer the reader to Ref. [204] where an extensive discussion of these decays is made.

### Expressions for $\mathcal{B}(h \rightarrow P\ell^+\ell^-)$

In our notation,  $P$  denotes the pseudoscalar quarkonium carrying momentum  $k$ , while  $Z$  flies with momentum  $p_Z$ . The dilepton invariant mass squared in the  $P\ell^+\ell^-$  final state is considered as  $q^2 = (p_\ell + p_{\bar{\ell}})^2$ , with  $p_{\ell,\bar{\ell}}$  being the momentum of the outgoing leptons.

In the SM, the decay  $h \rightarrow P\ell^+\ell^-$  occurs via the diagrams shown in Fig. 3.15. The dominant contribution comes from  $h \rightarrow Z^*Z^* \rightarrow P\ell\ell$  (Fig. 3.15c), which is much larger than the direct ones,  $h \rightarrow Z\bar{q}q \rightarrow ZP$  (Fig. 3.15a and 3.15b), and the one generated at loop level,  $h \rightarrow Z^*\gamma^* \rightarrow P\ell\ell$ , (Fig. 3.15d).<sup>18</sup> The contribution from the dominant diagram to the SM amplitude reads

$$\begin{aligned} \mathcal{M}(h \rightarrow P\ell^+\ell^-)^{2c} = & -\frac{1}{4} \left( \frac{g}{\cos\theta_W} \right)^3 m_Z \frac{g_A^q f_P}{(q^2 - m_Z^2)(k^2 - m_Z^2)} \left( -g_\mu^\alpha + \frac{q^\mu q_\alpha}{m_Z^2} \right) \\ & \times \left( -g^{\nu\alpha} + \frac{k^\nu k^\alpha}{m_Z^2} \right) k_\nu \bar{u}_\ell \gamma^\mu (g_V^\ell - g_A^\ell \gamma_5) v_\ell. \end{aligned} \quad (3.93)$$

The full expression, which includes all contributions depicted in Fig. 3.15, is given in the Appendix of Ref. [204]. We note, however, that the contribution of the diagram in Fig. 3.15d vanishes in the decay rate. Notice also that Eq. (3.93) must be multiplied by  $\sin(\beta - \alpha)$  to obtain the equivalent 2HDM amplitude.

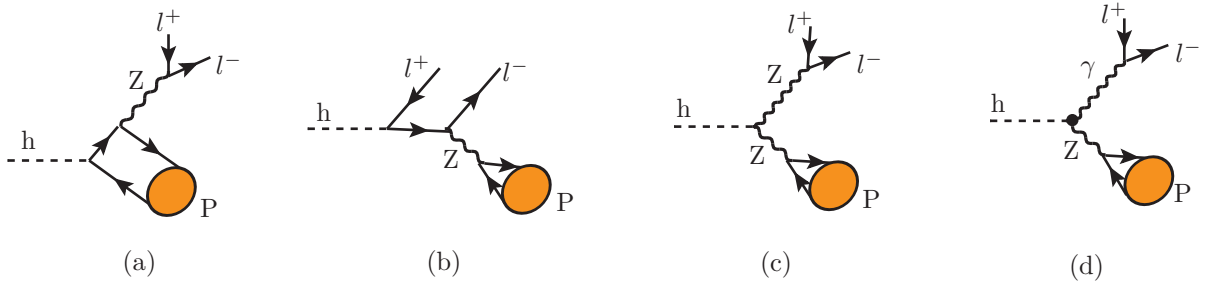


**Figure 3.15:** Diagrams relevant to  $h \rightarrow P\ell^+\ell^-$  decay in the SM. The full dot in the diagram (d) indicates that the vertex is loop-induced. Its contribution to the decay rate is nevertheless zero.

Diagrams arising in the 2HDM setup are shown in Fig. 3.16, of which the first two are numerically much less significant than the remaining three. The contributions of those latter (dominant) diagrams to the decay amplitude read:

$$\mathcal{M}(h \rightarrow P\ell^+\ell^-)^{3c} = - \left( \frac{g}{2 \cos\theta_W} \right)^2 \frac{m_q \xi_A^q m_P^2 f_P}{v} \frac{\cos(\beta - \alpha)}{(q^2 - m_Z^2)(k^2 - m_A^2)}$$

<sup>18</sup>Notice that the photon cannot couple directly to  $P$  because the vector matrix elements vanishes due to parity conservation.

$$\times \left( -g_{\mu\nu} + \frac{q_\mu q_\nu}{m_Z^2} \right) (k+p)^\mu \bar{u}_\ell \gamma^\nu (g_V^\ell - g_A^\ell \gamma_5) v_\ell, \quad (3.94)$$

$$\begin{aligned} \mathcal{M}(h \rightarrow P\ell^+\ell^-)^{3d} &= \left( \frac{g}{2 \cos \theta_W} \right)^2 \frac{m_\ell \xi_A^\ell}{v} \frac{g_A^q f_P \cos(\beta - \alpha)}{(q^2 - m_A^2)(k^2 - m_Z^2)} \\ &\times \left( -g_{\mu\nu} + \frac{k_\mu k_\nu}{m_Z^2} \right) (q+p)^\mu k^\nu \bar{u}_\ell \gamma_5 v_\ell, \end{aligned} \quad (3.95)$$

$$\mathcal{M}(h \rightarrow P\ell^+\ell^-)^{3e} = -\lambda_{hAA} v \frac{m_q \xi_A^q}{v} \frac{m_\ell \xi_A^\ell}{v} \frac{m_P^2 f_P}{2m_q} \frac{1}{(q^2 - m_A^2)(k^2 - m_A^2)} \bar{u}_\ell \gamma_5 v_\ell. \quad (3.96)$$

In the limit in which  $\Gamma_A/m_A \ll 1$ , one can work in the narrow width approximation, which amounts to replacing

$$\frac{1}{(q^2 - m_X^2)^2 + m_X^2 \Gamma_X^2} \rightarrow \delta(q^2 - m_X^2) \frac{\pi}{m_X \Gamma_X}. \quad (3.97)$$

This approximation is adopted throughout this thesis both for  $X = Z$  and  $X = A$ . We emphasize that, for clarity, we disregarded the direct contributions to the amplitude because they are numerically much smaller and can be safely neglected. Therefore, to a very good approximation the decay rate can be written as

$$\Gamma(h \rightarrow P\ell^+\ell^-) \simeq \Gamma(h \rightarrow PZ^* \rightarrow P\ell^+\ell^-) + \Gamma(h \rightarrow PA^* \rightarrow P\ell^+\ell^-). \quad (3.98)$$

We checked that the interference terms are indeed very small and the above formula is useful for the phenomenology we are interested in. For the explicit expressions of the separate rates in Eq. (3.98) we obtain,

$$\begin{aligned} \Gamma(h \rightarrow PZ^* \rightarrow P\ell^+\ell^-) &= \frac{f_P^2 m_Z^3}{384\pi^2 \Gamma_Z m_h^3 v^6} [\cos^2(2\theta_W) + 4 \sin^4 \theta_W] \\ &\left( g_A^q - \frac{\xi_A^q m_P^2 \cos(\beta - \alpha)}{2(m_A^2 - m_P^2)} \right)^2 \lambda^{3/2}(m_h, m_P, m_Z), \end{aligned} \quad (3.99)$$

$$\begin{aligned} \Gamma(h \rightarrow PA^* \rightarrow P\ell^+\ell^-) &= \frac{f_P^2 m_A}{512\pi^2 \Gamma_A m_h^3 v^2} \left( \frac{m_\ell \xi_A^\ell}{v} \right)^2 \left[ \lambda_{hAA} \frac{m_P^2}{m_A^2 - m_P^2} \frac{\xi_A^q}{v} v^2 \right. \\ &\left. + 2 \cos(\beta - \alpha) \frac{g_A^q}{v} (m_h^2 - m_A^2) \right]^2 \lambda^{1/2}(m_h, m_P, m_A). \end{aligned} \quad (3.100)$$

In the above formulas  $g_V^f = T_f^3 - 2Q_f \sin^2 \theta_W$ ,  $g_A^f = T_f^3$ , and we neglected the additive terms  $\propto m_\ell^2/m_Z^2$ . We emphasize once again that the above expression for  $\Gamma(h \rightarrow P\ell^+\ell^-)$  should be viewed as a very good approximation, whereas the full expressions are provided in the Appendix of Ref. [204]. Essential hadronic quantities needed to evaluate the amplitudes defined above are [205, 206]:

$$f_{\eta_c} = 391 \pm 4 \text{ MeV}, \quad f_{\eta_b} = 667 \pm 7 \text{ MeV}. \quad (3.101)$$

To get the branching fraction in a 2HDM setup, one should also be particularly careful with the width of the Higgs boson  $\Gamma_h$  which should not be much larger than its SM value, e.g.  $\Gamma_h/\Gamma_h^{\text{SM}} \lesssim 1.4$ , a condition that provides a particularly stringent bound on the coupling of  $h$  to two light CP-odd Higgses in the situation in which  $m_A \leq m_h/2$ . Finally, since the

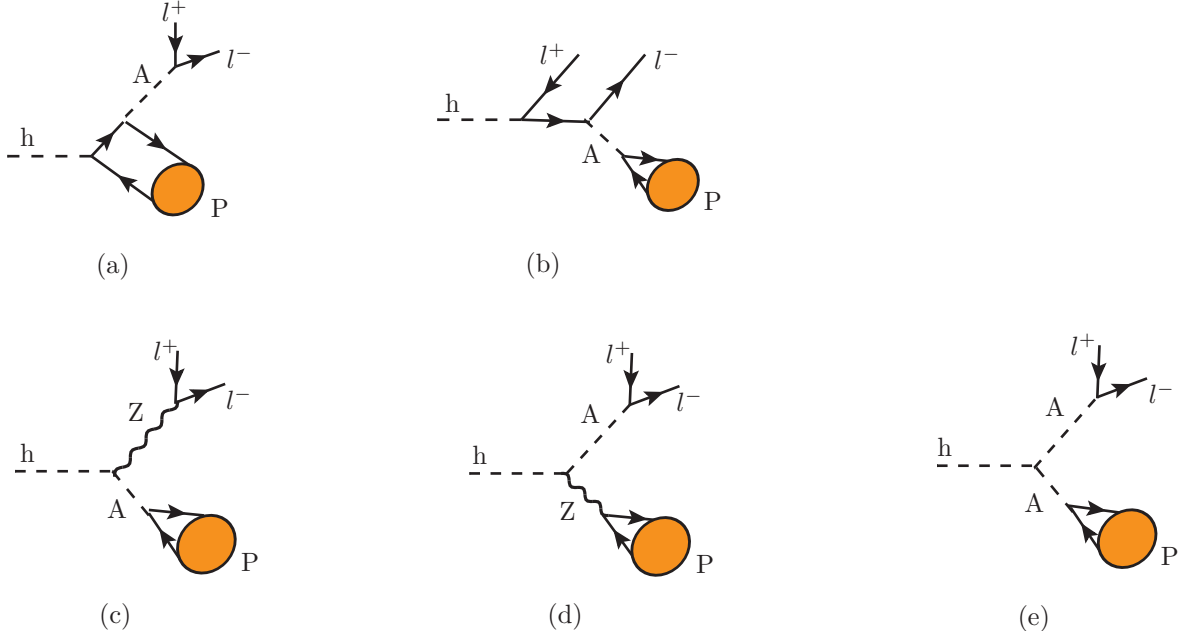


**Figure 3.16:** Contributions to the  $h \rightarrow P\ell^+\ell^-$  decay amplitude in a 2HDM scenario.

above formulas require the knowledge of the width of  $A$ , we give that expression too, in which we include  $\Gamma_A = \Gamma(A \rightarrow f\bar{f}) + \Gamma(A \rightarrow \gamma\gamma)$ , which are given by

$$\Gamma(A \rightarrow f\bar{f}) = \theta(m_A - 2m_f) |\xi_A^f|^2 \frac{N_c m_f^2}{8\pi v^2} m_A \sqrt{1 - \frac{4m_f^2}{m_A^2}},$$

$$\Gamma(A \rightarrow \gamma\gamma) = \frac{\alpha_{\text{em}}^2}{16\pi^3 v^2} m_A^3 \left| \sum_f \xi_A^f N_c Q_f^2 x_f F_{\gamma\gamma}(x_f) \right|^2, \quad (3.102)$$

where  $N_c = 3$  for quarks and  $N_c = 1$  for leptons, the electric charge for leptons, up-type and down-type quarks is  $Q_\ell = -1$ ,  $Q_u = 2/3$ ,  $Q_d = -1/3$ , respectively, and  $f$  runs over all available quark and lepton flavors. In the above expression we used the notation  $x_f = m_f^2/m_A^2$ , and the loop function reads

$$F_{\gamma\gamma}(x) = \begin{cases} \frac{1}{2} \left( i\pi + \log \left[ \frac{1 + \sqrt{1-4x}}{1 - \sqrt{1-4x}} \right] \right)^2, & \text{for } x < 1/4 \\ -2 \arcsin^2 \left( \frac{1}{2\sqrt{x}} \right), & \text{otherwise} \end{cases}. \quad (3.103)$$

Notice that  $\Gamma(A \rightarrow \gamma\gamma) \ll \Gamma(A \rightarrow f\bar{f})$  and our conclusion would remain the same even if we neglected  $\Gamma(A \rightarrow \gamma\gamma)$ . For the same reason we neglect the  $\Gamma(A \rightarrow gg)$  contribution to the full width of  $A$ .

## Phenomenology

In this Section we combine the results of the scan discussed in Sec. 3.6.1 with the expressions give above to evaluate

$$R_{\eta_{cb}}^{\tau\tau} = \frac{\mathcal{B}(h \rightarrow \eta_{cb}\tau^+\tau^-)^{2\text{HDM}}}{\mathcal{B}(h \rightarrow \eta_{cb}\tau^+\tau^-)^{\text{SM}}} \quad \text{and} \quad R_{\eta_{cb}}^{\mu\mu} = \frac{\mathcal{B}(h \rightarrow \eta_{cb}\mu^+\mu^-)^{2\text{HDM}}}{\mathcal{B}(h \rightarrow \eta_{cb}\mu^+\mu^-)^{\text{SM}}}, \quad (3.104)$$

where  $\eta_{cb}$  means either  $\eta_c$  or  $\eta_b$ . The range of values for each of the ratios (3.104), that we obtain by using the results of the scan for each of the 2HDM realizations are summarized in Tab. 3.4.

Ratio	$R_{\eta_c}^Z$	$R_{\eta_b}^Z$	$R_{\eta_c}^{\mu\mu}$	$R_{\eta_b}^{\mu\mu}$	$R_{\eta_c}^{\tau\tau}$	$R_{\eta_b}^{\tau\tau}$
Type I	(0.7, 1.0)	(0.7, 1.0)	(0.7, 1.0)	(0.7, 1.0)	(0.7, 3.3)	(0.7, 3.6)
Type II	(0.7, 1.0)	(0.3, 1.7)	(0.7, 1.0)	(0.7, 1.7)	(0.8, 2.3)	(0.9, 130)
Type X	(0.7, 1.0)	(0.7, 1.0)	(0.7, 1.1)	(0.7, 1.1)	(0.7, 21)	(0.7, 23)
Type Z	(0.7, 1.0)	(0.3, 1.7)	(0.7, 1.0)	(0.7, 1.7)	(0.7, 1.2)	(0.7, 1.7)

**Table 3.4:** Resulting intervals for the ratios obtained from the scans in various types of 2HDM.

In order to exacerbate the sensitivity to the CP-odd Higgs, one should consider  $\tau$ -leptons in the final state. This is because the second part in Eq. (3.98) becomes important,  $\Gamma(h \rightarrow PA^* \rightarrow P\ell^+\ell^-) \propto m_\ell^2$ , which can also be seen by using an approximate relation,  $\Gamma(h \rightarrow \eta_{cb}\tau\tau) \approx \Gamma(h \rightarrow \eta_{cb}A) \mathcal{B}(A \rightarrow \tau\tau)$ . Indeed, on the basis of the results presented in Tab. 3.4 we see that the ratios  $R_{\eta_c}^{\tau\tau}$  and  $R_{\eta_b}^{\tau\tau}$  depend much more on the light CP-odd Higgs than the ones with the light leptons in the final state. This is particularly true for the Type I, II and X models, the results highlighted in Tab. 3.4, and illustrated in Fig. 3.17 for Type II and X. We already stressed that the Type II model is far more constrained than Type X because of the constraint coming from  $B \rightarrow X_s\gamma$ . Yet the results for  $R_{\eta_b}^{\tau\tau}$  exhibit the similar enhancement in both models, which can be traced back to  $\Gamma(h \rightarrow PA^* \rightarrow P\ell^+\ell^-) \propto m_\ell^2 \tan^2 \beta$ , a common feature of both models. Notice, however, that for larger values of  $m_A$ , the value of  $\mathcal{B}(h \rightarrow \eta_{cb}\tau^+\tau^-)$  rapidly approaches its SM result, which is why we focus on these decay modes as possible probes of the light CP-odd Higgs ( $m_A \lesssim m_h$ ).

Finally, it is worth mentioning a correlation between  $R_{\eta_c}^{\tau\tau}$  and  $R_{\eta_b}^{\tau\tau}$  in Type I and Type X models, which is shown in Fig. 3.18. It is easy to understand its origin once one realizes that  $\Gamma(h \rightarrow PA^* \rightarrow P\ell^+\ell^-)$  dominates the full decay rate (3.98), and since the couplings to charm and to bottom quarks are equal in both models,  $|\xi_A^c| = |\xi_A^b| = 1/\tan \beta$ , the correlation becomes quite obvious. Similar reasoning, but this time with respect to  $\xi_A^\tau$ , can be used to explain why the enhancement in Type X model ( $|\xi_A^\tau| = \tan \beta$ ) is much more pronounced than the one in Type I model ( $|\xi_A^\tau| = 1/\tan \beta$ ).

In conclusion, the decay rates  $\mathcal{B}(h \rightarrow P\ell^+\ell^-)$  can be enhanced by as a factor of  $\approx 3$  and even a factor of  $\approx 50$  with respect to the SM predictions if a light CP-odd Higgs is present, as highlighted in Table 3.4. The origin of that enhancement is due to  $m_A \lesssim m_h$  and it is related to the Yukawa couplings to the CP-odd Higgs, which explains why the effect is so pronounced in the case of  $\tau$ -leptons in the final state (in contrast to the case of muons or electrons). Therefore, these observables offer new experimental opportunities to investigate the presence of a light CP-odd Higgs  $A$  and help to disentangle among various 2HDM scenarios. Finally, we should also add that in this study we focused on the lowest lying pseudoscalar quarkonia, but that our discussion could be trivially extended to the excited pseudoscalar quarkonia. Strategies for their detections have been discussed in Ref. [207] and references therein.

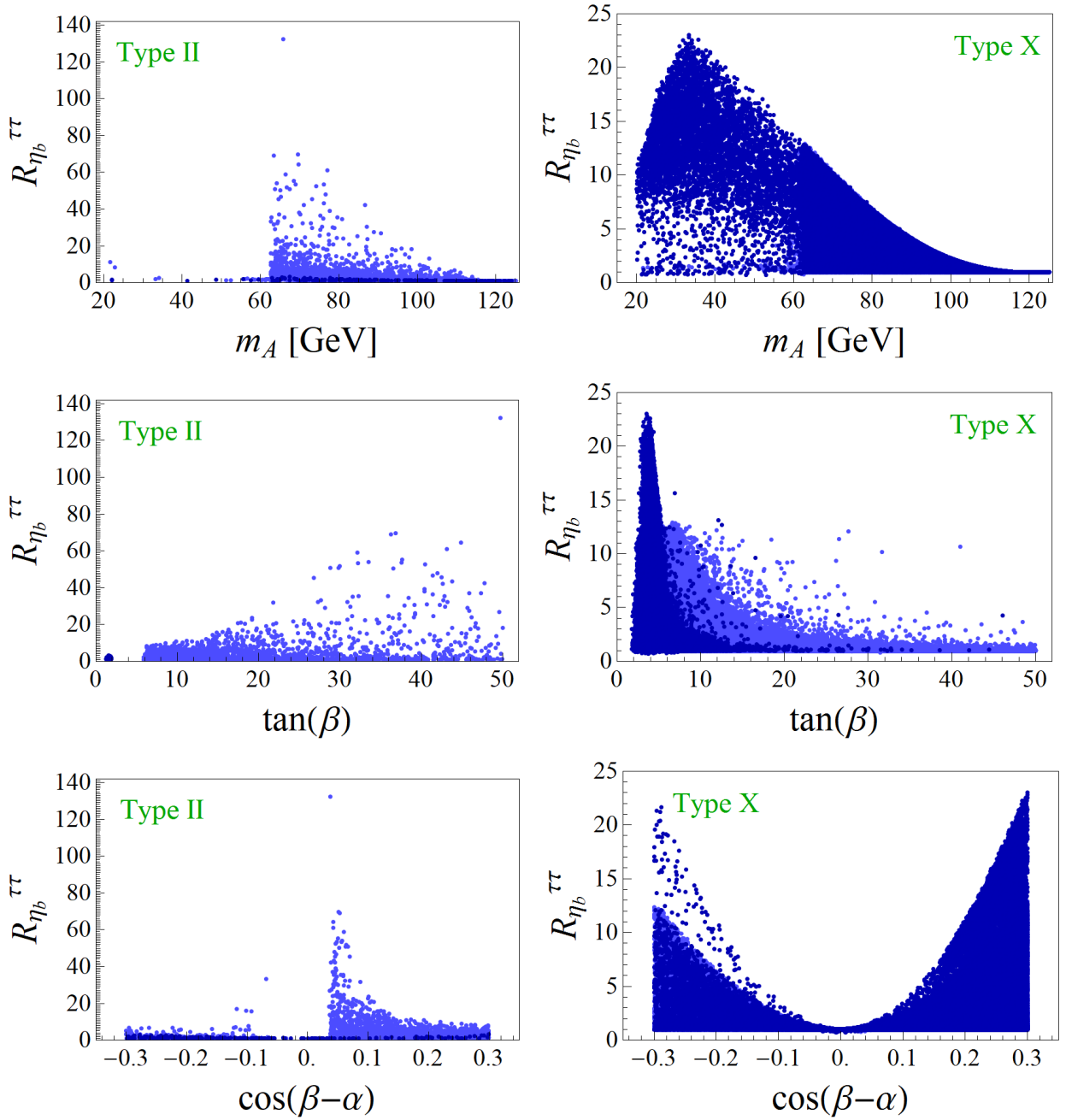


**Figure 3.17:** Results of the scan of parameters (3.86) after imposing constraints discussed in the text. Darker/lighter points correspond to the free/fine-tuned scan.

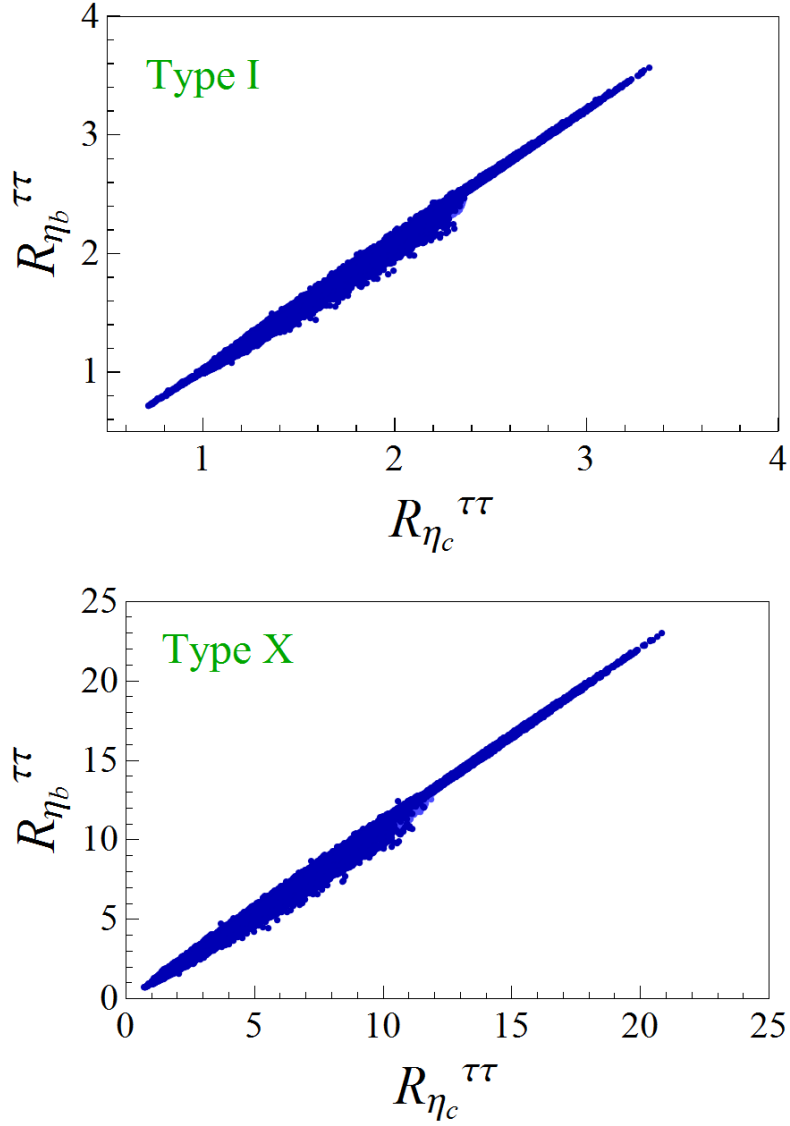


**Figure 3.18:** Correlation of the ratios  $R_{\eta_c}^{\tau\tau}$  and  $R_{\eta_b}^{\tau\tau}$  in Type I and Type X models arises from the fact that the Yukawa couplings of the charm and bottom quarks to the CP-odd Higgs are equal in these two models.

## 3.8 Probing a light CP-odd Higgs through quarkonia decays

In this Section we discuss the processes  $P \rightarrow \ell^+\ell^-$ , where  $P$  stands for a pseudoscalar quarkonia, namely,  $\eta_c$  or  $\eta_b$ . In the SM, these processes proceed through the exchange of a  $Z$  boson or via electroweak boxes. The tree-level and the leading loop contributions are shown in Fig. 3.19. The box diagrams with the  $W^\pm$  and  $Z^0$  bosons running in the loop are negligible in comparison

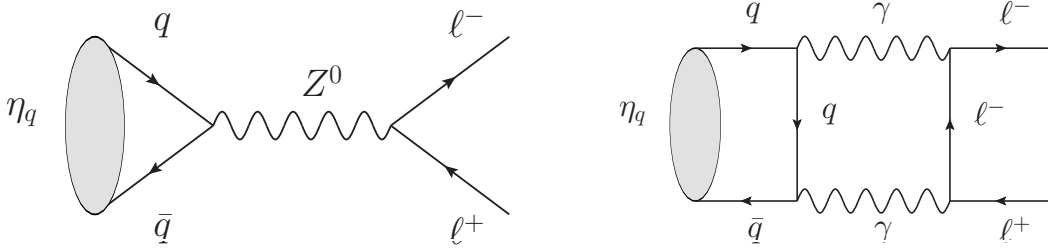


**Figure 3.19:** Dominant diagrams for the decays  $\eta_q \rightarrow \ell^+\ell^-$  in the SM.

The contribution from the photon is obviously absent at tree-level due to parity conservation, i.e. the matrix element  $\langle 0|\bar{b}\gamma^\mu b|\eta_b(p)\rangle = 0$  vanishes identically. Therefore, the SM predictions for  $\mathcal{B}(P \rightarrow \ell^+\ell^-)$  are very small and open the possibility for using these decays to look for NP. In particular, a CP-odd Higgs would give a tree-level contribution to this decay, as shown in Fig. 3.20, which can be orders of magnitude larger than the SM one for light values of  $m_A$ .

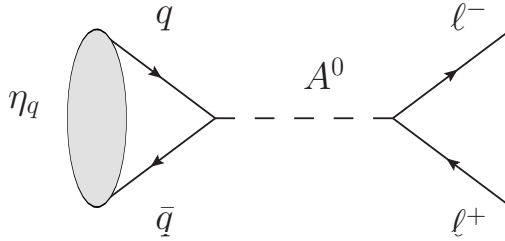


**Figure 3.20:** CP-odd contribution to the decay  $\eta_q \rightarrow \ell^+\ell^-$  in the SM.

In the following, we derive the general expressions for  $\mathcal{B}(P \rightarrow \ell^+\ell^-)$  in the SM extended with a second Higgs doublet. We use the results of the scan of parameters discussed in Sec. 3.6.1 and check on the sensitivity of these decays to the light CP-odd Higgs.

### Expressions for $\mathcal{B}(P \rightarrow \ell\ell)$

The total amplitude for the decay  $\eta_b \rightarrow \ell^+\ell^-$  can be decomposed as

$$\mathcal{M}_{\text{tot}}(\eta_q \rightarrow \ell^+\ell^-) = \mathcal{M}_Z + \mathcal{M}_{\text{em}} + \mathcal{M}_{\text{NP}}, \quad (3.105)$$

where  $q = c, b$  and each of these terms is associated to one type of contribution in Fig. 3.19 and Fig. 3.20. The  $Z$ -exchange amplitude can be trivially computed in terms of the decay

constant  $f_{\eta_b}$ ,

$$\mathcal{M}_Z = \frac{g^2}{2 \cos^2 \theta_W^2} \frac{f_{\eta_q} m_\ell}{m_Z^2} g_A^q g_A^\ell [\bar{u}(p_1) \gamma_5 v(p_2)] , \quad (3.106)$$

where  $g_A^f = T_f^3$  is the third component of weak isospin. The electromagnetic boxes have been estimated in Ref. [208, 209], giving

$$\mathcal{M}_{\text{em}} = 8Q_q^2 \alpha_{\text{em}}^2 f \left( \frac{m_\ell^2}{m_q^2} \right) \frac{f_{\eta_q} m_\ell}{m_{\eta_q}^2} [\bar{u}(p_1) \gamma_5 v(p_2)] , \quad (3.107)$$

where the loop function  $f(r)$  reads

$$f(r) = \frac{1}{\beta} \left[ \frac{1}{4} \log^2 \left( \frac{1+\beta}{1-\beta} \right) - \log \left( \frac{1+\beta}{1-\beta} \right) + \frac{\pi^2}{12} + \text{Li}_2 \left( -\frac{1-\beta}{1+\beta} \right) - \frac{i\pi}{2} \log \left( \frac{1+\beta}{1-\beta} \right) \right] , \quad (3.108)$$

with  $\beta_\ell = \sqrt{1 - m_\ell^2/m_b^2}$ . By using the values of the decay constants given in Eq. (3.101), we obtained the SM predictions

$$\begin{aligned} \mathcal{B}(\eta_c \rightarrow \mu^+ \mu^-) &= (4.2 \pm 0.2) \times 10^{-11} , \\ \mathcal{B}(\eta_b \rightarrow \mu^+ \mu^-) &= (5.6 \pm 2.4) \times 10^{-11} , \\ \mathcal{B}(\eta_b \rightarrow \tau^+ \tau^-) &= (4.0 \pm 1.7) \times 10^{-9} . \end{aligned} \quad (3.109)$$

The only experimental limits available so far for these decays are  $\mathcal{B}(\eta_b \rightarrow \mu^+ \mu^-) < 9 \times 10^{-3}$  [210] and  $\mathcal{B}(\eta_b \rightarrow \tau^+ \tau^-) < 8 \times 10^{-2}$  [211], which are still orders of magnitude from the SM values given above. Even though the electromagnetic contribution appears only at loop level, the box diagrams give comparable contributions to the ones generated at tree-level by a  $Z$  exchange. The suppression of the latter diagram comes from the  $Z$  propagator which gives a multiplicative factor  $m_{\eta_q}^2/m_Z^2$  to the amplitude.

The NP contributions to these decays can be generically written as

$$\mathcal{M}_{\text{NP}} = -\frac{m_q \xi_A^q}{v} \frac{m_\ell \xi_A^\ell}{v} \frac{m_{\eta_q}^2 f_{\eta_q}}{2m_q} \frac{1}{m_{\eta_q}^2 - m_A^2} [\bar{u}(p_1) \gamma_5 v(p_2)] , \quad (3.110)$$

where the couplings  $\xi_A^f$  were defined in Eq. (3.19). By combining the expressions given above, we obtain for the decay rate

$$\Gamma(\eta_q \rightarrow \ell^+ \ell^-) = \frac{\sqrt{m_{\eta_q}^2 - 4m_\ell^2}}{8\pi} \left( \frac{f_{\eta_q} m_\ell}{m_{\eta_q}^2} \right)^2 \left| 8Q_q^2 \alpha_{\text{em}}^2 f \left( \frac{m_\ell^2}{m_q^2} \right) + \frac{2m_{\eta_q}^2}{v^2} g_A^q g_A^\ell - \frac{m_{\eta_q}^4}{2v^2} \frac{\xi_A^q \xi_A^\ell}{m_{\eta_q}^2 - m_A^2} \right|^2 . \quad (3.111)$$

Notice that we neglect the mixing of  $\eta_{c,b}$  with  $A$  on the above expression since the range of  $m_A$  is chosen to be  $m_A \in (20 \text{ GeV}, m_h)$ , see discussion following Eq. (3.86).

## Phenomenology

We are now in position to combine the results of our scan described in Sec. 3.6.1 with the branching ratio formula (3.111) to investigate the impact of the different 2HDMs on the

decay channel  $\eta_q \rightarrow \ell\ell$ . To that purpose, we define the ratios of the decay rates with respect to the SM ones,

$$R_{\eta_q \rightarrow \ell\ell} = \frac{\mathcal{B}(\eta_q \rightarrow \ell^+\ell^-)}{\mathcal{B}(\eta_q \rightarrow \ell^+\ell^-)^{\text{SM}}}. \quad (3.112)$$

Our results for the different 2HDM realizations are summarized in Table 3.5, where we can see that  $\mathcal{B}(\eta_b \rightarrow \mu^+\mu^-)$  and  $\mathcal{B}(\eta_b \rightarrow \tau^+\tau^-)$  can be exacerbated by five orders of magnitude in comparison to the SM values given in Eq. (3.109). This happens only in the type II scenario due to the  $\tan\beta$  enhancement of the CP-odd Higgs couplings  $\xi_A^{d,\ell}$  both to down-type quarks and leptons. For the other scenarios, the CP-odd contribution turns out to be indistinguishable from the SM. Furthermore, we have also checked that the NP contributions to  $\eta_c \rightarrow \ell^+\ell^-$  are negligibly small in all the scenarios we consider here. This can be understood from the fact that the up-type quark couplings, given by  $\xi_A^u = 1/\tan\beta$ , cannot be large due to the stringent constraints on low  $\tan\beta$  values coming from  $B_s \rightarrow \mu^+\mu^-$  and  $B \rightarrow K\mu^+\mu^-$ , as discussed in Sec. 3.5.

Ratio	$R_{\eta_c \rightarrow \mu\mu}$	$R_{\eta_b \rightarrow \mu\mu}$	$R_{\eta_b \rightarrow \tau\tau}$
Type I	$\approx 1$	(1, 1.1)	(1, 1.2)
Type II	$\approx 1$	(1, $5.1 \times 10^4$ )	(1, $3.4 \times 10^5$ )
Type X	$\approx 1$	(0.75, 1)	(0.5, 1)
Type Z	$\approx 1$	(0.75, 1)	(0.5, 1)

**Table 3.5:** Resulting intervals for the ratios  $R_{\eta_q \rightarrow \ell\ell} = \mathcal{B}(\eta_q \rightarrow \ell^+\ell^-)/\mathcal{B}(\eta_q \rightarrow \ell^+\ell^-)^{\text{SM}}$  obtained from the scans in various types of 2HDM.

In Fig. 3.21, we plot the dependence of the ratios  $R_{\eta_q \rightarrow \ell\ell}$  on the CP-odd Higgs mass  $m_A$  and  $\tan\beta$ . We found that a large enhancement is present even for the parameters without fine-tuning. For the fine-tuned scenarios, the enhancement is more pronounced for  $m_A > m_h/2$ , since the light  $A$  is not constrained by the Higgs total width in this case, as shown before in Fig. 3.14. Interestingly, the large enhancement is not present only in the mode with  $\tau$ -leptons in the final state, but also in the channel  $\eta_b \rightarrow \mu^+\mu^-$ . The latter decay mode is more accessible experimentally, since it avoids the complicated reconstruction of the  $\tau$ 's. This feature can be more easily seen in Fig. 3.22, where we plot  $R_{\eta_b \rightarrow \tau\tau}$  as a function of  $R_{\eta_b \rightarrow \mu\mu}$ . The strong correlation between these channels can be understood from Eq. (3.111), since the lepton mass appears as an overall factor in the decay rates, i.e.  $\Gamma(\eta_q \rightarrow \ell^+\ell^-) \propto m_\ell^2$ . There is a residual dependence on  $m_\ell$  in the loop factor  $f(m_\ell^2/m_q^2)$ , but this effect is very mild in comparison to the overall factor  $m_\ell^2$ .

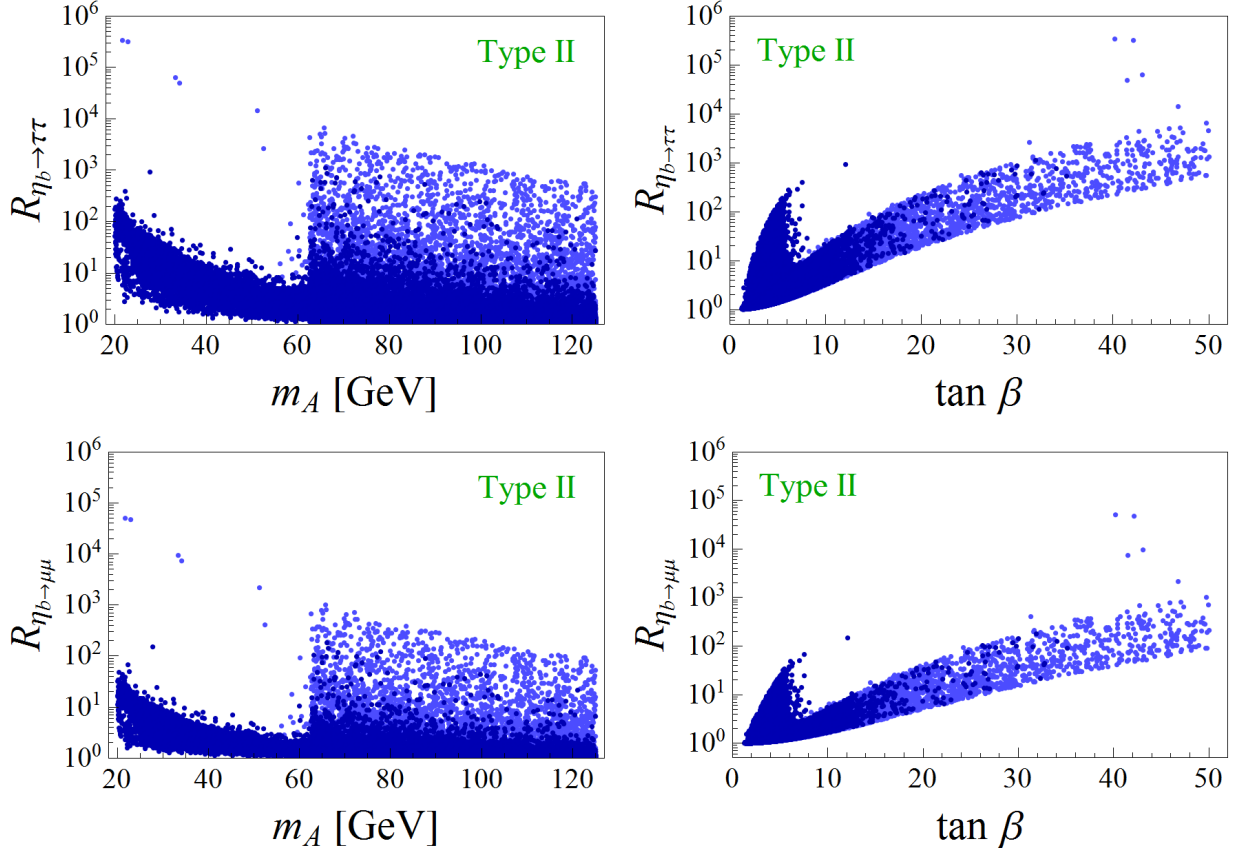


**Figure 3.21:** Results of the scan of parameters (3.86) for  $R_{\eta_q \rightarrow \ell\ell} = \mathcal{B}(\eta_q \rightarrow \ell^+\ell^-)/\mathcal{B}(\eta_q \rightarrow \ell^+\ell^-)^{\text{SM}}$  after imposing constraints discussed in the text. Darker/lighter points correspond to the free/fine-tuned scan.

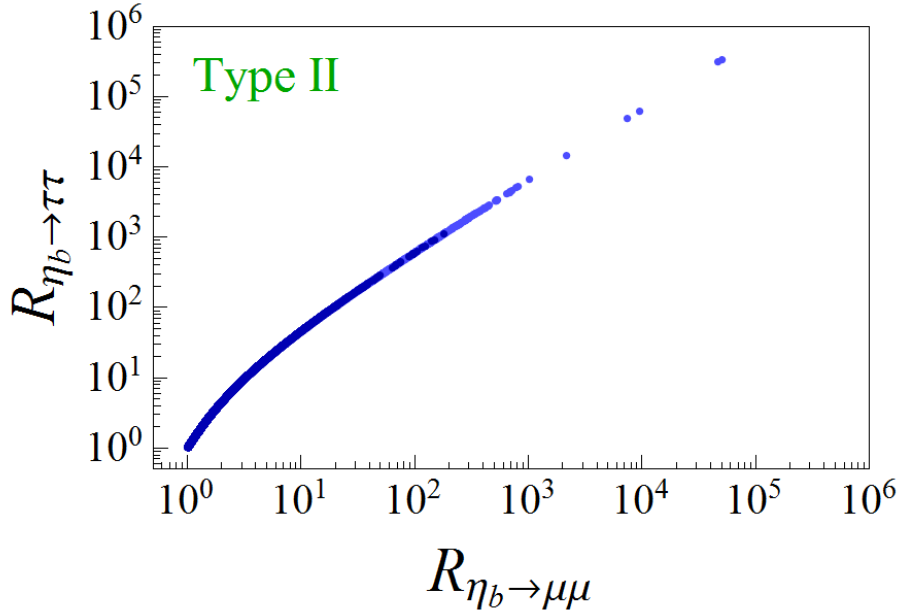


**Figure 3.22:** Correlation of the ratios  $R_{\eta_b \rightarrow \mu\mu}$  and  $R_{\eta_b \rightarrow \tau\tau}$  for the type II model, cf. Eq. (3.112). See Fig. 3.17 for the color code.

In conclusion, the processes  $\eta_b \rightarrow \mu^+\mu^-$  and  $\eta_b \rightarrow \tau^+\tau^-$ , which have been scarcely studied in experiments thus far, can provide additional information about the scalar sector beyond the SM. The SM rates for these processes are negligibly small, since the pseudoscalar quarkonia at tree-level decay to two leptons only weakly. For that reason, the observables  $\mathcal{B}(\eta_b \rightarrow \mu^+\mu^-)$  and  $\mathcal{B}(\eta_c \rightarrow \mu^+\mu^-)$  are sensitive to the light CP-odd Higgs contributions, which contributes at tree-level to the amplitude of this decay. Clearly, the contribution from the light CP-odd is more pronounced for light values of  $m_A$ . We have showed that these processes can be enhanced by almost five orders of magnitudes, being possibly within reach of current (LHCb) and future experiments (Belle-II), and providing complementary information to the decays  $h \rightarrow \eta_b\tau^+\tau^-$ , which were discussed in Sec. 3.7.

### Comments on $V \rightarrow \gamma\ell^+\ell^-$

Before closing this Section, we will briefly comment on other proposals to probe a light CP-odd Higgs by using the decays of quarkonia. An attempt has been made in Ref. [212–215] to consider the processes  $\Upsilon \rightarrow \gamma\ell^+\ell^-$ , with  $\ell = \mu, \tau$ , where it is claimed that these processes are highly sensitive to the contribution of a light pseudoscalar. We will argue that this statement is implausible, since the authors of Ref. [212–215] neglected an important contribution for the SM.

For these decays, the only NP contribution stems from QCD structure dependent diagram shown in Fig. 3.23.

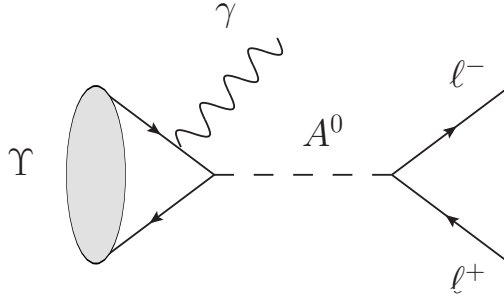


**Figure 3.23:** CP-odd contribution to the decay  $\Upsilon \rightarrow \gamma\ell^+\ell^-$ .

A similar diagram where the photon is emitted by a lepton is obviously forbidden by parity symmetry. The light-CP odd diagram should be added to the dominant SM contributions shown in Fig. 3.24.

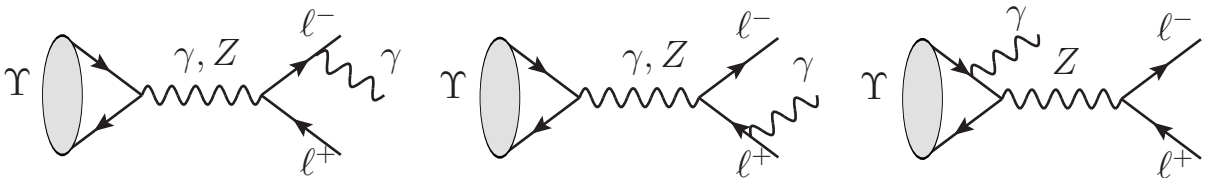


**Figure 3.24:** Leading contributions to the decay  $\Upsilon \rightarrow \gamma\ell^+\ell^-$  in the SM.

By comparing the diagrams 3.23 and 3.24, it becomes clear that the observable  $\mathcal{B}(\Upsilon \rightarrow \gamma\ell^+\ell^-)$  is insensitive to the CP-odd Higgs contribution. This conclusion comes from the fact that the first diagram in Fig. 3.24 is a tree-level electromagnetic contribution, thus orders of magnitude bigger than the one generated by NP. In Ref. [212–215], the SM decay

rate was estimated by making the approximation,

$$\Gamma(\Upsilon \rightarrow \gamma \ell^+ \ell^-) \stackrel{!}{\approx} \Gamma(\Upsilon \rightarrow \gamma \eta_b) \times \mathcal{B}(\eta_b \rightarrow \ell^+ \ell^-). \quad (3.113)$$

The study of  $\Upsilon \rightarrow \gamma \ell^+ \ell^-$  proceeds through the dominant electromagnetic tree-level contribution, which is huge compared to the CP-odd contribution. Disentangling the NP contributions from the large SM contribution becomes therefore complicated. In particular, even if one manages to subtract a part of bremsstrahlung, the validity of Eq. (3.113) is very questionable.

# Chapter 4

## Leptoquarks at low and high energies

Leptoquarks (LQ) are hypothetical bosons with simultaneous couplings to leptons and quarks. They emerge in most scenarios aiming to unify the SM fermions in the same representation of a gauge group larger than  $\mathcal{G}_{\text{SM}}$ . Examples of such scenarios are provided by Grand Unified Theories (GUT), where LQs appear as gauge bosons of the unified group, or as additional (colored) states in the scalar multiplets. The interest in scenarios with light LQs was recently renewed by the indications of lepton flavor universality violation (LFUV) in  $B$  meson decays, which can be accommodated by LQs lying around the TeV scale. In the viable LQ scenarios, LFUV can imply significant LFV signatures as it will be described in Chapter 5.

This Chapter is organized as follows: in Sec. 4.1 we discuss the general aspects of models with LQs. In Sec. 4.2, we present a concrete example of a  $SU(5)$  unification scenario with light LQs. In Sec. 4.3, we derive the effective Lagrangian for the LQ that will be considered in the next Chapter. Finally, the status of the direct searches for LQs at the LHC is briefly reviewed in Sec. 4.4.

### 4.1 Introduction

LQs are fields which admit simultaneous interactions with quarks and leptons via renormalizable operators [8, 216]. These states can be scalar or vector particles and they were firstly considered in the context of unified models based on the gauge group  $SU(5)$  [217] and the Pati-Salam group [218].<sup>1</sup> In addition to unification scenarios, LQs naturally arise in composite Higgs models [219–221] and models aiming at explaining the origin of neutrino masses [222] and other phenomena.

LQs with baryon number violating couplings must be very heavy in order to avoid proton decay constraints, as it was originally thought in the first grand unification papers. However, in scenarios with baryon number conservation, LQ masses and couplings have to satisfy much weaker constraints, which allow them to be considerably lighter, as explored in recent publications [223–225]. The phenomenology of TeV-scale LQ states is very rich and it includes sizable effects in rare meson decays and processes with LFV, as well as potential signatures in direct searches performed at the LHC [8].

There exist 12 LQ states which can be classified by their spin and by their transformation under the SM group. Since quarks are color triplets, the  $SU(3)_c$  gauge invariance imposes that a simultaneous interaction to leptons are possible if and only if LQs belong to the

---

<sup>1</sup>The Pati-Salam gauge group is  $SU(4) \times SU(2)_L \times SU(2)_R$  which can be embedded in  $SO(10)$ .

representations  $\mathbf{3}$  or  $\bar{\mathbf{3}}$  of  $SU(3)_c$ . A similar reasoning can be used to determine all the  $SU(2)_L \times U(1)_Y$  representations allowing gauge invariant and renormalizable interactions to leptons and quarks, as listed in Table 4.1. We adopt the notation of Ref. [226] and specify the LQ states by their quantum numbers with respect to the SM gauge group,  $(SU(3)_c, SU(2)_L)_Y$ , where the electric charge,  $Q = Y + T_3$ , is the sum of hypercharge ( $Y$ ) and the component of the third weak isospin ( $T_3$ ). Moreover, these states can be classified in terms of the fermion number  $F = 3B + L$ , where  $B$  is the baryon number and  $L$  is the lepton number defined in such a way that  $B = 1/3$  for quarks and  $L = 1$  for leptons.

$(SU(3)_c, SU(2)_L)_{U(1)_Y}$	Spin	Symbol	BNC	$F$
$(\bar{\mathbf{3}}, \mathbf{3})_{1/3}$	0	$S_3$	$\times$	-2
$(\bar{\mathbf{3}}, \mathbf{1})_{4/3}$	0	$\tilde{S}_1$	$\times$	-2
$(\bar{\mathbf{3}}, \mathbf{1})_{1/3}$	0	$S_1$	$\times$	-2
$(\bar{\mathbf{3}}, \mathbf{1})_{-2/3}$	0	$\bar{S}_1$	$\times$	-2
$(\mathbf{3}, \mathbf{2})_{7/6}$	0	$R_2$	$\checkmark$	0
$(\mathbf{3}, \mathbf{2})_{1/6}$	0	$\tilde{R}_2$	$\checkmark^*$	0
$(\bar{\mathbf{3}}, \mathbf{2})_{5/6}$	1	$V_2$	$\times$	-2
$(\bar{\mathbf{3}}, \mathbf{2})_{-1/6}$	1	$\tilde{V}_2$	$\times$	-2
$(\mathbf{3}, \mathbf{3})_{2/3}$	1	$U_3$	$\checkmark$	0
$(\mathbf{3}, \mathbf{1})_{5/3}$	1	$\tilde{U}_1$	$\checkmark$	0
$(\mathbf{3}, \mathbf{1})_{2/3}$	1	$U_1$	$\checkmark$	0
$(\mathbf{3}, \mathbf{1})_{-1/3}$	1	$\bar{U}_1$	$\checkmark$	0

**Table 4.1:** Classification of scalar and vector LQs. The column BNC refer to baryon number conservation. See text for details [8].

Throughout this Chapter the flavor indices of LQ couplings will refer to the mass eigenstates of down-type quarks and charged leptons, unless stated otherwise. In other words, the left-handed doublets are defined as  $Q_i = [(V^\dagger u_L)_i \ d_{Li}]^T$  and  $L_i = [(U \nu_L)_i \ \ell_{Li}]^T$ , where  $V$  and  $U$  are the Cabibbo-Kobayashi-Maskawa (CKM) and the Pontecorvo-Maki-Nakagawa-Sakata (PMNS) matrices, respectively. The fields  $u_L, d_L, \ell_L$  are the fermion mass eigenstates, whereas  $\nu_L$  stand for the massless neutrino flavor eigenstates. Since the tiny neutrino masses play no role for the purpose of this thesis, we may choose the PMNS matrix to be the unity matrix in the phenomenological discussion,  $U = \mathbf{1}$ . Right-handed field indices will always refer to the mass eigenbasis.

### 4.1.1 $SU(5)$ unification and light leptoquarks

The equality of electron and proton charges  $|Q_p| = |Q_e|$  is one of the great mysteries of the SM. Gauge theories do not constraint the quantum charges of an Abelian group, which can be any real number. The fact that the  $U(1)_Y$  charges of the SM fermions are such that  $|Q_p| = |Q_e|$  appears to be a very unpleasant coincidence. A well-known solution to this problem is to embed the SM gauge group  $\mathcal{G}_{\text{SM}}$  in a larger non-Abelian semi-simple group  $\mathcal{G}$ , where

leptons and quarks are included in the same representation of  $\mathcal{G}$ . The non-Abelian nature of  $\mathcal{G}$  implies then that the  $U(1)_Y$  charges of fermions are rational fractions, as observed in nature. This idea also agrees with the reductionist trend of theoretical physics of unifying the forces in simpler interactions, as it happened with Maxwell electromagnetism and the electroweak theory of Glashow and Salam. Notice, however, that the naive extrapolation of this historical feature might be a theoretical prejudice which is not necessarily satisfied in nature.

The first model unifying leptons and quarks was proposed by Pati and Salam in 1974 [218]. The minimal simple group containing  $\mathcal{G}_{\text{SM}}$  is  $SU(5)$ , as it was shown by Georgi and Glashow in the same year [217]. Unification models based on the gauge group  $SO(10)$  are also possible [227, 228], but these have a huge number of degrees of freedom, which reduce considerably the predictivity of these scenarios. In all these models, vector LQ states appear as gauge bosons of the unified group and scalar LQs appear as degrees of freedom in the scalar multiplets. The purpose of this Section is not to cover the vast literature on GUT, but to discuss whether LQs coming from unification scenarios can be light enough to be observed in low and high energy experiments. We will consider  $SU(5)$  as our gauge group due to its simplicity and we will illustrate the viability of this type of GUT scenario in Sec. 4.2 with the concrete model introduced in Ref. [229].

We follow the notation of [230] and denote the  $SU(5)$  representations by their dimensions. The SM fermions are embedded in three ten-dimensional representations  $(\mathbf{10})_i$  and three five-dimensional representations  $(\mathbf{5})_i$  of  $SU(5)$ , where  $i, j$  denote family indices. More precisely, for each fermion generation

$$\begin{aligned}\mathbf{10} &\equiv (\mathbf{1}, \mathbf{1})_1 \oplus (\bar{\mathbf{3}}, \mathbf{1})_{-2/3} \oplus (\mathbf{3}, \mathbf{2})_{1/6} = (\ell_R^C, u_R^C, Q), \\ \mathbf{5} &\equiv (\mathbf{1}, \mathbf{2})_{-1/2} \oplus (\bar{\mathbf{3}}, \mathbf{1})_{1/3} = (L, \ell_R^C),\end{aligned}\tag{4.1}$$

where one can recognize the left-handed SM fermion multiplets. The representations with lowest dimension containing LQ states are listed in Tab. 4.2. By analyzing all the possible  $SU(5)$  contractions with the fermion representations, one can show that only the **5**-, **10**-, **15**-, **45**-, and **50**-dimensional scalar representations can couple to SM fermions at the renormalizable level. On the other hand, the only representations that can get a vev without breaking color and electric charge are **5**-, **15**-, **24**- and **45**-dimensional representations. Among the representations mentioned above, only the **24**-plet does not contain scalar LQs (see Table 4.2), but this representation does not couple to SM fermions. Therefore, we can state that at least one scalar representation containing LQs is needed to generate electroweak symmetry breaking and to give mass to fermions. Moreover, the vector LQ  $V_2 = (\bar{\mathbf{3}}, \mathbf{2})_{5/6}$  appears in the adjoint representation **24** for every  $SU(5)$  scenario.<sup>2</sup> By combining these facts, one can say that there is in general at least one scalar and one vector LQ in any  $SU(5)$  unification model [8].

In the original  $SU(5)$  model of Georgi and Glashow, the scalar sector consists of an additional **5**, which contains the SM Higgs, and a **24** representation used to spontaneously break  $SU(5)$  down to  $\mathcal{G}_{\text{SM}}$ ,

$$\begin{aligned}\mathbf{24}_H &\equiv (\mathbf{8}, \mathbf{1})_0 \oplus (\mathbf{1}, \mathbf{3})_0 \oplus (\mathbf{3}, \mathbf{2})_{-5/6} \oplus (\bar{\mathbf{3}}, \mathbf{2})_{5/6} \oplus (\mathbf{1}, \mathbf{1})_0, \\ \mathbf{5}_H &\equiv (\mathbf{1}, \mathbf{2})_{-1/2} \oplus (\bar{\mathbf{3}}, \mathbf{1})_{1/3}.\end{aligned}\tag{4.2}$$

<sup>2</sup>It is customary in the  $SU(5)$  literature to call  $X$  and  $Y$  the states in the  $V_2$  multiplet with electric charge  $4/3$  and  $1/3$ , respectively.

The particles in the  $\mathbf{24}$  representation acquire masses at the unification scale  $\Lambda_{\text{GUT}} \gg v$ , having no phenomenological impact at low-energies. The scalar LQ  $(\bar{\mathbf{3}}, \mathbf{1})_{1/3}$  coming from  $\mathbf{5}_H$  is assumed to be much heavier than the SM Higgs to not disturb the proton stability, as it will be discussed in Sec. 4.1.2. To achieve this large mass splitting in the  $\mathbf{5}_H$  multiplet, a fine-tuning of the parameters in the scalar potential is needed, which is known as the doublet-triplet splitting problem.

Despite its elegance and simplicity, it is well-known that the minimal  $SU(5)$  model described above [217] is no longer viable. It suffers from several issues including: (i) doublet-triplet splitting; (ii) Yukawa relations in disagreement with experiment; (iii) massless neutrinos; and perhaps most strikingly, (iv) fails to achieve unification. However, with the exception of the first problem, there are straightforward, non-supersymmetric extensions of the original model which can solve each of these issues. The fermion mass relations can be addressed using higher-dimension operators [231] or a Higgs in the  $\mathbf{45}$  representation [232], while the addition of singlet right-handed neutrinos allows for neutrino masses via the Type-I seesaw [52–55]. Furthermore, there exist several models which introduce additional split multiplets in order to achieve gauge coupling unification consistent with the current experimental measurements [233–237].

Before presenting a viable  $SU(5)$  unification scenario with light LQs in Sec. 4.2, we will briefly discuss the generalities of proton decay in GUT models.

$(SU(3)_c, SU(2)_L)_{U(1)_Y}$	Symbol	$SU(5)$
$(\bar{\mathbf{3}}, \mathbf{3})_{1/3}$	$S_3$	$\bar{\mathbf{45}}, \bar{\mathbf{70}}$
$(\bar{\mathbf{3}}, \mathbf{1})_{4/3}$	$\tilde{S}_1$	$\mathbf{45}$
$(\bar{\mathbf{3}}, \mathbf{1})_{1/3}$	$S_1$	$\bar{\mathbf{5}}, \bar{\mathbf{45}}, \bar{\mathbf{50}}, \bar{\mathbf{70}}$
$(\bar{\mathbf{3}}, \mathbf{1})_{-2/3}$	$\bar{S}_1$	$\mathbf{10}, \mathbf{40}$
$(\mathbf{3}, \mathbf{2})_{7/6}$	$R_2$	$\bar{\mathbf{45}}, \bar{\mathbf{50}}$
$(\mathbf{3}, \mathbf{2})_{1/6}$	$\tilde{R}_2$	$\mathbf{10}, \mathbf{15}, \mathbf{40}$
$(\bar{\mathbf{3}}, \mathbf{2})_{5/6}$	$V_2$	$\mathbf{24}, \mathbf{75}$
$(\bar{\mathbf{3}}, \mathbf{2})_{-1/6}$	$\tilde{V}_2$	$\bar{\mathbf{10}}, \bar{\mathbf{40}}$
$(\mathbf{3}, \mathbf{3})_{2/3}$	$U_3$	$\bar{\mathbf{35}}, \bar{\mathbf{40}}$
$(\mathbf{3}, \mathbf{1})_{5/3}$	$\tilde{U}_1$	$\mathbf{75}$
$(\mathbf{3}, \mathbf{1})_{2/3}$	$U_1$	$\bar{\mathbf{10}}, \bar{\mathbf{40}}$
$(\mathbf{3}, \mathbf{1})_{-1/3}$	$\bar{U}_1$	$\mathbf{5}, \mathbf{45}, \mathbf{50}, \mathbf{70}$

**Table 4.2:** List of LQ states and the corresponding lowest dimension  $SU(5)$  representations. [8].

### 4.1.2 Proton stability

One of the most important constraint on unification scenarios comes from the proton stability. The proton decay can be induced both by scalar and vector LQs if these states violate baryon number, as listed in Table 4.1.

The issue of matter stability is directly related to the presence of the diquark couplings, which violate both baryon and lepton number. To illustrate the impact of experimental

bounds on the proton lifetime  $\tau_p$ , we consider the decay mode  $p \rightarrow \pi^0 e^+$  which is illustrated in Fig. 4.1 for both vector and scalar LQs. For vector LQs, the rate for this process is estimated by naive dimensional analysis to be

$$\Gamma(p \rightarrow \pi^0 e^+) \approx \frac{|g_1 g_2|^2}{m_{\text{LQ}}^4} m_p^5, \quad (4.3)$$

where  $m_p$  is the proton mass and  $g_{1,2}$  are the gauge couplings shown in Fig. 4.1. By taking  $g_1 = g_2 = 1/2$  and the limit  $\tau_{p \rightarrow \pi^0 e^+}^{\text{exp}} > 8.2 \times 10^{33}$  years (90% CL) [238], we obtain the naive bound  $m_{\text{LQ}} \gtrsim 10^{16}$  GeV. For the scalar mediated proton decay, we can write

$$\Gamma(p \rightarrow \pi^0 e^+) \approx \frac{|yz|^2}{m_{\text{LQ}}^4} m_p^5, \quad (4.4)$$

where  $y$  and  $z$  denote the Yukawa couplings appearing in Fig. 4.1 for the quark-lepton and quark-quark pairs, respectively. For couplings of the same order than the up-quark Yukawa ( $|y| = |z| = 10^{-5}$ ), we obtain the bound  $m_{\text{LQ}} \gtrsim 2 \times 10^{11}$  GeV, which is about five orders of magnitude weaker than the limit obtained above for vector LQs. These lower bounds on the LQ masses are rough estimates, but they give an idea of the spectrum of particles and unification scales needed in order to be consistent with current experimental limits on the proton lifetime. These estimations can certainly be refined for concrete unification scenarios, like the one we will present in Sec. 4.2.

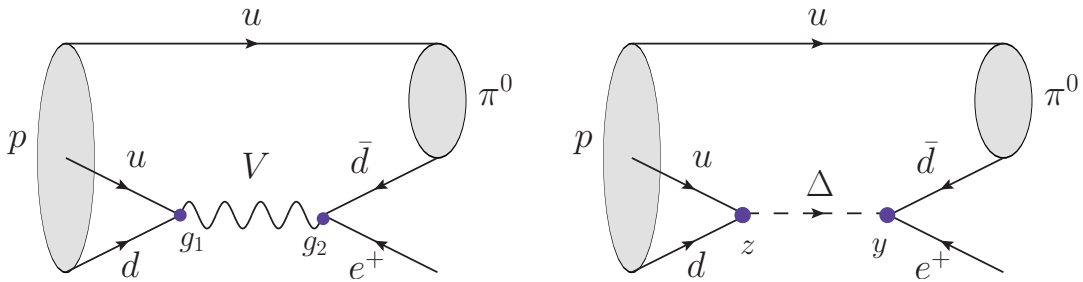


**Figure 4.1:** Illustration of proton decay mediated by vector  $V$  (left panel) and scalar  $\Delta$  (right panel) LQs.

Besides the usual types of proton decay which proceed via dimension-6 operators generated by diquark couplings, as discussed above, the proton decay can also be induced via higher dimensional operators. To be more precise, in the  $\tilde{R}_2 = (\mathbf{3}, \mathbf{2})_{1/6}$  scenario, the gauge symmetry allows for the following interaction term

$$\mathcal{L} \supset \lambda \varepsilon_{ijk} (H^\dagger \Delta_i) (\tilde{\Delta}_j^\dagger \Delta_k), \quad (4.5)$$

where  $H$  denotes the SM Higgs,  $\Delta$  the doublet LQ and  $\lambda$  is a generic coupling. We remind the reader that  $\tilde{\Delta} = i\sigma_2 \Delta^*$  is the conjugate  $SU(2)$  doublet. Note also that, we explicitly wrote the color indices  $(i, j, k)$ . After integrating out the LQ particles, this coupling generates dimension-9 operators which induce the decay  $p \rightarrow \pi^+ \pi^+ e^- \nu \nu$ , as illustrated in Fig. 4.2. The naive estimate of this decay rate gives

$$\Gamma(p \rightarrow \pi^+ \pi^+ e^- \nu \nu) = \frac{v^2 |\lambda y^3|^2}{m_{\text{LQ}}^{12}} m_p^{11}, \quad (4.6)$$

where  $y$  is a generic Yukawa coupling to down-type quarks and leptons. In this case, there is no dedicated search for this specific decay mode. The best limit that can be used is

$\tau_p^{\text{exp}} > 8.2 \times 10^{33}$  [239], which was obtained independently of proton the decay channel. Note that this limit is considerably lower than the one quoted above for  $p \rightarrow \pi^0 e^+$ . By taking  $\lambda = 1$  and once again  $y = 10^{-5}$ , we obtain the bound  $m_{\text{LQ}} \gtrsim 960$  GeV, which is orders of magnitude lower than the ones obtained above. Interestingly, this lower limit on the LQ mass falls precisely in the mass region which is being studied at the LHC. Therefore, from a phenomenologically point of view, this type of proton decay is not as problematic as the decays induced by dimension-6 operators, which were discussed above, but it offers different opportunities for future proton decay experiments.

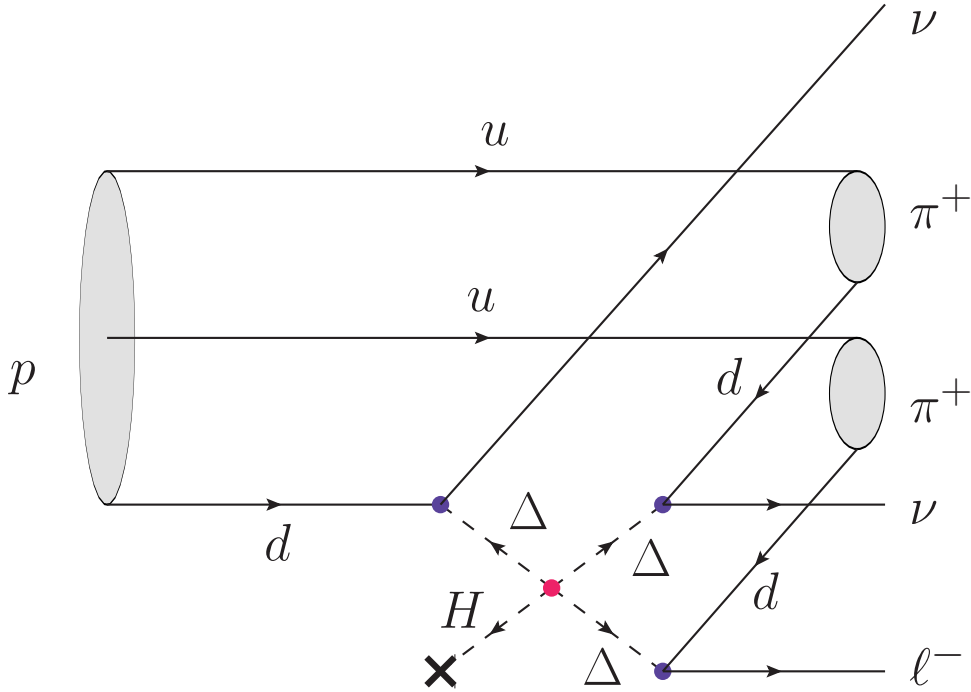


**Figure 4.2:** Proton decay  $p \rightarrow \pi^+ \pi^+ \ell^- \nu \nu$  induced by the coupling (4.5) for the scalar LQ  $\tilde{R}_2 = (3, 2)_{1/6}$ .

## 4.2 A concrete $SU(5)$ realization with light leptoquarks

As an illustration of a viable GUT scenario with light LQs, we consider the model proposed in Ref. [229], which is an extension of the minimal  $SU(5)$  model of Georgi and Glashow. The main interest of this model comes from the lightness of the leptoquark masses, which are not only a possibility, but the key assumption which leads to unification. Therefore, this unification scenario might be within reach of the current low and high energy experiments, such as the LHC and the meson factories, a possibility which is rarely encountered in the standard GUT literature.

The idea behind this model was originally introduced in Ref. [233], as an attempt to achieve  $SU(5)$  gauge unification without relying on supersymmetry. In this paper it was shown that the introduction of two  $(\mathbf{3}, \mathbf{2})_{1/6}$  scalar LQs and a second Higgs doublet at the electroweak scale can be used to achieve gauge coupling unification. The original proposal faces several difficulties, including a low unification scale ( $\approx 5 \times 10^{14}$  GeV) potentially in tension with the bounds from Super Kamiokande, as well as additional contributions

to proton decay mediated by the light LQs. In this Section, we show that the model of Ref. [233] in fact still remains viable when confronted with the latest experimental constraints. Firstly, we point out that extending the model to introduce splitting in the  $\mathbf{24}$  Higgs can preserve unification, while also allowing one to significantly raise the scale of unification. Furthermore, we discuss how dangerous contributions to proton decay, mediated by the light leptoquarks, can be forbidden by a  $U(1)_{PQ}$  symmetry.

### 4.2.1 Model setup

As anticipated above, the setup of the original model is a minimal extension of the Georgi-Glashow model [217]. The scalar sector of this model is extended to include an additional  $\bar{\mathbf{5}}$  Higgs  $H_{\bar{\mathbf{5}}}$ , as well as two new scalars,  $\Phi_{10}^{(1)}$  and  $\Phi_{10}^{(2)}$ , transforming in the  $\mathbf{10}$  representation. Experimental bounds on the proton lifetime provide a lower limit ( $m_T \gtrsim 10^{11}$  GeV) on the masses of the colour-triplet Higgs in the  $\mathbf{5}$  and  $\bar{\mathbf{5}}$ , leading to the well-known doublet-triplet splitting problem. These triplet scalars are therefore assumed to acquire GUT scale masses. This motivates the assumption that such splitting could in fact be a generic feature of the scalar sector, which then opens new avenues to achieve unification.

The decouplets,  $\Phi_{10}$ , can be decomposed under the SM gauge group as

$$\mathbf{10} = (\mathbf{3}, \mathbf{2})_{1/6} \oplus (\bar{\mathbf{3}}, \mathbf{1})_{-2/3} \oplus (\mathbf{1}, \mathbf{1})_1. \quad (4.7)$$

Splitting of the  $\mathbf{10}$  is assumed such that the LQ states  $\Delta \equiv (\mathbf{3}, \mathbf{2})_{1/6}$  can remain light, while the rest of the multiplet acquires GUT scale masses. A similar splitting is also considered for the  $\bar{\mathbf{5}}$  multiplet by assuming that the additional Higgs doublet remains light. These are the key assumptions that lead to unification in this model.

Departing from the original model, we will also consider the case where there is a splitting of the  $\Sigma_{24}$  Higgs by lowering the mass of the  $(\mathbf{8}, \mathbf{1})_0$  and  $(\mathbf{1}, \mathbf{3})_0$ ,

$$\mathbf{24}_H \equiv (\mathbf{8}, \mathbf{1})_0 \oplus (\mathbf{1}, \mathbf{3})_0 \oplus (\mathbf{3}, \mathbf{2})_{-5/6} \oplus (\bar{\mathbf{3}}, \mathbf{2})_{5/6} \oplus (\mathbf{1}, \mathbf{1})_0. \quad (4.8)$$

Naively, one would expect this additional splitting to disrupt unification. However, if the octet and triplet are approximately degenerate in mass, then their combined effect on the RGEs is such that unification can be preserved. As we shall demonstrate in the following section, splitting of the  $\mathbf{24}$ -plet then provides a straightforward way to raise the unification scale. Such behaviour was first pointed out in the context of supersymmetric, string-motivated models in Ref. [240]. However, in the case where  $\Sigma_{24}$  is the field which obtains an  $SU(5)$  breaking vev, it should be noted that the octet and triplet cannot be arbitrarily light. If their masses lie significantly below  $\langle \Sigma_{24} \rangle$ , one finds that  $\Gamma(\Sigma_3 \rightarrow hh)/m_{\Sigma_3} \gg 1$ . In the remainder of this paper we take the triplet/octet mass,  $m_{38}$ , to be a free parameter. It should be understood that in the case  $m_{38}/\langle \Sigma_{24} \rangle \ll 1$ , these states are assumed to arise from an additional  $\mathbf{24}$  multiplet, not associated with the breaking of  $SU(5)$ .<sup>3</sup>

The Yukawa Lagrangian of the model is given by

$$\mathcal{L}_Y = \mathbf{y}_d \bar{\Psi}_{10}^c H_{\bar{\mathbf{5}}} \Psi_{\bar{\mathbf{5}}} + \mathbf{y}_u \bar{\Psi}_{10}^c H_{\mathbf{5}} \Psi_{\mathbf{10}} + \sum_{a=1}^2 \mathbf{Y}^{(a)} \bar{\Psi}_{\bar{\mathbf{5}}}^c \Phi_{10}^{(a)} \Psi_{\bar{\mathbf{5}}} + \text{h.c.}, \quad (4.9)$$

where  $(\Psi_{\bar{\mathbf{5}}} + \Psi_{\mathbf{10}})$  corresponds to a single generation of SM fermions and there is an implicit sum over generations. Other Yukawa terms in this Lagrangian are forbidden by the

<sup>3</sup>In this case, for example, a potential of the form  $m^2 \Phi_{24}^2 + \lambda' \text{Tr}([\Sigma_{24}, \Phi_{24}]^2)$ , with  $\langle \Sigma_{24} \rangle = V \text{diag}(2, 2, 2, -3, -3)$ , can give GUT scale masses to the rest of the  $\Phi_{24}$  while the octet/triplet are tuned to be light with  $m_{38} = m$ .

$U(1)_{PQ}$  symmetry, which will be discussed in Sec. 4.2.4. When considering the low energy phenomenology, we will be particularly interested in the couplings of the light LQ states  $\Delta_a$  (with  $a = 1, 2$ ),

$$\begin{aligned} \mathcal{L}_Y \supset & \sum_{a=1}^2 Y_{ij}^{(a)} \varepsilon_{\alpha\beta} \bar{d}_{Ri} \Delta_a^\beta L_j^\alpha + \text{h.c.} \\ & = \sum_{a=1}^2 Y_{ij}^{(a)} \bar{d}_{Ri} \left[ \Delta_a^{(-1/3)} \nu_{Lj} - \Delta_a^{(2/3)} \ell_{Lj} \right] + \text{h.c.}, \end{aligned} \quad (4.10)$$

where  $\alpha, \beta$  are  $SU(2)$  indices,  $\mathbf{Y}^{(a)}$  are two generic  $3 \times 3$  complex matrices, and  $\Delta_a$  are mass eigenstates satisfying  $m_{\Delta_1} \leq m_{\Delta_2}$ . In the second line we decompose the weak doublets in terms of the fields  $\Delta_a^{(-1/3)}$  and  $\Delta_a^{(2/3)}$ , where the superscripts denote the corresponding electric charge. Notice that the matrices  $\mathbf{Y}^{(a)}$  should be anti-symmetric in flavour indices if  $d_{Rj}$  and  $L_{Lj}$  belong to the same  $SU(5)$  multiplet  $\bar{\mathbf{5}}$ . However, this is not always the case as suggested by the violation of the GUT relations  $m_d = m_e$  and  $m_s = m_\mu$  [241]. Finally, one can also read the Yukawa interactions of the two Higgs doublets from the first two terms in Eq. (4.9), which coincide with the couplings of a type-II 2HDM.

### 4.2.2 RGE equations

The two-loop renormalisation group equations (RGEs) for the gauge couplings take the form [242]

$$\mu \frac{dg_i}{d\mu} = \frac{b_i g_i^3}{16\pi^2} + \frac{g_i^3}{(16\pi^2)^2} \left( \sum_{j=1}^3 B_{ij} g_j^2 \right), \quad (4.11)$$

where the relevant coefficients  $b_i, B_{ij}$ , are given above each mass threshold by

$$b_i = \begin{pmatrix} \frac{41}{10} \\ -\frac{19}{6} \\ -7 \end{pmatrix} + \Theta(\mu - m_H) \begin{pmatrix} \frac{1}{10} \\ \frac{1}{6} \\ 0 \end{pmatrix} + 2\Theta(\mu - m_\Delta) \begin{pmatrix} \frac{1}{30} \\ \frac{1}{2} \\ \frac{1}{3} \end{pmatrix} + \Theta(\mu - m_{38}) \begin{pmatrix} 0 \\ \frac{2}{3} \\ 1 \end{pmatrix}, \quad (4.12)$$

and

$$\begin{aligned} B_{ij} = & \begin{pmatrix} \frac{199}{50} & \frac{27}{10} & \frac{44}{5} \\ \frac{9}{10} & \frac{35}{6} & 12 \\ \frac{11}{10} & \frac{9}{2} & -26 \end{pmatrix} + \Theta(\mu - m_H) \begin{pmatrix} \frac{9}{50} & \frac{9}{10} & 0 \\ \frac{3}{10} & \frac{13}{6} & 0 \\ 0 & 0 & 0 \end{pmatrix} + 2\Theta(\mu - m_\Delta) \begin{pmatrix} \frac{1}{150} & \frac{3}{10} & \frac{8}{15} \\ \frac{1}{10} & \frac{13}{2} & 8 \\ \frac{1}{15} & 3 & \frac{22}{3} \end{pmatrix} \\ & + \Theta(\mu - m_{38}) \begin{pmatrix} 0 & 0 & 0 \\ 0 & \frac{56}{3} & 0 \\ 0 & 0 & 42 \end{pmatrix}, \end{aligned} \quad (4.13)$$

where  $m_H$  is the mass of the second Higgs doublet,  $m_\Delta$  is the mass of the two light LQs and  $m_{38}$  is the mass of the states  $(\mathbf{8}, \mathbf{1})_0$  and  $(\mathbf{1}, \mathbf{3})_0$ , as defined previously. We have assumed two mass degenerate LQs in Eqs. (4.12) and (4.13). The extension of these expressions to the non-degenerate case is straightforward. There are also two-loop contributions proportional to  $g_i^3 \text{Tr}(y^\dagger y)$ . However, even in the case of the top quark Yukawa, these do not have a

significant impact due to their smaller numerical coefficients. We therefore neglect them in order to avoid introducing dependence on  $\tan\beta$ . We use the following values for the SM parameters, defined at  $\mu = m_Z$  in the  $\overline{\text{MS}}$  scheme [22]:

$$\begin{aligned}\alpha_3(m_Z) &= 0.1181 \pm 0.0011, \\ \alpha_{\text{em}}^{-1}(m_Z) &= 127.950 \pm 0.017, \\ \sin^2\theta_W(m_Z) &= 0.23129 \pm 0.00005.\end{aligned}\tag{4.14}$$

Taking the mass of the second Higgs doublet to be  $m_H = 3$  TeV, along with the light LQ masses  $m_{\Delta_1} = m_{\Delta_2} = 3$  TeV, and the triplet-octet mass  $m_{38} = 10$  TeV then leads to unification at a scale  $\Lambda_{\text{GUT}} = 1.2 \times 10^{16}$  GeV, as shown in Fig. 4.3.

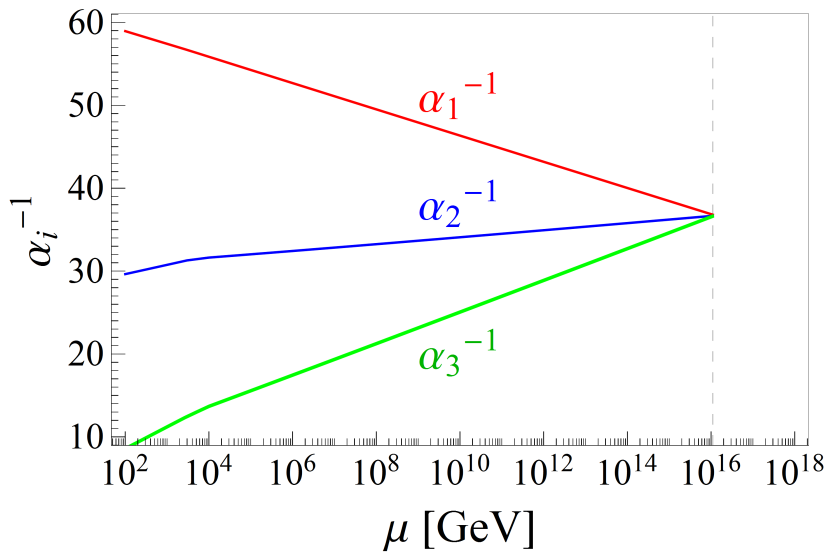


**Figure 4.3:** Running coupling constants with  $m_H = m_{\Delta_1} = m_{\Delta_2} = 3$  TeV and  $m_{38} = 10$  TeV. See text for details.

### 4.2.3 Scan of parameters

To fully explore the viable parameter space of the model, we performed a random scan over the masses in the ranges

$$m_{\Delta_1}, m_{\Delta_2} \in [400, 10^7] \text{ GeV}, \quad m_H \in [480, 10^7] \text{ GeV}, \quad m_{38} \in [10^3, 10^{16}] \text{ GeV}, \tag{4.15}$$

using logarithmic priors. The lower bound on the mass of the second Higgs doublet is motivated by constraints on the charged Higgs mass from  $B \rightarrow X_s \gamma$  [193], while the LQs are constrained by direct searches, to be discussed in Sec. 4.4. The model parameters for which unification is achieved (within  $2\sigma$  uncertainties on the gauge couplings) are shown in Fig. 4.4. From the left panel, it is evident that unification leads to an upper limit on the mass of the lightest LQ,  $\Delta_1$ . This is attained for degenerate LQ masses,  $m_{\Delta_1} = m_{\Delta_2}$ , and when  $m_H$  takes its minimum value. This case is shown by the red shaded band in Ref. 4.4. We therefore find that unification requires at least one LQ to have a mass below  $\lesssim 16$  TeV. Furthermore, it is clear from the right panel of Fig. 4.4 that the second LQ,  $\Delta_2$ , cannot be

arbitrarily heavy. The upper limit on  $m_{\Delta_2}$  is determined by the minimal allowed values for  $m_{\Delta_1}$  and  $m_H$ , which are constrained by experiment. Finally, note that the scale of gauge coupling unification  $\Lambda_{\text{GUT}}$ , denoted by the colour of the points, is strongly correlated with  $m_{38}$  and only mildly sensitive to the other mass thresholds.

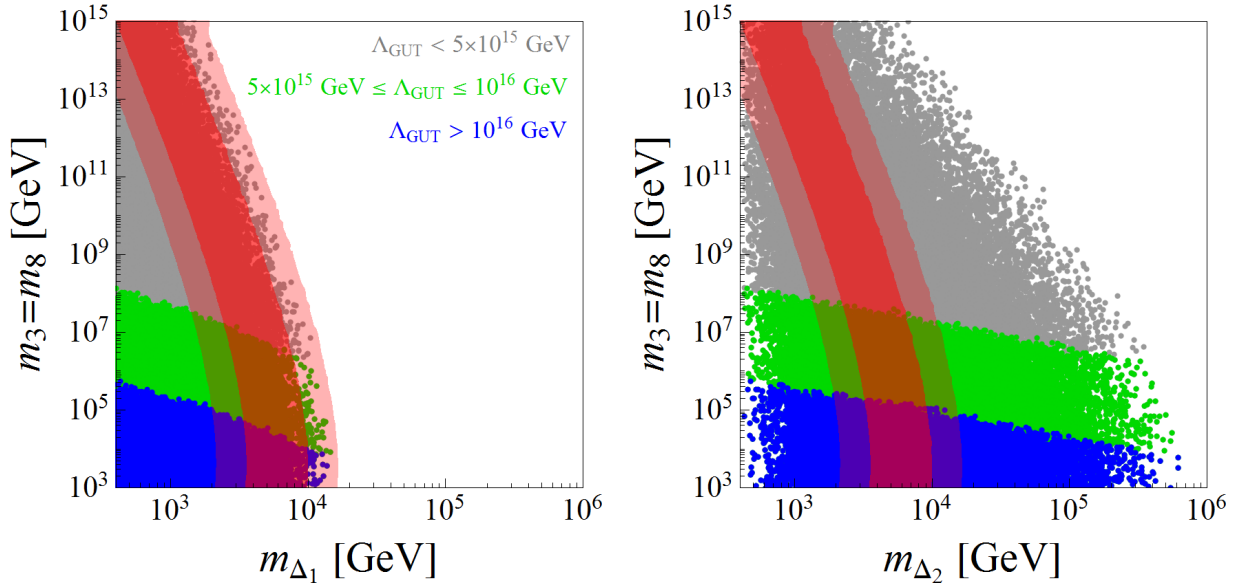


**Figure 4.4:** Regions of parameter space in which unification is obtained. The (green, blue) points correspond to a unification scale  $\Lambda_{\text{GUT}} > (5 \times 10^{15}, 10^{16})$  GeV, respectively, while the grey points satisfy  $\Lambda_{\text{GUT}} < 5 \times 10^{15}$  GeV. The dark (light) red shaded band shows the region where the couplings unify at  $1\sigma$  ( $2\sigma$ ) in the case of degenerate LQ masses,  $m_{\Delta_1} = m_{\Delta_2}$ , and  $m_H = 480$  GeV.

Let us now comment on the minimal case, where the **24**-plet is instead described by a real scalar containing a single triplet and single octet degree of freedom. Repeating the above analysis, we find results qualitatively similar to those shown in Fig. 4.4. However, in this case the upper bound on the lightest leptoquark mass becomes stronger, giving  $m_{\Delta_1} \lesssim 5$  TeV. Perhaps more interestingly, the unification scale is now restricted to lie below  $4 \times 10^{15}$  GeV. While still consistent with existing bounds on the proton lifetime, this lower unification scale could potentially lead to observable proton decay at future experiments, such as Hyper Kamiokande [243].

#### 4.2.4 Unification scale and proton decay

Even in cases where the unification scale is beyond  $10^{16}$  GeV, this model has a potentially disastrous problem due to rapid proton decay. This is because in addition to the usual dimension-6 operators obtained by integrating out the  $X$  and  $Y$   $SU(5)$  gauge bosons, the light LQs  $(\mathbf{3}, \mathbf{2})_{1/6}$  can also mediate the proton decay, as discussed in the previous Section. This occurs via the following terms in the scalar potential

$$\begin{aligned} \mathcal{L} \supset & \lambda' H_{\bar{5}} \Phi_{10} \Phi_{10} \Phi_{10} + \lambda'' H_{\bar{5}}^* \Phi_{10} \Phi_{10} \Phi_{10} + \text{h.c.}, \\ & \supset \lambda \epsilon_{ijk} \Delta^a \Delta^b \Delta^c H + \text{h.c.}, \end{aligned} \quad (4.16)$$

where  $i, j, k$  are colour indices and we omitted  $SU(2)$  indices. Proton decay then proceeds via the 5-body decay  $p \rightarrow \pi^+ \pi^+ e^- \nu \nu$  [244]. Although this decay corresponds to a dimension-9 operator, it might still be problematic as the suppression scale is only  $m_{\Delta} \sim \text{TeV}$ .

This proton decay channel was not originally identified, but was subsequently believed to be a strong reason to disfavour this model [8]. However, we wish to point out that the terms in Eq. (4.16) can be forbidden by imposing a  $U(1)_{\text{PQ}}$  symmetry. Such a symmetry has additional motivation in the context of the strong CP problem and was originally considered as motivation for introducing the additional  $\bar{\mathbf{5}}$  Higgs. By choosing the  $U(1)_{\text{PQ}}$  charge assignments

$$Q(H_5) = Q(H_{\bar{5}}) = Q(\Phi_{10}^{(a)}) = -2, \quad (4.17)$$

we clearly forbid the dangerous terms. The assignment  $Q = 1$  for the left-handed quarks and leptons  $(\Psi_{\bar{5}} + \Psi_{10})_L$ , then ensures the Yukawa terms in Eq. (4.9) are allowed by the symmetry. After PQ symmetry breaking, the terms in Eq. (4.16) will be generated by higher dimension operators, suppressed by  $\Lambda_{\text{PQ}}^2/M_{\text{Pl}}^2 \sim 10^{-18} - 10^{-12}$ . Substituting this value for  $\lambda$  into Eq. (4.6), it is clear that the proton remains sufficiently long-lived to satisfy the existing bounds. It would however be interesting to perform a dedicated search sensitive to decays  $p \rightarrow \pi^+ \pi^+ e^- \nu \nu$ , as this could be expected to improve the current limit by several orders of magnitude.

Of course, proton decay can still proceed via the usual dimension-6 operators and experimental bounds on the proton lifetime can then be used to place a lower bound on the unification scale. Focusing on the decay channel  $p \rightarrow \pi^0 e^+$ , the partial width is given by

$$\Gamma(p \rightarrow \pi^0 e^+) = \frac{m_p}{8\pi} A^2 \left( \frac{g_{\text{GUT}}}{\sqrt{2} m_{X,Y}} \right)^4 \left( |c(e^c, d) \langle \pi^0 | (ud)_{L u_R} | p \rangle|^2 + |c(e, d^c) \langle \pi^0 | (ud)_{R u_L} | p \rangle|^2 \right), \quad (4.18)$$

where  $g_{\text{GUT}}$  is the unified coupling evaluated at the mass of the  $X$  and  $Y$  gauge bosons,  $m_{X,Y}$ . The coefficients  $c(e^c, d)$  and  $c(e, d^c)$  depend on the fermion mixing matrices and are defined in Ref. [245]. Finally, the factor  $A$  accounts for running of the four-fermion operators from  $m_{X,Y}$  down to  $\approx \text{GeV}$  and is given by

$$A = A_{\text{QCD}} \left( \frac{\alpha_3(m_Z)}{\alpha_3(m_\Delta)} \right)^{\frac{2}{7}} \left( \frac{\alpha_3(m_\Delta)}{\alpha_3(m_{38})} \right)^{\frac{6}{19}} \left( \frac{\alpha_3(m_{38})}{\alpha_3(m_{X,Y})} \right)^{\frac{6}{16}}, \quad (4.19)$$

where  $A_{\text{QCD}} \approx 1.2$  includes the effect of running from  $m_Z$  to  $Q \approx 2.3 \text{ GeV}$ , and the light LQs are assumed to be degenerate in mass. For the hadronic matrix elements we use the lattice determined values from Ref. [246], which gives  $\langle \pi^0 | (ud)_{R u_L} | p \rangle = \langle \pi^0 | (ud)_{L u_R} | p \rangle = 0.103(41)$ .

In Fig. (4.5) we again plot the results of the parameter scan, showing the scale of unification  $\Lambda_{\text{GUT}}$ , for different octet/triplet masses. Notice once again that the unification scale is only mildly dependent of the masses of the LQs and second Higgs doublet. Furthermore, for octet masses close to the LHC lower bound of 1.5 TeV [247], the unification scale can be pushed all the way up to  $\sim 2 \times 10^{16} \text{ GeV}$ . The dashed line shows the lower bound on the unification scale derived from the Super Kamiokande limit on the proton lifetime,  $\tau(p \rightarrow \pi^0 e^+) > 1.29 \times 10^{34} \text{ years}$  [248]. For simplicity, we have neglected possible threshold corrections from fermions and scalars with masses near  $m_{X,Y}$ , such that  $\Lambda_{\text{GUT}} = e^{-1/21} m_{X,Y} \simeq 0.95 m_{X,Y}$ .

Fig. 4.5 suggests that triplet/octet masses below  $\approx 10^{10} \text{ GeV}$  are required in order to satisfy the bounds from Super Kamiokande. However, it should be noted that the precise bound on  $m_{X,Y}$  also depends upon the details of the model at the GUT scale. This dependence is contained in the coefficients  $c(e^c, d)$  and  $c(e, d^c)$ , which take the values

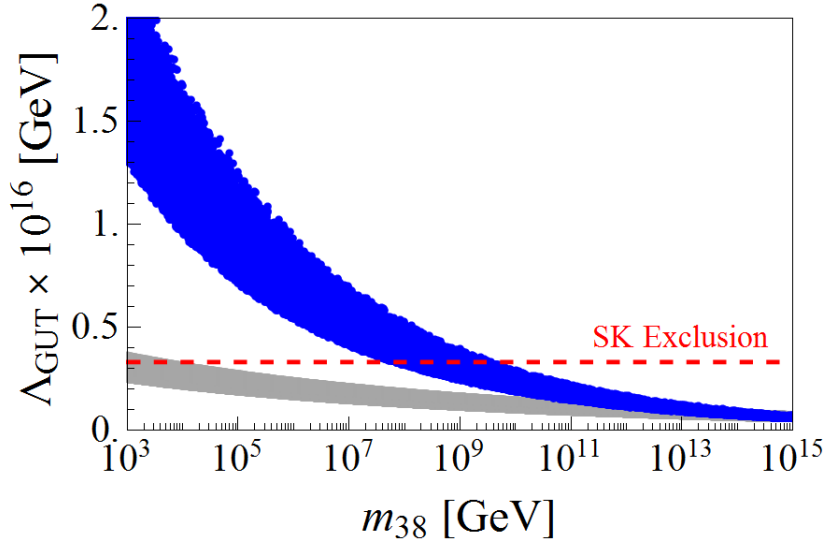


**Figure 4.5:** Unification scale as a function of the octet/triplet mass. The grey (blue) points correspond to a real (complex) octet and triplet. The dashed line shows the bound from Super Kamiokande ( $\tau_p > 1.29 \times 10^{34}$  years at 90% CL.) [238], assuming  $c(e^c, d) = 2$  and  $c(e, d^c) = 1$ . In evaluating (4.18) we have used the same masses as 4.3, however both the value of  $g_{\text{GUT}}$  and the factor  $A$  defined in (4.19) are approximately constant across the parameter space.

$c(e^c, d) = 2$  and  $c(e, d^c) = 1$  in the Georgi-Glashow model. These particular values also yield the maximum partial width in Eq. (4.18) that is consistent with unitarity of the fermion mixing matrices. However, at the very least we know that the relation  $Y_D = Y_E^T$  for the Yukawa matrices must be broken, which leads to some freedom in the mixing matrices. This issue was investigated in detail in [249], where it was shown that it is possible to forbid the decay  $p \rightarrow \pi^0 e^+$ , along with all decays into a meson and anti-neutrinos. The leading decay mode is then into second generation fermions,  $p \rightarrow K^0 \mu^+$ , and is suppressed by the CKM angle  $\sin^2 \theta_{13}$ . The bound on this decay channel from Super Kamiokande is  $1.6 \times 10^{33}$  years, which leads to the most conservative bound on the mass of heavy gauge bosons  $m_{X,Y} \gtrsim 7.4 \times 10^{13}$  GeV.

Finally, we comment on the low and high energy signatures of the light LQ states. The LHC constraints on LQ masses are very model dependent, since they depend on the couplings to fermions, which are free parameters in the Yukawa Lagrangian (4.9). By reinterpreting the bounds from the direct searches, one can show that LQs as light as  $\approx 400$  GeV are still allowed by current data [229]. We will overview the current status of the LHC searches for LQs in Sec. 4.4. Furthermore, the couplings to fermions in (4.10) can induce signatures in several low-energy observables provided these are non-negligible. Among the interesting signatures, the light LQs can induce sizable contributions to  $\Delta F = 1$  processes, such as  $B \rightarrow K^{(*)} \ell \ell$  ( $\ell = e, \mu, \tau$ ) and  $B \rightarrow K^{(*)} \nu \nu$ , and to several LFV processes, such as  $\tau \rightarrow \mu \phi$  and  $B \rightarrow K \mu \tau$ , which are being studied experimentally [155].

The model presented above served as a illustration of a viable unification scenario with light LQs. The novelty of this model is that unification implies that the lightest LQ must have a mass in the range  $\approx 0.4 - 16$  TeV. This unification scenario is therefore of particular interest as the LQs may be within reach of current and/or future experiments. In the following Sections, we will leave aside the unification scenarios and consider the LQ states in a model independent approach. Our focus will be their phenomenology at low-energies.

### 4.3 Specific leptoquark states

In this Section, we describe in details the models containing the LQ states that will be used in the following Sections, and we derive the corresponding effective Lagrangians which will be relevant for the low-energy phenomenology.

◦  $\mathbf{R}_2 = (\mathbf{3}, \mathbf{2})_{7/6}$ :

We start our discussion in the scenario with a LQ state transforming under the SM gauge group as  $(\mathbf{3}, \mathbf{2})_{7/6}$ . The relevant Lagrangian for this model reads,

$$\begin{aligned}\mathcal{L}_{\Delta(7/6)} &= (y_R)_{ij} \bar{Q}_i \Delta^{(7/6)} \ell_{Rj} + (y_L)_{ij} \bar{u}_{Ri} \widetilde{\Delta}^{(7/6)\dagger} L_j + \text{h.c.} \\ &= (V y_R)_{ij} \bar{u}_{Li} \ell_{Rj} \Delta^{(5/3)} + (y_R)_{ij} \bar{d}_{Li} \ell_{Rj} \Delta^{(2/3)} \\ &\quad + (y_L U)_{ij} \bar{u}_{Ri} \nu_{Lj} \Delta^{(2/3)} - (y_L)_{ij} \bar{u}_{Ri} \ell_{Lj} \Delta^{(5/3)} + \text{h.c.},\end{aligned}\tag{4.20}$$

where  $y_{L(R)}$  denote the Yukawa coupling matrices and  $\widetilde{\Delta} = i\sigma_2 \Delta^*$  is the conjugate  $SU(2)_L$  doublet. Color indices are omitted for simplicity. In the second line we decompose the weak doublet in terms of the fields  $\Delta^{(5/3)}$  and  $\Delta^{(2/3)}$ , where the superscripts refer to the electric charge of the two mass degenerate LQ states,  $m_\Delta \equiv m_{\Delta^{(5/3)}} = m_{\Delta^{(2/3)}}$ .<sup>4</sup> To determine the effective Lagrangian, we write the full Lagrangian of our model<sup>5</sup>

$$\mathcal{L} = \mathcal{L}_{\text{SM}} + \mathcal{L}_{\Delta(7/6)} + \left( D^\mu \Delta^{(7/6)} \right)^\dagger \left( D_\mu \Delta^{(7/6)} \right) - m_\Delta^2 \Delta^{(7/6)\dagger} \Delta^{(7/6)}.\tag{4.21}$$

By integrating out the heavy LQ fields, we obtain

$$\frac{\partial \mathcal{L}}{\partial \Delta} = -m_\Delta^2 \Delta^\dagger + \frac{\partial \mathcal{L}_{\Delta(7/6)}}{\partial \Delta} = 0,\tag{4.22}$$

where for shortness we use  $\Delta \equiv \Delta^{(7/6)}$ . The derivative appearing in the above equation reads

$$\frac{\partial \mathcal{L}_{\Delta(7/6)}}{\partial \Delta_\alpha} = (y_R)_{ij} \bar{Q}_{i,\alpha} \ell_{Rj} + (y_L)_{ij} \bar{u}_{Ri} L_{j,\beta} \varepsilon_{\beta\alpha},\tag{4.23}$$

where we have explicitly written the  $SU(2)$  indexes  $\alpha, \beta = 1, 2$ . Moreover,  $\varepsilon_{ij}$  denotes the total anti-symmetric tensor with convention  $\varepsilon_{12} = -\varepsilon_{21} = +1$ . The replacement of Eq. (4.23) in Eq. (4.22) after neglecting the kinetic terms allow us to obtain the effective Lagrangian in a gauge invariant form<sup>6</sup>

$$\mathcal{L}_{\text{eff}}^{(7/6)} = \frac{(y_R)_{ij} (y_R)_{i'j'}^*}{m_\Delta^2} \left( \bar{Q}_{i,\alpha} \ell_{Rj} \right) \left( \bar{\ell}_{Rj'} Q_{i',\alpha} \right) + \frac{(y_L)_{ij} (y_L)_{i'j'}^*}{m_\Delta^2} \left( \bar{L}_{j',\alpha} u_{Ri'} \right) \left( \bar{u}_{Ri} L_{j,\alpha} \right)$$

<sup>4</sup>Note that the electroweak oblique corrections do not allow for large splittings between the two states of the doublet [8, 250, 251].

<sup>5</sup>In principle, the quartic couplings to the Higgs doublet such as  $(\Delta^\dagger \Delta)(H^\dagger H)$  should also be included in the Lagrangian. We will neglect these terms since they play no role in the phenomenology that we are considering.

<sup>6</sup>This result for the effective Lagrangian can be more rigorously obtained by integrating-out the LQs in the path integral approach.

$$+ \left[ \frac{(y_R)_{ij}(y_L)_{i'j'}^*}{m_\Delta^2} \varepsilon_{\alpha\beta} \left( \bar{Q}_{i,\alpha} \ell_{Rj} \right) \left( \bar{L}_{j',\alpha} u_{Ri'} \right) + \text{h.c.} \right]. \quad (4.24)$$

One can then use the Fierz rearrangement for anti-commuting fields to write the effective Lagrangian as

$$\mathcal{L}_{\text{eff}}^{(7/6)} = \mathcal{L}_{d \rightarrow d' \ell \ell'}^{(7/6)} + \mathcal{L}_{u \rightarrow u' \ell \ell'}^{(7/6)} + \mathcal{L}_{d \rightarrow u \ell \ell'}^{(7/6)} + \mathcal{L}_{u \rightarrow u' \nu \nu'}^{(7/6)}, \quad (4.25)$$

where the terms contributing to neutral currents read

$$\mathcal{L}_{d \rightarrow d' \ell \ell'}^{(7/6)} = - \frac{(y_R)_{ij}(y_L)_{i'j'}^*}{2m_\Delta^2} \left( \bar{d}_i \gamma^\mu P_L d_{i'} \right) \left( \bar{\ell}_{j'} \gamma_\mu P_R \ell_j \right), \quad (4.26)$$

$$\mathcal{L}_{u \rightarrow u' \nu \nu'}^{(7/6)} = - \frac{(y_L U)_{i'j'}(y_L U)_{ij}^*}{2m_\Delta^2} \left( \bar{u}_i \gamma^\mu P_R u_{i'} \right) \left( \bar{\nu}_{j'} \gamma_\mu P_L \nu_j \right), \quad (4.27)$$

$$\begin{aligned} \mathcal{L}_{u \rightarrow u' \ell \ell'}^{(7/6)} = & \left\{ \frac{(y_R)_{ij}(y_L)_{i'j'}^*}{2m_\Delta^2} \left[ \left( \bar{u}_i P_R u_{i'} \right) \left( \bar{\ell}_{j'} P_R \ell_j \right) + \frac{1}{4} \left( \bar{u}_i \sigma_{\mu\nu} P_R u_{i'} \right) \left( \bar{\ell}_{j'} \sigma^{\mu\nu} P_R \ell_j \right) \right] + \text{h.c.} \right\} \\ & - \frac{(y_R)_{ij}(y_R)_{i'j'}^*}{2m_\Delta^2} \left( \bar{u}_i \gamma^\mu P_L u_{i'} \right) \left( \bar{\ell}_{j'} \gamma_\mu P_R \ell_j \right) - \frac{(y_L)_{ij}(y_L)_{i'j'}^*}{2m_\Delta^2} \left( \bar{u}_i \gamma^\mu P_R u_{i'} \right) \left( \bar{\ell}_{j'} \gamma_\mu P_L \ell_j \right). \end{aligned} \quad (4.28)$$

Similarly, the contribution to charged currents reads

$$\mathcal{L}_{d \rightarrow u \ell \ell'}^{(7/6)} = \frac{(y_R)_{ij}(y_L U)_{i'j'}^*}{2m_\Delta^2} \left[ \left( \bar{d}_i P_R u_{i'} \right) \left( \bar{\nu}_{j'} P_R \ell_j \right) + \frac{1}{4} \left( \bar{d}_i \sigma_{\mu\nu} P_R u_{i'} \right) \left( \bar{\nu}_{j'} \sigma^{\mu\nu} P_R \ell_j \right) \right] + \text{h.c.} \quad (4.29)$$

From Eq. (4.26), one can see that the only non-zero Wilson coefficients, relevant to  $b \rightarrow s \ell_1^- \ell_2^+$ , are

$$C_9^{\ell_1 \ell_2} = C_{10}^{\ell_1 \ell_2} = - \frac{\pi v^2}{2V_{tb} V_{ts}^* \alpha_{\text{em}}} \frac{(y_R)_{s\ell_1} (y_R)_{b\ell_2}^*}{m_\Delta^2}, \quad (4.30)$$

which correspond to the chirality non-flipped operators in Eq. (2.54). The operators appearing in Eq. 4.29 can contribute significantly to the transition  $b \rightarrow c \tau \nu$ , which will be discussed in Sec. 5.3. The other contributions turn out to be less relevant for phenomenology because there are few experimental results for the transitions  $u \rightarrow u' \ell \ell'$  and  $u \rightarrow u' \nu \nu'$ , the only exception being the strong experimental limits  $\mathcal{B}(D^0 \rightarrow \mu \mu) < 6.2 \times 10^{-9}$  and  $\mathcal{B}(D^+ \rightarrow \pi^+ \mu \mu) < 7.3 \times 10^{-8}$  [252, 253].

○  $\tilde{\mathbf{R}}_2 = (\mathbf{3}, \mathbf{2})_{1/6}$ :

The model containing the state  $(\mathbf{3}, \mathbf{2})_{1/6}$  was originally proposed as a viable explanation of  $R_K^{\text{exp}} < R_K^{\text{SM}}$  in Ref. [118]. The Yukawa Lagrangian reads,

$$\begin{aligned}\mathcal{L}_{\Delta^{(1/6)}} &= (y_L)_{ij} \bar{d}_{Ri} \widetilde{\Delta}^{(1/6)\dagger} L_j + \text{h.c.} \\ &= (y_L U)_{ij} \bar{d}_i P_L \nu_j \Delta^{(-1/3)} - (y_L)_{ij} \bar{d}_i P_L \ell_j \Delta^{(2/3)} + \text{h.c.},\end{aligned}\quad (4.31)$$

where  $y_L$  is a generic matrix of couplings.<sup>7</sup> In the second line we explicitly write the terms with  $\Delta^{(-1/3)}$  and  $\Delta^{(2/3)}$  where the superscripts refer to the electric charge of the  $Y = 1/6$  LQ states. As before, the masses of the two physical states are assumed to be equal for simplicity,  $m_{\Delta^{(2/3)}} = m_{\Delta^{(-1/3)}} \equiv m_\Delta$ . Notice also that we have neglected the possibility of having RH neutrinos when writing Eq. (4.31). The latter case will be discussed in Sec. 5.3 along with the models proposed to simultaneously explain  $R_{K^{(*)}}$  and  $R_{D^{(*)}}$ .

The effective Lagrangian for this model can be deduced in the same way as in the discussion above. We obtained

$$\mathcal{L}_{\text{eff}}^{(1/6)} = \frac{(y_L)_{ij} (y_L)_{i'j'}^*}{m_\Delta^2} \left( \bar{d}_{Ri} L_{j,\alpha} \right) \left( \bar{L}_{j',\alpha} d_{Ri'} \right), \quad (4.32)$$

which can be rewritten as

$$\begin{aligned}\mathcal{L}_{\text{eff}}^{(1/6)} &= - \frac{(y_L)_{ij} (y_L)_{i'j'}^*}{2m_\Delta^2} \left( \bar{d}_i \gamma^\mu P_R d_{i'} \right) \left( \bar{\ell}_{j'} \gamma_\mu P_L \ell_j \right) \\ &\quad + \frac{(y_L U)_{ij} (y_L U)_{i'j'}^*}{2m_\Delta^2} \left( \bar{d}_i \gamma^\mu P_R d_{i'} \right) \left( \bar{\nu}_{j'} \gamma_\mu P_L \nu_j \right).\end{aligned}\quad (4.33)$$

From this equation, one can identify the chirality flipped operators from the  $b \rightarrow s \ell_1^- \ell_2^+$  effective Hamiltonian (2.54), with the corresponding Wilson coefficients given by

$$\left( C_9^{\ell_1 \ell_2} \right)' = - \left( C_{10}^{\ell_1 \ell_2} \right)' = - \frac{\pi v^2}{2V_{tb} V_{ts}^* \alpha_{\text{em}}} \frac{(y_L)_{s\ell_1} (y_L)_{b\ell_2}^*}{m_\Delta^2}. \quad (4.34)$$

The phenomenology of this scenario will be discussed as a particular case of the model introduced in Sec. 5.3.

○  $\mathbf{S}_1 = (\bar{\mathbf{3}}, \mathbf{1})_{1/3}$ :

Being an electroweak singlet, this scalar LQ model is the simplest one. Its Lagrangian is given by,

$$\begin{aligned}\mathcal{L}_{\Delta^{(1/3)}} &\supset (y_L)_{ij} \overline{Q_i^C} i\tau_2 L_j \Delta^{(1/3)} + (y_R)_{ij} \overline{u_{Ri}^C} \ell_{Rj} \Delta^{(1/3)} + \text{h.c.} \\ &= \Delta^{(1/3)} \left[ (V^* y_L)_{ij} \overline{u_i^C} P_L \ell_j - (y_L)_{ij} \bar{d}_i^C P_L \nu_j + (y_R)_{ij} \overline{u_i^C} P_R \ell_j \right] + \text{h.c.},\end{aligned}\quad (4.35)$$

where the superscript  $C$  stands for the charge conjugation, which is defined as  $\Psi^C \equiv \gamma_0 C \Psi^*$  with  $C = i\gamma_2 \gamma_0$ .<sup>8</sup> In addition to terms shown in (4.35) one can also write terms involving diquarks, namely,

<sup>7</sup>The matrix  $y_L$  should not be confused with the one appearing in Eq. (4.20).

<sup>8</sup>It should be clear that  $y_{L,R}$  in Eq. (4.35) are entirely different couplings from those appearing in Eq. (4.31) or in Eq. (4.20).

$$\mathcal{L}_{\Delta^{(1/3)}} \supset (z_L)_{ij} \overline{Q_{L i, \alpha}^C} Q_{L j \beta} \Delta^{(1/3)*} \varepsilon_{\alpha\beta} + (z_R)_{ij} \overline{u_{R i}^C} d_{R j} \Delta^{(1/3)*} \varepsilon_{\alpha\beta} + \text{h.c.}, \quad (4.36)$$

which are manifestly gauge invariant. These terms violate baryon and lepton number if they coexist with the ones present in (4.35). To avoid a conflict with the stringent proton decay bounds those couplings must be negligibly small. If we neglect the diquark couplings, the effective Lagrangian of this model becomes

$$\mathcal{L}_{\text{eff}}^{(1/3)} = \mathcal{L}_{d \rightarrow u \ell \ell'}^{(1/3)} + \mathcal{L}_{d \rightarrow d' \nu \nu'}^{(1/3)} + \mathcal{L}_{u \rightarrow u' \ell \ell'}^{(1/3)}, \quad (4.37)$$

where the different terms are given by

$$\begin{aligned} \mathcal{L}_{d \rightarrow u \ell \ell'}^{(1/3)} &= -\frac{(y_L)_{ij} (y_L)_{i'j'}^*}{2m_\Delta^2} (\overline{u}_{i'} \gamma^\mu P_L d_i) (\overline{\ell}_{j'} \gamma^\mu P_L \nu_j) \\ &+ \frac{(y_L)_{ij} (y_R)_{i'j'}^*}{2m_\Delta^2} \left[ (\overline{u}_{i'} P_L d_i) (\overline{\ell}_{j'} P_L \nu_j) - \frac{1}{4} (\overline{u}_{i'} \sigma_{\mu\nu} P_L d_i) (\overline{\ell}_{j'} \sigma^{\mu\nu} P_L \nu_j) \right] + \text{h.c.}, \end{aligned} \quad (4.38)$$

$$\mathcal{L}_{d \rightarrow d' \nu \nu'}^{(1/3)} = \frac{(y_L)_{ij} (y_L)_{i'j'}^*}{2m_\Delta^2} (\overline{d}_{i'} \gamma^\mu P_L d_i) (\overline{\nu}_{j'} \gamma^\mu P_L \nu_j), \quad (4.39)$$

and

$$\begin{aligned} \mathcal{L}_{u \rightarrow u' \ell \ell'}^{(1/3)} &= \frac{(V^* y_L)_{ij} (V^* y_L)_{i'j'}^*}{2m_\Delta^2} (\overline{u}_{i'} \gamma^\mu P_L u_i) (\overline{\ell}_{j'} \gamma^\mu P_L \ell_j) \\ &+ \frac{(y_R)_{ij} (y_R)_{i'j'}^*}{2m_\Delta^2} (\overline{u}_{i'} \gamma^\mu P_R u_i) (\overline{\ell}_{j'} \gamma^\mu P_R \ell_j) \\ &- \left\{ \frac{(y_R)_{ij} (V^* y_L)_{i'j'}^*}{2m_\Delta^2} \left[ (\overline{u}_{i'} P_R u_i) (\overline{\ell}_{j'} P_R \ell_j) - \frac{1}{4} (\overline{u}_{i'} \sigma_{\mu\nu} P_R u_i) (\overline{\ell}_{j'} \sigma^{\mu\nu} P_R \ell_j) \right] + \text{h.c.} \right\}. \end{aligned} \quad (4.40)$$

In deriving these equations we have used the Fierz identity and the following fermion conjugation properties

$$\begin{aligned} \overline{\psi^C} P_L \phi^C &= \overline{\phi} P_L \psi, \\ \overline{\psi^C} \gamma_\mu P_L \phi^C &= -\overline{\phi} \gamma_\mu P_R \psi, \\ \overline{\psi^C} \sigma_{\mu\nu} P_L \phi^C &= -\overline{\phi} \sigma_{\mu\nu} P_L \psi, \end{aligned} \quad (4.41)$$

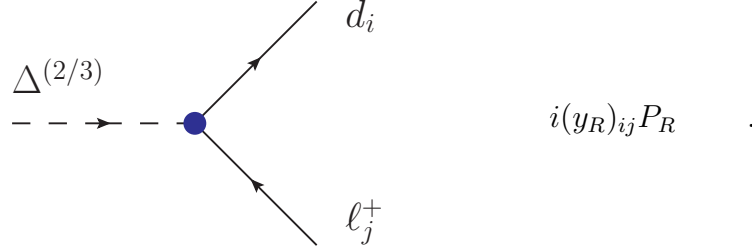
where  $\psi \equiv \psi(x)$  and  $\phi \equiv \phi(x)$  stand for generic (anti-commuting) fermionic fields.

Finally, notice that this LQ does not contribute to the transition  $b \rightarrow s \ell_1^- \ell_2^+$  at tree-level. The  $b \rightarrow s \ell \ell$  Wilson coefficients appear only at one-loop level via box diagrams with LQs running in the loop [254, 255]. The phenomenology of this scenario will be discussed in Sec. 5.2.4.

**Remarks on sign “ambiguity” in deriving  $\mathcal{L}_{\text{eff}}$** 

Before moving to the next Section, let us comment on a subtle point regarding the derivation of  $\mathcal{L}_{\text{eff}}$  in models with leptoquark states. As we are going to show, one should be careful when computing the effective Lagrangian by using Feynman rules to account for an extra minus sign coming from the anti-commutation of the operators.

To illustrate this issue, let us consider the model  $(\mathbf{3}, \mathbf{2})_{7/6}$  and derive the effective Lagrangian for  $b \rightarrow s\ell_1\ell_2$  by using Feynman rules instead of the approach describe above. The Feynman rule needed to this computation is given by



The amplitude for the process  $b(p_b) \rightarrow s(p_s)\ell_1^-(p_1)\ell_2^+(p_2)$  is then given by <sup>9</sup>

$$\begin{aligned} \mathcal{M}(b \rightarrow s\ell_1^-\ell_2^+) &= i(y_R)_{s\ell_2}^* [\bar{u}_s(p_s)P_R v_{\ell_2}(p_2)] \frac{i}{q^2 - m_\Delta^2} i(y_R)_{b\ell_1} [\bar{u}_{\ell_1}(p_1)P_L u_b(p_b)] \\ &\approx i \frac{(y_R)_{b\ell_1}(y_R)_{s\ell_2}^*}{m_\Delta^2} [\bar{u}_s(p_s)P_R v_{\ell_2}(p_2)] [\bar{u}_{\ell_1}(p_1)P_L u_b(p_b)] \\ &= i \frac{(y_R)_{b\ell_1}(y_R)_{s\ell_2}^*}{2m_\Delta^2} [\bar{u}_s(p_s)\gamma_\mu P_L u_b(p_b)] [\bar{u}_{\ell_1}(p_1)\gamma^\mu P_R v_{\ell_2}(p_2)] , \end{aligned} \quad (4.42)$$

where the Fierz identity for spinors was used in the last line, cf. Appendix A.1. By comparing this equation with the Lagrangian (4.26), we realize that Eq. (4.26) would generate an amplitude with a different sign. We will show in the following that the missing minus sign in the computation we just described comes from the anti-commutation of the fermion fields and from the choice of asymptotic states, which must be specified in this type of computation.

To elucidate this apparent paradox, let us compute the  $S$ -matrix for the following effective operator

$$\mathcal{O} = (\bar{s}\gamma^\mu P_L b)(\bar{\ell}_1\gamma_\mu P_R \ell_2). \quad (4.43)$$

We define the fermionic fields in terms of creation (annihilation) operators as

$$\psi(x) = \int \frac{d^3\vec{p}}{\sqrt{(2\pi)^3 2E_p}} \sum_\sigma [a(p, \sigma)u(p, \sigma)e^{-ip\cdot x} + b(p, \sigma)^\dagger v(p, \sigma)e^{ip\cdot x}] , \quad (4.44)$$

where  $\sigma$  denotes the spin of the field. In the following, we will omit the  $\sigma$  dependence on the spinors and operators to simplify our notation. To compute the  $S$ -matrix, we will adopt

<sup>9</sup>For simplicity we will write spinors for the quark fields. It should be clear that this computation is just an illustration and that one should appropriately treat the hadronic matrix element in a realistic computation.

the following convention for the asymptotic states

$$|b\rangle \equiv \sqrt{2E_{p_b}} a_b^\dagger(p_b)|0\rangle, \quad (4.45)$$

and

$$\langle \ell_2^+(p_2) \ell_1^-(p_1) s(p_s) | \equiv \langle 0 | b_{\ell_2}(p_2) a_{\ell_1}(p_1) a_s(p_s) \sqrt{2E_{p_s} 2E_{p_1} 2E_{p_2}}, \quad (4.46)$$

where the subscript in the operators denote the type of fermion we are considering. Note that a different ordering of the fermionic operators could lead to a different (global) sign of the amplitudes. By using these conventions, the  $S$ -matrix at leading order reads

$$S_{fi} = \langle \ell_2^+(p_2) \ell_1^-(p_1) s(p_s) | \int d^4x i : (\bar{s} \gamma^\mu P_L b) (\bar{\ell}_1 \gamma_\mu P_R \ell_2) : | b(p_b) \rangle, \quad (4.47)$$

where  $: \mathcal{O} :$  denotes the normal ordering of the operator. By replacing the fermion fields, one can show that

$$\begin{aligned} S_{fi} &= i \int d^4x \prod_{i=1}^4 \int \frac{d^3 \vec{k}_i}{\sqrt{(2\pi)^3 2E_{k_i}}} \sum_{\sigma_i} \sqrt{2E_{p_b} 2E_{p_s} 2E_{p_1} 2E_{p_2}} \\ &\times \langle 0 | b_{\ell_2}(p_2) a_{\ell_1}(p_1) a_s(p_s) : [a_s^\dagger(k_1) \bar{u}_s(k_1) e^{ik_1 \cdot x}] \gamma^\mu P_L [a_b(k_2) u_b(k_2) e^{-ik_2 \cdot x}] \\ &\quad [a_{\ell_1}^\dagger(k_3) \bar{u}_{\ell_1}(k_3) e^{ik_3 \cdot x}] \gamma^\mu P_R [b_{\ell_2}^\dagger(k_4) v_{\ell_2}(k_4) e^{ik_4 \cdot x}] : a_b^\dagger(p_b) | 0 \rangle, \end{aligned} \quad (4.48)$$

which gives, after integration and contracting the fermionic operators,

$$S_{fi} = i(2\pi)^4 \delta(p_b - p_s - p_{\ell_1} - p_{\ell_2}) [\bar{u}_s(p_s) \gamma^\mu P_L u_b(p_b)] [\bar{u}_{\ell_1}(p_1) \gamma^\mu P_R v_{\ell_2}(p_2)]. \quad (4.49)$$

This is the result we expected. Note that our choice of initial states was such that no additional sign due to the anti-commutation of the creation (annihilation) operators appeared.

Let us perform now the same computation but after applying the Fierz transformation to the operator  $\mathcal{O}$ . In this case, we can write

$$\mathcal{O} = (\bar{s} \gamma^\mu P_L b) (\bar{\ell}_1 \gamma_\mu P_R \ell_2) = -2(\bar{s} P_R \ell_2) (\bar{\ell}_1 P_L b). \quad (4.50)$$

The corresponding  $S$ -matrix is then given by

$$\begin{aligned} S_{fi} &= -2 \langle \ell_2^+(p_2) \ell_1^-(p_1) s(p_s) | \int d^4x i : (\bar{s} P_R \ell_2) (\bar{\ell}_1 P_L b) : | b(p_b) \rangle \\ &= -2i \int d^4x \prod_{i=1}^4 \int \frac{d^3 \vec{k}_i}{\sqrt{(2\pi)^3 2E_{k_i}}} \sum_{\sigma_i} \sqrt{2E_{p_b} 2E_{p_s} 2E_{p_1} 2E_{p_2}} \\ &\times \langle 0 | b_{\ell_2}(p_2) a_{\ell_1}(p_1) a_s(p_s) : [a_s^\dagger(k_1) \bar{u}_s(k_1) e^{ik_1 \cdot x}] P_R [b_{\ell_2}^\dagger(k_4) v_{\ell_2}(k_4) e^{ik_4 \cdot x}] \\ &\quad [a_{\ell_1}^\dagger(k_3) \bar{u}_{\ell_1}(k_3) e^{ik_3 \cdot x}] P_L [a_b(k_2) u_b(k_2) e^{-ik_2 \cdot x}] : a_b^\dagger(p_b) | 0 \rangle. \end{aligned} \quad (4.51)$$

To simplify this equation it is necessary necessary to permute the anti-commuting fields, which generates an extra minus sign in the final result:

$$\begin{aligned}
 \langle 0 | b_{\ell_2}(p_2) a_{\ell_1}(p_1) a_s(p_s) : [a_s^\dagger(k_1) b_{\ell_2}^\dagger(k_4) a_{\ell_1}^\dagger(k_3) a_b(k_2)] : a_b^\dagger(p_b) | 0 \rangle \\
 = -(2\pi)^6 \delta^{(3)}(p_s - k_1) \delta^{(3)}(p_b - k_2) \delta^{(3)}(p_1 - k_3) \delta^{(3)}(p_2 - k_4).
 \end{aligned} \tag{4.52}$$

Therefore, the final result is

$$S_{fi} = i(2\pi)^4 \delta(p_b - p_s - p_{\ell_1} - p_{\ell_2}) 2[\bar{u}_s(p_s) P_R v_{\ell_2}(p_2)][\bar{u}_{\ell_1}(p_1) P_L u_b(p_b)]. \tag{4.53}$$

where an extra minus sign appears due to the definition of the asymptotic states. This result coincides with Eq. (4.49) after performing the Fierz transformation for spinors, cf. Appendix A.1.

The conclusion of this exercise is that one should be careful when matching operators with amplitudes where the fermion ordering is different, since an extra sign due to the anti-commutation of the fields appears. To be more explicit, in order to match operators of the type  $(\bar{\psi}_1 \Gamma \psi_2)(\bar{\psi}_3 \Gamma \psi_4)$  onto amplitudes of the type  $(\bar{u}_{\psi_1} \Gamma u_{\psi_4})(\bar{u}_{\psi_3} \Gamma u_{\psi_2})$ , one should add an extra sign coming from the choice of the final states. An unambiguous way of avoiding this issue is to perform the Fierz at the operator level and then match the amplitudes, which have now the same ordering of the fermion fields.

## 4.4 Direct searches at the LHC

In this Section, we summarize the status of direct searches for LQs performed by CMS and ATLAS by using data collected at  $\sqrt{s} = 13$  TeV. For LQs with perturbative Yukawa couplings, the dominant production mechanism at the LHC is pair production via gluon-gluon fusion processes,  $gg \rightarrow \Delta \bar{\Delta}$ , which are fully determined by the strong interactions and by the LQ mass  $m_\Delta$ . In particular, the pair production rates are independent of the Yukawa couplings of the LQ states. The branching ratio of a LQ decay into a lepton and a quark is the only model dependent quantity that needs to be estimated. In practice, the experimental searches can set limit limits on the products

$$\sigma(gg \rightarrow \Delta \bar{\Delta}) \times \mathcal{B}(\Delta^{(Q)} \rightarrow \text{quark} + \text{lepton})^2, \tag{4.54}$$

where  $Q \in \{-1/3, 2/3, 5/3\}$  denotes the LQ charge, which fixes the possible quarks (up-type or down-type quarks) and leptons ( $\nu$  or  $\ell = e, \mu, \tau$ ) in the final state.<sup>10</sup> Therefore, for a given LQ branching ratio, which depends on the Yukawa structure of the model, one can directly determine a lower bound on the LQ mass from the experimental limit.

We will focus on a pair of LQs decaying mostly to second and third generation fermions, since the LQ couplings to the first generation are already highly constrained by several low energy observables, such as atomic parity violation [8] and the kaon physics observables, which include  $\mathcal{B}(K \rightarrow \mu\nu)$  and limits on  $\mathcal{B}(K^+ \rightarrow \pi^+ \nu \bar{\nu})$  [22]. As a curiosity, we quote the lower bounds on first and second generation LQs obtained by ATLAS [256] and CMS [257, 258], which give  $m_\Delta \gtrsim 1130(1165)$  GeV, assuming a 100% branching ratio  $\Delta^{(2/3)} \rightarrow eq(\mu q)$ , where  $q = d, s$ . These bounds are considerably smaller if the LQ states decay into heavier fermions, since the corresponding searches have a much smaller sensitivity. In the case of third generation LQs, the CMS collaboration released improved bounds on LQs

<sup>10</sup>In principle, one can search for a pair of LQs decaying into a distinct quark-lepton pair. However, most of the experimental limits derived so far focus on a pair of LQs decaying into the same final state.

decaying into  $b\tau$ , obtaining a lower bound on the LQ mass of 900 GeV, with the assumption  $\mathcal{B}(\Delta^{(2/3)} \rightarrow b\tau) = 1$  [259, 260]. Searches with third-generation quarks and neutrinos in the final state have much weaker bounds. By assuming again 100% branching ratios for the decay channels  $\Delta^{(-1/3)} \rightarrow b\nu$  and  $\Delta^{(2/3)} \rightarrow t\nu$ , the ATLAS collaboration obtained the limits  $m_\Delta < 625$  GeV and  $m_\Delta < 640$  GeV, respectively [261]. Similarly, CMS excludes LQs decaying into  $t\tau$  with masses  $m_\Delta > 685$  GeV if  $\mathcal{B}(\Delta^{(-1/3)} \rightarrow t\tau) = 1$  [262]. Note that, with the exception of Ref. [260], these searches currently only make use of the 2015 dataset and we can therefore expect these bounds to improve in the near future, using the significantly greater integrated luminosity collected in 2016.

In most realistic scenarios, the limits quoted above must be reinterpreted to account for LQ branching ratios smaller than one. The exclusions on  $m_\Delta$  for different branching ratios are shown in Fig. 4.6 for the decays  $\Delta^{(2/3)} \rightarrow \tau b$ ,  $\Delta^{(2/3)} \rightarrow \tau\nu$ ,  $\Delta^{(-1/3)} \rightarrow b\nu$  and  $\Delta^{(-1/3)} \rightarrow t\tau$ , where we see that the upper bounds on  $m_\Delta$  drop considerably for branching ratios smaller than  $\approx 50\%$ . One should have in mind that branching ratios of  $\mathcal{O}(50\%)$  can appear even in the scenarios with only one non-vanishing Yukawa coupling. For instance, in the scenario where a doublet LQ couples to a doublet of leptons, the couplings contributing to  $\mathcal{B}(\Delta^{(2/3)} \rightarrow \tau b)$  and  $\mathcal{B}(\Delta^{(-1/3)} \rightarrow b\nu)$  are related by gauge invariance, giving comparable contributions. In Sec. 5.3.3, we will give a concrete example in Sec. 5.3.3 where the bound  $m_\Delta \gtrsim 900$  GeV coming from  $\Delta^{(2/3)} \rightarrow b\tau$  searches can be considerably lowered for the complete model to  $m_\Delta \gtrsim 600$  GeV, while being consistent with other searches and indirect constraints. The lesson from this exercise being that one should carefully reinterpret the limits quoted by ATLAS and CMS for concrete scenarios, by using the rescaled limits similar to the ones shown in Fig. 4.6.

Before closing this section, we should also mention that another possibility to probe LQ contributions is to study the indirect LQ effects in the tails of the kinematic distributions of  $pp \rightarrow \ell\ell$ , with  $\ell = \mu, \tau$ . This strategy has been used to constraint four-fermion effective operators of the form  $\ell\ell b\bar{b}$  in Ref. [263, 264], which can then be translated on constraints on LQ couplings. The constraints on LQs derived as of now are still very limited, but the situation will change with more data accumulated at the LHC.

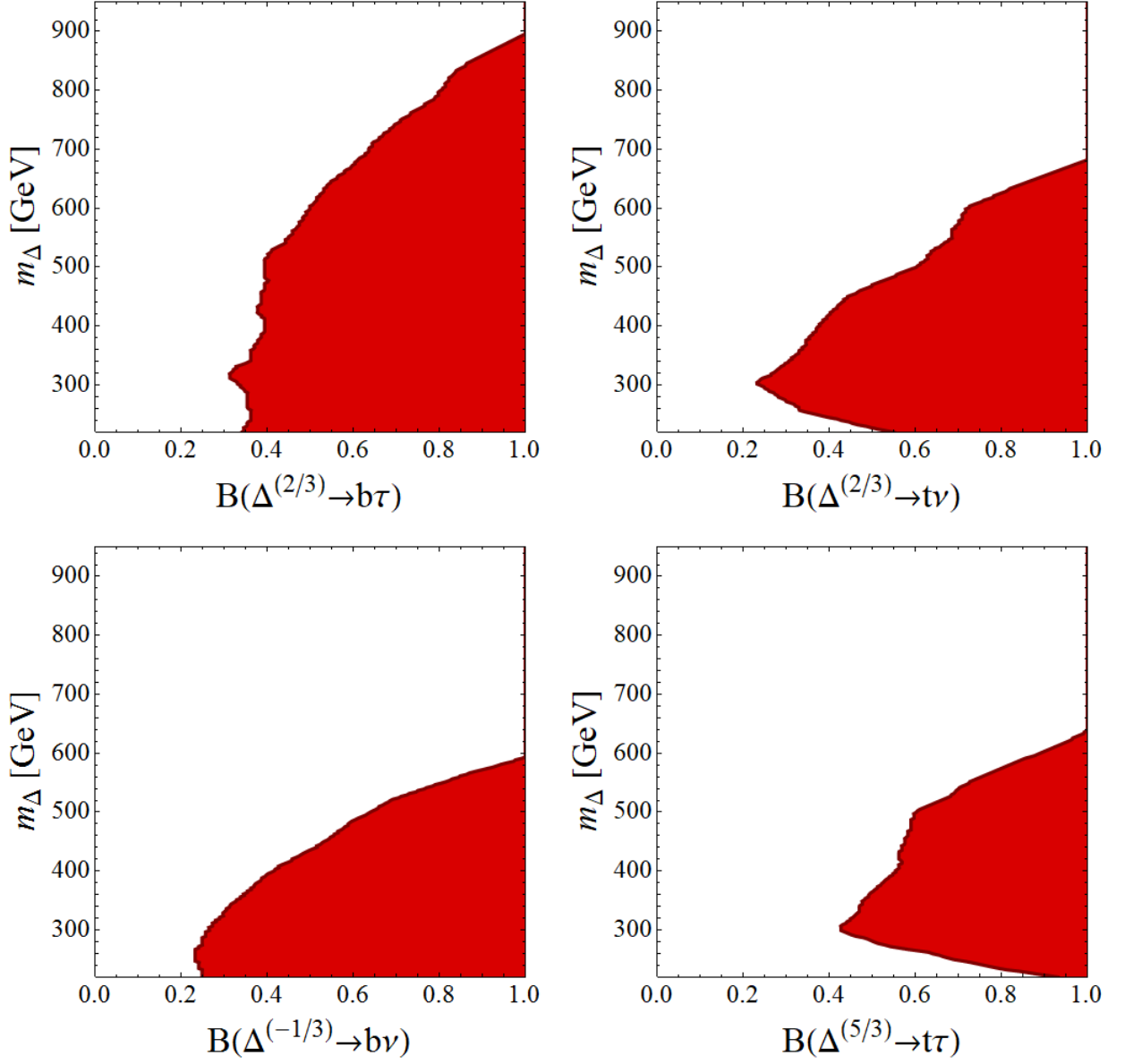


**Figure 4.6:** Exclusions on  $m_\Delta$  as a function of the branching ratio of LQs decaying into  $\Delta^{(2/3)} \rightarrow \tau b$ ,  $\Delta^{(2/3)} \rightarrow t\nu$ ,  $\Delta^{(-1/3)} \rightarrow b\nu$  [260, 261], and  $\Delta^{(-1/3)} \rightarrow t\tau$  [262].

# Chapter 5

## Lepton flavor (universality) violation

Even though the direct searches at LHC did not unveil the NP particles, the  $B$ -physics experiments at LHCb and at the  $B$ -factories point at very intriguing effects of lepton flavor universality violation (LFUV). These discrepancies appeared in both the neutral and the charged  $B$  meson semileptonic decays, and they cannot be accounted for by minimal extensions of the SM. The observed pattern of deviations triggered a considerable interest in the theory community since it could be a first manifestation of flavor breaking effects emerging beyond the SM. The purpose of this Chapter is to critically review the theoretical and experimental status of these anomalies and to describe the viable NP explanations proposed thus far.

This Chapter is organized as follows: In Sec. 5.1, we define the relevant observables and review the current status of these puzzles. In Sec. 5.2, we discuss the interpretation of the LFUV puzzles in neutral currents by using an EFT approach, which is then matched onto several concrete scenarios. Finally, we extend our discussion to the anomalies in tree-level decays in Sec. 5.3, where we also comment on the attempts to simultaneously explain all the LFUV hints.

### 5.1 Introduction

Lepton flavor universality (LFU) is an accidental symmetry of the SM gauge sector which is broken in the Higgs sector by the Yukawa couplings. Experimental studies of LFU offer then a fine test of validity of the SM, since most models of NP introduce additional LFU breaking effects. Furthermore, the LFU ratios have the advantage that some of the hadronic uncertainties and the dependence on the CKM matrix cancel out in these ratios, providing theoretically clean observables.

The first LFU experimental tests of the SM started many years ago with pion, kaon and  $\tau$  leptonic decays. For instance, the following ratios of decays to different charged leptons were measured [22]

$$R_\tau = \frac{\mathcal{B}(\tau \rightarrow \mu\nu\bar{\nu})}{\mathcal{B}(\tau \rightarrow e\nu\bar{\nu})} = 0.9762 \pm 0.0028, \quad \text{and} \quad r_K^\ell = \frac{\mathcal{B}(K \rightarrow e\bar{\nu})}{\mathcal{B}(K \rightarrow \mu\bar{\nu})} = (2.488 \pm 0.009) \times 10^{-5}, \quad (5.1)$$

which were found to be in quite a good agreement with the precise theoretical predictions  $R_\tau^{\text{SM}} = (0.972559 \pm 0.000005)$  [265] and  $r_K^{\ell, \text{SM}} = (2.477 \pm 0.001) \times 10^{-5}$  [266, 267], which will be improved by NA62 and Belle-II in the near future.

Despite the success of the SM in describing the observables based on the first two generations of quarks, the couplings to the third generation were poorly constrained before the advent of the  $B$ -factories and LHCb. These new experiments allowed us to measure with great precision many transitions related to the  $b$  quark, where the LFU discrepancies appeared in both the tree-level and loop-induced  $B$  meson semi-leptonic decays. More specifically, the LHCb Collaboration measured the partial branching ratios of  $B^+ \rightarrow K^+ \ell \ell$  in the bin  $q^2 \in [1, 6]$   $\text{GeV}^2$  and found

$$R_K = \frac{\mathcal{B}(B^+ \rightarrow K^+ \mu \mu)}{\mathcal{B}(B^+ \rightarrow K^+ e e)} \Big|_{q^2 \in (1,6) \text{ GeV}^2} = 0.745 \pm_{0.074}^{0.090} \pm 0.036, \quad (5.2)$$

which lies  $2.6\sigma$  below the the clean SM prediction  $R_K^{\text{SM}} = 1.00(1)$  [13, 268]. The choice of low values of  $q^2$  is wisely made to avoid the narrow charmonium resonances which are notoriously non-perturbative and cannot be described by first principle computations. This observation of LFUV was recently corroborated by the most recent LHCb results [12],

$$R_{K^*}^{\text{low}} = \frac{\mathcal{B}(B \rightarrow K^* \mu \mu)_{q^2 \in [0.045, 1.1] \text{ GeV}^2}}{\mathcal{B}(B \rightarrow K^* e e)_{q^2 \in [0.045, 1.1] \text{ GeV}^2}} = 0.660 \pm_{0.070}^{0.110} \pm 0.024,$$

$$R_{K^*}^{\text{central}} = \frac{\mathcal{B}(B \rightarrow K^* \mu \mu)_{q^2 \in [1.1, 6] \text{ GeV}^2}}{\mathcal{B}(B \rightarrow K^* e e)_{q^2 \in [1.1, 6] \text{ GeV}^2}} = 0.685 \pm_{0.069}^{0.113} \pm 0.047, \quad (5.3)$$

thus again  $\approx (2.2 - 2.4)\sigma$  below the Standard Model (SM) prediction, as illustrated in Fig. 5.1. When combined in the same fit, these results amount to a discrepancy with respect to the SM at the  $4\sigma$  level [269]. Since the hadronic uncertainties largely cancel out in  $R_{K^{(*)}}$ , if confirmed, these would be an unambiguous manifestation of NP. Nonetheless, it should be stressed that the electron-channel measurement has a lower statistics and larger bremsstrahlung effects in comparison to the muon channel. Therefore, the confirmation from an independent experiment, which will be Belle-II, is mandatory before claiming that these deviations are indeed NP effects.

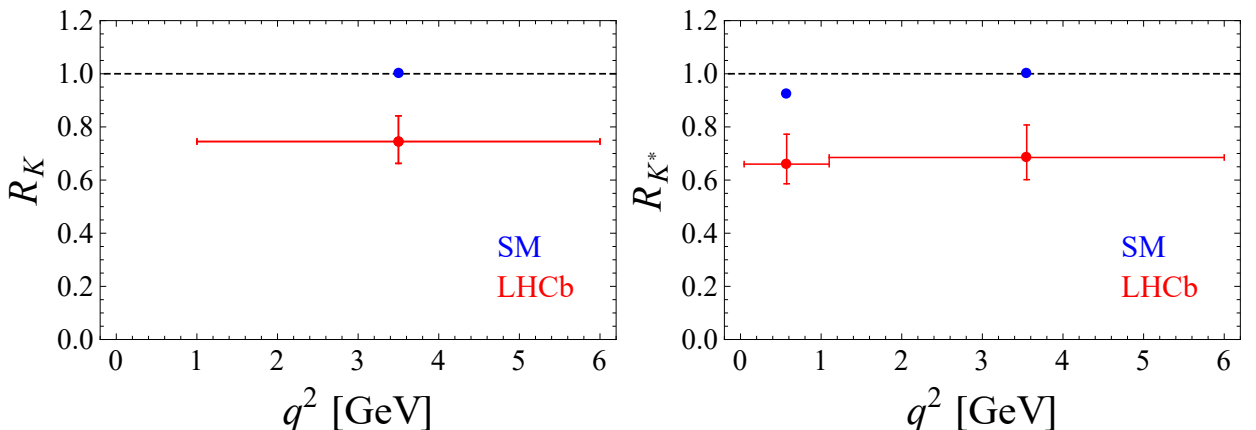


**Figure 5.1:** Experimental results of  $R_K$  and  $R_{K^*}$  in the low and central  $q^2$  bin.

Another intriguing observation of LFUV comes from the tree-level decays based on the transition  $b \rightarrow c \tau \nu$ . The average of the experimental results from the B-factories reads [71, 73],

$$R_D = \frac{\mathcal{B}(B \rightarrow D\tau\nu)}{\mathcal{B}(B \rightarrow Dl\nu)} \Big|_{l=e,\mu} = 0.41 \pm 0.05, \quad (5.4)$$

where the average in the denominator is taken over the possible light lepton in the final state. The theoretical situation of  $R_D$  is different from  $R_{K^{(*)}}$ , since the  $\tau$ -lepton mass is not negligible in comparison to the energy scale of this problem,  $m_B$ . For this reason, the hadronic uncertainties associated to the shape of the form factors do not fully cancel out in the ratio (5.4) and it becomes necessary to reliably assess those by nonperturbative methods. By solely relying on the lattice QCD data for both the vector and the scalar form factors, recently presented in Ref. [16], we obtain  $R_D^{\text{SM}} = 0.286 \pm 0.012$  which turns out to be  $\approx 2.5\sigma$  lower than the experimental measurement (5.4), as shown in the left panel of Fig. 5.2. This result is corroborated by the experimentally established [14]

$$R_{D^*} = \frac{\mathcal{B}(B \rightarrow D^*\tau\nu)}{\mathcal{B}(B \rightarrow D^*l\nu)} \Big|_{l=e,\mu} = 0.310 \pm 0.015 \pm 0.008, \quad (5.5)$$

which appears to be  $3.3\sigma$  larger than the SM prediction,  $R_{D^*}^{\text{SM}} = 0.252 \pm 0.003$  [17], as illustrated in the right panel of Fig. 5.2. Note, however, that the theoretical estimate of  $R_{D^*}^{\text{SM}}$  relies strongly on experimental information extracted from the differential distribution of  $d\Gamma(B \rightarrow D^*\ell\nu)/dq^2$  (with  $\ell = e, \mu$ ) and on the validity of leading order Heavy Quark Effective Theory (HQET) in evaluating the pseudoscalar form factors. The LQCD result for the full set of  $B \rightarrow D^*$  form factors is still not available, and those are mandatory to reliably predict  $R_{D^*}$ , as it will be discussed in Sec. 5.3. From the experimental point of view, the combined fit of the anomalies indicates a  $\approx 4\sigma$  deviation with respect to the SM. However, the experimental situation is still not clear since Belle results for  $R_{D^{(*)}}$  and the most recent LHCb result for  $R_{D^*}$  agree with the quoted SM predictions. Since  $\tau$ -leptons are complicated objects to deal with in particle detectors, the final verdict on the  $b \rightarrow c\ell\nu$  anomalies will depend on the effort to reduce the experimental uncertainties and to have a better understanding of the theoretical uncertainties. In particular, a very promising route would be to focus on decays for which the hadronic uncertainties can be more easily tamed by LQCD simulations, such as  $B_{(s)} \rightarrow D_{(s)}\ell\nu$  and  $B_c \rightarrow \eta_c\ell\nu$ . As discussed in Sec. 2.2.2, the SM predictions for these decays depend only on two form factors which satisfy the condition  $f_+(0) = f_0(0)$  at large-recoil, which is especially useful in constraining the slope of  $f_0(q^2)/f_+(q^2)$ .

Despite the intense theoretical effort to understand the  $b \rightarrow c$  and  $b \rightarrow s$  anomalies, very few concrete and fully viable solutions have emerged so far. The main challenge is to formulate a model which can explain these results while being consistent with the plethora of flavor constraints and with the limits from the direct searches performed at the LHC. Therefore, the theory community is at crossroads: (i) either one chooses to introduce different sets of new particles to address the current anomalies, producing rather complicated and sometimes even unappealing models, or (ii) one decides to focus on a subset of deviations by renouncing to explain the others. We will prefer to adopt the minimalist approach by following the latter route, since the experimental situation of these anomalies still needs further clarification.

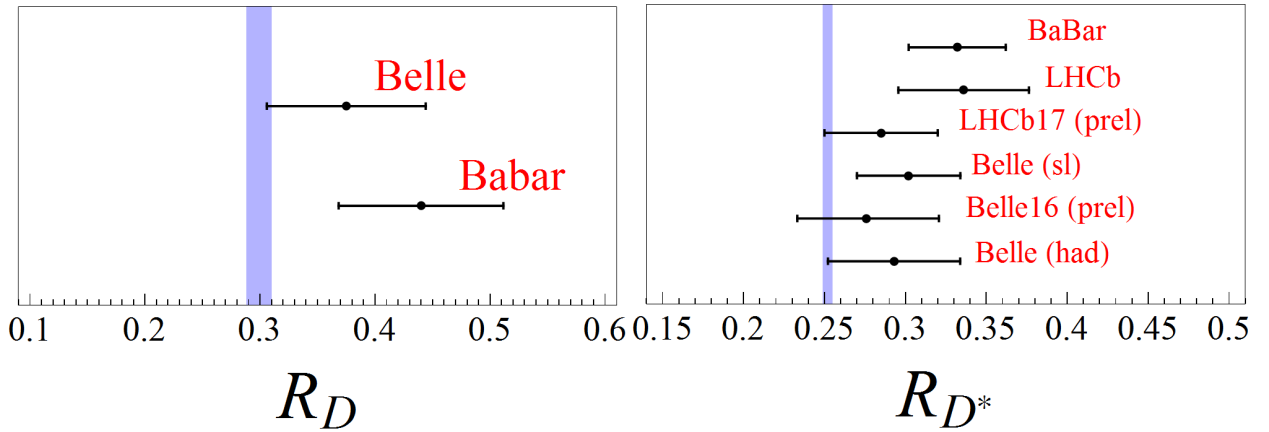


**Figure 5.2:** Experimental results for  $R_D$  and  $R_{D^*}$  obtained by LHCb [74, 270], Babar [72] and Belle [73, 75, 76] compared to the SM predictions [14, 17].

## 5.2 Lepton flavor (universality) violation in $b \rightarrow s\ell_1\ell_2$

In this Section, we will focus on  $R_{K^{(*)}}$  and discuss the implications if these hints of NP persist in the future. We start our discussion with an effective description of the experimental results in Sec. 5.2.1. In Sec. 5.2.2, we briefly overview the concrete models proposed in the literature to explain the observed deviations. We focus then our discussion on leptoquark models by exploring the possible tree-level solutions in Sec. 5.2.3 and the ones proposed at loop-level in Sec. 5.2.4 and Sec. 5.2.5.

### 5.2.1 Effective description of the deviations

In this Section, we use a model independent approach to explore the consistency of the observed deviations in  $R_{K^{(*)}}$  with the established experimental data for the exclusive  $b \rightarrow s\mu\mu$  processes. To that end we consider the effective Hamiltonian (2.54) and assume that NP contributes only to the transition  $b \rightarrow s\mu\mu$ . In other words, we assume that the NP contribution to the  $b \rightarrow see$  effective coefficients are negligible. This assumption is motivated by the observation that the measurement of  $\mathcal{B}(B \rightarrow K\mu\mu)$  in the high  $q^2$  bin was found to be about  $2\sigma$  lower than predicted, as discussed in Sec. 2.3. This small deviation is consistent with the discrepancy found in  $R_K$  if the deficit is coming from the muonic rate.

In the following, to simplify our notation we will denote the NP contribution to the Wilson coefficients by simply  $C_i$  instead of  $\delta C_i$ , as defined in Eq. (2.62). In other words, the SM case corresponds to  $C_i = 0 \forall i$  in our notation. We consider then two effective NP scenarios: (i) in **Scenario I** we assume that  $C_9$  and  $C_{10}$  are the only non-zero Wilson coefficients, while (ii) in **Scenario II** we consider the flipped coefficients  $(C_9)'$  and  $(C_{10})'$  instead. The fit to the experimental data leads to stringent bounds on the Wilson coefficients we are interested in, and ultimately provides  $R_{K,K^*} < 1$  for some combinations of the Wilson coefficients, as we shall see below.

#### Low-energy fits

In the first fit to the  $b \rightarrow s\mu\mu$  data, we use the two most reliable decay modes, as far as hadronic uncertainties are concerned, namely  $B_s \rightarrow \mu\mu$  and  $B \rightarrow K\mu\mu$ . More specifically,

to compare the measured [130]

$$\mathcal{B}(B_s \rightarrow \mu^+\mu^-)^{\text{exp}} = (3.0 \pm 0.6_{-0.2}^{+0.3}) \times 10^{-9}, \quad (5.6)$$

with theory, the only needed quantity is the decay constant  $f_{B_s}$  which has been computed by many lattice QCD collaborations. The most recent average value is  $f_{B_s} = 224(5)$  MeV [77], cf. Table 2.1. Similarly, the lattice QCD results for the  $B \rightarrow K$  form factors have been computed at large values of  $q^2$  by two collaborations [131, 132]. Their results agree and can be used to compare with the measured [116]

$$\mathcal{B}(B \rightarrow K\mu^+\mu^-)_{q^2 \in [15,22]}^{\text{exp}} \text{ GeV}^2 = (8.5 \pm 0.3 \pm 0.4) \times 10^{-8}. \quad (5.7)$$

We refer the reader to Sec. 2.3, where we provide a more extensive discussion about the theoretical robustness of these observables. The result of this procedure will be called “**Fit A**”. It is important to stress the difference between our approach and the usual global fits considered in the literature, where observables for which the hadronic uncertainties are not fully under control are also included in the fit [271, 272]. For instance, the form factors needed to compute the amplitudes of  $B \rightarrow K^*\ell^+\ell^-$  and  $B_s \rightarrow \phi^*\ell^+\ell^-$  in the low  $q^2$  bin are not available from LQCD. The situation is even worse for some angular observables of  $B \rightarrow K^*\mu^+\mu^-$  which strongly depend on the unknown  $c\bar{c}$  contribution, as we will comment on in the end of this Section. We prefer to choose a more conservative set of observables in order to avoid a misinterpretation of hadronic errors as a signal of NP.

The results of our first fit are shown in Fig. 5.3 for both NP scenarios. The specific realizations  $C_9^{(\prime)} = C_{10}^{(\prime)}$  are disfavored by current data, while the scenarios with an opposite sign,  $C_9^{(\prime)} = -C_{10}^{(\prime)}$ , can give a substantial improvement with respect to the SM. We obtained from the one-dimensional fit to  $2\sigma$  accuracy

$$C_9 = -C_{10} \in (-0.70, -0.04) \Big|_{\text{Fit A}}, \quad (5.8)$$

and

$$(C_9)' = -(C_{10})' \in (-0.60, 0.03) \Big|_{\text{Fit A}}, \quad (5.9)$$

where the predictions for  $\mathcal{B}(B \rightarrow K^*\mu\mu)_{q^2 \in [15,22]} \text{ GeV}^2$  obtained with the form factors computed in Ref. [131] and Ref. [132] were combined in average.

Another possibility is to, in addition to the above two quantities, also consider a few “clean” quantities extracted from the study of the  $B \rightarrow K^*\mu\mu$  decay mode. In particular, the measured [119]

$$\mathcal{B}(B \rightarrow K^*\mu^+\mu^-)_{q^2 \in [15,19]}^{\text{exp}} \text{ GeV}^2 = (1.95 \pm 0.16) \times 10^{-7} \quad (5.10)$$

can be combined with form factors computed on the lattice at large values of  $q^2$  [134]. Furthermore, the three observables obtained from the decay’s angular distribution, all three depending only on the so-called transverse amplitudes,  $A_{\parallel,\perp}(q^2)$ , with respect to the spin of the on-shell  $K^*$ . These quantities, which also appear to be very mildly sensitive to hadronic uncertainties [137], are known as  $A_T^{(2)}$ ,  $A_T^{(\text{re})}$  and  $A_T^{(\text{im})}$ , are translated into  $P_{1,2,3}$  in Ref. [273], the notation also respected by the experimentalists.<sup>1</sup> More specifically,

<sup>1</sup> Note that,  $P_1 \equiv A_T^{(2)}$ ,  $P_2 \equiv A_T^{(\text{re})}/2$ ,  $P_3 \equiv -A_T^{(\text{im})}/2$ , where we take into account the correct signs [156] to correctly compare with experimental results.

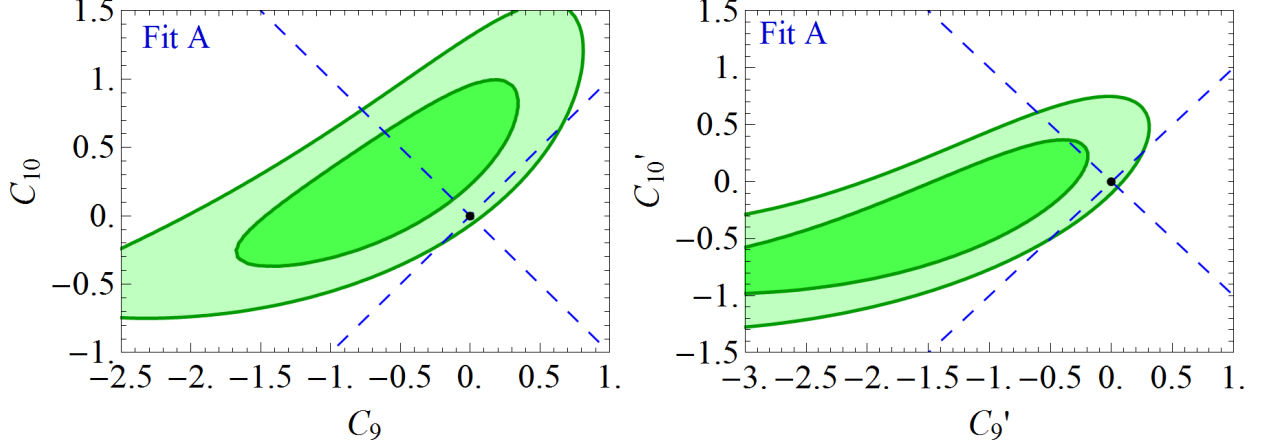


**Figure 5.3:** Regions in the plane  $(C_9^{\mu\mu}, C_{10}^{\mu\mu})$  (left panel) and  $((C_9^{\mu\mu})', (C_{10}^{\mu\mu})')$  (right panel) in agreement with the experimental of  $\mathcal{B}(B_s \rightarrow \mu\mu)$  and  $\mathcal{B}(B^+ \rightarrow K^+ \mu\mu)_{\text{large } q^2}$  to  $1\sigma$  (dark green) and  $2\sigma$  (light green) accuracy. The dashed lines correspond to the scenarios  $C_9 = \pm C_{10}$  and  $(C_9)' = \pm(C_{10})'$ .

$$\begin{aligned}
 P_1 &= \frac{\langle |A_{\perp}^{L,R}|^2 - |A_{\parallel}^{L,R}|^2 \rangle}{\langle |A_{\perp}^{L,R}|^2 + |A_{\parallel}^{L,R}|^2 \rangle}, & P_1^{\text{exp}} &= \{0.08(25)_{\text{low } q^2}, -0.50(10)_{\text{high } q^2}\}, \\
 P_2 &= -\frac{\langle \text{Re} [A_{\perp}^L A_{\parallel}^{L*} - A_{\perp}^R A_{\parallel}^{R*}] \rangle}{\langle |A_{\perp}^{L,R}|^2 + |A_{\parallel}^{L,R}|^2 \rangle}, & P_2^{\text{exp}} &= \{-0.16(7)_{\text{low } q^2}, 0.36(3)_{\text{high } q^2}\}, \\
 P_3 &= \frac{\langle \text{Im} [A_{\perp}^L A_{\parallel}^{L*} - A_{\perp}^R A_{\parallel}^{R*}] \rangle}{\langle |A_{\perp}^{L,R}|^2 + |A_{\parallel}^{L,R}|^2 \rangle}, & P_3^{\text{exp}} &= \{0.21(14)_{\text{low } q^2}, 0.08(6)_{\text{high } q^2}\}, \quad (5.11)
 \end{aligned}$$

where the full expressions for  $A_{\parallel,\perp} \equiv A_{\parallel,\perp}(q^2)$ , in terms of form factors and Wilson coefficients, can be found eg. in Ref. [127]. In the above notation,  $\langle \dots \rangle$  means that the numerator and denominator have been partially integrated over a specific window of  $q^2$ . The experimental values for  $P_{1,2,3}$  in two (wide) bins, corresponding to  $q^2 \in [1.1, 6] \text{ GeV}^2$  and  $q^2 \in [15, 19] \text{ GeV}^2$ , which are referred to as “low  $q^2$ ” and “high  $q^2$ ”, are extracted from Ref. [119]. Thus, from the fit in which we use

$$\begin{aligned}
 &\mathcal{B}(B_s \rightarrow \mu\mu), \mathcal{B}(B \rightarrow K\mu\mu)_{q^2 \in [15,22] \text{ GeV}^2}, \\
 &\mathcal{B}(B \rightarrow K^* \mu\mu)_{q^2 \in [15,19] \text{ GeV}^2}, (P_1, P_2, P_3)_{\text{low } q^2}, (P_1, P_2, P_3)_{\text{high } q^2}, \quad (5.12)
 \end{aligned}$$

to  $2\sigma$  accuracy, which will be referred to as “**Fit B**”.

By using the second procedure, we obtained the following interval to  $2\sigma$  accuracy for the scenario  $C_9 = -C_{10}$ ,

$$C_9 = -C_{10} \in (-0.70, -0.16) \Big|_{\text{Fit B}}, \quad (5.13)$$

which is in very good agreement with the result from Fit A, cf. Eq. (5.8). The two-dimensional fit on the plane  $(C_9, C_{10})$  is shown in Fig. 5.4, where we see again the preference

for the combination  $C_9 = -C_{10}$  over the combination with a plus sign. For the scenarios with primed operators, we found that the NP cannot substantially improve the SM description of data when the  $B \rightarrow K^*$  “clean” observables are also included in the fit. The reason for that is that there is a  $\approx 2\sigma$  discrepancy in  $(P_2)_{\text{low } q^2}$  which can only be explained by a contribution to  $C_9$ . Therefore, the Fit B seems to favor the scenarios with  $C_9$  and  $C_{10}$  over the scenarios with primed operators. Notice, however, that any conclusion drawn from the  $B \rightarrow K^*$  angular coefficients depends on the theoretical input for the  $c\bar{c}$  contributions to  $C_9$ , which is still not under full theoretical control. For instance, if the contributions of the tails of the charmonia resonances to the bin  $q^2 \in [1, 6]$  GeV<sup>2</sup> are underestimated, then the conclusions from Fit B would change. For this reason, the conclusions drawn from Fit A are more robust than the ones obtained from Fit B. Nonetheless, as we are going to see, the scenarios with primed operator cannot accommodate the LFUV ratios  $R_{K^{(*)}}$ , for which the unknown non-perturbative  $c\bar{c}$  contribution cancel out to a large extent.

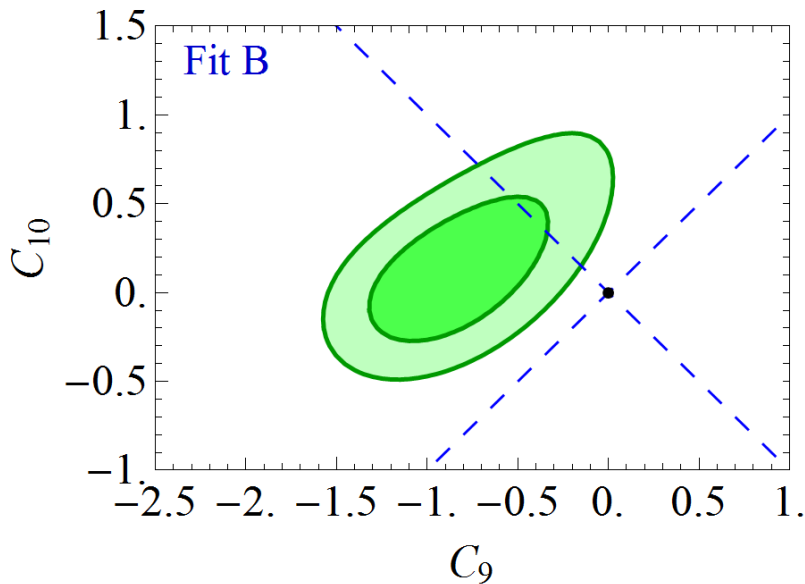


**Figure 5.4:** Regions in the plane  $(C_9^{\mu\mu}, C_{10}^{\mu\mu})$  in agreement with the experimental of  $\mathcal{B}(B_s \rightarrow \mu\mu)$ ,  $\mathcal{B}(B^+ \rightarrow K^+\mu\mu)_{\text{large } q^2}$  and the  $B \rightarrow K^*$  angular observables discussed in the text to  $1\sigma$  (dark green) and  $2\sigma$  (light green) accuracy. The dashed lines correspond to the scenarios  $C_9 = \pm C_{10}$ .

### Predictions for LFU ratios

We can then use the results for  $C_9 = -C_{10}$  and  $(C_9)' = -(C_{10})'$  obtained by the two fits described above, and compute

$$R_{K^{(*)}} = \frac{\mathcal{B}(B \rightarrow K^{(*)}\mu\mu)_{q^2 \in [q_1^2, q_2^2]}}{\mathcal{B}(B \rightarrow K^{(*)}ee)_{q^2 \in [q_1^2, q_2^2]}}, \quad (5.14)$$

by relying on the expressions given in our Refs. [127, 155], and for three separate intervals in  $q^2$ . To make the comparison with experiment easier we consider three intervals:  $q^2 \in [0.045, 1.1]$  GeV<sup>2</sup>,  $[1.1, 6]$  GeV<sup>2</sup> and  $[15, 19]$  GeV<sup>2</sup> and call them low, central and large  $q^2$ -bin, respectively.<sup>2</sup> In Fig. (5.5), we plot  $R_K$  and  $R_{K^*}$  in the central bin for the choices of Wilson

<sup>2</sup>The LHCb Collaboration considers  $q^2 \in [1, 6]$  GeV<sup>2</sup> instead of  $q^2 \in [1.1, 6]$  GeV<sup>2</sup> as the central bin for  $R_K$ , a choice that we also adopt. Notice, however, that the difference between the two is immaterial.

coefficients favored by the clean observables  $\mathcal{B}(B_s \rightarrow \mu\mu)$  and  $\mathcal{B}(B \rightarrow K\mu\mu)_{q^2 \in [15,22]} \text{ GeV}^2$ , i.e.  $C_9 = -C_{10}$  and  $(C_9)' = -(C_{10})'$ . From this plot, it is clear that  $C_9 = -C_{10}$  is the only scenario which provides a reasonable explanation to both  $R_K$  and  $R_{K^*}$ . This is corroborated our second fit to which the somewhat clean  $B \rightarrow K^*$  angular observables are include, as discussed above. For this reason, we will focus on this scenario in the following.

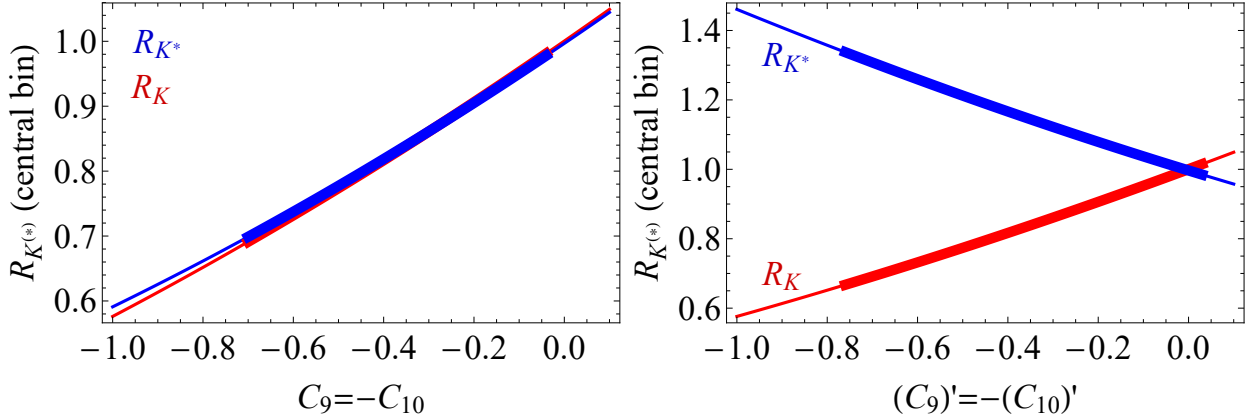


**Figure 5.5:** Predictions for  $R_{K^{(*)}}$  in the central  $q^2$  bin as a function of  $C_9 = -C_{10}$  (left panel) and  $(C_9)' = -(C_{10})'$  (right panel). The thicker line correspond to the results from the fit A, cf. Eqs. (5.8) and (5.9). See text for details.

In Fig. 5.6 we plot the resulting  $R_K$  and  $R_{K^*}$  in the three  $q^2$  bins by relying only on the effective theory and on the value of  $C_9^{\mu\mu} = -C_{10}^{\mu\mu}$  obtained from the fit with the data as discussed above. We see that in the central bin our results are in very good agreement with experiment, at the  $1\sigma$  level, regardless of the  $C_9^{\mu\mu}$  value we use, Eq. (5.8) or (5.13). The situation is not as favorable in the low  $q^2$ -bin, in which the agreement between ours and the measured values of  $R_{K^*}$  is not better than  $1.5\sigma$ . This, however, is a very good agreement too. Notice also that the low  $q^2$  bin is more sensitive to form factor uncertainties, since  $d\Gamma/dq^2$  varies quickly near the muon threshold in a flavor non-universal way [13]. The values shown in Fig. 5.6 are also listed in Tab. 5.1. The high  $q^2$  bin has not been explored experimentally yet for  $R_K$  and  $R_{K^*}$ , but it will serve as an additional test to the observed anomalies. Another interesting measurement that would be very useful to corroborate this picture is the measurement of  $R_K$  in the low  $q^2$  bin, since a deviation larger than  $R_{K^*}$  is expected in this case, as well as other ratios based on the  $b \rightarrow s\ell\ell$  transitions, such as  $R_\phi = \mathcal{B}(B_s \rightarrow \phi\mu^+\mu^-)/\mathcal{B}(B_s \rightarrow \phi e^+e^-)$ .

In conclusion, the scenario with effective coefficients  $C_9 = -C_{10}$  is strongly favored by current  $b \rightarrow s\mu\mu$  exclusive data. By making this minimal assumption for the effective coefficients, one can use the most reliable data for the transition  $b \rightarrow s$  to determine these coefficients and predict  $R_{K^{(*)}}$ , which are in good agreement with the most recent LHCb findings. We have also checked that this conclusion is corroborated by studies with more observables which are not as safe as  $\mathcal{B}(B_s \rightarrow \mu\mu)$  and  $\mathcal{B}(B \rightarrow K\mu^+\mu^-)_{q^2 \in [15,22]}^{\text{exp}} \text{ GeV}^2$  from the point of view of hadronic uncertainties. The other combinations of Wilson coefficients are disfavored by the  $b \rightarrow s\mu\mu$  fits and/or cannot accommodate the deviations observed by LHCb. In Section 5.2.2, we will discuss the specification realizations that have been proposed to generate the allowed combination of Wilson coefficients to explain  $R_{K^{(*)}}$ .

Quantity	Fit A	Fit B
$R_K$ (low $q^2$ )	[0.64, 0.96]	[0.66, 0.91]
$R_{K^*}$ (low $q^2$ )	[0.83, 0.92]	[0.84, 0.91]
$R_K$ (central $q^2$ )	[0.66, 0.98]	[0.69, 0.93]
$R_{K^*}$ (central $q^2$ )	[0.67, 0.98]	[0.69, 0.93]
$R_K$ (high $q^2$ )	[0.65, 0.98]	[0.68, 0.93]
$R_{K^*}$ (high $q^2$ )	[0.64, 0.98]	[0.67, 0.92]

**Table 5.1:** Intervals of  $R_K$  and  $R_{K^*}$  obtained solely from the values for the Wilson coefficient  $C_9^{\mu\mu} = -C_{10}^{\mu\mu}$  obtained from the Fit A [Eq. (5.8)] and Fit B [Eq. (5.13)], as discussed in the text.

### Anomalies in $B \rightarrow K^*\mu^+\mu^-$ angular distributions?

Before closing this Section, we need to comment on the other discrepancies related to the transition  $b \rightarrow s\mu\mu$  that have been reported in the past years. The most significant one is the so-called  $P'_5(q^2)$  observable proposed in Ref. [274] and constructed from the angular distribution of the decay  $B \rightarrow K^*\mu^+\mu^-$ ,

$$P'_5(q^2) = \frac{I_5(q^2)}{\sqrt{-4I_2^c(q^2)I_2^s(q^2)}}, \quad (5.15)$$

where the angular coefficients  $I_i(q^2)$  are defined in Eq. (2.127). The measurement of this quantity in the interval  $q^2 \in [4.3, 8.68]$  GeV<sup>2</sup> by LHCb [157, 275] turned out to be about  $4\sigma$  away from the SM prediction  $\langle P'_5 \rangle_{[4.3-8.68]}^{\text{SM}} = -0.90(5)$  [121, 276], a result that was also confirmed by the Belle experiment [277]. Even though the experimental situation seems to be under control, the theoretical prediction of  $P'_5$  in these bins is the source of many controversies which are mostly related to various sources of hadronic uncertainties. Most importantly, the estimate of the  $c\bar{c}$  contribution to the  $b \rightarrow s$  transition is crucial in order to reliably determine the SM predictions. Currently, there is no first principles computation of these contributions, which are so far evaluated by QCD sum rules [278]. Interestingly, the authors of Ref. [122] showed that the current discrepancies in  $P'_5$  can be explained by the unknown charm correction to the effective coefficient  $C_9^{\text{SM}}$ . Therefore, the question that must be answered is if the needed contribution to  $C_9$  originates from underestimated charm corrections or from NP. While the interpretation of these discrepancies remains subject of controversies, it is nevertheless intriguing that these deviations can be accommodated by the same NP scenarios needed to explain  $R_{K^{(*)}}^{\text{exp}} < R_{K^{(*)}}^{\text{SM}}$ , which are largely independent on hadronic uncertainties.<sup>3</sup>

<sup>3</sup>We focused our discussion of  $R_{K^{(*)}}$  on the choice of effective coefficients  $C_9 = -C_{10} < 0$ , since these appear naturally in several NP scenarios. Nonetheless, one can see from Figs. 5.3 and 5.4 that an explanation relying only on  $C_9 < 0$  is equally possible, a choice which also predicts  $R_{K^{(*)}}^{\text{exp}} < R_{K^{(*)}}^{\text{SM}}$  [269].

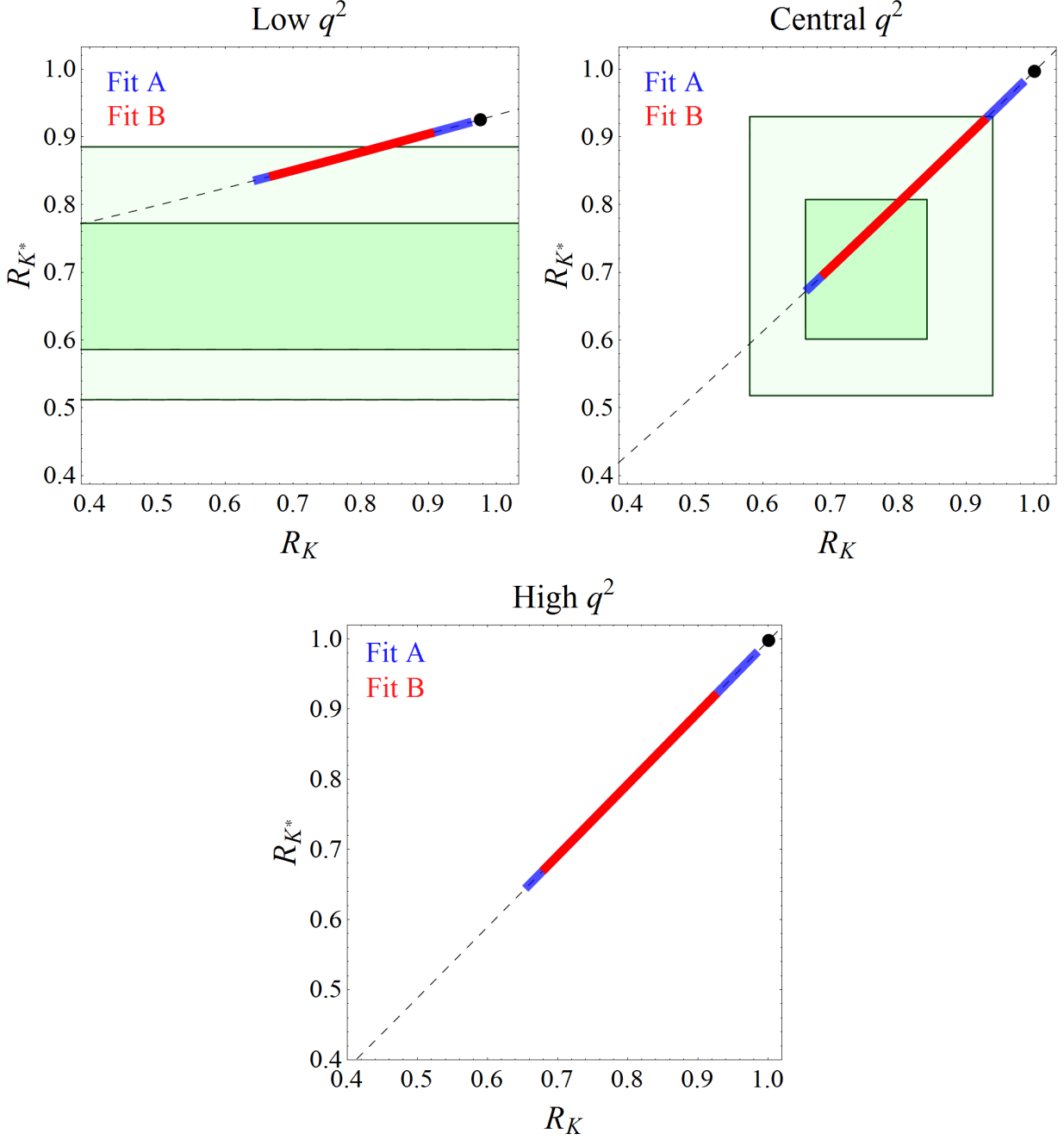


**Figure 5.6:** Results for  $R_K$  and  $R_{K^*}$  obtained solely from the values for the Wilson coefficient  $C_9^{\mu\mu} = -C_{10}^{\mu\mu}$  obtained from the Fit A [Eq. (5.8)] and Fit B [Eq. (5.13)] as discussed in the text. The shaded area correspond to the measured values to  $1\sigma$  and  $2\sigma$ , cf. Eqs. (5.2,5.3). The thick dot corresponds to the SM result.

### 5.2.2 Proposed explanations of $R_K$ and $R_{K^*}$

Several concrete models have been proposed to explain  $R_K$  and  $R_{K^*}$ . The strategy usually adopted is to introduce new heavy particles that generate the effective coefficients  $C_9^{\mu\mu} = -C_{10}^{\mu\mu}$  or  $C_9^{\mu\mu}$  at low energies, after being integrated out. The great majority of these models can be separated into two general classes: (i) models containing heavy neutral vector bosons  $Z'$  or (ii) scenarios with light scalar or vector LQs.

In the first class of models, the  $Z'$  particle is considered to be the gauge boson associated to a new gauge symmetry. Several suitable non-anomalous Abelian gauge symmetries have

been proposed in the literature, such as  $L_\mu - L_\tau$  [279–282],  $B - L$  [283],  $B_3 - 3L_\mu$  [284], and the so-called Branco-Lavoura-Grimus (BGL) group [285]. Proposals based on an additional Abelian symmetry related to a dark sector have also been made in Ref. [286,287]. Moreover, some groups based on non-Abelian symmetries have been proposed, cf. Refs. [288–292]. An interesting possibility is that the needed  $Z'$  particles are associated to the mechanism of generation of fermion masses. This route was considered in Ref. [293], where it was shown that a scenario with Yukawa generated dynamically can accommodate  $R_{K^{(*)}}^{\text{exp}} < R_{K^{(*)}}^{\text{SM}}$ , while explaining the quark and lepton Yukawa patterns. Note that, in all of the above-mentioned scenarios, the flavor violating couplings to  $b$  and  $s$  are generated at tree-level either via mixing with vector-like quarks [279], or by the rotation from the flavor to the mass basis [153]. A different possibility is to couple the  $Z'$  boson to a heavy particle which generates the current  $J_q^\mu = \bar{s}\gamma^\mu P_L b$  via loops, as recently considered in Ref. [294]. The advantage of this scenario is that the masses of the heavy mediator  $Z'$  is considerably lower, and thus accessible at the LHC. Finally, it should be clear that to distinguish among the plethora of viable  $Z'$  scenarios, it will be essential to have additional experimental information from other types of indirect searches, and also from the searches of heavy resonances at the LHC. Among the indirect signatures, searches of LFV  $B$  meson decays can be particularly helpful [127, 153, 154]. Furthermore, the study of high- $p_T$  dilepton tails can provide complementary information to the searches performed at low energies [264].

Models based on LQ states have also been extensively proposed in the literature. For instance, vector LQs have been considered in Ref. [295,296]. It should be stressed that one-particle extensions of the SM with (massive) vector LQs are non-renormalizable. Therefore, the loop processes cannot be computed in these effective scenarios, a fact that reduces considerably their predictivity unless a UV completion is explicitly specified, see discussion in Ref. [297]. Note that a partial UV completion to one of these scenarios has been recently considered in Ref. [298] by extending the minimal composite Higgs model. On the other hand, models postulating the existence of scalar LQs are simpler since they are renormalizable. As we shall discuss in detail in Sec. 5.2.3, the only LQ state that can explain both  $R_K$  and  $R_{K^*}$  via a tree-level exchange is the  $SU(2)_L$  triplet  $(\bar{\mathbf{3}}, \mathbf{3})_{1/3}$  [299, 300]. However, in order to ensure the proton stability one needs to devise an extra symmetry to forbid the diquark couplings.<sup>4</sup> The scenario with the weak doublet  $(\mathbf{3}, \mathbf{2})_{1/6}$  has been also proposed to explain  $R_K$ , but it has been disfavored by the recent measurement of  $R_{K^*}$ , as we shall discuss below. Another viable possibility is to consider scenarios where the LQ contribution to  $b \rightarrow s\ell\ell$  appears only at loop-level. There are two proposals which postulate the existence of a scalar singlet  $(\mathbf{3}, \mathbf{1})_{1/3}$  [254] or a scalar doublet  $(\mathbf{3}, \mathbf{2})_{7/6}$  [155]. The phenomenology of these scenarios will be discussed in detail in Sec. 5.2.4 and Sec. 5.2.5, respectively. The models that contribute to  $R_{K^{(*)}}$  through loops require relatively light masses for the LQs, due to the loop suppression factor, being for this reason phenomenologically more appealing and possibly within reach at the LHC. Furthermore, there are more non-minimal models that postulate the existence of both new fermions and scalars [302, 303]. In this case, the contribution to  $b \rightarrow s\ell\ell$  arises via box diagrams, which can reduce the tensions with the experimental findings if the new particles are light enough.

Departing from the usual assumption that the boson responsible for the LFUV is much heavier than the electroweak scale, the authors of Ref. [304] have considered the intriguing possibility that the  $Z'$  boson has a mass of a few GeV, giving a resonant contribution to  $B \rightarrow K^{(*)}\ell^+\ell^-$ . In this case, they predicted a strong  $q^2$ -dependence for  $R_{K^{(*)}}$  that will be tested in the near future by the measurement of  $R_{K^*}$  in the high  $q^2$  bin, where they predict

<sup>4</sup>See Ref. [222, 301] for an example of such a mechanism within a  $SU(5)$  model.

no observable effect. Finally, there have been also proposals to accommodate the LFUV hints in other classes of models, such as scenarios with a warped extra-dimension [305, 306] and composite Higgs model [307, 308].

In the following, we will focus our discussion on the various LQ scenarios proposed to explain  $R_{K^{(*)}}$ , since there are fewer possibilities for LQs than in the  $Z'$  case. In Sec. 5.2.3, we will discuss the scalar LQ models that can explain  $R_{K^{(*)}}$  at tree-level. The models which contribute to  $b \rightarrow s\ell\ell$  at tree-level will be discussed in Sec. 5.2.4 and Sec. 5.2.5.

### 5.2.3 Tree-level leptoquark models for $R_{K^{(*)}}$

In this Section, we discuss whether the Wilson coefficients needed to describe  $R_{K^{(*)}}^{\text{exp}} < R_{K^{(*)}}^{\text{SM}}$  can arise from the exchange of light LQs. We will focus on the scalar LQ scenarios and assume that the SM is extended by only one LQ state. Vector LQs will be disregarded, since these models are not renormalizable and become problematic when computing the loop induced processes. Observables such as  $\mathcal{B}(\tau \rightarrow \mu\gamma)$  and the  $B_s - \bar{B}_s$  mixing amplitude arise only at loop-level in LQ scenarios, but these are known to impose severe constraints on any attempt to address the LFUV puzzles. Therefore, the predictivity of these models is compromised unless a renormalizable and gauge invariant UV completion is explicitly specified which is quite a nontrivial task as discussed in Ref. [297].

We will consider modifications only of  $b \rightarrow s\mu\mu$ , as suggested by current data, and use the absence of diquark couplings as a criteria to choose the viable models from Table 4.1. The models that can contribute to the transition  $b \rightarrow s\ell_1\ell_2$  at tree-level are listed in Table 5.2 along with the Wilson coefficient combination generated at the effective level and the implications for  $R_K$  and  $R_{K^*}$ . From this table, we see that only the scenario with a scalar triplet  $(\bar{\mathbf{3}}, \mathbf{3})_{1/3}$  can accommodate  $R_K^{\text{exp}} < R_K^{\text{SM}}$  and  $R_{K^*}^{\text{exp}} < R_{K^*}^{\text{SM}}$  through the effective coefficients  $C_9 = -C_{10}$ . Nonetheless, this model violated baryon number via the diquark couplings [8],

$$\mathcal{L}_{\Delta(1/3)} \supset (y_L)_{ij} \bar{Q}_i^C i\tau_2 \boldsymbol{\tau} \cdot \boldsymbol{\Delta} L_j + (z_L)_{ij} \bar{Q}_i^C i\tau_2 (\boldsymbol{\tau} \cdot \boldsymbol{\Delta})^\dagger Q_j + \text{h.c.} \quad (5.16)$$

where we omitted color indices. This Lagrangian can be expanded in terms of the charge eigenstates, giving [8]

$$\begin{aligned} \mathcal{L}_{\Delta(1/3)} \supset & -(y_L U)_{ij} \bar{d}_{Li}^C \nu_{Lj} \Delta^{(1/3)} - \sqrt{2} (y_L)_{ij} \bar{d}_{Li}^C \ell_{Lj} \Delta^{(4/3)} \\ & + \sqrt{2} (V^T y_L U)_{ij} \bar{u}_{Li}^C \nu_{Lj} \Delta^{(-2/3)} - (V^T y_L)_{ij} \bar{u}_{Li}^C \ell_{Lj} \Delta^{(1/3)} \\ & - (z_L V^\dagger)_{ij} \bar{d}_{Li}^C u_{Lj} \Delta^{(1/3)*} + \sqrt{2} (V^T z_L V^\dagger)_{ij} \bar{u}_{Li}^C u_{Lj} \Delta^{(4/3)*} \\ & - \sqrt{2} (z_L)_{ij} \bar{d}_{Li}^C d_{Lj} \Delta^{(-2/3)*} - (V^T z_L)_{ij} \bar{u}_{Li}^C d_{Lj} \Delta^{(1/3)*} + \text{h.c.}, \end{aligned} \quad (5.17)$$

From this equation, we can see that the decay  $p \rightarrow K\nu$  is induced at tree-level via the coupling  $z_L V^\dagger$  and  $y_L$ , as illustrated in Fig. 5.7. The decay  $p \rightarrow \pi^0 e^+$  is protected at tree-level by the anti-symmetric nature of  $z_L$  in flavor space, which implies that  $(z_L)_{11} = (V^T z_L V^\dagger)_{11} = 0$ . However, this decay is induced at one-loop level by box diagrams. In conclusion, the introduction of an additional *ad hoc* symmetry is mandatory to forbid the diquark couplings.

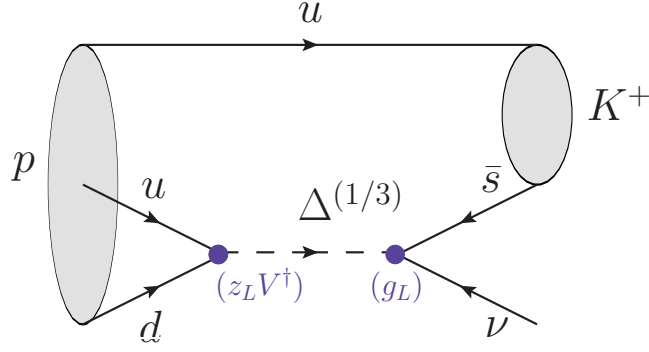


**Figure 5.7:** Contribution at tree-level for the proton decay in the  $(\bar{\mathbf{3}}, \mathbf{3})_{1/3}$  scenario.

$(SU(3)_c, SU(2)_L)_{U(1)_Y}$	BNC	Interaction	Eff. Coefficients	$R_K/R_K^{\text{SM}}$	$R_{K^*}/R_{K^*}^{\text{SM}}$
$(\bar{\mathbf{3}}, \mathbf{3})_{1/3}$	$\times$	$\overline{Q^C} i\tau_2 \tau \cdot \Delta L$	$C_9 = -C_{10}$	$< 1$	$< 1$
$(\bar{\mathbf{3}}, \mathbf{1})_{4/3}$	$\times$	$\overline{d_R^C} \Delta \ell_R$	$(C_9)' = (C_{10})'$	$\approx 1$	$\approx 1$
$(\mathbf{3}, \mathbf{2})_{7/6}$	$\checkmark$	$\overline{Q} \Delta \ell_R$	$C_9 = C_{10}$	$> 1$	$> 1$
$(\mathbf{3}, \mathbf{2})_{1/6}$	$\checkmark$	$\overline{d_R} \widetilde{\Delta}^\dagger L$	$(C_9)' = -(C_{10})'$	$< 1$	$> 1$

**Table 5.2:** List of LQ states which can modify the transition  $b \rightarrow s\mu\mu$  at tree-level. The conservation of baryon number (BNC), the interaction term and the corresponding Wilson coefficients are also listed along with the prediction for  $R_K$ . Couplings to electrons are set to zero.

Regarding the other scenarios, the weak doublet  $(\mathbf{3}, \mathbf{2})_{1/6}$  can accommodate  $R_K^{\text{exp}} < R_K^{\text{SM}}$  and it has the advantage of not disturbing the proton decay by diquark couplings. This model will be described in detail in Sec. 5.3 along with the proposed explanations of  $R_{D^{(*)}}$ . Nonetheless, it predicts  $R_{K^*}$  to be slightly larger than the SM prediction [118, 229], in contradiction with current experimental results. The states  $(\mathbf{3}, \mathbf{2})_{7/6}$  and  $(\bar{\mathbf{3}}, \mathbf{1})_{4/3}$  induce tree-level contributions which are either too small or incompatible with observations, cf. Fig. 5.3. Finally, another possibility is to consider LQ scenarios for which the leading contribution to  $b \rightarrow s\ell\ell$  appears only at loop-level, as it will be discussed in Sec. 5.2.4 and 5.2.5

### 5.2.4 Loop induced leptoquark models: A first attempt

The first attempt to explain the  $b \rightarrow s\mu\mu$  anomalies via LQ loops was proposed in Ref. [254]. The authors of this paper claimed that the singlet LQ state  $(\bar{\mathbf{3}}, \mathbf{1})_{1/3}$  with  $m_\Delta = 1$  TeV and  $\mathcal{O}(1)$  left-handed couplings could simultaneously accommodate the observed LFU violation hints in  $R_K$  and  $R_{D^{(*)}}$ . The main idea in this paper was to explain the puzzles in tree-level decays,  $R_{D^{(*)}}$ , via tree-level LQ contributions and the ones appearing in loop processes,  $R_{K^{(*)}}$ , via loop-level contributions. This claim was soon realized to be incorrect in Ref. [155], where a complete flavor analysis showed that this scenario cannot make  $R_K$  significantly smaller than one, without running into serious difficulties with other measured quantities, namely, the ratio  $R_D^{\mu/e} = \mathcal{B}(B \rightarrow D\mu\nu)/\mathcal{B}(B \rightarrow De\nu)$ . After the measurement of  $R_{K^*}$  by LHCb, this model was revived in Ref. [309] where it was shown that one can avoid the constraints introduced in Ref. [155] by significantly increasing the LQ mass and by choosing a different pattern of Yukawa couplings. However, this proposal cannot make  $R_{K^{(*)}}$  compatible with the  $1\sigma$  intervals of  $R_{K^{(*)}}^{\text{exp}}$  reported by LHCb, as we will show in this

Section.

The Lagrangian for the model  $(\bar{\mathbf{3}}, \mathbf{1})_{1/3}$  was already given in Eq. (4.35) and we rewrite it here for the reader's convenience,

$$\begin{aligned} \mathcal{L}_{\Delta^{(1/3)}} &\supset (y_L)_{ij} \overline{Q_i^C} i\tau_2 L_j \Delta^{(1/3)} + (y_R)_{ij} \overline{u_{Ri}^C} \ell_{Rj} \Delta^{(1/3)} + \text{h.c.}, \\ &= \Delta^{(1/3)} \left[ (V^* y_L)_{ij} \overline{u_i^C} P_L \ell_j - (y_L)_{ij} \overline{d_i^C} P_L \nu_j + (y_R)_{ij} \overline{u_i^C} P_R \ell_j \right] + \text{h.c.}, \end{aligned} \quad (5.18)$$

where  $y_{L(R)}$  are generic Yukawa matrices with flavor indices  $i, j$ . In addition to these terms, one should included diquark couplings which mediate the proton decay and must be forbidden by hand to make the model viable. To discuss the phenomenology of this model, we consider the following pattern of left-handed Yukawas,

$$y_L = \begin{pmatrix} 0 & 0 & 0 \\ 0 & (y_L)_{s\mu} & (y_L)_{s\tau} \\ 0 & (y_L)_{b\mu} & (y_L)_{b\tau} \end{pmatrix}, \quad V y_L = \begin{pmatrix} 0 & V_{us}(g_L)_{s\mu} + V_{ub}(y_L)_{b\mu} & V_{us}(y_L)_{s\tau} + V_{ub}(y_L)_{b\tau} \\ 0 & V_{cs}(g_L)_{s\mu} + V_{cb}(y_L)_{b\mu} & V_{cs}(y_L)_{s\tau} + V_{cb}(y_L)_{b\tau} \\ 0 & V_{ts}(g_L)_{s\mu} + V_{tb}(y_L)_{b\mu} & V_{ts}(y_L)_{s\tau} + V_{tb}(y_L)_{b\tau} \end{pmatrix}, \quad (5.19)$$

where the first matrix connects down-type quarks to neutrinos, and the second up-type quarks to charged leptons.<sup>5</sup> Notice that the couplings to the first generation of leptons are assumed to be zero for simplicity. They are tightly constrained by the limits on  $\mu - e$  conversion and the atomic parity violation (APV) experiments [8]. In our approach, the couplings to the  $d$  quark are also set to zero, since their nonzero values can induce significant contributions to processes such as  $K \rightarrow \pi\nu\nu$  and the  $K^0 - \bar{K}^0$  mixing. Even though we fix  $(y_L)_{d\mu} = (y_L)_{d\tau} = 0$ , from Eq. (5.19), we see that the couplings to the  $u$  quark are generated via the CKM matrix. Therefore, constraints from the kaon and the  $D$ -meson sectors should be taken into account too. For the right-handed couplings, which were assumed to be small in the original proposal, we adopt the ansatz introduced in Ref. [309], namely,

$$y_R = \begin{pmatrix} 0 & 0 & 0 \\ 0 & 0 & (y_L)_{c\tau} \\ 0 & (y_R)_{t\mu} & 0 \end{pmatrix}. \quad (5.20)$$

With this choice of flavor couplings, one aims at explaining  $R_{D^{(*)}}$  via large couplings  $(y_L)_{c\tau}$ , while the coupling  $(y_R)_{t\mu}$  must remain small to satisfy the bounds on  $\mathcal{B}(\tau \rightarrow \mu\gamma)$  and to be consistent the  $b \rightarrow s\mu\mu$  exclusive modes.

The effective coefficients  $C_9^{\ell_1\ell_2} \pm C_{10}^{\ell_1\ell_2}$  are loop induced and the results are given by [254, 255]:

$$\begin{aligned} C_9^{\ell_1\ell_2} - C_{10}^{\ell_1\ell_2} &= \frac{m_t^2}{8\pi\alpha_{\text{em}}m_\Delta^2} (V^* y_L)_{t\ell_1}^* (V^* y_L)_{t\ell_2} - \frac{1}{64\pi\alpha_{\text{em}}} \frac{v^2}{m_\Delta^2} \frac{(y_L \cdot y_L^\dagger)_{bs}}{V_{tb}V_{ts}^*} (y_L^\dagger \cdot y_L)_{\ell_1\ell_2}, \\ C_9^{\ell_1\ell_2} + C_{10}^{\ell_1\ell_2} &= \frac{m_t^2}{16\pi\alpha_{\text{em}}m_\Delta^2} (y_R)_{t\ell_1}^* (y_R)_{t\ell_2} \left[ \log \frac{m_\Delta^2}{m_t^2} - f(x_t) \right] \\ &\quad - \frac{1}{64\pi\alpha_{\text{em}}} \frac{v^2}{m_\Delta^2} \frac{(y_L \cdot y_L^\dagger)_{bs}}{V_{tb}V_{ts}^*} (y_R^\dagger \cdot y_R)_{\ell_1\ell_2}, \end{aligned} \quad (5.21)$$

<sup>5</sup>We reiterate that the PMNS matrix  $U$  is set to unity since the neutrino masses are neglected in this study.

where  $x_t = m_t^2/m_W^2$  and

$$f(x_t) = 1 + \frac{3}{x_t - 1} \left( \frac{\log x_t}{x_t - 1} - 1 \right). \quad (5.22)$$

As discussed in Sec. 5.2.1, the combination  $C_9^{\mu\mu} + C_{10}^{\mu\mu}$  is disfavored by the current  $b \rightarrow s\mu\mu$  exclusive data, so that the coefficient  $(y_R)_{t\mu}$  must be small. Furthermore, notice that the term in  $C_9^{\ell_1\ell_2} - C_{10}^{\ell_1\ell_2}$  proportional to  $m_t^2$  comes with a positive sign, which is also disfavored by the the  $b \rightarrow s\mu\mu$  fit and by the experimental results of  $R_{K^{(*)}}$ , cf. discussion in Sec. 5.2.1. Therefore, the contribution proportional to  $|(y_L)_{t\mu}|^2$  should be compensated by the second term in Eq. (5.21), which must come with a minus sign. This was the main reason that led to the conclusion that this model is not phenomenologically viable for  $m_\Delta \approx 1$  TeV. In this case, a large coupling  $(y_L)_{c\mu}$  is needed to produce  $C_9^{\mu\mu} + C_{10}^{\mu\mu} < 0$ , which would be in disagreement with the constraint  $R_D^{\mu/e} = \mathcal{B}(B \rightarrow D\mu\nu)/\mathcal{B}(B \rightarrow D e\nu)$  that will be described below [155].

We will now describe the constraints on this model considered in our analysis. One of the most important constraints comes from the  $B_s - \bar{B}_s$  mixing amplitude. We obtain

$$\frac{\Delta m_{B_s}^{\text{th}}}{\Delta m_{B_s}^{\text{SM}}} = 1 + \frac{\eta_1 (y_L \cdot y_L^\dagger)_{bs}^2}{32G_F^2 m_W^2 |V_{tb}V_{ts}^*|^2 \eta_B S_0(x_t) m_\Delta^2}, \quad (5.23)$$

where  $\eta_1 = 0.82(1)$  accounts for the QCD running from  $\mu = m_\Delta \simeq 1$  TeV down to  $\mu = m_b$ ,  $S_0(x_t)$  is the Inami-Lim function, and  $\eta_B$  encodes the short distance QCD corrections. We combine the experimental value  $\Delta m_{B_s}^{\text{exp}} = 17.7(2)$  ps<sup>-1</sup> [310], with the SM prediction  $\Delta m_{B_s}^{\text{SM}} = 17.3(17)$  ps<sup>-1</sup>, to get  $\Delta m_{B_s}^{\text{exp}}/\Delta m_{B_s}^{\text{SM}} = 1.02(10)$  [127]. Another very important constraint at loop-level comes from the partial decay widths of the  $Z$  boson, which have been precisely measured at LEP [22],

$$\mathcal{B}(Z \rightarrow \mu\mu)^{\text{exp}} = 3.366(7) \%, \quad \mathcal{B}(Z \rightarrow \tau\tau)^{\text{exp}} = 3.370(8) \%. \quad (5.24)$$

We computed the full amplitude for the decays  $Z \rightarrow \ell_1\ell_2$  and matched it onto the effective Lagrangian,

$$\mathcal{L}_{\text{eff}} = \frac{g}{2 \cos \theta_W} C_{VL}^{\ell_1\ell_2} \bar{\ell}_1 \gamma^\mu P_L \ell_2 Z^\mu + (L \rightarrow R), \quad (5.25)$$

obtaining the following expressions for  $\ell = \ell_1 = \ell_2$ ,

$$C_{VL}^{\ell\ell} = -\frac{3}{16\pi^2} \left\{ |(y_L)_{t\ell}|^2 \frac{m_t^2}{m_\Delta^2} \left( 1 + \log \frac{m_t^2}{m_\Delta^2} \right) - \frac{|(y_L)_{c\ell}|^2 m_Z^2}{3 m_\Delta^2} \left[ \left( 1 - \frac{4s_W^2}{3} \right) \left( \log \frac{m_\Delta^2}{m_Z^2} + i\pi + \frac{1}{3} \right) - \frac{s_W^2}{9} \right] \right\}, \quad (5.26)$$

$$C_{VR}^{\ell\ell} = +\frac{3}{16\pi^2} \left\{ |(y_R)_{t\ell}|^2 \frac{m_t^2}{m_\Delta^2} \left( 1 + \log \frac{m_t^2}{m_\Delta^2} \right) - \frac{|(y_R)_{c\ell}|^2 m_Z^2}{3 m_\Delta^2} \left[ \left( -\frac{4s_W^2}{3} \right) \left( \log \frac{m_\Delta^2}{m_Z^2} + i\pi + \frac{1}{3} \right) - \frac{s_W^2}{9} \right] \right\} \quad (5.27)$$

which agree with the expressions given in Ref. [254].

In addition to the loop constraints described above, there are several observable to which the LQ state contribute at tree-level. A very important constraint stems from the ratio

$R_{\nu\nu} = \mathcal{B}(B \rightarrow K\nu\nu)_{\text{th}}/\mathcal{B}(B \rightarrow K\nu\nu)_{\text{SM}}$ , which should satisfy  $R_{\nu\nu}^{\text{exp}} < 4.3$ , as established by BaBar [311, 312]. By using the effective Lagrangian (4.39), one can show that, in this model, this observable is modified as follows,

$$R_{\nu\nu} = 1 - \frac{1}{6 C_L^{\text{SM}}} \text{Re} \left[ \frac{(y_L \cdot y_L^\dagger)_{sb}}{N m_\Delta^2} \right] + \frac{1}{48 (C_L^{\text{SM}})^2} \frac{(y_L \cdot y_L^\dagger)_{ss} (y_L \cdot y_L^\dagger)_{bb}}{|N|^2 m_\Delta^4}, \quad (5.28)$$

where  $N = G_F V_{tb} V_{ts}^* \alpha_{\text{em}} / (\sqrt{2}\pi)$ , and  $C_L^{\text{SM}} = -6.38(6)$  as defined in Ref. [313]. Furthermore, a peculiarity of this model is the modification of (semi-)leptonic meson decays. By matching the Lagrangian (4.38) to the effective Hamiltonian (2.3), we obtain the Wilson coefficients

$$g_V = -g_A \Big|_{d \rightarrow u\ell\nu_{\ell'}} = \frac{1}{4\sqrt{2}G_F V_{ud}} \frac{(y_L)_{u\ell}^* (y_L)_{d\nu_{\ell'}}}{m_\Delta^2}, \quad (5.29)$$

$$g_S(\mu = m_\Delta) = -g_P(\mu = m_\Delta) \Big|_{d \rightarrow u\ell\nu_{\ell'}} = -\frac{1}{4\sqrt{2}G_F V_{ud}} \frac{(y_R)_{u\ell}^* (y_L)_{d\nu_{\ell'}}}{m_\Delta^2}, \quad (5.30)$$

$$g_T(\mu = m_\Delta) \Big|_{d \rightarrow u\ell\nu_{\ell'}} = -\frac{1}{4} g_S(\mu = m_\Delta) \Big|_{d \rightarrow u\ell\nu_{\ell'}}, \quad (5.31)$$

where  $u$  and  $d$  stand for a generic up- and down-type quark flavors. These expressions can be inserted into the expressions for decay rates, explicitly given in Chapter 2, cf. Eqs. (2.9) and (2.29). We should stress that LQs can induce new contributions in which the neutrino has a different flavor from the charged lepton. One should therefore sum over the unobserved neutrino flavors in order to compare with the experimentally measured rates, e.g.  $\mathcal{B}(B \rightarrow D\ell\nu) = \sum_{\ell'} \mathcal{B}(B \rightarrow D\ell\nu_{\ell'})$ , with  $\ell' \in \{\mu, \tau\}$ . Considering the ansatz given in Eq. (5.19) for the Yukawa matrix, the relevant leptonic modes for our study are  $K \rightarrow \mu\nu$ ,  $D_s \rightarrow (\mu, \tau)\nu$ , and  $B \rightarrow \tau\nu$ . We consider the experimental values given in Ref. [310] and we use the values for the decay constants computed in lattice QCD, which are summarized in Sec. 2.2.1. In addition to the leptonic constraints, it is crucial to also consider the semileptonic ratio

$$R_D^{\mu/e} = \frac{\mathcal{B}(B \rightarrow D\mu\nu)}{\mathcal{B}(B \rightarrow De\nu)}, \quad (5.32)$$

which is constrained by the Belle measurement  $R_D^{\mu/e} = 0.995(22)(39)$  [314].<sup>6</sup> It is well known that large values of this quantity would be implausible, since the  $\mathcal{B}(B \rightarrow De\nu)$  and  $\mathcal{B}(B \rightarrow D\mu\nu)$  data have been successfully combined in  $B$ -factory experiments to extract  $\mathcal{G}(1)|V_{cb}|$ . In Ref. [316] it was argued that such a deviation from lepton flavor universality cannot be larger than 2%, which is considered as a constraint in our analysis. It should be stressed that this limit is the main constraint for masses  $m_\Delta \approx 1$  TeV, as argued in Ref. [155], where it was shown that an explanation of  $R_K$  as originally proposed in Ref. [254] would imply unacceptably large values for  $R_D^{\mu/e}$ . Finally, useful constraints stem from the experimental limits  $\mathcal{B}(\tau \rightarrow \mu\gamma) < 4.4 \times 10^{-8}$  [317] and  $\mathcal{B}(D^0 \rightarrow \mu^+\mu^-) < 7.6 \times 10^{-9}$  [253]. We computed the LQ contributions to these decays and obtained

$$\mathcal{B}(\tau \rightarrow \mu\gamma) = \tau_\tau \frac{\alpha_{\text{em}} (m_\tau^2 - m_\mu^2)^3}{4m_\tau^3} \left( |\sigma_L|^2 + |\sigma_R|^2 \right), \quad (5.33)$$

<sup>6</sup>A similar ratio has been also measured with a  $D^*$  meson in the final state, yielding  $R_{D^*}^{e/\mu} = 1.04(5)(1)$  in good agreement with  $\mu/e$  universality [315].

with

$$\sigma_{L(R)} = -i \frac{N_C m_\tau}{192\pi^2 m_\Delta^2} \left\{ (y_{R(L)})_{t\tau} (y_{R(L)})_{t\mu}^* - \frac{m_t}{m_\tau} (y_{L(R)})_{t\tau} (y_{L(R)})_{t\mu}^* \left[ 14 + 8 \log \left( \frac{m_t^2}{m_\Delta^2} \right) \right] \right\}, \quad (5.34)$$

and

$$\begin{aligned} \mathcal{B}(D^0 \rightarrow \mu^+ \mu^-) &= \frac{f_D^2 m_D^3}{512\pi m_\Delta^4 \Gamma_D} \left( \frac{m_D}{m_c} \right)^2 \beta_\mu \left[ \beta_\mu^2 \left| (y_L)_{c\mu} (y_R)_{u\mu}^* - (y_R)_{c\mu} (y_L)_{u\mu}^* \right|^2 \right. \\ &\quad \left. + \left| (y_L)_{c\mu} (y_R)_{u\mu}^* + (y_R)_{c\mu} (y_L)_{u\mu}^* - \frac{2m_\mu m_c}{m_D^2} \left[ (y_L)_{c\mu} (y_L)_{u\mu}^* + (y_R)_{c\mu} (y_R)_{u\mu}^* \right] \right|^2 \right], \end{aligned} \quad (5.35)$$

where  $m_c = m_c(m_\Delta)$  is the running charm quark mass.

To assess the viability of this model, we combine the above-mentioned constraints to  $2\sigma$  accuracy with the perturbativity condition,  $|(y_L)_{ij}| < \sqrt{4\pi}$ , and look for the parameters which would simultaneously satisfy the observed  $R_K^{\text{exp}}$  and  $R_D^{\text{exp}}$ . We vary the LQ mass in the region  $m_\Delta \in [1, 5]$  TeV and impose the flavor ansatz of Eq. (5.19) and Eq. (5.20) for the Yukawa matrices  $y_L$  and  $y_R$ . The results from our scan are shown in Fig. 5.8, where  $R_K$  in the central bin is plotted against  $R_D$ . As it can be seen from this plot, we were not able to find parameters that would result in values for  $R_K$  consistent with the  $1\sigma$  region reported by LHCb. This model can only somewhat reduce the tension with respect to the SM for this specific observable. On the other hand, the deviation in  $R_D$  can be easily accommodated by this LQ state, a fact that was already demonstrated years ago in Ref. [318]. From the same plot, we also learn that a simultaneous improvement of both observables is difficult, since an improvement of  $R_K$  compromises the explanation of  $R_D$ . This fact can be better understood in Fig. 5.9, where  $R_K$  is plotted against the LQ mass  $m_\Delta$ . To substantially reduce the value of  $R_K$ , the LQ masses must be larger than  $\approx 4$  TeV, in order to avoid the constraint from  $R_D^{\mu/e}$  described above. This observation is the source of disagreement with  $R_{D^{(*)}}$ , since an explanation of the latter requires relatively light NP ( $m_\Delta \approx 1$  TeV) with sizable couplings. Finally, we plot the correlation between  $(y_L)_{b\mu}$  and  $m_\Delta$  in Fig. (5.10). In the same plot, we highlight the parameters which would be consistent with  $R_K$  and  $R_{K^*}$  in the central bin at the  $1.5\sigma$  level. As it can be seen from this plot, to produce this improvement in the description of  $R_{K^{(*)}}$ , one should have  $m_\Delta \gtrsim 4$  TeV and  $|(y_L)_{b\mu}| \approx \sqrt{4\pi}$ , saturating the perturbativity limit.

### 5.2.5 A viable leptoquark explanation of $R_{K^{(*)}} < 1$ through loops

In this Section we discuss another scalar LQ model proposed to accommodate  $R_{K^{(*)}}^{\text{exp}} < R_{K^{(*)}}^{\text{SM}}$  via loop-level contributions [319]. This model invokes the doublet  $R_2 = (3, 2)_{7/6}$  LQ state and it was inspired by the singlet scenario described above. Differently from the singlet scenario, where there was no tree-level contribution to  $b \rightarrow s\ell\ell$ , this state contributes to this transition at tree-level, but it cannot accommodate  $R_{K^{(*)}}^{\text{exp}} < R_{K^{(*)}}^{\text{SM}}$ , as discussed in Sec. 5.2.3. The new idea introduced in Ref. [319] is to impose a flavor ansatz that will forbid the tree-level contribution to  $b \rightarrow s\ell\ell$ . As we will show in this Section, the loop-level contribution to  $b \rightarrow s\ell\ell$  will generate the combination  $C_9 = -C_{10}$ , which can then explain the experimental findings. Notice, however, that this model cannot simultaneously explain  $R_{D^{(*)}}$ , the fact that was already (implicitly) shown in Ref. [224].

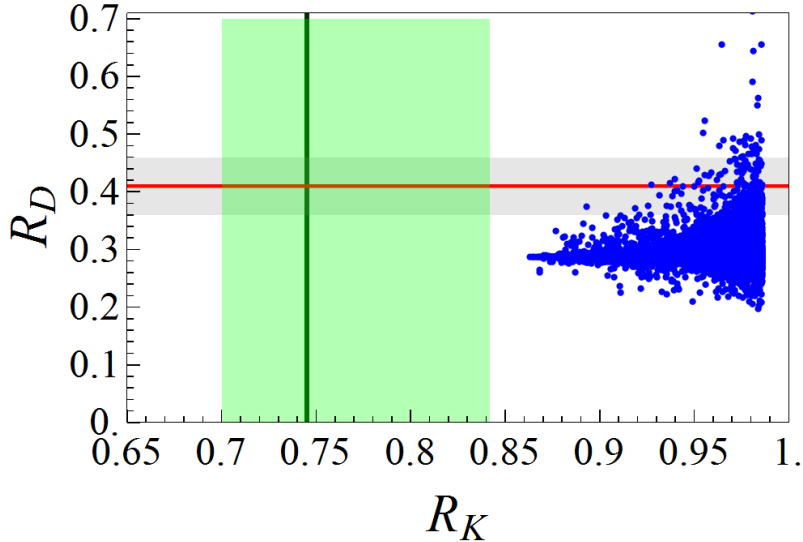


**Figure 5.8:**  $R_D$  is plotted against  $R_K$  in the central bin. The allowed points are compared with the experimental values (green and grey bands) at  $1\sigma$ .

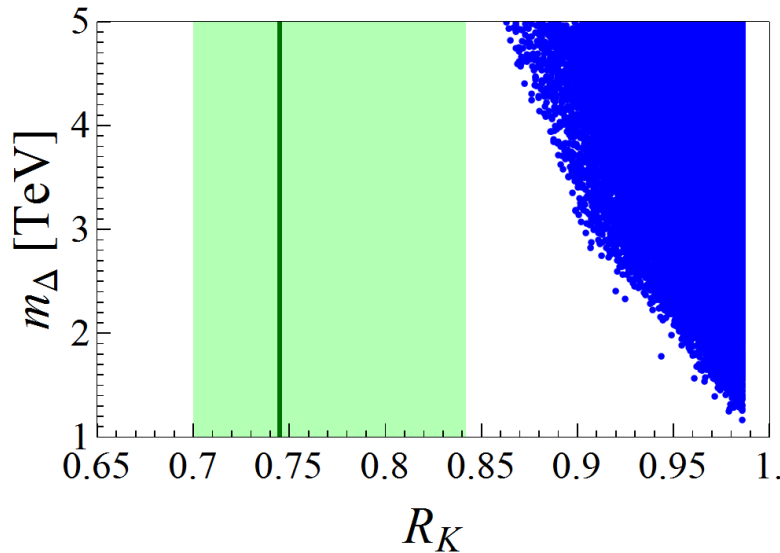


**Figure 5.9:**  $R_K$  in the central bin is plotted against the LQ mass  $m_\Delta$ . The allowed points are compared with the experimental value for  $R_K$  (green band) at  $1\sigma$ .

Before introducing our model and its phenomenology, we would like to emphasize the advantages of this scenario in comparison to the singlet model presented in Sec. 5.2.4. Firstly, this scenario conserves baryon number by construction, as shown in Table 4.1. Therefore, no additional *ad-hoc* symmetry is needed to preserve the proton stability. Furthermore, in our model, the top quark contribution naturally induces  $C_9^{\mu\mu} = -C_{10}^{\mu\mu} < 0$ , as needed. In the singlet scenario, the dominant top-quark contribution generates  $C_9^{\mu\mu} > 0$ , so that it was mandatory to compensate that effect with a very large charm-muon Yukawa, which induces problems in other observables, or by increasing the LQ mass, which lies far beyond the current sensitivity of LHC. These limitations are not present in the scenario we will describe below.

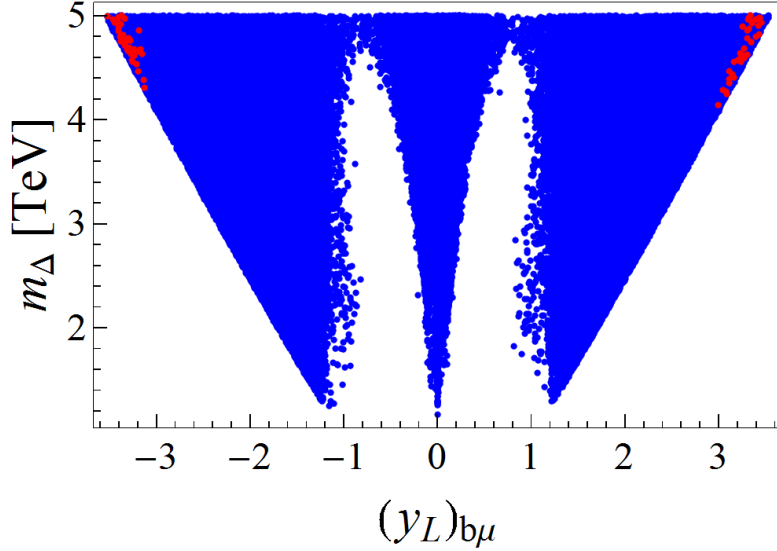


**Figure 5.10:** Projection of the allowed points from Fig. 5.9 in the plane  $(y_L)_{b\mu}$  vs.  $m_\Delta$ . We highlight in red the points which can be consistent with  $R_K$  and  $R_{K^*}$  in the central bin to  $1.5\sigma$  accuracy.

### Description of the model

The general Yukawa Lagrangian for this model was already given in Eq. (4.20) and reads

$$\begin{aligned} \mathcal{L}_{\Delta^{(7/6)}} &= (y_R)_{ij} \bar{Q}_i \Delta^{(7/6)} \ell_{Rj} + (y_L)_{ij} \bar{u}_{Ri} \widetilde{\Delta}^{(7/6)\dagger} L_j + \text{h.c.}, \\ &= (V y_R)_{ij} \bar{u}_i P_R \ell_j \Delta^{(5/3)} + (y_R)_{ij} \bar{d}_i P_R \ell_j \Delta^{(2/3)} \\ &\quad + (U y_L)_{ij} \bar{u}_i P_L \nu_j \Delta^{(2/3)} - (y_L)_{ij} \bar{u}_i P_L \ell_j \Delta^{(5/3)} + \text{h.c.}, \end{aligned} \quad (5.36)$$

where  $y_{L,R}$  are the matrices of Yukawa couplings, that we assume to be

$$y_L = \begin{pmatrix} 0 & 0 & 0 \\ 0 & y_L^{c\mu} & y_L^{c\tau} \\ 0 & y_L^{t\mu} & y_L^{t\tau} \end{pmatrix}, \quad y_R = \begin{pmatrix} 0 & 0 & 0 \\ 0 & 0 & 0 \\ 0 & 0 & y_R^{b\tau} \end{pmatrix}, \quad V y_R = \begin{pmatrix} 0 & 0 & V_{ub} y_R^{b\tau} \\ 0 & 0 & V_{cb} y_R^{b\tau} \\ 0 & 0 & V_{tb} y_R^{b\tau} \end{pmatrix}, \quad (5.37)$$

which is the main peculiarity of our model. The superscript in  $\Delta^{(5/3)}$  and  $\Delta^{(2/3)}$  refer to the electric charge of the two mass degenerate leptoquark states, as before. The above choice of Yukawa couplings, and in particular  $y_R^{s\ell} = 0$ , means that the contributions of the leptoquark  $\Delta^{(7/6)}$  to the transitions  $b \rightarrow s\ell\ell$  can only be a loop effect and not generated at tree level. The only diagram contributing (in the unitary gauge) is the one shown in Fig. 5.11.

We computed the corresponding amplitude, matched it onto the effective theory (2.54), and found

$$C_9^{\ell_1\ell_2} = -C_{10}^{\ell_1\ell_2} = \sum_{u,u' \in \{u,c,t\}} \frac{V_{ub} V_{u's}^*}{V_{tb} V_{ts}^*} y_L^{u'\ell_1} (y_L^{u\ell_2})^* \mathcal{F}(x_u, x_{u'}), \quad (5.38)$$

where  $x_i = m_i^2/m_W^2$ , and the loop function reads,

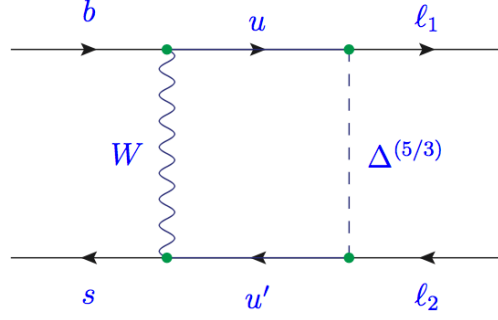


**Figure 5.11:** The only diagram contributing  $b \rightarrow s\ell_1\ell_2$  decay in the LQ scenario considered here. In a non-unitary gauge there is an extra diagram similar to the one depicted above, with  $W$  replaced by a Goldstone boson.

$$\mathcal{F}(x_u, x_{u'}) = \frac{\sqrt{x_u x_{u'}}}{32\pi\alpha_{\text{em}}} \left[ \frac{x_{u'}(x_{u'} - 4) \log x_{u'}}{(x_{u'} - 1)(x_u - x_{u'})(x_{u'} - x_\Delta)} + \frac{x_u(x_u - 4) \log x_u}{(x_u - 1)(x_{u'} - x_u)(x_u - x_\Delta)} - \frac{x_\Delta(x_\Delta - 4) \log x_\Delta}{(x_\Delta - 1)(x_\Delta - x_u)(x_\Delta - x_{u'})} \right]. \quad (5.39)$$

We checked that the above result is finite and gauge invariant by doing the computation in both the Feynman and the unitary gauge. The loop function vanishes when sending the quark mass to zero, and therefore the dominant contributions are those coming from  $u = u' = t$ , and the one in which  $u = t$ ,  $u' = c$ , latter being CKM enhanced. This closes our discussion of the  $R_2$  model with our particular setup specified by the structure of the  $y_{L,R}$  matrices, as given in Eq. (5.37).

### Phenomenology: Low-energy constraints

The model described above can induce important contributions to some observables which have already been accurately measured. In other words, we check which quantity can be particularly sensitive to our model and then use its measured value to constrain the non-zero entries in the matrices  $y_{L,R}$  (5.37).

First of all, by switching on the couplings to the leptoquark of the top quark and to  $\mu$  and to  $\tau$  leptons, one necessarily generates an extra term to the  $\tau \rightarrow \mu\gamma$  decay amplitude. In order to comply with the experimentally established upper bound,  $\mathcal{B}(\tau \rightarrow \mu\gamma) < 4.4 \times 10^{-8}$  [317], we checked the expression derived in Ref. [8, 320] with which we agree, and write:

$$\mathcal{B}(\tau \rightarrow \mu\gamma) = \tau_\tau \frac{\alpha_{\text{em}}(m_\tau^2 - m_\mu^2)^3}{4m_\tau^3} (|\sigma_L|^2 + |\sigma_R|^2), \quad (5.40)$$

with

$$\begin{aligned} \sigma_L &= 0, \\ \sigma_R &= \frac{3im_\tau}{64\pi^2 m_\Delta^2} \sum_{q \in \{c,t\}} y_L^{q\mu*} \left[ y_L^{q\tau} + \frac{2}{3} \frac{m_q}{m_\tau} V_{qb} y_R^{b\tau} \left( 1 + 4 \log \frac{m_t^2}{m_\Delta^2} \right) \right]. \end{aligned} \quad (5.41)$$

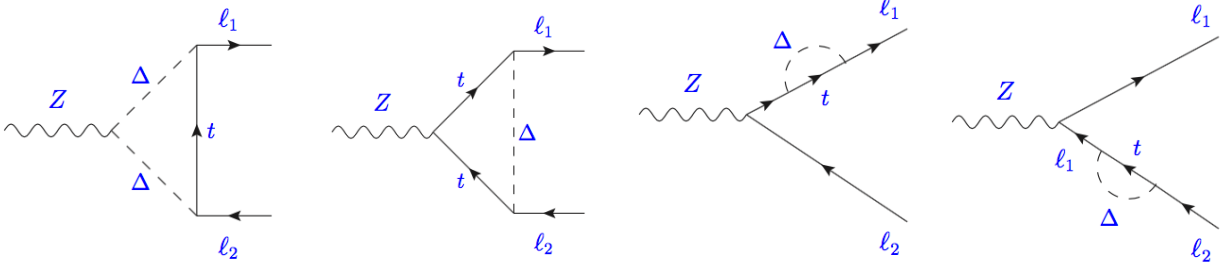


**Figure 5.12:** Contributions to the  $Z \rightarrow \ell_1\ell_2$  decay amplitude generated in our  $R_2$  model, where  $\Delta \equiv \Delta^{(5/3)}$ . Another set of diagrams, similar to those shown above is obtained by replacing  $t \rightarrow c$ .

Since we need a significant value for  $y_L^{t\mu}$  and  $y_L^{c\mu}$  to describe the exclusive  $b \rightarrow s\mu\mu$  decay rates, the above condition proves to be a severe bound on  $y_R^{b\tau}$ , due to the  $m_t/m_\tau$  enhancement.

Another important constraint comes from the contributions to the muon's  $g-2$ . Current deviation between the measured and the SM values is  $\Delta a_\mu^{\text{exp}} = a_\mu^{\text{exp}} - a_\mu^{\text{SM}} = (2.8 \pm 0.9) \times 10^{-9}$ , where  $a_\mu = (g_\mu - 2)/2$ , as usual. Since the SM estimate of this quantity is not yet fully assessed [321], we require the leptoquark contribution to be smaller than  $2\sigma$  error on  $\Delta a_\mu^{\text{exp}}$ . To do so we use the expression [8]:

$$\Delta a_\mu = -\frac{3m_\mu^2}{8\pi^2 m_\Delta^2} \sum_{q \in \{c,t\}} |y_L^{q\mu}|^2 \left[ \frac{5}{3} f_S(m_q^2/m_\Delta^2) - f_F(m_q^2/m_\Delta^2) \right],$$

$$f_S(x) = \frac{x+1}{4(1-x)^2} + \frac{x \log x}{2(1-x)^3}, \quad f_F(x) = \frac{x^2 - 5x - 2}{12(x-1)^3} + \frac{x \log x}{2(1-x)^4}. \quad (5.42)$$

A very efficient constraint on  $y_L^{t\ell}$  and  $y_L^{c\ell}$  comes from the branching fractions  $\mathcal{B}(Z \rightarrow \ell\ell)$ , which have been very accurately measured at LEP [22], cf. Eq. (5.24). In our model the diagrams contributing to  $Z \rightarrow \ell\ell$  (or, more generally, to  $Z \rightarrow \ell_1\ell_2$ ) are shown in Fig. 5.12. We computed the full amplitude, matched it with the effective Lagrangian,

$$\mathcal{L}_{\text{eff}} = \frac{g}{2 \cos \theta_W} C_{VL}^{\ell_1\ell_2} \bar{\ell}_1 \gamma^\mu P_L \ell_2 Z^\mu, \quad (5.43)$$

and obtained, for  $\ell_1 = \ell_2 \equiv \ell$ ,

$$C_{VL}^{\ell_1\ell_2} = -\frac{3}{16\pi^2} \left\{ y_L^{t\ell_1} y_L^{t\ell_2*} \frac{m_t^2}{m_\Delta^2} \left( 1 + \log \frac{m_t^2}{m_\Delta^2} \right) + \frac{4}{9} y_L^{c\ell_1} y_L^{c\ell_2*} \frac{m_c^2}{m_\Delta^2} \left[ \sin^2 \theta_W \left( \log \frac{m_c^2}{m_\Delta^2} - i\pi - \frac{1}{12} \right) + \frac{1}{8} \right] \right\}. \quad (5.44)$$

The top contribution in the above formula agrees with the result of Ref. [322] while the contribution arising from charm is new. Using the Lagrangian (5.43), we then obtain

$$\mathcal{B}(Z \rightarrow \ell\ell) = \frac{m_Z^3}{24\pi v^2 \Gamma_Z} \left[ |C_{VL}^{\ell\ell}|^2 - 2 \text{Re}(1 + C_{VL}^{\ell\ell}) \cos(2\theta_W) + 2 + \cos(4\theta_W) \right]. \quad (5.45)$$

In practice, we find it more convenient to consider

$$R_Z^{\ell\ell} = \frac{\mathcal{B}(Z \rightarrow \ell\ell)}{\mathcal{B}(Z \rightarrow \ell\ell)^{\text{SM}}}, \quad (5.46)$$

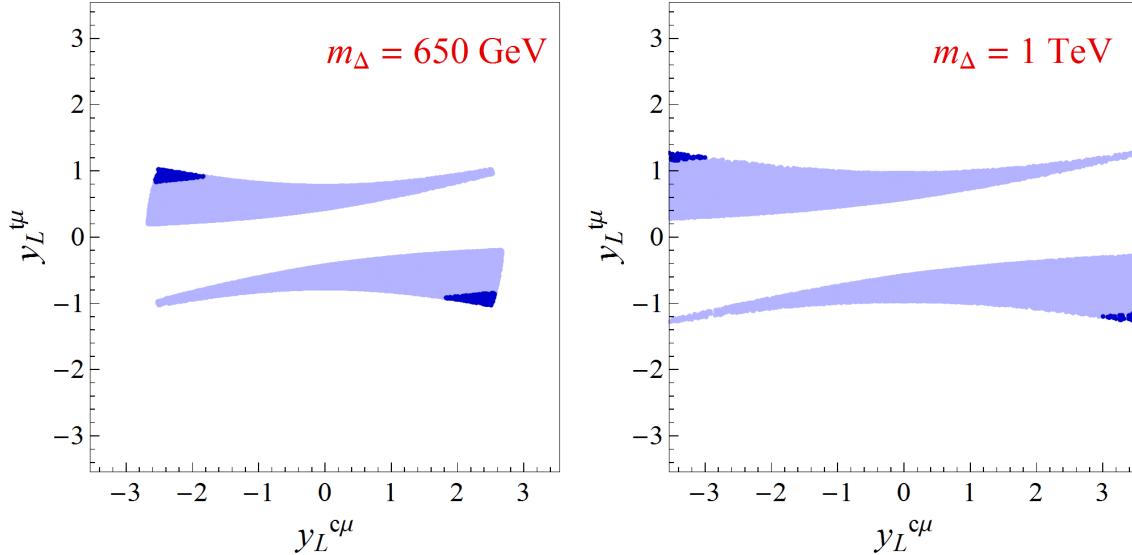


**Figure 5.13:** Allowed values for the couplings  $y_L^{t\mu}$  and  $y_L^{c\mu}$  consistent with all the constraints discussed in the previous section. Plots are provided for  $m_\Delta = 650$  GeV and  $m_\Delta = 1$  TeV. Highlighted regions correspond to the values of the couplings that ensure the  $1.5\sigma$  agreement of  $R_K$  and  $R_{K^*}$  with experiment in the central  $q^2$ -bin.

and to use the values (5.24) to  $2\sigma$  accuracy.

Finally, the major constraint on the model comes from the exclusive  $b \rightarrow s\mu\mu$  decays, for which we will consider the constraint (5.8), as obtained in Sec. 5.2.1. Before closing this section we believe it is worth emphasizing that the model we consider here does not give any contribution to the  $B_s - \bar{B}_s$  mixing amplitude (at the one-loop level).

### Phenomenology: $R_K$ and $R_{K^*}$

We next focus on our model and beside  $C_9^{\mu\mu} = -C_{10}^{\mu\mu}$  obtained in Eqs. (5.8) and (5.13) we also use the constraints discussed in the previous section. These constraints appear to be quite severe. Consistency with  $C_9^{\mu\mu}$  requires rather large values of the muonic couplings to the leptoquark. For that reason, the experimental bound on  $\mathcal{B}(\tau \rightarrow \mu\gamma)$  will necessarily restrain  $y_R^{b\tau}$  to very small values. The values of  $y_L^{t\mu}$  [ $y_L^{t\tau}$ ] and  $y_L^{c\mu}$  [ $y_L^{c\tau}$ ] are then saturated by  $\Delta a_\mu$  and by the required consistency with the measured  $\mathcal{B}(Z \rightarrow \mu\mu)$  [ $\mathcal{B}(Z \rightarrow \tau\tau)$ ].

We performed several scans of the model parameters. We first fixed the mass of leptoquark to either  $m_\Delta = 650$  GeV or to  $m_\Delta = 1$  TeV, and varied all the couplings within  $|y_{L,R}^{q\ell}| \leq \sqrt{4\pi}$ . As we anticipated above, the allowed values of  $y_R^{b\tau}$  are indeed negligibly small, and for our phenomenological purposes this coupling can be safely neglected. In the following we set it to zero. On the other hand, constraints on the couplings to muon result in the regions shown in Fig. 5.13. Clearly, for larger  $m_\Delta$  the couplings grow and for reasonable values of  $m_\Delta$  (less than a few TeV) the only coupling that hits the perturbativity bound is  $y_L^{c\mu}$  while the other ones remain well below  $\sqrt{4\pi}$ .

Notice also that in Fig. 5.13 we highlight the regions of couplings that are needed to provide a  $1.5\sigma$  compatibility of  $R_K$  and  $R_{K^*}$  with experimental results in the central  $q^2$ -bin. In other words, to get close to the measured values of  $R_K^{\text{exp}}$  and  $R_{K^*}^{\text{exp}}$  the values of couplings  $y_L^{c\mu}$  and  $y_L^{t\mu}$  indeed need to be large (larger than 1). The values for  $R_K$  and  $R_{K^*}$  obtained with our model are given in Tab. 5.3. We see that the situation regarding the agreement with experimental values (5.2) and (5.3) remains similar to the discussion based only on

$C_9^{\mu\mu}$ , i.e. our values for  $R_K$  and  $R_{K^*}$  are compatible with experiment in the central  $q^2$ -bin to  $1.1\sigma$ , while in the low- $q^2$ -bin the agreement of our  $R_{K^*}$  with the value in (5.3) is at the  $1.8\sigma$  level.

Quantity	$m_\Delta = 650$ GeV	$m_\Delta = 1$ TeV
$R_K$ (low $q^2$ )	[0.80, 0.96]	[0.82, 0.96]
$R_{K^*}$ (low $q^2$ )	[0.88, 0.92]	[0.88, 0.92]
$R_K$ (central $q^2$ )	[0.82, 0.98]	[0.85, 0.98]
$R_{K^*}$ (central $q^2$ )	[0.82, 0.98]	[0.85, 0.98]
$R_K$ (high $q^2$ )	[0.81, 0.98]	[0.84, 0.98]
$R_{K^*}$ (high $q^2$ )	[0.81, 0.98]	[0.83, 0.98]

**Table 5.3:** Intervals of  $R_K$  and  $R_{K^*}$  obtained in our model by using all the constraints discussed in the text, and  $C_9^{\mu\mu} = -C_{10}^{\mu\mu}$  in Eq. (5.8) in particular.

As a curiosity we can now proceed the other way around and perform a scan of parameters by leaving  $m_\Delta$  as a free parameter, and then check how large one can take  $m_\Delta$  and still remain e.g.  $1.5\sigma$ -compatible with  $R_K$  and  $R_{K^*}$  reported by LHCb in the central  $q^2$ -bin. The result of this exercise is shown in Fig. 5.14, from which we see that  $m_\Delta < 1.2$  TeV.

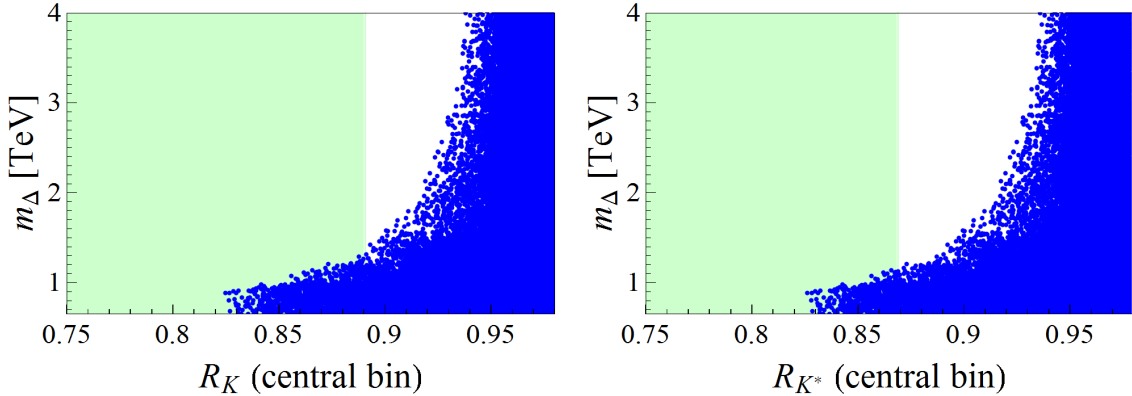


**Figure 5.14:** Results of our scan of parameters consistent with all constraints discussed in the previous section in which the leptoquark mass  $m_\Delta$  is varied too. We see that the  $1.5\sigma$  consistency requirement with the values of LHCb for  $R_K$  and  $R_{K^*}$  in the central  $q^2$ -bin (shaded area) results in  $m_\Delta < 1.2$  TeV.

We now enumerate the predictions of this model:

1. Like we mentioned before, this model does not induce the tree-level or the one-loop contribution to the  $B_s - \bar{B}_s$  mixing amplitude.

2. Using Eq. (5.38) and by taking into account the constraints on the couplings  $g_{L,R}^{q\tau}$ , we were able to compute  $C_9^{\tau\tau} = -C_{10}^{\tau\tau}$  from which we computed the branching fractions  $\mathcal{B}(B_s \rightarrow \tau\tau)$  and  $\mathcal{B}(B \rightarrow K^{(*)}\tau\tau)_{\text{large } q^2}$ . We obtain,  $-0.46 \leq C_9^{\tau\tau} \leq 0.06$  for  $m_\Delta = 650$  GeV, which then gives:

$$\begin{aligned} 0.78 &\leq \frac{\mathcal{B}(B_s \rightarrow \tau\tau)}{\mathcal{B}(B_s \rightarrow \tau\tau)^{\text{SM}}} \leq 1.03, \\ 0.79 &\leq \frac{\mathcal{B}(B \rightarrow K\tau\tau)_{q^2 \in [15,19] \text{ GeV}^2}}{\mathcal{B}(B \rightarrow K\tau\tau)_{q^2 \in [15,19] \text{ GeV}^2}^{\text{SM}}} \leq 1.03, \\ 0.77 &\leq \frac{\mathcal{B}(B \rightarrow K^*\tau\tau)_{q^2 \in [15,19] \text{ GeV}^2}}{\mathcal{B}(B \rightarrow K^*\tau\tau)_{q^2 \in [15,19] \text{ GeV}^2}^{\text{SM}}} \leq 1.03. \end{aligned} \quad (5.47)$$

For  $m_\Delta = 1$  TeV, we obtain,  $-0.17 \leq C_9^{\tau\tau} \leq 0.03$ , which leads to:

$$\begin{aligned} 0.92 &\leq \frac{\mathcal{B}(B_s \rightarrow \tau\tau)}{\mathcal{B}(B_s \rightarrow \tau\tau)^{\text{SM}}} \leq 1.01, \\ 0.92 &\leq \frac{\mathcal{B}(B \rightarrow K\tau\tau)_{q^2 \in [15,19] \text{ GeV}^2}}{\mathcal{B}(B \rightarrow K\tau\tau)_{q^2 \in [15,19] \text{ GeV}^2}^{\text{SM}}} \leq 1.01, \\ 0.91 &\leq \frac{\mathcal{B}(B \rightarrow K^*\tau\tau)_{q^2 \in [15,19] \text{ GeV}^2}}{\mathcal{B}(B \rightarrow K^*\tau\tau)_{q^2 \in [15,19] \text{ GeV}^2}^{\text{SM}}} \leq 1.01. \end{aligned} \quad (5.48)$$

3. Our model allows for lepton flavor violation, as in most scenarios aiming to explain the LFUV effects [153]. Again, after inserting the values (intervals) of the couplings  $y_L^{q\mu}$  and  $y_L^{q\tau}$  into Eq. (5.38), we obtain

$$\mathcal{B}(B \rightarrow K\mu\tau) \lesssim \left\{ (4.6 \times 10^{-9})_{m_\Delta=650 \text{ GeV}}, (1.5 \times 10^{-9})_{m_\Delta=1 \text{ TeV}} \right\}, \quad (5.49)$$

whereas the branching fractions for similar decay modes can be obtained from the ratios (2.149) which are independent on the Wilson coefficients [127]:

$$\frac{\mathcal{B}(B \rightarrow K^*\mu\tau)}{\mathcal{B}(B \rightarrow K\mu\tau)} \approx 1.8 \quad \text{and} \quad \frac{\mathcal{B}(B_s \rightarrow \mu\tau)}{\mathcal{B}(B \rightarrow K\mu\tau)} \approx 0.9. \quad (5.50)$$

Since the LFV and lepton flavor conserving modes are related by the same model parameters, there is obviously a correlation between various rates. A typical one is shown in Fig. 5.15, where we see that the LFV mode can be significant even for  $\mathcal{B}(B_s \rightarrow \tau\tau)$  perfectly consistent with its Standard Model value.

4. Another interesting LFV mode is  $Z \rightarrow \mu\tau$ . The expression given in Eq. (5.44) is trivially extended to the LFV case by simply replacing  $y_L^{q\ell} y_L^{q\ell^*} \rightarrow y_L^{q\ell_1} y_L^{q\ell_2^*}$ . We obtain that the maximal allowed values can be quite large, namely,

$$\mathcal{B}(Z \rightarrow \mu\tau) \lesssim \left\{ (4 \times 10^{-7})_{m_\Delta=650 \text{ GeV}}, (2.1 \times 10^{-7})_{m_\Delta=1 \text{ TeV}} \right\}, \quad (5.51)$$

and could be an opportunity for future experiments.

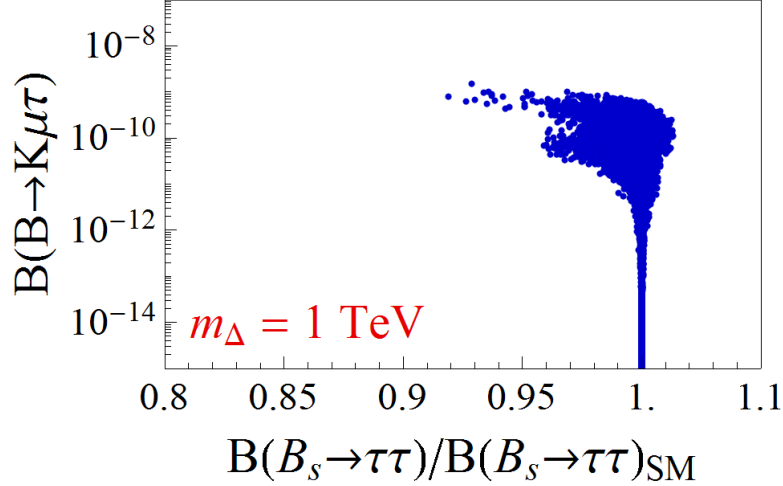


**Figure 5.15:** Correlation between  $\mathcal{B}(B_s \rightarrow \tau\tau)$  and  $\mathcal{B}(B \rightarrow K\mu\tau)$  as obtained in our model.

5. We have checked that our model provides a very small contribution to  $\mathcal{B}(t \rightarrow b\tau\nu)$ , which is well within the experimental error [323].
6. We also computed the Wilson coefficient relevant to  $\mathcal{B}(B \rightarrow K\nu\nu)$  and found that our model can bring only a small reduction with respect to the Standard Model value, i.e.

$$0.94 \leq \frac{\mathcal{B}(B \rightarrow K\nu\nu)}{\mathcal{B}(B \rightarrow K\nu\nu)^{\text{SM}}} \leq 1, \quad (5.52)$$

the reduction being more pronounced for smaller leptoquark masses, namely  $m_\Delta = 650$  GeV.

### Comments on Direct Searches

So far we have assumed the value of the leptoquark mass to be either  $m_\Delta = 650$  GeV or  $m_\Delta = 1$  TeV, both being consistent with direct searches, cf. Sec. 4.4. We find that the experimental bound,  $m_\Delta \gtrsim 650$  GeV, is very conservative and the reason for this can be understood from the assumptions made in the LHC searches. So far the attempts for direct detection of the leptoquark states, present in our model, only included the decays [261,262]

$$\Delta^{(2/3)} \rightarrow t\nu, \quad \text{and} \quad \Delta^{(5/3)} \rightarrow t\tau, \quad (5.53)$$

for which they assumed  $\mathcal{B}(\Delta^{(2/3)} \rightarrow t\nu) = 1$ , and  $\mathcal{B}(\Delta^{(5/3)} \rightarrow t\tau) = 1$ . The resulting bound,  $m_\Delta \gtrsim 650$  GeV, would be considerably lower if one also considered

$$\Delta^{(2/3)} \rightarrow c\nu, \quad \text{and} \quad \Delta^{(5/3)} \rightarrow t\mu, \quad c\tau, \quad c\mu, \quad (5.54)$$

and then used the fact that the branching fractions of the above-mentioned modes are less than one. With our couplings we can compute the relevant decay rates. We derived the necessary expression for the decay of  $\Delta^{(2/3,5/3)}$ , namely,

$$\Gamma(\Delta^{(2/3)} \rightarrow u\nu_i) = \Gamma(\Delta^{(5/3)} \rightarrow u\ell_i) = |y_L^{ui}|^2 \frac{(m_\Delta^2 - m_u^2)^2}{16\pi m_\Delta^3}, \quad (5.55)$$

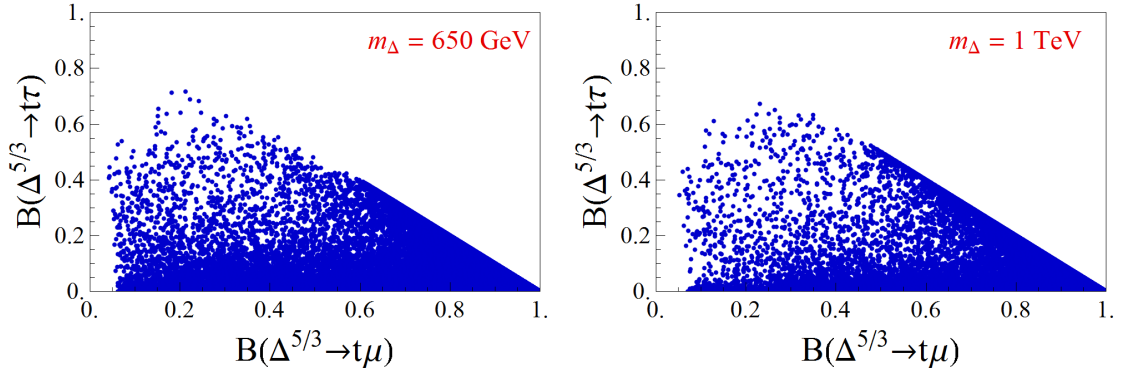


**Figure 5.16:** Branching fractions of the dominant decay modes of  $\Delta^{(5/3)}$  as obtained from the constraints on the relevant couplings discussed in the body of this paper.

where  $u \in \{c, t\}$  and  $i \in \{\mu, \tau\}$ . Notice that we neglect the contribution proportional to  $g_R^{b\tau}$  due to its smallness. Furthermore, the decay rate  $\Gamma(\Delta^{(2/3)} \rightarrow b\tau)$  is indeed completely negligible. From the above formulas it is then easy to reconstruct the relevant branching fractions for the modes searched experimentally. The net result is that the bound on  $m_\Delta$  becomes lower. In other words, the values we use,  $m_\Delta \geq 650$  GeV, are in fact very conservative. Note also that the modes with the charm quark are experimentally very challenging at the LHC.

In Fig. 5.16 we show the possible values for  $\mathcal{B}(\Delta^{(5/3)} \rightarrow t\tau)$  and  $\mathcal{B}(\Delta^{(5/3)} \rightarrow t\mu)$ , consistent with all the constraints discussed above. This information can be used in the forthcoming attempts at LHC to detect the leptoquark through  $\Delta^{(5/3)} \rightarrow t\mu$  channel.

### 5.3 Lepton flavor universality violation in $b \rightarrow c\ell\nu$

In this Section, we discuss the current status of the discrepancies  $R_{D^{(*)}}$  and we will elaborate on the possible connections with the observed deviations in  $R_{K^{(*)}}$ , which were discussed in the previous Section. These observables are defined as,

$$R_{D^{(*)}} = \left. \frac{\mathcal{B}(B \rightarrow D^{(*)}\tau\nu)}{\mathcal{B}(B \rightarrow D^{(*)}l\nu)} \right|_{l=e,\mu}, \quad (5.56)$$

where light leptons have been averaged in the denominator. There are several phenomenological differences between  $R_{K^{(*)}}$  and  $R_{D^{(*)}}$ . Firstly, the SM predictions of  $R_{D^{(*)}}$  depends on hadronic parameters and most particularly on the shape of the form factors, which was not the case for  $R_{K^{(*)}}$ . This comes from the fact that the  $\tau$ -lepton mass is non-negligible in comparison to  $m_B$ , introducing a large LFU breaking already in the SM. Therefore, we stress once again that the determination of shape of the form factors becomes a crucial point to reliably estimate  $R_{D^{(*)}}^{\text{SM}}$ , as implicitly stated in Sec. 2.2.2 and Sec. 2.2.3. Furthermore, in terms of the viable NP explanations,  $B \rightarrow D^{(*)}l\nu$  are tree-level decays with relatively large predictions in the SM. To satisfactorily explain the large deviations which were observed, NP must be relatively light and/or have large couplings. This is not necessarily the case for  $R_{K^{(*)}}$ , where the tree-level explanations remain perturbative all the way up to  $\Lambda_{\text{NP}} \approx 30$  TeV. In other words, the hints  $R_{K^{(*)}}$  and  $R_{D^{(*)}}$  point at different scales for the NP or at very different ballparks for the NP couplings.<sup>7</sup>

<sup>7</sup>An interesting possibility is that this hierarchy of couplings comes from a flavor symmetry which enforces the new bosons to couple mostly to third generation fermions [316].

The remainder of this Section is organized as follows: In Sec. 5.3.1, we describe the SM predictions for  $R_D$  and  $R_{D^*}$  focusing on the potential sources of hadronic uncertainties. In Sec. 5.3.2, we discuss the attempts proposed so far in the literature to simultaneously explain  $R_{K^{(*)}}$  and  $R_{D^{(*)}}$ . We conclude in Sec. 5.3.3, where we propose a minimal model that can explain  $R_K$  and  $R_{D^{(*)}}$  but which cannot account for  $R_{K^*}$ . This last Section will serve as an illustration of the difficulty to conceive simultaneous explanations to all LFUV hints which remains consistent with the plethora of constraints from flavor observables.

### 5.3.1 Standard Model predictions for $R_D$ and $R_{D^*}$

Regarding the SM prediction for these observables, the  $B \rightarrow D$  decays seem to be under good theoretical control as the scalar and vector form factors have been computed on the Lattice by two collaborations and their results are found to be consistent [15, 16]. The SM prediction is then obtained by combining the LQCD results with the  $B \rightarrow D l \nu$  ( $l = e, \mu$ ) experimental distributions, giving [77]

$$R_D^{\text{SM}} = 0.300 \pm 0.008, \quad (5.57)$$

which is about  $2\sigma$  lower than the experimental results, cf. Eq. (5.4). The value obtained by MILC, by solely relying on LQCD estimates, would be  $R_D = 0.286 \pm 0.012$  [15]. This value is slightly lower than (5.57), but still perfectly consistent with it. Therefore, the determination of  $R_D^{\text{SM}}$  is quite robust and it is independent of the information extracted from experimental data.

In contrast, the determination of the  $B \rightarrow D^*$  matrix elements are not as solid as the one for  $B \rightarrow D$ . As already mentioned in Sec. 2.2.3, there are no available LQCD results at non-zero recoil for the relevant form factors. Only normalization [ $h_{A_1}(1)$ ] has been computed on the lattice while the shapes of the helicity amplitudes were extracted from the angular distribution of  $B \rightarrow D^*(\rightarrow D\pi)l\nu$ . Those values are then combined with the leading order HQET formulas to fix the value of the scalar form factor and then predict  $\mathcal{B}(B \rightarrow D^* \tau \nu_\tau)$ . Extraction of the form factors from the full angular distribution received quite a bit of interest recently. In Refs. [324, 325] the parametrization used to extract the values and shapes of form factors was questioned, and the value of the scalar form factor which was used in the theory paper in which the SM prediction was provided [93] has been recently questioned in Ref. [332]. For all of these reasons, it is fair to say that the value of  $R_{D^*}^{\text{SM}}$  is not nearly as robust as that of  $R_D^{\text{SM}}$ , at least not to the claimed accuracy.

We remind the reader that the decomposition of the matrix elements relevant to the semileptonic  $B \rightarrow D^*$  transition, in terms of form factors, reads

$$\begin{aligned} \langle \bar{D}^*(k, \varepsilon) | \bar{c} \gamma^\mu b | \bar{B}(p) \rangle &= \varepsilon^{\mu\nu\rho\sigma} \varepsilon_\nu^* p_\rho k_\sigma \frac{2V(q^2)}{m_B + m_{D^*}}, \\ \langle \bar{D}^*(k, \varepsilon) | \bar{c} \gamma^\mu \gamma_5 b | \bar{B}(p) \rangle &= i\varepsilon^{*\mu} (m_B + m_{D^*}) A_1(q^2) - i(p+k)^\mu (\varepsilon^* \cdot q) \frac{A_2(q^2)}{m_B + m_{D^*}} \\ &\quad - iq^\mu (\varepsilon^* \cdot q) \frac{2m_{D^*}}{q^2} [A_3(q^2) - A_0(q^2)], \end{aligned} \quad (5.58)$$

where  $\varepsilon^\mu(0, \pm)$  stands for the polarization of the  $D^*$  meson. Similar decomposition in HQET

looks as,

$$\begin{aligned}\langle \bar{D}^*(v', \varepsilon) | \bar{c} \gamma^\mu b | \bar{B}(v) \rangle &= h_V(w) \varepsilon^{\mu\nu\rho\sigma} \varepsilon_\nu^* v_\rho k'_\sigma, \\ \langle \bar{D}^*(v', \varepsilon) | \bar{c} \gamma^\mu \gamma_5 b | \bar{B}(v) \rangle &= i h_{A_1}(w) \varepsilon^{*\mu}(w+1) - i(\varepsilon \cdot v) [h_{A_2}(w)v^\mu + h_{A_3}(w)v'^\mu],\end{aligned}\quad (5.59)$$

where at leading order in the heavy quark expansion  $h_V(w) = h_{A_1}(w) = h_{A_3}(w) = \xi(w)$  where the universal Isgur–Wise function depends on the relative velocity  $w = v \cdot v' = (m_B^2 + m_{D^*}^2 - q^2)/(2m_B m_{D^*})$ , and it is normalized to unity at the zero recoil,  $\xi(1) = 1$ , by virtue of the heavy quark spin/flavor symmetry.

By expanding around the zero recoil, it appears that the form factor  $h_{A_1}(w)$  is the best suited form factor, i.e. closest to the Isgur–Wise function even when the heavy quark power corrections are included.<sup>8</sup> Furthermore it appears to be a very good approximation to retain only the two non-trivial terms in the expansion:

$$\xi(w) = 1 - \rho^2(w-1) + c(w-1)^2 \quad \longrightarrow \quad h_{A_1}(w) = h_{A_1}(1) \left[ 1 - \rho_{A_1}^2(w-1) + c_{A_1}(w-1)^2 \right]. \quad (5.60)$$

Notice that we keep  $h_{A_1}(1)$  since its value is in principle different from unity due to the small power corrections. Using the analyticity and unitarity of QCD one can use the dispersion relation for the form factors in order to relate the slope  $\rho_{A_1}^2$  and the curvature  $c_{A_1}$ . In Refs. [326, 327, 331] the authors derived such constraints on the shape of the form factor

$$A_1(w) = \frac{w+1}{2} \mathcal{R}_{D^*} h_{A_1}(w), \quad (5.61)$$

in the  $z$ -space, i.e. on the disk of radius unity which corresponds to the whole  $q^2$  (or  $w$ ) after applying the conformal mapping

$$z(w) = \frac{\sqrt{w+1} - \sqrt{2}}{\sqrt{w+1} + \sqrt{2}}. \quad (5.62)$$

Unitarity and analyticity then tightly constrain  $c_{A_1}$  which can be expressed in terms of  $\rho_{A_1}^2$  so that in the end one has

$$\frac{A_1(w)}{A_1(1)} = 1 - 8\rho^2 z + (53\rho^2 - 15)z^2 - (231\rho^2 - 91)z^3. \quad (5.63)$$

As for the other form factors that enter the expression for the differential decay rate, by factoring out  $|A_1(w)|^2$ , one deals with the following ratios

$$\begin{aligned}R_1(w) &= \frac{w+1}{2} \mathcal{R}_{D^*} \frac{V(w)}{A_1(w)}, & R_2(w) &= \frac{w+1}{2} \mathcal{R}_{D^*} \frac{A_2(w)}{A_1(w)}, \\ R_0(w) &= \frac{w+1}{2} \mathcal{R}_{D^*} \frac{A_0(w)}{A_1(w)},\end{aligned}\quad (5.64)$$

where, again,  $q^2 = m_B^2 + m_{D^*}^2 - 2m_B m_{D^*} w$ . The shapes of the functions  $R_i(w)$ ,  $i \in (0, 1, 2)$ , cannot be fully inferred on the basis of HQET and additional phenomenological information

---

<sup>8</sup>It is also protected by the so-called Luke theorem which states that the leading order power corrections are absent and only the second order corrections in heavy quark expansion can modify the form factor  $h_{A_1}(w)$ . This is in fact the equivalent to the Ademollo–Gatto theorem in the kaon physics.

is often used. In particular, in Ref. [327] the authors heavily relied on HQET and after expanding around  $w = 1$  they suggested an expansion

$$\begin{aligned} R_1(w) &= R_1(1) - 0.12(w - 1) + 0.05(w - 1)^2, \\ R_2(w) &= R_2(1) + 0.11(w - 1) - 0.06(w - 1)^2, \\ R_0(w) &= R_0(1) - 0.11(w - 1) + 0.01(w - 1)^2, \end{aligned} \quad (5.65)$$

thus only two extra parameters are needed to be extracted from the fit with the angular distribution of the  $B \rightarrow D^* l \nu$  [ $l \in (e, \mu)$ ] data, namely  $R_1(1)$  and  $R_2(1)$ . Even though the authors argued there are also uncertainties in slopes of  $R_1(w)$  and  $R_2(w)$ , the experimentalists used only the central values in the fit. In such a way, for example Belle collaboration reported in Ref. [328]:

$$\begin{aligned} h_{A_1}(1)|V_{cb}| &= (34.6 \pm 1.0) \times 10^{-3}, & \rho^2 &= 1.214 \pm 0.035, \\ R_1(1) &= 1.401 \pm 0.038, & R_2(1) &= 0.864 \pm 0.025. \end{aligned} \quad (5.66)$$

The fact that the slopes of  $R_1(w)$  and  $R_2(w)$  were fixed to the values (partly) dictated by relying on HQET was strongly criticized in Refs. [324, 325], mostly because the HQET predicts  $R_2(1) = 0.80$ , which is about  $2\sigma$  smaller than the value determined by Belle. In other words fixing the slopes by using HQET can be misleading as the tests elsewhere suggest significant deviations at the level of the aimed precision. After the recent publication of the unfolded data by Belle [315], theorists were able to perform the fit to experimental data by leaving these parameters free in the so-called Boyd Grinstein Lebed (BGL) parameterization [331]. The authors of Ref. [324, 325] found then that the values for  $R_2(w^2)$  become systematically larger than the ones obtained in the CLN parameterization. Moreover, the CLN and BGL parameterizations lead to quite different results for  $|V_{cb}|^{\text{excl.}}$ . While the former predicts the value  $|V_{cb}|^{\text{CLN}} = (38.71 \pm 0.75) \times 10^{-3}$  [14], which disagrees with the value determined from the inclusive decays,  $|V_{cb}|^{\text{incl.}} = (41.98 \pm 0.45) \times 10^{-3}$  [14], the fit with the BGL parameterization leads to values which are perfectly consistent with  $|V_{cb}|^{\text{incl.}}$  [324, 325]. Since the fits to the experimental data are equally good, we cannot say that one specific parameterization is better than the other. However, this disagreement is a clear indication that the hadronic inputs entering the  $R_{D^*}$  prediction need to be better understood.

As for  $R_0(w)$ , which enters the prediction for  $\Gamma(B \rightarrow D^* \tau \nu)$ , its value has been obtained in Ref. [93] in a manner similar to what has been advocated by the authors of Ref. [327], but also by fixing the value of  $R_0(1)$  following Ref. [329, 330]

$$R_3(1) \equiv \frac{R_2(1)(1 - r) + r [R_0(1)(1 + r) - 2]}{(1 - r)^2} = 0.97, \quad (5.67)$$

valid to leading order in the power expansion  $1/m_{b,c}$ , where we also for shortness wrote  $r = m_{D^*}/m_B$ . In that way the result reported in Ref. [93]

$$R_0(1) = 1.14 \pm 0.11, \quad (5.68)$$

where the 10% error is a simple guesstimate. Note that this value is consistent with the HQET result  $R_0(1) = 1.22$ . Very recently that result has been revisited by the authors of Ref. [332] who employed the QCD sum rule technique applied to the HQET correlation functions, and found

$$R_0(1) = 1.17 \pm 0.02. \quad (5.69)$$

This value too should be tested by making the explicit computation of the ratio of the form factors on the lattice.

In the following, we will assume that the observed discrepancies in  $R_{D^{(*)}}$  are due to NP. We will focus our discussion on the possible connections between the anomalies in  $b \rightarrow c\tau\nu$  and  $b \rightarrow s\ell\ell$ . As already anticipated in the introduction of Sec. 5.2, the proposed solutions have a compromise between the simplicity of the model and the capability to explain all deviations. We prefer to opt for the latter possibility, since the LFUV deviations in neutral currents still need to be confirmed by another experiment, which will be Belle-II, and because the experimental situation of  $R_{D^{(*)}}$  still needs to be clarified.

### 5.3.2 Simultaneous explanations of $R_{K^{(*)}}$ and $R_{D^{(*)}}$

So far several models have been proposed to simultaneously describe  $R_{K^{(*)}}$  and  $R_{D^{(*)}}$ , see Ref. [333] for a recent review. While many authors considered effective scenarios, very few concrete solutions to the puzzle of  $B$ -physics anomalies have been proposed [334–336]. By using a set of gauge invariant operators the authors usually assume that only the coupling to one generation in the interaction basis is non-zero so that the LFUV comes from the misalignment between the interaction and mass bases [153, 334]. The set of  $SU(3)_c \times SU(2)_L \times U(1)_Y$  gauge invariant operators usually considered is given by

$$\begin{aligned}\mathcal{O}_1^{ijkl} &= (\bar{Q}_i \gamma^\mu Q_j)(\bar{L}_k \gamma^\mu L_l), \\ \mathcal{O}_3^{ijkl} &= (\bar{Q}_i \gamma^\mu \sigma^a Q_j)(\bar{L}_k \gamma^\mu \sigma^a L_l),\end{aligned}\tag{5.70}$$

where  $i, j, k, l$  are family indices and  $\sigma^a$  ( $a = 1, 2, 3$ ) are Pauli matrices. Interestingly, the operator  $\mathcal{O}_3$  generates both charged and neutral currents, which could explain the ensemble of LFUV observations for an appropriate choice of couplings, as first pointed out in Ref. [334].<sup>9</sup> One should, however, be cautious because the renormalization group running from the NP scale to the relevant low energy scale can generate sizable contributions to others operators, such as the ones contributing to the  $Z$ -pole observables and to leptonic  $\tau$  decays. The authors of Ref. [337] argued that an EFT explanation of  $R_{D^{(*)}}$  by means of the operators described in Eq. (5.70) would induce large contributions to  $\mathcal{B}(\tau \rightarrow \mu\nu\nu)/\mathcal{B}(\tau \rightarrow e\nu\nu)$  that would be in conflict with current experimental results, disfavoring a simultaneous EFT explanation based on this set of operators.

The main challenge to build a concrete model to accommodate the  $b \rightarrow s$  and  $b \rightarrow c$  anomalies is that we observe in both cases  $\mathcal{O}(10\%)$  deviations compared to the corresponding SM amplitudes, which are induced at tree-level for the transition  $b \rightarrow c\ell\nu$  and at loop-level for  $b \rightarrow s\ell^+\ell^-$ . As a consequence, an explanation of  $R_{D^{(*)}}$  would require tree-level bosonic mediators in the TeV range, while a tree-level explanation of  $R_{K^{(*)}}$  with similar couplings would point at much larger scales, in the ballpark of  $\approx 30$  TeV [338]. Therefore, a mechanism is needed to explain this hierarchy between the needed contributions. A very appealing solution would be to reproduce the same pattern found in the SM, i.e. to explain  $R_{D^{(*)}}$  via tree-level contributions and  $R_{K^{(*)}}$  through loops. Nonetheless, no fully viable model has been proposed along these lines thus far.<sup>10</sup> Another interesting possibility, which is certainly easier to implement, is to introduce a hierarchial pattern for

<sup>9</sup>This can be easily seen from the identity  $\sigma_{ij}^a \sigma_{kl}^b = 2\delta_{il}\delta_{jk} - \delta_{ij}\delta_{kl}$ .

<sup>10</sup>A first attempt in this direction was made in Ref. [254] by using the LQ state  $(\bar{\mathbf{3}}, \mathbf{1})_{1/3}$ , but we showed in Ref. [155] that this model is not viable, as discussed in Sec. 5.2.4.

the NP couplings to fermions. In this case, the new bosons would couple mostly to the third generation fermions, also providing an explanation for the good experimental agreement found in LFU ratios with kaon and pion decays. This strategy has been followed in Ref. [296, 298, 316, 339] by introducing a minimally broken flavor symmetry  $\mathcal{G}_F$  which, after an appropriate assignment of quantum charges, enforces that only operators with third generation fermions are allowed. The operators containing first and second are then generated by a suitable breaking of this symmetry, which would explain why the effects observed in  $b \rightarrow c\tau\nu$  are larger than the ones found in  $b \rightarrow s\mu\mu$ .

One of the first concrete proposals to explain the observed excess  $R_{D^{(*)}}$  were the 2HDM of different types, including the aligned 2HDM [180] and the (fine-tuned) model of type III [340]. These models face now severe constraints stemming from the  $B_c$  meson lifetime [341–343] and from the studies of high- $p_T$   $\tau$ -leptons tails at the LHC [263].<sup>11</sup> Nonetheless, as it was implicitly stated in Sec. 3.4, the only LFUV contributions in 2HDM to  $b \rightarrow s\ell^+\ell^-$  come from the scalar and pseudoscalar operators, which are not enough to explain the observed deviations in  $R_{K^{(*)}}$ . Therefore, these models cannot simultaneously explain  $R_{K^{(*)}}$  and  $R_{D^{(*)}}$ . Among the models containing color-singlet particles, another proposal is the one of vector-boson weak triplets with hierarchial couplings to fermions [290, 316]. In these scenarios, the  $Z'$  and  $W'$  bosons contribute at tree-level to the transitions  $b \rightarrow s\ell^+\ell^-$  and  $b \rightarrow c\tau\nu$ , respectively. A very comprehensive analysis of this model was performed in Ref. [316], where it was shown that its minimal realization is ruled out by the LHC searches of heavy resonances decaying into  $\tau$  pairs.

Several scenarios with hypothetical light LQ states have also been proposed. While the scenarios with vector LQs are the easiest ones [295, 296, 298] they become problematic when computing the loop corrections unless the vector LQs are promoted into the “light” gauge bosons  $\mathcal{O}(1 \text{ TeV})$ , in which case one runs into contradiction as such gauge bosons are supposed to be associated with a gauge group relevant to the scales of grand unification. Otherwise the loop corrections in a theory with a light vector LQ are UV-cutoff dependent unless the UV completion is explicitly specified. This fact considerably reduces the predictivity of these scenarios, since loop observables which pose severe constraints on LQ scenarios, such as the  $B_s - \bar{B}_s$  mixing amplitude and  $\mathcal{B}(\tau \rightarrow \mu\gamma)$ , cannot be computed. Concerning the light scalar LQ scenarios, instead, they do not exhibit such a problem but in their minimal form they are suitable to either describe  $R_{K^{(*)}}$  [300] or  $R_{D^{(*)}}$  [224], but not both. The only possibility left is to consider non-minimal models where the existence of more than one scalar LQ is postulated. This route was taken in Ref. [344] by considering the pair of scalar LQs  $(\bar{\mathbf{3}}, \mathbf{1})_{1/3}$  and  $(\bar{\mathbf{3}}, \mathbf{3})_{1/3}$  in the context of a minimally broken flavor symmetry. Similarly, the authors of Ref. [301] postulated the existence of two light scalar LQs transforming as  $(\mathbf{3}, \mathbf{2})_{1/6}$  and  $(\bar{\mathbf{3}}, \mathbf{3})_{1/3}$  in a concrete GUT realization. Interestingly, the problematic diquark couplings of the LQ triplet are forbidden in this latter scenario by a suitable choice of the  $SU(5)$  quantum charges.

Finally, we attempted to simultaneously address the  $b \rightarrow c$  and  $b \rightarrow s$  anomalies by minimally extending the model with the scalar LQ  $(\mathbf{3}, \mathbf{2})_{1/6}$ . By postulating the existence of light right-handed neutrinos we showed in Ref. [345] that this model can satisfactorily explain  $R_K^{\text{exp}} < R_K^{\text{SM}}$  and  $R_{D^{(*)}}^{\text{exp}} > R_{D^{(*)}}^{\text{SM}}$ . However, the recent measurement of  $R_{K^*}$  by LHCb disfavored this scenario, since it predicts  $R_{K^*}$  to be slightly larger than the SM prediction. In the following Section, we will describe this model to illustrate the situation in model building in flavor physics: it is a very challenging task to propose a minimal model capable

<sup>11</sup>See Ref. [343] for a recent and comprehensive analysis of effective scenarios aiming to explain  $R_{D^{(*)}}$  via scalar operators.

of explaining both  $R_{K^{(*)}}$  and  $R_{D^{(*)}}$  while being consistent with the plethora of constraints coming from the flavor physics observables.

### 5.3.3 $(\mathbf{3}, 2)_{1/6}$ and light right-handed neutrinos

The model containing the state  $(\mathbf{3}, 2)_{1/6}$  was originally proposed as a viable explanation of  $R_K^{\text{exp}} < R_K^{\text{SM}}$  in Ref. [118]. In this Section, we will show that the minimal inclusion of light RH neutrinos to this scenario induces new contributions to charged current processes, which can accommodate  $R_{D^{(*)}}^{\text{exp}} > R_{D^{(*)}}^{\text{SM}}$  [345].

In the presence of three gauge singlets  $\nu_{Rj}$  ( $j = 1, 2, 3$ ), the Lagrangian (4.31) becomes

$$\mathcal{L}_{\Delta^{(1/6)}} = (y_L)_{ij} \bar{d}_{Ri} \widetilde{\Delta}^{(1/6)\dagger} L_j + (y_R)_{ij} \bar{Q}_i \Delta^{(1/6)} \nu_{R,j} + \text{h.c.}, \quad (5.71)$$

where  $y_{L,R}$  are generic  $3 \times 3$  Yukawa matrices. This expression can be further developed in terms of the fermionic mass eigenstates

$$\begin{aligned} \mathcal{L}_{\Delta^{(1/6)}} = & (y_L U)_{ij} \bar{d}_{Ri} \nu_{Lj} \Delta^{(-1/3)} - (y_L)_{ij} \bar{d}_{Ri} \ell_{Lj} \Delta^{(2/3)} \\ & + (V y_R)_{ij} \bar{u}_{Li} \nu_{Rj} \Delta^{(2/3)} + (y_R)_{ij} \bar{d}_{Li} \nu_{Rj} \Delta^{(-1/3)} + \text{h.c.}, \end{aligned} \quad (5.72)$$

where  $U$  denotes the leptonic mixing matrix, and  $\Delta^{(\mathcal{Q})}$  denote the LQ mass eigenstates with electric charge  $\mathcal{Q}$ , as before. From this expression, we observe that a coupling between up-type quarks and neutrinos is induced by the RH couplings which could potentially contribute to the  $b \rightarrow c\tau\nu$  decays and to  $R_{D^{(*)}}$  in particular. To study the charged currents with RH neutrinos, we find it convenient to define the effective Lagrangian

$$\begin{aligned} \mathcal{L}_{\text{eff}} = & -2\sqrt{2} G_F V_{ud} \left[ (\bar{u}_L \gamma_\mu d_L) (\bar{\ell}_L \gamma^\mu \nu_L) + g_S^R(\mu) (\bar{u}_L d_R) (\bar{\ell}_L \nu_R) \right. \\ & \left. + g_T^R(\mu) (\bar{u}_L \sigma_{\mu\nu} d_R) (\bar{\ell}_L \sigma^{\mu\nu} \nu_R) \right] + \text{h.c.}, \end{aligned} \quad (5.73)$$

where  $u/d$  stands for a generic up-/down-type quark, while  $g_{S,T}^R \equiv g_{S,T}^R|_{d \rightarrow u\ell\nu}$  are the effective couplings induced by New Physics. This equation should be compared to Eq. (2.3), where the possibility of having RH neutrinos was not considered.

In the following, we assume that the neutrino masses are negligible in comparison with the hadronic mass scales, so that it is legitimate to take  $U = \mathbb{1}$  for the PMNS matrix. We consider neutrinos to be Dirac particles, even though this issue is immaterial in the limit of  $m_\nu \rightarrow 0$ .<sup>12</sup> We describe below the effective Lagrangian of the  $(\mathbf{3}, \mathbf{2})_{1/6}$  scenario extended with RH neutrinos, and we discuss the phenomenological implications.

#### Effective Lagrangian

The low energy effective theory obtained by integrating out the heavy  $\Delta$  has the following Lagrangian

$$\mathcal{L}_{\text{eff}} = \mathcal{L}_{\text{eff}}^{d \rightarrow d' \ell \ell'} + \mathcal{L}_{\text{eff}}^{d \rightarrow d' \nu \nu} + \mathcal{L}_{\text{eff}}^{d \rightarrow u \ell \nu} + \mathcal{L}_{\text{eff}}^{u \rightarrow u' \nu \nu'}, \quad (5.74)$$

where the piece affecting the  $b \rightarrow s\mu\mu$  transition described in Eq. (4.32) remains unchanged:

<sup>12</sup>Notice that the effective Lagrangian for  $b \rightarrow c\tau\nu$  would be the same for Dirac and Majorana neutrinos.

$$\mathcal{L}_{\text{eff}}^{d \rightarrow d' \ell \ell'} = -\frac{(y_L)_{ij}(y_L)_{kl}^*}{2m_\Delta^2} (\bar{d}_i \gamma^\mu P_R d_k) (\bar{\ell}_l \gamma_\mu P_L \ell_j). \quad (5.75)$$

The novelty of our model is the presence of the following terms

$$\mathcal{L}_{\text{eff}}^{d \rightarrow u \ell \nu} = \frac{(V y_R)_{ij}(y_L)_{kl}^*}{2m_\Delta^2} \left[ (\bar{u}_i P_R d_k) (\bar{\ell}_l P_R \nu_j) + \frac{1}{4} (\bar{u}_i \sigma_{\mu\nu} P_R d_k) (\bar{\ell}_l \sigma^{\mu\nu} P_R \nu_j) \right] + \text{h.c.}, \quad (5.76)$$

which are induced by the right-handed couplings. This Lagrangian can modify the transition  $b \rightarrow c\ell\nu$ , with  $\ell = e, \mu, \tau$ , as mentioned before. Notice that the flavor of the neutrino is generic in this expression and one should compare the experimental results with

$$\mathcal{B}(B \rightarrow D\ell\nu) \equiv \sum_{\ell'=e,\mu,\tau} \mathcal{B}(B \rightarrow D\ell\nu_{\ell'}), \quad (5.77)$$

where a similar expression should also be used for leptonic decays. Finally, the last two pieces in Eq. 5.74 are given by

$$\begin{aligned} \mathcal{L}_{\text{eff}}^{d \rightarrow d' \nu \nu} = & - \sum_{\alpha=L,R} \frac{(y_\alpha)_{ij}(y_\alpha)_{kl}^*}{2m_\Delta^2} (\bar{d}_i \gamma^\mu (1 - P_\alpha) d_k) (\bar{\nu}_l \gamma_\mu P_\alpha \nu_j) \\ & - \frac{(y_L)_{ij}(y_R)_{kl}^*}{2m_\Delta^2} \left[ (\bar{d}_i P_L d_k) (\bar{\ell}_l P_L \nu_j) + \frac{1}{4} (\bar{d}_i \sigma_{\mu\nu} P_L d_k) (\bar{\ell}_l \sigma^{\mu\nu} P_L \nu_j) \right], \end{aligned} \quad (5.78)$$

where two new terms induced by the couplings  $(y_R)_{k\ell}$  appeared, and by

$$\mathcal{L}_{\text{eff}}^{u \rightarrow u' \nu \nu'} = -\frac{(V y_R)_{ij}(V y_R)_{kl}^*}{2m_\Delta^2} (\bar{u}_i \gamma^\mu P_R u_k) (\bar{\nu}_l \gamma_\mu P_L \nu_j), \quad (5.79)$$

which is not phenomenologically interesting, since there are no compelling experimental results regarding this transition.<sup>13</sup> These expressions will be used in the phenomenological discussion below.

### Flavor physics constraints

Similarly to the discussion of Sec. 5.2.5, we take the couplings to the first generation to be zero in order to avoid the potential problems with the atomic parity violating experiments, as well as the experimental limits on  $\mathcal{B}(K \rightarrow \pi\nu\nu)$  and  $\mathcal{B}(B_s \rightarrow \mu e)$ . We will assume the following structure of the matrices of Yukawa couplings:

$$y_{L,R} = \begin{pmatrix} 0 & 0 & 0 \\ 0 & (y_{L,R})_{s\mu} & (y_{L,R})_{s\tau} \\ 0 & (y_{L,R})_{b\mu} & (y_{L,R})_{b\tau} \end{pmatrix}, \quad (5.80)$$

<sup>13</sup>To our knowledge, the only available experimental limit is  $\mathcal{B}(J/\Psi \rightarrow \bar{\nu}\nu) < 3.9 \times 10^{-3}$  [311], which is still significantly away from the SM prediction.

which implies that

$$Vy_R = \begin{pmatrix} 0 & V_{us}(y_R)_{s\mu} + V_{ub}(y_R)_{b\mu} & V_{us}(y_R)_{s\tau} + V_{ub}(y_R)_{b\tau} \\ 0 & V_{cs}(y_R)_{s\mu} + V_{cb}(y_R)_{b\mu} & V_{cs}(y_R)_{s\tau} + V_{cb}(y_R)_{b\tau} \\ 0 & V_{ts}(y_R)_{s\mu} + V_{tb}(y_R)_{b\mu} & V_{ts}(y_R)_{s\tau} + V_{tb}(y_R)_{b\tau} \end{pmatrix}. \quad (5.81)$$

Although the couplings to first generation fermions are set to zero in Eq. (5.71), it is clear from Eq. (5.81) that contributions to the leptonic and semileptonic decays of kaons ( $s \rightarrow u$ ) or  $B$ -mesons ( $b \rightarrow u$ ) are not absent. Therefore, constraints involving the up quark, such as  $\mathcal{B}(B^+ \rightarrow \tau^+\nu)$  and  $\mathcal{B}(K^+ \rightarrow \mu^+\nu)$  must be taken into account.

The values of the couplings  $(y_{L,R})_{ij}$ , which we take to be real, are varied within the perturbative limits,  $|(y_{L,R})_{ij}| < \sqrt{4\pi}$ , and are subject to many constraints of which the following ones are found to be particularly relevant:

- $b \rightarrow s\mu\mu$ :

As described in Sec. 5.2.1, we consider the cfrom the experimentally established  $\mathcal{B}(B_s \rightarrow \mu\mu)$  and  $\mathcal{B}(B^+ \rightarrow K^+\mu\mu)$  in the large  $q^2$  bin, which imply the constraints  $(C_9^{\mu\mu})' = -(C_{10}^{\mu\mu})' \in (-0.44, -0.12)$  to  $1\sigma$  accuracy. This results can be translated as a constraint on the combination  $(y_L)_{b\mu}(y_L)_{s\mu}^*/m_\Delta^2$  by using Eq. (4.34). The allowed values lead to the prediction  $R_K = 0.88(8)$ , consistent with the experimental value found by LHCb, cf. (5.2). This model also predicts  $R_{K^*}^{\text{central}} = 1.11(9)$  which is slightly larger than the SM prediction. Therefore, this model would be ruled out if  $R_{K^*} < 1$  is confirmed, cf. Eq. (5.3).

- $\Delta m_{B_s}$ :

Another important constraint stems from the  $B_s - \bar{B}_s$  amplitude. We computed  $R_{B_s} = \Delta m_{B_s}/\Delta m_{B_s}^{\text{SM}}$  in our model, which reads

$$R_{B_s} = 1 + \frac{\eta_1}{16G_F^2 m_W^2 (V_{tb}V_{ts}^*)^2 \eta_B S_0(x_t) m_\Delta^2} \times \left[ (y_L \cdot y_L^\dagger)_{bs}^2 + \frac{1}{2} (y_R \cdot y_R^\dagger)_{bs}^2 - \eta_{41} \frac{3}{2} (y_L \cdot y_L^\dagger)_{bs} (y_R \cdot y_R^\dagger)_{bs} \left( \frac{m_{B_s}}{m_b(m_b) + m_s(m_b)} \right)^2 \frac{B_4(m_b)}{B_1(m_b)} \right], \quad (5.82)$$

where we use the standard notation for  $\Delta m_{B_s}^{\text{SM}}$ ,  $\eta_1 = 0.82(1)$  and  $\eta_{41} = 4.4(1)$  account for the QCD evolution from  $\mu \simeq 1$  TeV down to  $\mu = m_b$ . After combining the lattice QCD values for bag parameters  $B_{1,4}$  [77, 346], with the experimental  $R_{B_s}^{\text{exp}} = 1.02(10)$ , we obtain a rather stringent constraint on the couplings shown in the brackets of Eq. (5.82).

- $\tau \rightarrow \mu\phi$ :

The experimental upper limit  $\mathcal{B}(\tau \rightarrow \mu\phi) < 8.4 \times 10^{-8}$  [310] can be used to constraint  $(y_L)_{s\mu}/m_\Delta$  and  $(y_L)_{s\tau}/m_\Delta$  via the expression

$$\mathcal{B}(\tau \rightarrow \mu\phi) = \frac{f_\phi^2 m_\tau^3}{512\pi\Gamma_\tau} \left| \frac{(y_L)_{s\tau}(y_L)_{s\mu}^*}{m_\Delta^2} \right|^2 (1-x)(1+x-2x^2), \quad (5.83)$$

where  $x = m_\phi^2/m_\tau^2$  and  $f_\phi = 241(18)$  MeV [347]. The terms proportional to  $m_\mu^2/m_\tau^2$  were omitted in this equation.

- $B \rightarrow K\nu\bar{\nu}$ :

The experimental upper limit on  $\mathcal{B}(B \rightarrow K\nu\bar{\nu})$  [310] turns out to be a very important constraint too. The relevant expression for this process computed in the SM extended by the effective Lagrangian is

$$\begin{aligned} \mathcal{B}(B \rightarrow K\nu_i\bar{\nu}_j) &= \frac{|\mathcal{N}|^2\lambda_B^{1/2}}{384\pi^3 m_B^3 \Gamma_B} \left\{ |f_+(q^2)|^2 \lambda_B \left[ |C_{LL}^{ij} + C_{LR}^{ij}|^2 + |C_{LR}^{ij}|^2 \right] \right. \\ &\quad + |f_0(q^2)|^2 \frac{3q^2}{2(m_b - m_s)^2} (m_B^2 - m_K^2)^2 |C_{S,LL}^{ij}|^2 \\ &\quad \left. + |f_T(q^2)|^2 \lambda_B \frac{2q^2}{(m_B + m_K)^2} |C_{T,LL}^{ij}|^2 \right\}, \end{aligned} \quad (5.84)$$

where  $\mathcal{N} = \alpha_{\text{em}} G_F V_{tb} V_{ts}^* / (\sqrt{2}\pi)$ . After summing over the neutrinos states, the auxiliary coefficients in the given above read

$$\begin{aligned} \sum_{ij} |C_{LL}^{ij} + C_{LR}^{ij}|^2 &= 3|C_L^{\text{SM}}|^2 + \frac{C_{LL}^{\text{SM}}}{2\mathcal{N}m_\Delta^2} \text{Re}(y_L \cdot y_L^\dagger)_{sb} + \frac{1}{16|\mathcal{N}|^2 m_\Delta^4} (y_L \cdot y_L^\dagger)_{ss} (y_L \cdot y_L^\dagger)_{bb}, \\ \sum_{ij} |C_{S,LL}^{ij}|^2 &= 16 \sum_{ij} |C_{T,LL}^{ij}|^2 = \frac{1}{16|\mathcal{N}|^2 m_\Delta^4} (y_L \cdot y_L^\dagger)_{ss} (y_R \cdot y_R^\dagger)_{bb}, \\ \sum_{ij} |C_{RR}^{ij}|^2 &= \frac{1}{16|\mathcal{N}|^2 m_\Delta^4} (y_R \cdot y_R^\dagger)_{ss} (y_R \cdot y_R^\dagger)_{bb}, \end{aligned} \quad (5.85)$$

where  $C_L^{\text{SM}} = -6.83(6)$  denotes the SM contribution, as before [348].

- Leptonic decays:

Also useful are the constraints coming from the (semi-)leptonic meson decays. Using the Lagrangian (5.73), one can easily compute the decay rates for various leptonic processes. For example, we obtained

$$\Gamma(D_s \rightarrow \ell\bar{\nu}) = \frac{G_F^2}{8\pi m_{D_s}^3} |V_{cs}|^2 f_{D_s}^2 (m_{D_s}^2 - m_\ell^2)^2 m_\ell^2 \left[ 1 + |g_S^R|^2 \frac{m_{D_s}^4}{m_\ell^2 (m_c + m_s)^2} \right], \quad (5.86)$$

where the matching of Eq. (5.73) and (5.76) gives

$$(g_S^R)_{c \rightarrow s\ell\nu_j} = \frac{(V y_R)^{cj} y_L^{si*}}{4\sqrt{2} G_F V_{cs} m_\Delta^2}, \quad (5.87)$$

at the scale  $\mu = m_\Delta \approx 1$  TeV, which is via the QCD running related to the scales where the LQCD simulations are performed, namely,  $g_S(\mu = 1 \text{ TeV}) \approx 0.5 \times g_S(\mu = m_b) \approx 0.37 \times g_S(\mu = 2 \text{ GeV})$ . Note that if we replace  $g_S \rightarrow g_S^R$ , then Eq. (5.86) coincides with Eq. (2.9) except for the interference term which does not exist for

RH neutrinos. Since neutrinos are unobserved, one should sum over all possible final states. The absence of interference term allow us to define

$$\left| \left( g_S^R \right)_{c \rightarrow s\mu\nu} \right|^2 \equiv \left| \left( g_S^R \right)_{c \rightarrow s\mu\nu_\mu} \right|^2 + \left| \left( g_S^R \right)_{c \rightarrow s\mu\nu_\tau} \right|^2, \quad (5.88)$$

which can be directly used in Eq. (5.86) to obtain  $\mathcal{B}(D_s \rightarrow \ell\nu) = \mathcal{B}(D_s \rightarrow \ell\nu_\mu) + \mathcal{B}(D_s \rightarrow \ell\nu_\tau)$ . The same expression can be applied *mutatis mutandis* for the other leptonic decays, namely,  $\mathcal{B}(K \rightarrow \mu\nu)$ ,  $\mathcal{B}(\tau \rightarrow K\nu)$  and  $\mathcal{B}(B \rightarrow \tau\nu)$ , for which the relevant decay constants are summarized in Tab. 2.1. Experimental results are taken from Ref. [310]. We do not include constraints from semi-leptonic decays in our analysis, since these are superseded by the analogous leptonic modes. This can be understood from the helicity suppression which is lifted by the scalar Wilson coefficient  $g_S^R$  in Eq. (5.86).

- $R_D^{\mu/e}$ :

An important constraint for NP scenarios with couplings to  $\mu$ 's is the ratio

$$R_D^{\mu/e} = \frac{\mathcal{B}(B \rightarrow D\mu\nu)}{\mathcal{B}(B \rightarrow De\nu)}, \quad (5.89)$$

which was first considered in Ref. [316] and then also used in Ref. [155] to challenge a putative simultaneous explanation of  $R_K$  and  $R_D$ , cf. Sec. 5.2.4. The relevant expression for the differential branching ratio, obtained by using the Lagrangian (5.73), is given by

$$\begin{aligned} \frac{d\mathcal{B}}{dq^2}(B \rightarrow D\ell\nu) = \mathcal{B}_0 |V_{cb}|^2 |f_+(q^2)|^2 & \left\{ c_+^\ell(q^2) + |g_T^R|^2 c_T^\ell(q^2) \left| \frac{f_T(q^2)}{f_+(q^2)} \right|^2 \right. \\ & \left. + \left( 1 + |g_S^R|^2 \frac{q^4}{m_\ell^2 (m_b - m_c)^2} \right) c_0^\ell(q^2) \left| \frac{f_0(q^2)}{f_+(q^2)} \right|^2 \right\}, \end{aligned} \quad (5.90)$$

where  $\mathcal{B}_l = G_F^2 \tau_B / (192\pi^3 m_B^3)$ , as before, and the coefficient functions are given again by Eq. (2.30). Using the form factors from Ref. [16] and requiring  $R_D^{\mu/e} < 1.02$  [314, 316], we obtain a powerful constraint on the couplings,

$$g_S^R(\mu = m_\Delta) \Big|_{b \rightarrow c\ell_i \bar{\nu}_j} = 4 g_T^R(\mu = m_\Delta) \Big|_{b \rightarrow c\ell_i \bar{\nu}_j} = \frac{(Vy_R)^{cj} y_L^{bi*}}{4\sqrt{2}G_F V_{cb} m_\Delta^2}, \quad (5.91)$$

where the QCD running accounts for  $g_T^R(\mu = 1 \text{ TeV}) \approx 1.3 \times g_T^R(\mu = m_b) \approx 1.4 \times g_T^R(\mu = 2 \text{ GeV})$ , and the tensor form factor is taken from Ref. [349]. We stress once again that modes with different neutrino flavors should be added to obtain the rates

$$\mathcal{B}(B \rightarrow D\mu\nu) = \sum_{\ell'=\mu,\tau} \mathcal{B}(B \rightarrow D\mu\nu_{\ell'}), \quad (5.92)$$

which can be effectively done by redefining the effective coefficients  $g_{S,T}^R$  similarly to Eq. (5.88).

Other observables, such as leptonic decays of  $\phi(nS)$  and  $\Upsilon(nS)$ , could in principle provide useful bounds on the LQ couplings, but the derived limits turn out to be less significant at this point. Flavor conserving leptonic decays, such as  $\Upsilon(nS) \rightarrow \tau\tau$ , are dominated by the very large tree-level electromagnetic contribution which undermines their sensitivity to NP. LFV modes, such as  $\Upsilon \rightarrow \mu\tau$ , are in principle sensitive to the LQ contribution but the current experimental limit  $\mathcal{B}(\Upsilon(1S) \rightarrow \mu\tau)^{\text{exp}} < 6 \times 10^{-6}$  [350] is still too weak to be useful. Moreover, an additional suppression to the decay rates comes from the larger width of the vector quarkonia. For instance, the width of  $\Upsilon$ ,  $\Gamma_\Upsilon = 54.02 \pm 1.25$  keV, is many orders of magnitude larger than the width of  $B_{(s)}$  mesons [22],

$$\frac{\Gamma_{\Upsilon(1S)}}{\Gamma_{B_{d(s)}}} \approx 10^8. \quad (5.93)$$

This can be easily understood from the fact that  $B_{(s)}$ -meson decays proceed through electroweak interactions, while  $\Upsilon(nS)$  can decay directly through strong and electromagnetic interactions. Therefore, potential NP contributions to electroweak decays of quarkonia are always diluted in the branching ratios by the large total width. Therefore, we can say on general grounds that any search for NP effects in quarkonia decay modes would require a much better accuracy than the one needed for instance in the  $B_{(s)}$  system.

Finally, we have also checked that the experimental limit on  $\mathcal{B}(\tau \rightarrow \mu\gamma) < 4.4 \times 10^{-8}$  [317] does not provide any additional constraint to this model because of an accidental cancellation of terms  $\propto 1/m_\Delta^2$  in the loop function [155]:

$$\sigma_L^{(1/6)} = 0, \quad \sigma_R^{(1/6)} = -i(y_L)_{b\mu}(y_L)_{b\tau}^* \frac{N_C m_b^2 m_\tau}{96\pi^2 m_\Delta^4} \left[ \frac{5}{2} + \log\left(\frac{m_b^2}{m_\Delta^2}\right) \right], \quad (5.94)$$

where we use the same notation as in Eq. (5.40).<sup>14</sup> This expression should be compared to Eq. (5.41), where the leading contribution is proportional to  $1/m_\Delta^2$ , instead of  $1/m_\Delta^4$ , and where the top quark mass can enhance the loop-function.

We are now in a position to combine the ingredients given above in order to constraint the Yukawa couplings  $(y_{L,R})_{ij}$ , which are then used to compute the effective coefficients (5.91). After inserting those couplings into Eq. (5.90) we can compute  $R_D = \mathcal{B}(B \rightarrow D\tau\nu)/\mathcal{B}(B \rightarrow D\ell\nu)$ . The result is shown in Fig. (5.17) where we see that with all of the constraints discussed above, our model not only gives  $R_K = 0.88(8)$  compatible with the experimental finding, but we are also able to find parameters which are compatible with  $R_D^{\text{exp}}$  at the  $\approx 1.1\sigma$  level. In this scan, we kept the leptoquark mass fixed at  $m_\Delta = 650$  GeV and also required consistency with the direct search limits [259, 261], which will be discussed at the end of this Section. We plot the correlation between the allowed couplings  $(y_L)_{b\tau}$ ,  $(y_R)_{b\tau}$  in Fig. 5.18, where we see that one needs  $|(y_L)_{b\tau}| \gtrsim 1.4$  to reduce the tension in  $R_D$ . The RH coupling  $(y_R)_{b\tau}$  can help reducing the tension in  $R_D$ , and it has an anti-correlation with  $(y_L)_{b\tau}$ , i.e. large  $(y_R)_{b\tau}$  implies small  $(y_L)_{b\tau}$ . In the same plot, we highlight the points consistent with  $R_D^{\text{exp}}$  to  $1.5\sigma$  accuracy (in black), which seem to be uniformly distributed. The correlation between  $(y_L)_{b\mu}$ ,  $(y_L)_{b\tau}$  is also shown in Fig. 5.17, where we see that they can take any value, but small values are preferred for a better description of  $R_D^{\text{exp}}$ , as expected. Finally, we use the expressions encountered in the literature for the  $B \rightarrow D^*$  form factors to estimate  $R_{D^*}/R_{D^*}^{\text{SM}}$  in Fig. 5.19, c.f. discussion in Sec. 5.3.1. Nonetheless, if one believes

<sup>14</sup>Notice that for the same reason  $(g-2)_\mu$  remains highly suppressed and experimentally indistinguishable from its SM prediction.

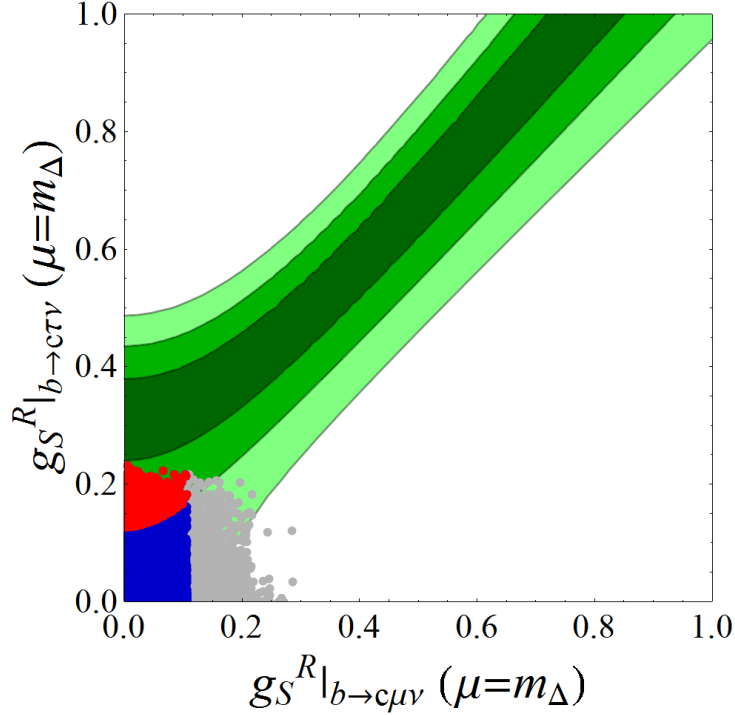


**Figure 5.17:** The ensemble of points (all colors combined) correspond to our model in the case  $m_\Delta = 650$  GeV after applying all the constraints on Yukawa couplings discussed in this Section except for the  $R_D^{\mu/e}$  constraint. They are shown in the plane  $g_S^R|_{b \rightarrow c\tau\nu}$  Vs.  $g_S^R|_{b \rightarrow c\mu\nu}$ , against the green regions which represent  $R_D$  at 1-, 2- and 3- $\sigma$ . Red and blue points are selected after imposing consistency with  $R_D^{\mu/e}$ . Finally the red points alone indicate the compatibility with  $R_D$  to  $2\sigma$ .

in these expression for the form factors, then this model can produce an enhancement of about 5% in addition to the quoted SM error. This statement needs to be confirmed by computing the  $B \rightarrow D^*$  form factors on the lattice.

We also performed a second scan of parameters by leaving  $m_\Delta$  as a free parameter, and then checked how the prediction of  $R_D$  changes as a function of the leptoquark mass. We considered the range  $m_\Delta \in (500, 3000)$  GeV and applied the direct searches constraints for third-generation LQs that will be described at the end of this Section. The result of this exercise is shown in Fig. 5.20, from which we learn that the  $2\sigma$  compatibility with  $R_D^{\text{exp}}$  implies  $m_\Delta \in (590, 1200)$  GeV. Larger LQ masses are excluded by the perturbative conditions, which is taken to be  $|(y_{L,R})| < \sqrt{4\pi}$ , while smaller masses are in conflict with the bounds obtained from the direct searches [259, 261].

## Predictions

With the Yukawa couplings constrained in a way discussed in the previous Section, we could show that we are able to accommodate  $R_K^{\text{exp}} < R_K^{\text{SM}}$  and  $R_{D^{(*)}}^{\text{exp}} > R_{D^{(*)}}^{\text{SM}}$ . In this Section, we discuss several predictions that could be used to test this scenario in modern day experiments. In the scenario  $m_\Delta = 650$  GeV, we obtained that:

- The value of  $\mathcal{B}(B_s \rightarrow \tau\tau)$  can be both larger and smaller than the SM one since the sign of the Wilson coefficient  $(C_{10}^{\tau\tau})'$  is not fixed by the flavor constraints. We found

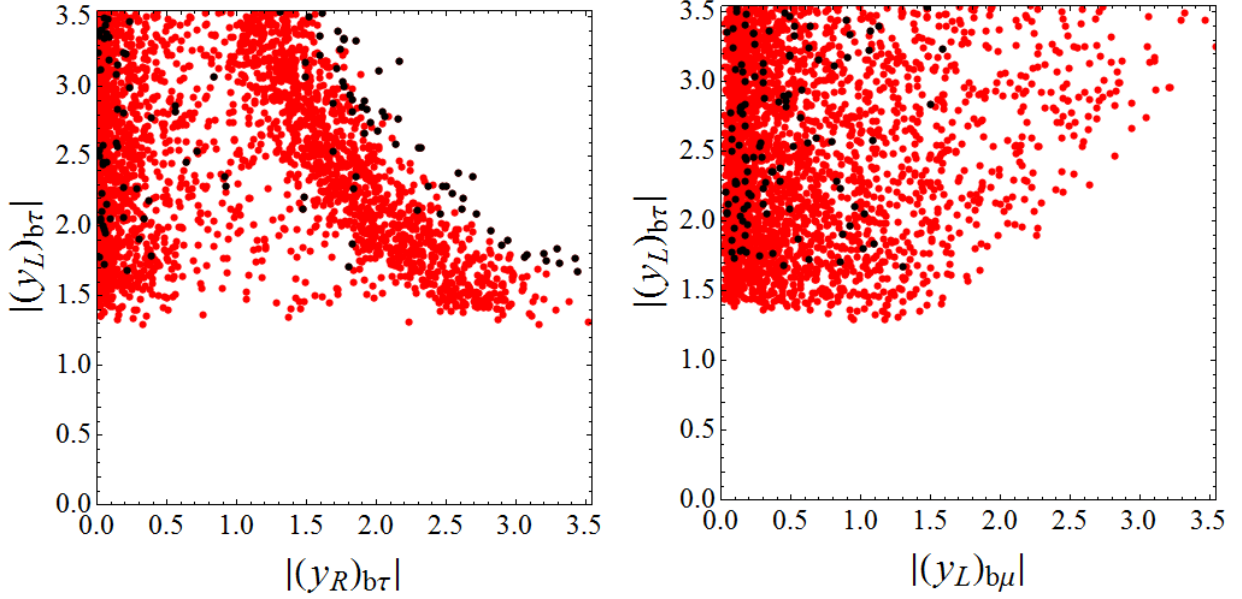


**Figure 5.18:** Correlations of allowed couplings in the planes  $((y_R)_{b\tau}, (y_L)_{b\tau})$  (left panel) and  $((y_L)_{b\mu}, (y_L)_{b\tau})$  (right plane). The red points are consistent with  $R_D^{\text{exp}}$  to  $2\sigma$  accuracy, as in Fig. 5.18. We highlight in black the points with a consistency with  $R_D^{\text{exp}}$  at the  $1.5\sigma$  level.

that

$$0 \leq \frac{\mathcal{B}(B_s \rightarrow \tau\tau)}{\mathcal{B}(B_s \rightarrow \tau\tau)^{\text{SM}}} < 15, \quad (5.95)$$

which is still far from the current limit  $\mathcal{B}(B_s \rightarrow \tau\tau) < 6.8 \times 10^{-3}$  (95% CL) obtained by the LHCb collaboration [352].<sup>15</sup>

- Using the expressions presented in Section 2.3, we also computed the lepton flavor violating decay rate  $\mathcal{B}(B \rightarrow K\mu\tau)$  and found that

$$8 \times 10^{-10} \leq \mathcal{B}(B \rightarrow K\mu\tau) \leq 5 \times 10^{-6}, \quad (5.96)$$

which is shown in Fig. 5.21. Notice that the similar LFV modes are easily inferred from the bounds given above, by using Eq. (2.149).

- Similarly to  $R_D > R_D^{\text{SM}}$ , we find that the ratio  $R_{\eta_c} = \mathcal{B}(B_c \rightarrow \eta_c \tau \nu) / \mathcal{B}(B_c \rightarrow \eta_c l \nu)$  can be larger than its SM value. Using the recent  $B_c \rightarrow \eta_c$  decay form factor values computed on the lattice [86] and the results for  $g_S^R|_{b \rightarrow c l_i \bar{\nu}_j}$  discussed above, we obtained

$$1.06 \leq \frac{R_{\eta_c}}{R_{\eta_c}^{\text{SM}}} \leq 1.22, \quad (5.97)$$

which is also plotted in Fig. 5.21.

<sup>15</sup>Notice that one could have  $\mathcal{B}(B_s \rightarrow \tau\tau) \approx 0$ , since the NP contribution to  $C_{10}$  can interfere destructively with the SM one.

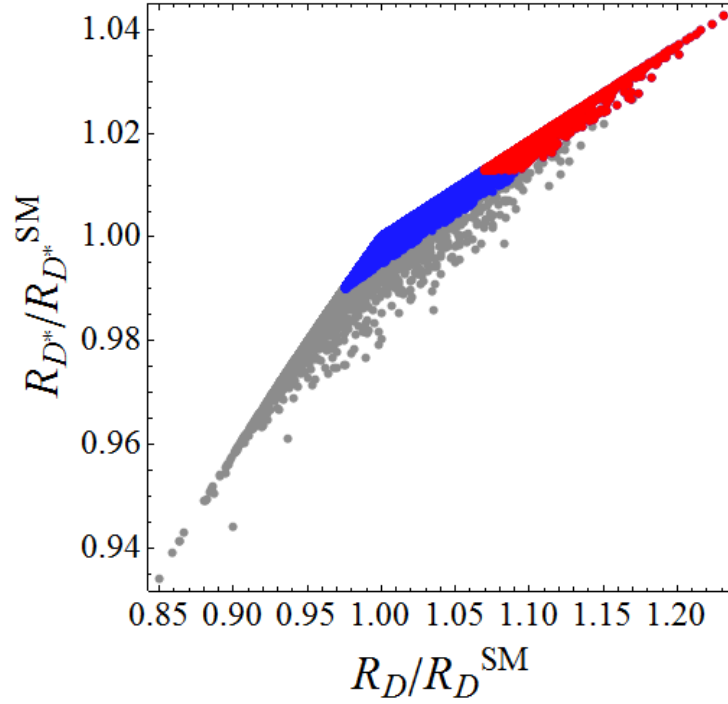


**Figure 5.19:** Correlation of  $R_D/R_D^{\text{SM}}$  and  $R_{D^*}/R_{D^*}^{\text{SM}}$  for the allowed points. For simplicity, we only show the central values for both observables. See Fig. 5.17 for the color code.

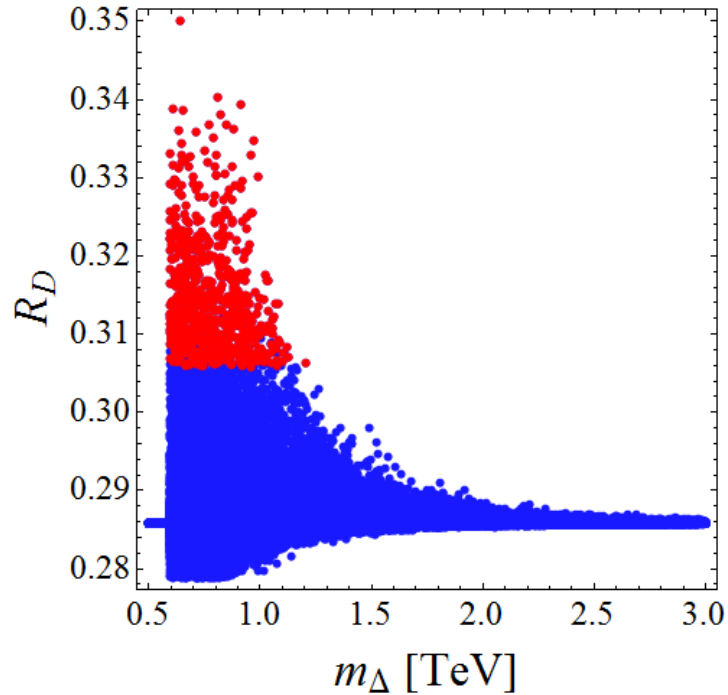


**Figure 5.20:** Results of our scan of parameters consistent with all constraints discussed in the previous section in which the leptoquark mass  $m_{\Delta}$  is varied too. We see that the combination of direct search limits with the  $2\sigma$  consistency requirement with  $R_D^{\text{exp}}$  results in  $m_{\Delta} \in (590, 1200)$  GeV. See Fig. 5.18 for the color code (gray points are not shown in this plot).

- A very interesting feature of this model is not only that the different leptonic decays of  $B_c$  are modified differently, but the fact that  $\mathcal{B}(B_c \rightarrow \tau\nu)$  we obtain is strictly larger than the SM value:

$$2.2 \leq \frac{\mathcal{B}(B_c \rightarrow \tau\nu)}{\mathcal{B}(B_c \rightarrow \tau\nu)^{\text{SM}}} \leq 5.0, \quad (5.98)$$

which offers another possibility to experimentally test the validity of our model. On the other hand, the value of  $\mathcal{B}(B_c \rightarrow \mu\nu)$  that we obtain can be either equal to its SM value or enhanced by up to a few orders of magnitude.

As extensively discussed in Section 5.2, scenarios with primed Wilson coefficients cannot accommodate the hints of  $R_{K^*}^{\text{exp}} < R_{K^*}^{\text{SM}}$ . If confirmed, this result would exclude the model discussed above as an explanation of the muons anomalies, since it predicts  $R_{K^*}$  to be slightly larger than the SM prediction. Nevertheless, it remains a viable model to describe  $R_{D^{(*)}}$ . This also illustrates the current situation in model building in the flavor physics community. Many new experimental data help either corroborating an hypothesis or to select among various models. Therefore, we indeed use data to do physics.

### Implications for Direct Searches

Finally, we comment on the attempts to detect the LQ states of this specific model at the LHC. Since the explanation of  $R_{D^{(*)}}$  requires large couplings to the third generation,  $(y_L)_{b\tau}$  and/or  $(y_R)_{b\tau}$ , the main decay modes of our model are

$$\Delta^{(-1/3)} \rightarrow b\nu, \quad \text{and} \quad \Delta^{(2/3)} \rightarrow b\tau, t\nu. \quad (5.99)$$

Other possible final states are

$$\Delta^{(-1/3)} \rightarrow s\nu, b\nu, \quad \text{and} \quad \Delta^{(2/3)} \rightarrow s\mu, b\mu, s\tau, c\nu, \quad (5.100)$$

depending on the structure of the Yukawa matrices  $y_{L,R}$ .<sup>16</sup> The expression for the relevant decay rates of  $\Delta^{(2/3)}$  are

$$\Gamma(\Delta^{(2/3)} \rightarrow d_i \ell_j) = \frac{m_\Delta}{16\pi} |(y_L)_{ij}|^2, \quad (5.101)$$

$$\Gamma(\Delta^{(2/3)} \rightarrow u_i \nu) = \frac{m_\Delta}{16\pi} \left(1 - \frac{m_{u_i}^2}{m_\Delta^2}\right)^2 \sum_{k=\mu,\tau} |(Vy_R)_{ik}|^2, \quad (5.102)$$

and similarly to the state  $\Delta^{(-1/3)}$ ,

$$\Gamma(\Delta^{(-1/3)} \rightarrow d_i \nu) = \frac{m_\Delta}{16\pi} \sum_{j=\mu,\tau} \left[ |(y_L)_{ik}|^2 + |(y_R)_{ik}|^2 \right], \quad (5.103)$$

where  $i, j$  are flavor indices. We only kept the up-type mass in the above equations, since  $m_t$  is the only fermion mass which is not negligible with respect to  $m_\Delta$ .

<sup>16</sup>The decay  $\Delta^{(2/3)} \rightarrow u\nu$  is also possible, but it is Cabibbo suppressed in our model.

So far, the most stringent limit on third generation leptoquark is  $m_\Delta > 900$  GeV, which was obtained by the CMS collaboration with the assumption  $\mathcal{B}(\Delta \rightarrow \tau b) = 1$  [260]. Similarly to the discussion at the end of Sec. 5.2.5, this bound becomes considerably weaker in a more realistic scenario where other decay modes are also allowed. For instance, we rescaled the limits from Ref. [259] in the case where  $\mathcal{B}(\Delta^{(2/3)} \rightarrow \tau b)$  is smaller than one, cf. discussion in Sec. 5.3.3. The result was shown in Fig. 4.6, where we can see that the bound drops considerably to  $m_\Delta \gtrsim 500$  GeV if  $\mathcal{B}(\Delta^{(2/3)} \rightarrow \tau b) = 0.5$ , for example. We showed in the same figure a similar recast of the searches performed in Ref. [261] for a pair of LQs decaying into  $\Delta^{(2/3)} \rightarrow \tau\nu$  and  $\Delta^{(-1/3)} \rightarrow b\nu$ . We stress once again that all these limits were considered in the scans of parameter space presented above, from which we extracted the interval  $m_\Delta \in (590, 1200)$  GeV, which is consistent with direct and indirect limits on LQs.

Finally, we should mention that the LQ model presented here is still perfectly consistent with the limits derived on Ref. [263] by studying the tails of high- $p_T$   $\tau$ -leptons at the LHC. By considering the  $t$ -channel LQ contribution to  $b\bar{b} \rightarrow \tau^+\tau^-$ , they derived the limit  $|(y_L)_{b\tau}| \lesssim 3$  for  $m_\Delta \approx 650$  GeV, which is still perfectly consistent with the results shown in Fig. 5.18. Note that the situation might change in the future with more data accumulated at the LHC. These searches have the potential to confirm or refute this scenario as an explanation of  $R_{D^{(*)}}$  since the couplings  $|(y_L)_{b\tau}|$  are bounded from below, as discussed above.

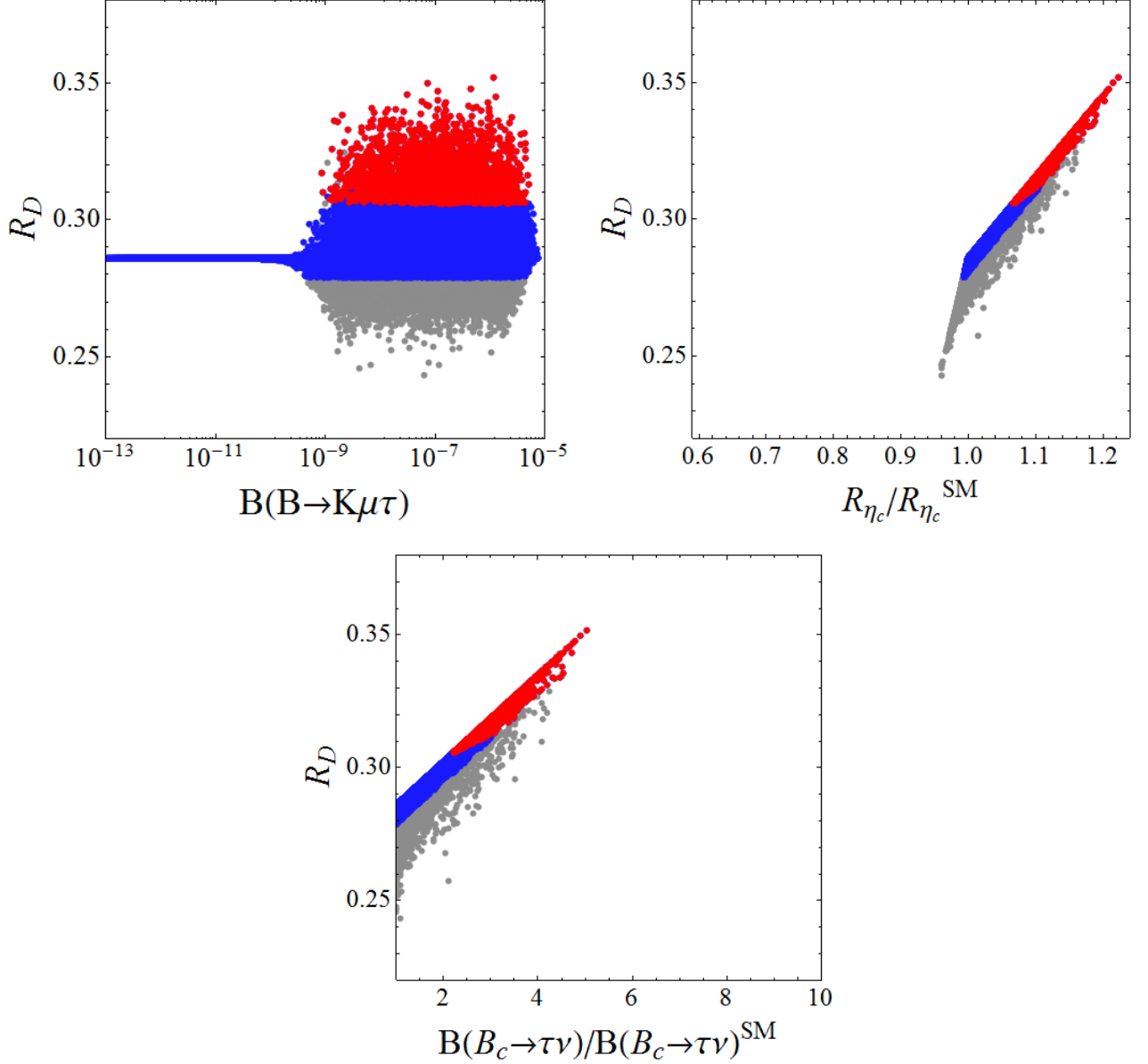


**Figure 5.21:** Colors of the points are the same as in Fig. 5.19: the blue points are obtained by subjecting the Yukawa couplings of our model to the constraints discussed in the text, and the red ones are selected from the blue ones after requiring the compatibility with  $R_D^{\text{exp}}$  to  $2\sigma$ . We plot our predictions for three selected quantities: limits on the LFV decay mode, i.e. its  $B(B \rightarrow K \mu \tau)$ , the ratio between  $R_{\eta_c} = \mathcal{B}(B_c \rightarrow \eta_c \tau \bar{\nu})/\mathcal{B}(B_c \rightarrow \eta_c l \bar{\nu})$  predicted by our model and its SM value, and a similar ratio of  $\mathcal{B}(B_c \rightarrow \tau \bar{\nu})$  which appears to be strictly larger than its SM estimate.

# Conclusion

In this thesis we aspired to extract information about physics beyond the SM by using the flavor physics observables. Our ultimate goal was to formulate a theory of flavor based on the experimental results which could explain the Yukawa structure in terms of fewer and more fundamental parameters. To that purpose, we used the experimental findings as the main guideline to choose the preferred NP scenarios. A first part of this thesis is dedicated to 2HDM. The Higgs sector was the last piece of the SM fixed by experiment, and the current level of precision still allows for observable signals both in indirect and direct searches related to the scalar sector. We discussed the general lessons that can be learned on the spectrum of 2HDM by using the theoretical and phenomenological constraints, and we explored the repercussion of the new degrees of freedom in different low energy observables, including tree-level and loop-level meson decays. In particular, we discussed the scenario with a CP-odd Higgs lighter than the scalar boson observed at the LHC which escaped observation thus far, and we propose strategies to probe this particle in modern day experiments. Such a boson would be most welcome as a new mediator between the SM and the dark sector. A second part of this thesis was devoted to the phenomenon of lepton flavor universality violation observed in the exclusive decays based on the transitions  $b \rightarrow s\ell^+\ell^-$  and  $b \rightarrow c\tau\nu$ . If confirmed, these signal would be a legitimate manifestation of NP which could be related to the flavor breaking mechanism beyond the SM. Within the 2HDM scenarios these effects are found to be small. To accommodate the observed LFUV we introduced the various scalar LQ scenarios, which provide one of the best candidates thus far. We scrutinized the proposed solutions, showing that one of the popular scenarios in the literature is not viable, and we proposed minimal models which can accommodate some of the observed discrepancies by relying on new mechanisms. Furthermore, we explored the possibilities of searching for signs of LFV through similar decay modes, which offer a clean alternative to test most of the NP explanations. The main results discussed in this thesis are summarized below:

- We discussed the general limits that can be derived on the spectrum of 2HDM by applying the general theory and phenomenology constraints. The allowed parameters were then confronted with the constraints from leptonic and semileptonic meson decays, which constrains the tree-level contribution from a charged Higgs. Furthermore, we showed that 2HDM scenarios with a light CP-odd Higgs ( $m_A < m_h$ ) are perfectly plausible with current theory and phenomenology constraints.
- We computed the complete set of Wilson coefficients for the transition  $b \rightarrow s\ell^+\ell^-$  in the context of 2HDM devised with a  $\mathbb{Z}_2$  symmetry [186]. Regarding the scalar and pseudoscalar operators, we elucidated the issue of appropriate matching between the full and the effective theory when keeping the external momenta different from zero is necessary. To that purpose, we introduced an extended basis of operators which

include the ones suppressed by  $1/m_W$  that must be used for the unambiguous matching. Finally, we confronted our results for the Wilson coefficients with the measured  $\mathcal{B}(B_s \rightarrow \mu^+\mu^-)$  and  $\mathcal{B}(B \rightarrow K\mu^+\mu^-)_{\text{high-}q^2}$ , and derived the repercussion for the various 2HDM.

- We proposed new strategies to investigate the presence of a light CP-odd Higgs in indirect searches: (i) We showed that the exclusive Higgs decays  $\mathcal{B}(h \rightarrow \eta_{c,b}\tau^+\tau^-)$  can be an order of magnitude larger than the SM prediction for the models of type II and X [204]; (ii) We proposed the observables  $\mathcal{B}(\eta_b \rightarrow \mu^+\mu^-)$  and  $\mathcal{B}(\eta_b \rightarrow \tau^+\tau^-)$  as a new probe of light pseudoscalar particles, since they can be enhanced by several orders of magnitude in the type II 2HDM. The experimental study of these observables, which have been scarcely explored so far, can help disentangling among the various 2HDM scenarios.
- We revisited a  $SU(5)$  scenario where the unification of gauge couplings is achieved via the simple addition of light scalar LQ  $(\mathbf{3}, \mathbf{2})_{1/6}$  from two  $\mathbf{10}$  multiplets [229]. We found that the lightest LQ state is required to have a mass in the range  $m_\Delta \in (0.4, 16)$  TeV, being possibly accessible at the LHC. Furthermore, we addressed two shortcomings of the original proposal: (i) We demonstrated that a mass splitting in the  $\mathbf{24}$ -plet preserves unification and provides a straightforward way to raise the unification scale, which can then avoid the current limits on the proton lifetime; (ii) We showed that a  $U(1)_{\text{PQ}}$  symmetry can be used to forbid a term in Lagrangian which would induce the proton decay via dimension-9 operators.
- We derived the expressions for the full decay rates of the decay modes  $B_s \rightarrow \ell_1^\pm \ell_2^\mp$  and  $B \rightarrow K^{(*)} \ell_1^\pm \ell_2^\mp$  with  $\ell_1, \ell_2 = e, \mu, \tau$  by relying on a general EFT. We used these expressions to explore the connection between LFUV and LFV in explicit scenarios, including  $Z'$  models [127] and the scenarios with the various LQ states [155]. As a by-product of our work, we also clarified some inconsistencies in the expressions for the  $B \rightarrow K^* \mu^+ \mu^-$  angular observables found in the literature [127].
- We explored to what extent the observed LFUV in  $R_{K^{(*)}}$  and  $R_{D^{(*)}}$  can be explained by LQ scenarios. By performing a complete flavor analysis, we argued that the singlet LQ state  $(\bar{\mathbf{3}}, 1)_{1/3}$  cannot provide a simultaneous explanation to the LFU puzzles in tree-level and loop-induced decays [155]. We proposed a new scalar LQ model which can explain the deviations in  $R_{K^{(*)}}$  through loop contributions [319]. This model is based on the state  $(\mathbf{3}, \mathbf{2})_{7/6}$ , to which a specific flavor ansatz on the Yukawa matrices is imposed to forbid the tree-level contributions to  $b \rightarrow s\ell^+\ell^-$ , which only appear at loop-level. We reinterpreted the limits from the direct searches performed at the LHC and showed that this scenario is consistent with those, as well as with the ensemble of indirect constraints. Furthermore, we predict that the mass of this LQ satisfies  $m_\Delta \lesssim 2$  TeV, a fact that can be directly tested at the LHC.
- We proposed a scalar LQ model which includes the light right-handed neutrinos that can explain the deviations in  $R_K$  and  $R_{D^{(*)}}$  [345]. This model has been disfavored

since the measurement of  $R_{K^*}$  by LHCb, but it remains a viable model to explain  $R_{D^{(*)}}$ . Among the predictions of this scenario, we showed that strong signatures can be observed in LFV  $B$  meson decays,  $B_s \rightarrow \mu^\pm \tau^\mp$  and  $B \rightarrow K^{(*)} \mu^\pm \tau^\mp$ . Furthermore, we predict an enhancement of  $\mathcal{B}(B_c \rightarrow \tau \nu)$  and  $R_{\eta_c} = \mathcal{B}(B_c \rightarrow \eta_c \tau \nu) / \mathcal{B}(B_c \rightarrow \eta_c l \nu)$  ( $l = e, \mu$ ) which can be tested at the LHC and at Belle-II in the near future.

It should be clear that the solutions to the problems addressed in this thesis remain a work in progress. Firstly, the question of whether the Higgs boson is the one predicted by the SM remains unanswered, the answer of which will require a combined effort of indirect and direct experimental searches. Furthermore, while the updated LHCb results on  $R_{K^{(*)}}$  and  $R_{D^{(*)}}$  and the Belle-II determination of the same observables are waited, the issue of LFUV remains an open question. One should also keep in mind that the anomalous magnetic momentum  $(g-2)_\mu$  presents a  $\approx 3.6\sigma$  discrepancy with respect to the SM [353]. This discrepancy will be soon confirmed or refuted by the joint effort between the experimental groups at Fermilab and the LQCD community, which are working on reducing the experimental and theoretical uncertainties. To propose a minimal scenario which can simultaneously explain the observed deviations while complying with the plethora of direct and indirect constraints is a very challenging task to which no convincing solution has emerged yet. Furthermore, it remains not clear if the observed pattern of deviations is a manifestation of flavor breaking beyond the SM, or other mechanism of NP possibly related to the one of the SM problems.

Hopefully, the answer to these above-mentioned questions will soon be provided by the collective effort of the flavor physics experiments at NA62, BES-III and LHCb with the future ones at Belle-II, KOTO, TREK,  $(g-2)_\mu$  and Mu2E, which will provide us with an unprecedented amount of data. The combination of these results with the direct searches performed at the LHC will serve as a guide to the theoretical effort towards a better understanding of the flavor breaking mechanism beyond the SM and will possibly help solving some of the long standing problems in theoretical physics.

## Publication List

1. **“Seeking the CP-odd Higgs via  $h \rightarrow \eta_{c,b} \ell^+ \ell^-$ ”**  
D. Bečirević, B. Melić, M. Patra and O. Sumensari.  
[arXiv:1705.01112](#) [hep-ph]
2. **“A leptoquark model to accommodate  $R_K^{\text{exp}} < R_K^{\text{SM}}$  and  $R_{K^*}^{\text{exp}} < R_{K^*}^{\text{SM}}$ ”**  
D. Bečirević and O. Sumensari.  
[arXiv:1704.05835](#) [hep-ph]  
JHEP **1708** (2017) 104
3. **“Two Higgs Doublet Models and  $b \rightarrow s$  exclusive decays”**  
P. Arnan, D. Bečirević, F. Mescia and O. Sumensari.  
[arXiv:1703.03426](#) [hep-ph]
4. **“Sterile neutrinos facing kaon physics experiments”**  
A. Abada, D. Bečirević, O. Sumensari, C. Weiland and R. Zukanovich Funchal.  
[arXiv:1612.04737](#) [hep-ph]  
Phys. Rev. D **95**, no. 7, 075023 (2017)
5. **“SU(5) Unification with TeV-scale Leptoquarks”**  
P. Cox, A. Kusenko, O. Sumensari and T. T. Yanagida.  
[arXiv:1612.03923](#) [hep-ph]  
JHEP **1703**, 035 (2017)
6. **“Leptoquark model to explain the  $B$ -physics anomalies,  $R_K$  and  $R_D$ ”**  
D. Bečirević, S. Fajfer, N. Košnik and O. Sumensari.  
[arXiv:1608.08501](#) [hep-ph]  
Phys. Rev. D **94**, no. 11, 115021 (2016)
7. **“Palatable leptoquark scenarios for lepton flavor violation in exclusive  $b \rightarrow s \ell_1 \ell_2$  modes”**  
D. Bečirević, N. Košnik, O. Sumensari and R. Zukanovich Funchal.  
[arXiv:1608.07583](#) [hep-ph]  
JHEP **1611** (2016) 035
8. **“Lepton flavor violation in exclusive  $b \rightarrow s$  decays”**  
D. Bečirević, O. Sumensari and R. Zukanovich Funchal.  
[arXiv:1602.00881](#) [hep-ph]  
Eur. Phys. J. C **76**, no. 3, 134 (2016)
9. **“Can the new resonance at LHC be a CP-Odd Higgs boson?”**  
D. Bečirević, E. Bertuzzo, O. Sumensari and R. Zukanovich Funchal.  
[arXiv:1512.05623](#) [hep-ph]  
Phys. Lett. B **757**, 261 (2016)
10. **“Limits on neutrinophilic two-Higgs-doublet models from flavor physics”**  
E. Bertuzzo, Y. F. Perez G., O. Sumensari and R. Zukanovich Funchal.  
[arXiv:1510.04284](#) [hep-ph]  
JHEP **1601**, 018 (2016)

11. **“On the viability of minimal neutrinophilic two-Higgs-doublet models”**  
P. A. N. Machado, Y. F. Perez, O. Sumensari, Z. Tabrizi and R. Zukanovich Funchal.  
[arXiv:1507.07550](https://arxiv.org/abs/1507.07550) [hep-ph]  
JHEP **1512**, 160 (2015)
  
12. **“Lepton flavor violating decays of vector quarkonia and of the  $Z$  boson”**  
A. Abada, D. Bečirević, M. Lucente and O. Sumensari.  
[arXiv:1503.04159](https://arxiv.org/abs/1503.04159) [hep-ph]  
Phys. Rev. D **91**, no. 11, 113013 (2015)

# Appendix A

## Useful identities

### A.1 Fierz identities

The Fierz identities used in this thesis are listed below:

$$(P_L)_{ij}(P_L)_{kl} = \frac{1}{2}(P_L)_{il}(P_L)_{kj} + \frac{1}{8}(\sigma^{\mu\nu}P_L)_{il}(\sigma_{\mu\nu}P_L)_{kj}, \quad (\text{A.1})$$

$$(P_L)_{ij}(P_R)_{kl} = \frac{1}{2}(\gamma^\mu P_R)_{il}(\gamma^\mu P_L)_{kj}, \quad (\text{A.2})$$

$$(\gamma_\mu P_L)_{ij}(\gamma^\mu P_L)_{kl} = -(\gamma_\mu P_L)_{il}(\gamma^\mu P_L)_{kj}, \quad (\text{A.3})$$

$$(\gamma_\mu P_L)_{ij}(\gamma^\mu P_R)_{kl} = 2(P_L)_{il}(P_R)_{kj}. \quad (\text{A.4})$$

The sign changes due to fermion field ordering are not included. The identities with a flipped chirality can be obtained by the trivial replacement  $P_{L,R} \rightarrow P_{R,L}$ .

### A.2 Passarino-Veltman Functions

In this appendix we list the analytic expression for some of the Passarino-Veltman (PV) functions. The scalar PV functions are defined in  $d = 4 - \varepsilon$  dimensions by the expressions [185]

$$A_0(m_0^2) = \frac{(2\pi\mu)^\varepsilon}{i\pi^2} \int d^d k \frac{1}{k^2 - m_0^2}, \quad (\text{A.5})$$

$$B_0(r_{10}^2, m_0^2, m_1^2) = \frac{(2\pi\mu)^\varepsilon}{i\pi^2} \int d^d k \prod_{i=0}^1 \frac{1}{[(k+r_i)^2 - m_i^2]}, \quad (\text{A.6})$$

$$C_0(r_{10}^2, r_{12}^2, r_{20}^2, m_0^2, m_1^2, m_2^2) = \frac{(2\pi\mu)^\varepsilon}{i\pi^2} \int d^d k \prod_{i=0}^2 \frac{1}{[(k+r_i)^2 - m_i^2]}, \quad (\text{A.7})$$

$$D_0(r_{10}^2, r_{12}^2, r_{23}^2, r_{30}^2, r_{20}^2, r_{13}^2, m_0^2, \dots, m_3^2) = \frac{(2\pi\mu)^\varepsilon}{i\pi^2} \int d^d k \prod_{i=0}^3 \frac{1}{[(k+r_i)^2 - m_i^2]}, \quad (\text{A.8})$$

where  $r_{ij} = (r_i - r_j)^2 \forall i, j \in \{0, 1, \dots, n-1\}$ . By convention  $r_0 = 0$ , so that  $r_{i0}^2 = r_i^2$ . These integrals can be computed by using dimension regularization in  $d = 4 - \varepsilon$  dimensions, and by using the Feynman trick. The general results for the first two functions are given by

$$A_0(m^2) = m^2 \left( \Delta_\varepsilon + 1 - \log \frac{m^2}{\mu^2} \right), \quad (\text{A.9})$$

$$B_0(p^2, m_0^2, m_1^2) = \Delta_\varepsilon - \int_0^1 dx \log \left[ \frac{-x(1-x)p^2 + xm_1^2 + (1-x)m_0^2}{\mu^2} \right], \quad (\text{A.10})$$

where  $\mu$  is the renormalization scale and  $\Delta_\varepsilon = 2/\varepsilon - \gamma_E + \log(4\pi)$  contains the UV divergent piece in  $d = 4$ . The three and four point PV functions are finite and given in general by

$$C_0(r_{10}^2, r_{12}^2, r_{20}^2, m_0^2, m_1^2, m_2^2) = - \int_0^1 dx \int_0^{1-y} dx \frac{1}{\Delta_C(x, y)}, \quad (\text{A.11})$$

$$D_0(r_{10}^2, r_{12}^2, r_{23}^2, r_{30}^2, r_{20}^2, r_{13}^2, m_0^2, \dots, m_3^2) = \int_0^1 dx \int_0^{1-x} dy \int_0^{1-x-y} dz \frac{1}{\Delta_D(x, y, z)^2}, \quad (\text{A.12})$$

where the functions in the denominators read

$$\begin{aligned} \Delta_C(x, y) &= m_0^2(1-x-y) + xm_1^2 + ym_2^2 - x(1-x)r_{10}^2 - y(1-y)r_{20}^2 \\ &\quad + xy(r_{10}^2 + r_{20}^2 - r_{21}^2), \end{aligned} \quad (\text{A.13})$$

and

$$\begin{aligned} \Delta_D(x, y, z) &= m_0^2(1-x-y-z) + xm_1^2 + ym_2^2 + zm_3^2 - x(1-x)r_{10}^2 \\ &\quad - y(1-y)r_{20}^2 - z(1-z)r_{30}^2 + xy(r_{20}^2 + r_{10}^2 - r_{21}^2) \\ &\quad + xz(r_{30}^2 + r_{10}^2 - r_{31}^2) + yz(r_{30}^2 + r_{20}^2 - r_{32}^2). \end{aligned} \quad (\text{A.14})$$

The analytical computation of the finite integrals given above can be particularly difficult for non-zero external momenta  $r_i$ . We give below the results when  $r_{ij}^2 = 0 \forall i, j$ :

$$B_0(0, m_0^2, m_1^2) = \Delta_\varepsilon + 1 - \frac{m_0^2 \log m_0^2 - m_1^2 \log m_1^2}{m_0^2 - m_1^2}, \quad (\text{A.15})$$

$$C_0(0, 0, 0, m_0^2, m_1^2, m_2^2) = - \frac{1}{m_0^2} \frac{1}{t_1 - t_2} \left[ \frac{t_1 \log t_1}{t_1 - 1} - \frac{t_2 \log t_2}{t_2 - 1} \right], \quad (\text{A.16})$$

$$\begin{aligned} D_0(0, \dots, 0, m_0^2, \dots, m_3^2) &= \frac{1}{2m_0^2} \left[ \frac{t_1^2 \log t_1}{(t_1 - 1)(t_1 - t_2)(t_1 - t_3)} \right. \\ &\quad \left. - \frac{t_2^2 \log t_2}{(t_2 - 1)(t_1 - t_2)(t_2 - t_3)} + \frac{t_3^2 \log t_3}{(t_3 - 1)(t_1 - t_3)(t_2 - t_3)} \right], \end{aligned} \quad (\text{A.17})$$

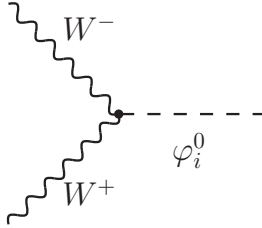
where  $t_i = m_i^2/m_0^2$  for  $i = 1, 2, 3$ .

# Appendix B

## 2HDM

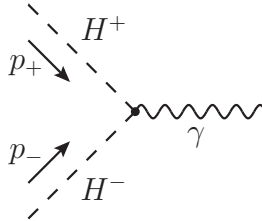
### B.1 Feynman rules for 2HDM

In this Appendix we collect the Feynman rules used in our computation. For the couplings between the gauge bosons and the scalars we have

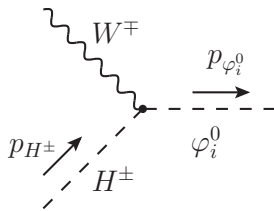


$$igm_W \lambda_{W^+W^-}^{\varphi_i^0} g^{\mu\nu}, \quad (\text{B.1})$$

where  $\lambda_{W^+W^-}^h = \sin(\beta - \alpha)$ ,  $\lambda_{W^+W^-}^H = \cos(\beta - \alpha)$  and  $\lambda_{W^+W^-}^A = 0$ . Similarly, we also have



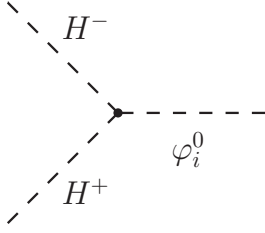
$$ie(p_- - p_+)^{\mu}, \quad (\text{B.2})$$



$$\pm \frac{ig}{2} \lambda_{H^{\pm}W^{\mp}}^{\varphi_i^0} (p_{H^{\pm}} + p_{\varphi_i^0})^{\mu}, \quad (\text{B.3})$$

where  $\lambda_{H^{\pm}W^{\mp}}^h = \cos(\beta - \alpha)$ ,  $\lambda_{H^{\pm}W^{\mp}}^H = -\sin(\beta - \alpha)$ , and  $\lambda_{H^{\pm}W^{\mp}}^A = \mp i$ , depending on the

charges of the initial particles. For the trilinear scalar interactions, we have



$$iv\lambda_{H^+H^-}^{\varphi_i^0} \quad (\text{B.4})$$

where the trilinear couplings read

$$\begin{aligned} \lambda_{H^+H^-}^h &= -\frac{m_h^2[3\cos(\alpha+\beta)+\cos(\alpha-3\beta)]+4\sin(2\beta)\sin(\beta-\alpha)m_{H^\pm}^2-4M^2\cos(\alpha+\beta)}{2v^2\sin(2\beta)}, \\ \lambda_{H^+H^-}^H &= -\frac{m_H^2[3\sin(\alpha+\beta)+\sin(\alpha-3\beta)]+4\sin(2\beta)\cos(\beta-\alpha)m_{H^\pm}^2-4M^2\sin(\alpha+\beta)}{2v^2\sin(2\beta)}, \\ \lambda_{H^+H^-}^A &= 0. \end{aligned} \quad (\text{B.5})$$

These results agree with the ones given in Refs. [182, 199] after the appropriate change of basis and/or conventions. <sup>1</sup>

## B.2 Auxiliary functions

In this Appendix we give the expressions for the functions ( $f_i$  and  $g_i$ ) used in this thesis. The auxiliary functions  $g_{0,1,2}$  used in Eq. (3.61) are defined by [186]

$$g_0 = \frac{1}{4(x_{H^\pm} - x_t)} \left\{ \zeta_d \zeta_u^* \left[ \frac{x_t}{x_{H^\pm} - x_t} \log\left(\frac{x_{H^\pm}}{x_t}\right) - 1 \right] + |\zeta_u|^2 \left[ \frac{x_t^2}{2(x_{H^\pm} - x_t)^2} \log\left(\frac{x_{H^\pm}}{x_t}\right) + \frac{x_{H^\pm} - 3x_t}{4(x_{H^\pm} - x_t)} \right] \right\}, \quad (\text{B.6})$$

$$g_1 = -\frac{3}{4} + \zeta_d \zeta_u^* \frac{x_t}{x_{H^\pm} - x_t} \left[ 1 - \frac{x_{H^\pm}}{x_{H^\pm} - x_t} \log\left(\frac{x_{H^\pm}}{x_t}\right) \right] + |\zeta_u|^2 \frac{x_t}{2(x_{H^\pm} - x_t)^2} \left[ \frac{x_{H^\pm} + x_t}{2} - \frac{x_{H^\pm} x_t}{x_{H^\pm} - x_t} \log\left(\frac{x_{H^\pm}}{x_t}\right) \right], \quad (\text{B.7})$$

$$g_2 = \zeta_d(\zeta_d \zeta_u^* + 1) f_1(x_t, x_{H^\pm}) + \zeta_d (\zeta_u^*)^2 f_2(x_t, x_{H^\pm}) + \zeta_d |\zeta_u|^2 f_3(x_t, x_{H^\pm}) + \zeta_u |\zeta_u|^2 f_4(x_t, x_{H^\pm}) - \zeta_u^* |\zeta_u|^2 f_5(x_t, x_{H^\pm}) + \zeta_u f_6(x_t, x_{H^\pm}) - \zeta_u^* f_7(x_t, x_{H^\pm}), \quad (\text{B.8})$$

with

$$f_1(x_t, x_{H^\pm}) = \frac{1}{2(x_{H^\pm} - x_t)} [-x_{H^\pm} + x_t + x_{H^\pm} \log x_{H^\pm} - x_t \log x_t], \quad (\text{B.9})$$

$$f_2(x_t, x_{H^\pm}) = \frac{1}{2(x_{H^\pm} - x_t)} \left[ x_t - \frac{x_{H^\pm} x_t}{x_{H^\pm} - x_t} \log\left(\frac{x_{H^\pm}}{x_t}\right) \right], \quad (\text{B.10})$$

<sup>1</sup>Notice that our  $\lambda$  is  $-\lambda$  of Ref. [182].

$$f_3(x_t, x_{H^\pm}) = \frac{1}{2(x_{H^\pm} - x_t)} \left[ x_{H^\pm} - \frac{x_{H^\pm}^2 \log x_{H^\pm}}{x_{H^\pm} - x_t} + \frac{x_t(2x_{H^\pm} - x_t) \log x_t}{x_{H^\pm} - x_t} \right], \quad (\text{B.11})$$

$$f_4(x_t, x_{H^\pm}) = \frac{1}{4(x_{H^\pm} - x_t)^2} \left[ \frac{x_t(3x_{H^\pm} - x_t)}{2} - \frac{x_{H^\pm}^2 x_t}{x_{H^\pm} - x_t} \log \left( \frac{x_{H^\pm}}{x_t} \right) \right], \quad (\text{B.12})$$

$$f_5(x_t, x_{H^\pm}) = \frac{1}{4(x_{H^\pm} - x_t)^2} \left[ \frac{x_t(x_{H^\pm} - 3x_t)}{2} - \frac{x_{H^\pm} x_t (x_{H^\pm} - 2x_t)}{x_{H^\pm} - x_t} \log \left( \frac{x_{H^\pm}}{x_t} \right) \right], \quad (\text{B.13})$$

$$f_6(x_t, x_{H^\pm}) = \frac{1}{2(x_{H^\pm} - x_t)} \left[ \frac{x_t(x_t^2 - 3x_{H^\pm} x_t + 9x_{H^\pm} - 5x_t - 2)}{4(x_t - 1)^2} \right. \quad (\text{B.14})$$

$$+ \frac{x_{H^\pm}(x_{H^\pm} x_t - 3x_{H^\pm} + 2x_t) \log x_{H^\pm}}{2(x_{H^\pm} - 1)(x_{H^\pm} - x_t)} \\ \left. + \frac{x_{H^\pm}^2(-2x_t^3 + 6x_t^2 - 9x_t + 2) + 3x_{H^\pm} x_t^2(x_t^2 - 2x_t + 3) - x_t^2(2x_t^3 - 3x_t^2 + 3x_t + 1)}{2(x_t - 1)^3(x_{H^\pm} - x_t)} \log x_t \right],$$

$$f_7(x_t, x_{H^\pm}) = \frac{1}{2(x_{H^\pm} - x_t)} \left[ \frac{(x_t^2 + x_t - 8)(x_{H^\pm} - x_t)}{4(x_t - 1)^2} - \frac{x_{H^\pm}(x_{H^\pm} + 2)}{2(x_{H^\pm} - 1)} \log x_{H^\pm} \right. \quad (\text{B.15}) \\ \left. + \frac{x_{H^\pm}(x_t^3 - 3x_t^2 + 3x_t + 2) + 3(x_t - 2)x_t^2}{2(x_t - 1)^3} \log x_t \right].$$

Notice that in the above expressions we assumed the couplings  $\zeta_f \in \mathbb{C}$  in order to keep our formulas as general as possible, although in the body of the paper we consistently used  $\zeta_f \in \mathbb{R}$ .

### B.2.1 Wilson Coefficients for the Derivative Operators

In this subsection we present the explicit expressions for the Wilson coefficients relevant to the derivative operators given in Eq. (3.65). From the  $Z$ -penguins we obtain,

$$C_{RR}^{\mathcal{T}q} = |\zeta_u|^2 \frac{\sqrt{x_b} x_t}{72} \left\{ \frac{3(x_{H^\pm}^2 - 5x_{H^\pm} x_t - 2x_t^2)}{(x_{H^\pm} - x_t)^3} + \frac{18x_{H^\pm} x_t^2}{(x_{H^\pm} - x_t)^4} \log \left( \frac{x_{H^\pm}}{x_t} \right) \right. \\ \left. - 2 \sin^2 \theta_W \left[ \frac{7x_{H^\pm}^2 - 5x_{H^\pm} x_t - 8x_t^2}{(x_{H^\pm} - x_t)^3} - \frac{6x_{H^\pm} x_t (2x_{H^\pm} - 3x_t)}{(x_{H^\pm} - x_t)^4} \log \left( \frac{x_{H^\pm}}{x_t} \right) \right] \right\} \quad (\text{B.16}) \\ + \zeta_u^* \zeta_d \frac{\sqrt{x_b} x_t}{24} \left\{ \frac{3(x_{H^\pm} - 3x_t)}{(x_{H^\pm} - x_t)^2} - \frac{6x_{H^\pm}(x_{H^\pm} - 2x_t)}{x_{H^\pm} - x_t} \log \left( \frac{x_{H^\pm}}{x_t} \right) \right. \\ \left. + 4 \sin^2 \theta_W \left[ \frac{5x_t - 3x_{H^\pm}}{(x_{H^\pm} - x_t)^2} + \frac{2x_{H^\pm}(2x_{H^\pm} - 3x_t)}{(x_{H^\pm} - x_t)^3} \log \left( \frac{x_{H^\pm}}{x_t} \right) \right] \right\},$$

and  $C_{RL}^{\mathcal{T}q} = C_{RR}^{\mathcal{T}q} \left( 1 - \frac{1}{2 \sin^2 \theta_W} \right)$ . Similarly, from the box diagrams we get

$$C_{LL}^{\mathcal{T}\ell} = -\zeta_u \zeta_\ell^* \frac{\sqrt{x_\ell} x_t}{4(x_{H^\pm} - x_t) \sin^2 \theta_W} \left[ -\frac{1}{(x_{H^\pm} - 1)} + \frac{x_{H^\pm}(1 - x_{H^\pm}) \log x_t}{(x_{H^\pm} - x_t)(x_t - 1)(x_{H^\pm} - 1)} \right. \quad (\text{B.17}) \\ \left. - \frac{x_{H^\pm}(x_t + 1 - 2x_{H^\pm}) \log x_{H^\pm}}{(x_{H^\pm} - x_t)(x_{H^\pm} - 1)^2} \right],$$

and  $C_{LL}^{\mathcal{T}\ell} = (C_{LR}^{\mathcal{T}\ell})^*$ .

### B.2.2 Wilson Coefficients Suppressed by $m_\ell$

In addition to the Wilson coefficients given in Section 3.4, in the computation of the box diagrams one gets contributions suppressed by the lepton mass. For completeness, we give these contributions here. We obtain:

$$C_{T(5)}^{\text{NP, box}} = \zeta_u^* \zeta_\ell \frac{\sqrt{x_b x_\ell x_t}}{32(x_{H^\pm} - x_t) \sin^2 \theta_W} \times \left[ \frac{x_t \log x_t}{(x_t - 1)(x_{H^\pm} - x_t)} - \frac{x_{H^\pm} \log x_{H^\pm}}{(x_{H^\pm} - 1)(x_{H^\pm} - x_t)} + \frac{x_t - \log x_t - 1}{(x_t - 1)^2} \right], \quad (\text{B.18})$$

and

$$C_9^{\text{NP, box}} = \frac{x_\ell x_t}{16 \sin^2 \theta_W} \left\{ |\zeta_u|^2 |\zeta_\ell|^2 \left[ -\frac{1}{x_{H^\pm} - x_t} + \frac{x_t}{(x_{H^\pm} - x_t)^2} \log \left( \frac{x_{H^\pm}}{x_t} \right) \right] + 2 \text{Re}[\zeta_u \zeta_\ell^*] \left[ \frac{(x_t + 2) \log x_t}{(x_{H^\pm} - x_t)(x_t - 1)} - \frac{(x_{H^\pm} + 2) \log x_{H^\pm}}{(x_{H^\pm} - x_t)(x_{H^\pm} - 1)} \right] \right\} + 2\sqrt{x_\ell} \text{Re} \left( C_{LL}^{T\ell} \right), \quad (\text{B.19})$$

$$C_{10}^{\text{NP, box}} = \frac{x_\ell x_t}{16 \sin^2 \theta_W} \left\{ |\zeta_u|^2 |\zeta_\ell|^2 \left[ -\frac{1}{x_{H^\pm} - x_t} + \frac{x_t}{(x_{H^\pm} - x_t)^2} \log \left( \frac{x_{H^\pm}}{x_t} \right) \right] + 2 \text{Re}[\zeta_u \zeta_\ell^*] \left[ \frac{(x_t - 2) \log x_t}{(x_{H^\pm} - x_t)(x_t - 1)} - \frac{(x_{H^\pm} - 2) \log x_{H^\pm}}{(x_{H^\pm} - x_t)(x_{H^\pm} - 1)} \right] \right\}. \quad (\text{B.20})$$

# Bibliography

- [1] G. Aad *et al.* [ATLAS Collaboration], Phys. Lett. B **716**, 1 (2012) doi:10.1016/j.physletb.2012.08.020 [arXiv:1207.7214 [hep-ex]].
- [2] S. Chatrchyan *et al.* [CMS Collaboration], Phys. Lett. B **716**, 30 (2012) doi:10.1016/j.physletb.2012.08.021 [arXiv:1207.7235 [hep-ex]].
- [3] H. Albrecht *et al.* [ARGUS Collaboration], Phys. Lett. B **192**, 245 (1987). doi:10.1016/0370-2693(87)91177-4
- [4] S. Abachi *et al.* [D0 Collaboration], Phys. Rev. Lett. **74**, 2632 (1995) doi:10.1103/PhysRevLett.74.2632 [hep-ex/9503003].
- [5] F. Abe *et al.* [CDF Collaboration], Phys. Rev. Lett. **74**, 2626 (1995) doi:10.1103/PhysRevLett.74.2626 [hep-ex/9503002].
- [6] M. Bona *et al.* [UTfit Collaboration], JHEP **0803**, 049 (2008) doi:10.1088/1126-6708/2008/03/049 [arXiv:0707.0636 [hep-ph]].
- [7] G. C. Branco, P. M. Ferreira, L. Lavoura, M. N. Rebelo, M. Sher and J. P. Silva, Phys. Rept. **516**, 1 (2012) doi:10.1016/j.physrep.2012.02.002 [arXiv:1106.0034 [hep-ph]].
- [8] I. Doršner, S. Fajfer, A. Greljo, J. F. Kamenik and N. Košnik, Phys. Rept. **641**, 1 (2016) doi:10.1016/j.physrep.2016.06.001 [arXiv:1603.04993 [hep-ph]].
- [9] C. Boehm, M. J. Dolan, C. McCabe, M. Spannowsky and C. J. Wallace, JCAP **1405**, 009 (2014) doi:10.1088/1475-7516/2014/05/009 [arXiv:1401.6458 [hep-ph]].
- [10] S. Ipek, D. McKeen and A. E. Nelson, Phys. Rev. D **90**, no. 5, 055021 (2014) doi:10.1103/PhysRevD.90.055021 [arXiv:1404.3716 [hep-ph]].
- [11] R. Aaij *et al.* [LHCb Collaboration], Phys. Rev. Lett. **113**, 151601 (2014) doi:10.1103/PhysRevLett.113.151601 [arXiv:1406.6482 [hep-ex]].
- [12] R. Aaij *et al.* [LHCb Collaboration], arXiv:1705.05802 [hep-ex].
- [13] M. Bordone, G. Isidori and A. Pattori, Eur. Phys. J. C **76**, no. 8, 440 (2016) doi:10.1140/epjc/s10052-016-4274-7 [arXiv:1605.07633 [hep-ph]].
- [14] Y. Amhis *et al.*, arXiv:1612.07233 [hep-ex].
- [15] H. Na *et al.* [HPQCD Collaboration], Phys. Rev. D **92**, no. 5, 054510 (2015) Erratum: [Phys. Rev. D **93**, no. 11, 119906 (2016)] doi:10.1103/PhysRevD.93.119906, 10.1103/PhysRevD.92.054510 [arXiv:1505.03925 [hep-lat]].

- 
- [16] J. A. Bailey *et al.* [MILC Collaboration], Phys. Rev. D **92**, no. 3, 034506 (2015) doi:10.1103/PhysRevD.92.034506 [arXiv:1503.07237 [hep-lat]].
- [17] S. Fajfer, J. F. Kamenik, I. Nisandzic and J. Zupan, Phys. Rev. Lett. **109**, 161801 (2012) doi:10.1103/PhysRevLett.109.161801 [arXiv:1206.1872 [hep-ph]].
- [18] G. S. Guralnik, C. R. Hagen and T. W. B. Kibble, Phys. Rev. Lett. **13**, 585 (1964). doi:10.1103/PhysRevLett.13.585
- [19] F. Englert and R. Brout, Phys. Rev. Lett. **13**, 321 (1964). doi:10.1103/PhysRevLett.13.321
- [20] P. W. Higgs, Phys. Rev. Lett. **13**, 508 (1964). doi:10.1103/PhysRevLett.13.508
- [21] P. W. Higgs, Phys. Lett. **12**, 132 (1964). doi:10.1016/0031-9163(64)91136-9
- [22] C. Patrignani *et al.* [Particle Data Group], Chin. Phys. C **40**, no. 10, 100001 (2016). doi:10.1088/1674-1137/40/10/100001
- [23] M. Baak *et al.*, Eur. Phys. J. C **72**, 2205 (2012) doi:10.1140/epjc/s10052-012-2205-9 [arXiv:1209.2716 [hep-ph]].
- [24] S. Schael *et al.* [ALEPH and DELPHI and L3 and OPAL and SLD Collaborations and LEP Electroweak Working Group and SLD Electroweak Group and SLD Heavy Flavour Group], Phys. Rept. **427**, 257 (2006) doi:10.1016/j.physrep.2005.12.006 [hep-ex/0509008].
- [25] M. Kobayashi and T. Maskawa, Prog. Theor. Phys. **49**, 652 (1973). doi:10.1143/PTP.49.652
- [26] K. S. Hirata *et al.* [Kamiokande-II Collaboration], Phys. Lett. B **205**, 416 (1988). doi:10.1016/0370-2693(88)91690-5
- [27] R. Becker-Szendy *et al.*, Phys. Rev. D **46**, 3720 (1992). doi:10.1103/PhysRevD.46.3720
- [28] Y. Fukuda *et al.* [Kamiokande Collaboration], Phys. Lett. B **335**, 237 (1994). doi:10.1016/0370-2693(94)91420-6
- [29] W. W. M. Allison *et al.*, Phys. Lett. B **391**, 491 (1997) doi:10.1016/S0370-2693(96)01609-7 [hep-ex/9611007].
- [30] Y. Fukuda *et al.* [Super-Kamiokande Collaboration], Phys. Rev. Lett. **81**, 1562 (1998) doi:10.1103/PhysRevLett.81.1562 [hep-ex/9807003].
- [31] K. Abe *et al.* [Super-Kamiokande Collaboration], Phys. Rev. Lett. **97**, 171801 (2006) doi:10.1103/PhysRevLett.97.171801 [hep-ex/0607059].
- [32] Y. Fukuda *et al.* [Kamiokande Collaboration], Phys. Rev. Lett. **77**, 1683 (1996). doi:10.1103/PhysRevLett.77.1683
- [33] B. T. Cleveland, T. Daily, R. Davis, Jr., J. R. Distel, K. Lande, C. K. Lee, P. S. Wildenhain and J. Ullman, Astrophys. J. **496**, 505 (1998). doi:10.1086/305343
- [34] J. N. Abdurashitov *et al.* [SAGE Collaboration], Phys. Rev. C **60**, 055801 (1999) doi:10.1103/PhysRevC.60.055801 [astro-ph/9907113].

- 
- [35] M. Altmann *et al.* [GNO Collaboration], Phys. Lett. B **490**, 16 (2000) doi:10.1016/S0370-2693(00)00915-1 [hep-ex/0006034].
- [36] Q. R. Ahmad *et al.* [SNO Collaboration], Phys. Rev. Lett. **87**, 071301 (2001) doi:10.1103/PhysRevLett.87.071301 [nucl-ex/0106015].
- [37] V. N. Gavrin [SAGE Collaboration], Nucl. Phys. Proc. Suppl. **91**, 36 (2001). doi:10.1016/S0920-5632(00)00920-8
- [38] S. N. Ahmed *et al.* [SNO Collaboration], Phys. Rev. Lett. **92**, 181301 (2004) doi:10.1103/PhysRevLett.92.181301 [nucl-ex/0309004].
- [39] J. P. Cravens *et al.* [Super-Kamiokande Collaboration], Phys. Rev. D **78**, 032002 (2008) doi:10.1103/PhysRevD.78.032002 [arXiv:0803.4312 [hep-ex]].
- [40] G. Bellini *et al.* [Borexino Collaboration], Phys. Rev. D **82**, 033006 (2010) doi:10.1103/PhysRevD.82.033006 [arXiv:0808.2868 [astro-ph]].
- [41] F. Kaether, W. Hampel, G. Heusser, J. Kiko and T. Kirsten, Phys. Lett. B **685**, 47 (2010) doi:10.1016/j.physletb.2010.01.030 [arXiv:1001.2731 [hep-ex]].
- [42] S. H. Ahn *et al.* [K2K Collaboration], Phys. Lett. B **511**, 178 (2001) doi:10.1016/S0370-2693(01)00647-5 [hep-ex/0103001].
- [43] D. G. Michael *et al.* [MINOS Collaboration], Phys. Rev. Lett. **97**, 191801 (2006) doi:10.1103/PhysRevLett.97.191801 [hep-ex/0607088].
- [44] K. Abe *et al.* [T2K Collaboration], Phys. Rev. Lett. **107**, 041801 (2011) doi:10.1103/PhysRevLett.107.041801 [arXiv:1106.2822 [hep-ex]].
- [45] K. Eguchi *et al.* [KamLAND Collaboration], Phys. Rev. Lett. **90**, 021802 (2003) doi:10.1103/PhysRevLett.90.021802 [hep-ex/0212021].
- [46] Y. Abe *et al.* [Double Chooz Collaboration], Phys. Rev. Lett. **108**, 131801 (2012) doi:10.1103/PhysRevLett.108.131801 [arXiv:1112.6353 [hep-ex]].
- [47] R. Leitner [Daya Bay Collaboration], Nucl. Part. Phys. Proc. **285-286**, 32 (2017). doi:10.1016/j.nuclphysbps.2017.03.007
- [48] J. K. Ahn *et al.* [RENO Collaboration], Phys. Rev. Lett. **108**, 191802 (2012) doi:10.1103/PhysRevLett.108.191802 [arXiv:1204.0626 [hep-ex]].
- [49] P. A. N. Machado, H. Minakata, H. Nunokawa and R. Zukanovich Funchal, JHEP **1205**, 023 (2012) doi:10.1007/JHEP05(2012)023 [arXiv:1111.3330 [hep-ph]].
- [50] I. Esteban, M. C. Gonzalez-Garcia, M. Maltoni, I. Martinez-Soler and T. Schwetz, JHEP **1701**, 087 (2017) doi:10.1007/JHEP01(2017)087 [arXiv:1611.01514 [hep-ph]].
- [51] E. W. Otten and C. Weinheimer, Rept. Prog. Phys. **71**, 086201 (2008) doi:10.1088/0034-4885/71/8/086201 [arXiv:0909.2104 [hep-ex]].
- [52] P. Minkowski, Phys. Lett. **67B**, 421 (1977). doi:10.1016/0370-2693(77)90435-X
- [53] T. Yanagida, Conf. Proc. C **7902131**, 95 (1979).

- [54] S. L. Glashow, NATO Sci. Ser. B **61**, 687 (1980). doi:10.1007/978-1-4684-7197-7\_15
- [55] M. Gell-Mann, P. Ramond and R. Slansky, Conf. Proc. C **790927**, 315 (1979) [arXiv:1306.4669 [hep-th]].
- [56] R. N. Mohapatra and J. W. F. Valle, Phys. Rev. D **34**, 1642 (1986). doi:10.1103/PhysRevD.34.1642
- [57] M. C. Gonzalez-Garcia and J. W. F. Valle, Phys. Lett. B **216**, 360 (1989). doi:10.1016/0370-2693(89)91131-3
- [58] F. Deppisch and J. W. F. Valle, Phys. Rev. D **72**, 036001 (2005) doi:10.1103/PhysRevD.72.036001 [hep-ph/0406040].
- [59] S. Weinberg, Phys. Rev. Lett. **43**, 1566 (1979). doi:10.1103/PhysRevLett.43.1566
- [60] A. Gando *et al.* [KamLAND-Zen Collaboration], Phys. Rev. Lett. **110**, no. 6, 062502 (2013) doi:10.1103/PhysRevLett.110.062502 [arXiv:1211.3863 [hep-ex]].
- [61] M. Agostini *et al.* [GERDA Collaboration], Phys. Rev. Lett. **111**, no. 12, 122503 (2013) doi:10.1103/PhysRevLett.111.122503 [arXiv:1307.4720 [nucl-ex]].
- [62] J. B. Albert *et al.* [EXO-200 Collaboration], Nature **510**, 229 (2014) doi:10.1038/nature13432 [arXiv:1402.6956 [nucl-ex]].
- [63] [ATLAS and CDF and CMS and D0 Collaborations], arXiv:1403.4427 [hep-ex].
- [64] M. Bona *et al.* [UTfit Collaboration], JHEP **0610**, 081 (2006) doi:10.1088/1126-6708/2006/10/081 [hep-ph/0606167].
- [65] J. Charles *et al.*, Phys. Rev. D **91**, no. 7, 073007 (2015) doi:10.1103/PhysRevD.91.073007 [arXiv:1501.05013 [hep-ph]].
- [66] L. Wolfenstein, Phys. Rev. Lett. **51**, 1945 (1983). doi:10.1103/PhysRevLett.51.1945
- [67] C. F. Kolda and H. Murayama, JHEP **0007**, 035 (2000) doi:10.1088/1126-6708/2000/07/035 [hep-ph/0003170].
- [68] S. L. Glashow, J. Iliopoulos and L. Maiani, Phys. Rev. D **2**, 1285 (1970). doi:10.1103/PhysRevD.2.1285
- [69] G. D'Ambrosio, G. F. Giudice, G. Isidori and A. Strumia, Nucl. Phys. B **645**, 155 (2002) doi:10.1016/S0550-3213(02)00836-2 [hep-ph/0207036].
- [70] G. Isidori and D. M. Straub, Eur. Phys. J. C **72**, 2103 (2012) doi:10.1140/epjc/s10052-012-2103-1 [arXiv:1202.0464 [hep-ph]].
- [71] J. P. Lees *et al.* [BaBar Collaboration], Phys. Rev. Lett. **109**, 101802 (2012) doi:10.1103/PhysRevLett.109.101802 [arXiv:1205.5442 [hep-ex]].
- [72] J. P. Lees *et al.* [BaBar Collaboration], Phys. Rev. D **88**, no. 7, 072012 (2013) doi:10.1103/PhysRevD.88.072012 [arXiv:1303.0571 [hep-ex]].
- [73] M. Huschle *et al.* [Belle Collaboration], Phys. Rev. D **92**, no. 7, 072014 (2015) doi:10.1103/PhysRevD.92.072014 [arXiv:1507.03233 [hep-ex]].

- [74] R. Aaij *et al.* [LHCb Collaboration], Phys. Rev. Lett. **115**, no. 11, 111803 (2015) Erratum: [Phys. Rev. Lett. **115**, no. 15, 159901 (2015)] doi:10.1103/PhysRevLett.115.159901, 10.1103/PhysRevLett.115.111803 [arXiv:1506.08614 [hep-ex]].
- [75] S. Hirose *et al.* [Belle Collaboration], Phys. Rev. Lett. **118**, no. 21, 211801 (2017) doi:10.1103/PhysRevLett.118.211801 [arXiv:1612.00529 [hep-ex]].
- [76] A. Abdesselam *et al.* [Belle Collaboration], arXiv:1603.06711 [hep-ex].
- [77] S. Aoki *et al.*, Eur. Phys. J. C **77**, no. 2, 112 (2017) doi:10.1140/epjc/s10052-016-4509-7 [arXiv:1607.00299 [hep-lat]].
- [78] B. Colquhoun *et al.* [HPQCD Collaboration], Phys. Rev. D **91**, no. 11, 114509 (2015) doi:10.1103/PhysRevD.91.114509 [arXiv:1503.05762 [hep-lat]].
- [79] N. Carrasco, P. Lami, V. Lubicz, L. Riggio, S. Simula and C. Tarantino, Phys. Rev. D **93**, no. 11, 114512 (2016) doi:10.1103/PhysRevD.93.114512 [arXiv:1602.04113 [hep-lat]].
- [80] J. Koponen, C. T. H. Davies, G. C. Donald, E. Follana, G. P. Lepage, H. Na and J. Shigemitsu, arXiv:1305.1462 [hep-lat].
- [81] V. Lubicz *et al.* [ETM Collaboration], arXiv:1706.03017 [hep-lat].
- [82] E. Dalgic, A. Gray, M. Wingate, C. T. H. Davies, G. P. Lepage and J. Shigemitsu, Phys. Rev. D **73**, 074502 (2006) Erratum: [Phys. Rev. D **75**, 119906 (2007)] doi:10.1103/PhysRevD.75.119906, 10.1103/PhysRevD.73.074502 [hep-lat/0601021].
- [83] J. A. Bailey *et al.* [Fermilab Lattice and MILC Collaborations], Phys. Rev. D **92**, no. 1, 014024 (2015) doi:10.1103/PhysRevD.92.014024 [arXiv:1503.07839 [hep-lat]].
- [84] J. M. Flynn, T. Izubuchi, T. Kawanai, C. Lehner, A. Soni, R. S. Van de Water and O. Witzel, Phys. Rev. D **91**, no. 7, 074510 (2015) doi:10.1103/PhysRevD.91.074510 [arXiv:1501.05373 [hep-lat]].
- [85] C. M. Bouchard, G. P. Lepage, C. Monahan, H. Na and J. Shigemitsu, Phys. Rev. D **90**, 054506 (2014) doi:10.1103/PhysRevD.90.054506 [arXiv:1406.2279 [hep-lat]].
- [86] A. Lytle, B. Colquhoun, C. Davies, J. Koponen and C. McNeile, PoS BEAUTY **2016**, 069 (2016) [arXiv:1605.05645 [hep-lat]].
- [87] D. Becirevic, S. Fajfer, I. Nisandzic and A. Tayduganov, arXiv:1602.03030 [hep-ph].
- [88] D. Bečirević, N. Košnik and A. Tayduganov, Phys. Lett. B **716**, 208 (2012) doi:10.1016/j.physletb.2012.08.016 [arXiv:1206.4977 [hep-ph]].
- [89] Z. Ligeti, M. Papucci and D. J. Robinson, JHEP **1701**, 083 (2017) doi:10.1007/JHEP01(2017)083 [arXiv:1610.02045 [hep-ph]].
- [90] R. Alonso, A. Kobach and J. Martin Camalich, Phys. Rev. D **94**, no. 9, 094021 (2016) doi:10.1103/PhysRevD.94.094021 [arXiv:1602.07671 [hep-ph]].
- [91] C. Bernard *et al.*, Phys. Rev. D **79**, 014506 (2009) doi:10.1103/PhysRevD.79.014506 [arXiv:0808.2519 [hep-lat]].

- [92] J. A. Bailey *et al.* [Fermilab Lattice and MILC Collaborations], Phys. Rev. D **89**, no. 11, 114504 (2014) doi:10.1103/PhysRevD.89.114504 [arXiv:1403.0635 [hep-lat]].
- [93] S. Fajfer, J. F. Kamenik and I. Nisandzic, Phys. Rev. D **85**, 094025 (2012) doi:10.1103/PhysRevD.85.094025 [arXiv:1203.2654 [hep-ph]].
- [94] S. Faller, A. Khodjamirian, C. Klein and T. Mannel, Eur. Phys. J. C **60**, 603 (2009) doi:10.1140/epjc/s10052-009-0968-4 [arXiv:0809.0222 [hep-ph]].
- [95] M. Bona *et al.* [UTfit Collaboration], Phys. Rev. Lett. **97**, 151803 (2006) doi:10.1103/PhysRevLett.97.151803 [hep-ph/0605213].
- [96] M. Freytsis, Z. Ligeti and J. T. Ruderman, Phys. Rev. D **92**, no. 5, 054018 (2015) doi:10.1103/PhysRevD.92.054018 [arXiv:1506.08896 [hep-ph]].
- [97] Y. Amhis *et al.* [Heavy Flavor Averaging Group (HFAG)], arXiv:1412.7515 [hep-ex].
- [98] M. Ablikim *et al.* [BESIII Collaboration], Phys. Rev. D **94**, no. 7, 072004 (2016) doi:10.1103/PhysRevD.94.072004 [arXiv:1608.06732 [hep-ex]].
- [99] A. Zupanc *et al.* [Belle Collaboration], JHEP **1309**, 139 (2013) doi:10.1007/JHEP09(2013)139 [arXiv:1307.6240 [hep-ex]].
- [100] P. del Amo Sanchez *et al.* [BaBar Collaboration], Phys. Rev. D **82**, 091103 (2010) Erratum: [Phys. Rev. D **91**, no. 1, 019901 (2015)] doi:10.1103/PhysRevD.82.091103, 10.1103/PhysRevD.91.019901 [arXiv:1008.4080 [hep-ex]].
- [101] J. P. Alexander *et al.* [CLEO Collaboration], Phys. Rev. D **79**, 052001 (2009) doi:10.1103/PhysRevD.79.052001 [arXiv:0901.1216 [hep-ex]].
- [102] P. Naik *et al.* [CLEO Collaboration], Phys. Rev. D **80**, 112004 (2009) doi:10.1103/PhysRevD.80.112004 [arXiv:0910.3602 [hep-ex]].
- [103] P. U. E. Onyisi *et al.* [CLEO Collaboration], Phys. Rev. D **79**, 052002 (2009) doi:10.1103/PhysRevD.79.052002 [arXiv:0901.1147 [hep-ex]].
- [104] M. Ablikim *et al.* [BESIII Collaboration], Chin. Phys. C **40**, no. 11, 113001 (2016) doi:10.1088/1674-1137/40/11/113001 [arXiv:1605.00208 [hep-ex]].
- [105] D. Besson *et al.* [CLEO Collaboration], Phys. Rev. D **80**, 032005 (2009) doi:10.1103/PhysRevD.80.032005 [arXiv:0906.2983 [hep-ex]].
- [106] M. Ablikim *et al.* [BESIII Collaboration], Phys. Rev. D **92**, no. 7, 072012 (2015) doi:10.1103/PhysRevD.92.072012 [arXiv:1508.07560 [hep-ex]].
- [107] L. Widhalm *et al.* [Belle Collaboration], Phys. Rev. Lett. **97**, 061804 (2006) doi:10.1103/PhysRevLett.97.061804 [hep-ex/0604049].
- [108] M. Ablikim *et al.* [BESIII Collaboration], Eur. Phys. J. C **76**, no. 7, 369 (2016) doi:10.1140/epjc/s10052-016-4198-2 [arXiv:1605.00068 [hep-ex]].
- [109] B. Kronenbitter *et al.* [Belle Collaboration], Phys. Rev. D **92**, no. 5, 051102 (2015) doi:10.1103/PhysRevD.92.051102 [arXiv:1503.05613 [hep-ex]].

- [110] J. P. Lees *et al.* [BaBar Collaboration], Phys. Rev. D **88**, no. 3, 031102 (2013) doi:10.1103/PhysRevD.88.031102 [arXiv:1207.0698 [hep-ex]].
- [111] K. Abe *et al.* [Belle Collaboration], Phys. Lett. B **526**, 258 (2002) doi:10.1016/S0370-2693(01)01483-6 [hep-ex/0111082].
- [112] B. Aubert *et al.* [BaBar Collaboration], Phys. Rev. Lett. **104**, 011802 (2010) doi:10.1103/PhysRevLett.104.011802 [arXiv:0904.4063 [hep-ex]].
- [113] J. J. Aubert *et al.* [E598 Collaboration], Phys. Rev. Lett. **33**, 1404 (1974). doi:10.1103/PhysRevLett.33.1404
- [114] J. E. Augustin *et al.* [SLAC-SP-017 Collaboration], Phys. Rev. Lett. **33**, 1406 (1974) [Adv. Exp. Phys. **5**, 141 (1976)]. doi:10.1103/PhysRevLett.33.1406
- [115] C. Bobeth, M. Gorbahn, T. Hermann, M. Misiak, E. Stamou and M. Steinhauser, Phys. Rev. Lett. **112**, 101801 (2014) doi:10.1103/PhysRevLett.112.101801 [arXiv:1311.0903 [hep-ph]].
- [116] R. Aaij *et al.* [LHCb Collaboration], JHEP **1406**, 133 (2014) doi:10.1007/JHEP06(2014)133 [arXiv:1403.8044 [hep-ex]].
- [117] C. Bobeth, G. Hiller, D. van Dyk and C. Wacker, JHEP **1201**, 107 (2012) doi:10.1007/JHEP01(2012)107 [arXiv:1111.2558 [hep-ph]].
- [118] D. Bečirević, S. Fajfer and N. Košnik, Phys. Rev. D **92**, no. 1, 014016 (2015) doi:10.1103/PhysRevD.92.014016 [arXiv:1503.09024 [hep-ph]].
- [119] R. Aaij *et al.* [LHCb Collaboration], JHEP **1611**, 047 (2016) doi:10.1007/JHEP11(2016)047, 10.1007/JHEP04(2017)142, 10.1007/JHEP11(2016)047, 10.1007/JHEP04(2017)142 [arXiv:1606.04731 [hep-ex]].
- [120] R. Aaij *et al.* [LHCb Collaboration], JHEP **1509**, 179 (2015) doi:10.1007/JHEP09(2015)179 [arXiv:1506.08777 [hep-ex]].
- [121] W. Altmannshofer and D. M. Straub, Eur. Phys. J. C **75**, no. 8, 382 (2015) doi:10.1140/epjc/s10052-015-3602-7 [arXiv:1411.3161 [hep-ph]].
- [122] M. Ciuchini, M. Fedele, E. Franco, S. Mishima, A. Paul, L. Silvestrini and M. Valli, JHEP **1606**, 116 (2016) doi:10.1007/JHEP06(2016)116 [arXiv:1512.07157 [hep-ph]].
- [123] W. Altmannshofer, P. Ball, A. Bharucha, A. J. Buras, D. M. Straub and M. Wick, JHEP **0901**, 019 (2009) doi:10.1088/1126-6708/2009/01/019 [arXiv:0811.1214 [hep-ph]].
- [124] A. J. Buras, M. Misiak, M. Munz and S. Pokorski, Nucl. Phys. B **424**, 374 (1994) doi:10.1016/0550-3213(94)90299-2 [hep-ph/9311345].
- [125] C. Greub, V. Pilipp and C. Schupbach, JHEP **0812**, 040 (2008) doi:10.1088/1126-6708/2008/12/040 [arXiv:0810.4077 [hep-ph]].
- [126] R. Alonso, B. Grinstein and J. Martin Camalich, Phys. Rev. Lett. **113**, 241802 (2014) doi:10.1103/PhysRevLett.113.241802 [arXiv:1407.7044 [hep-ph]].

- [127] D. Bečirević, O. Sumensari and R. Zukanovich Funchal, *Eur. Phys. J. C* **76**, no. 3, 134 (2016) doi:10.1140/epjc/s10052-016-3985-0 [arXiv:1602.00881 [hep-ph]].
- [128] K. De Bruyn, R. Fleischer, R. Knegjens, P. Koppenburg, M. Merk and N. Tuning, *Phys. Rev. D* **86**, 014027 (2012) doi:10.1103/PhysRevD.86.014027 [arXiv:1204.1735 [hep-ph]].
- [129] R. Aaij *et al.* [LHCb Collaboration], *Phys. Rev. Lett.* **114**, no. 4, 041801 (2015) doi:10.1103/PhysRevLett.114.041801 [arXiv:1411.3104 [hep-ex]].
- [130] R. Aaij *et al.* [LHCb Collaboration], *Phys. Rev. Lett.* **118**, no. 19, 191801 (2017) doi:10.1103/PhysRevLett.118.191801 [arXiv:1703.05747 [hep-ex]].
- [131] C. Bouchard *et al.* [HPQCD Collaboration], *Phys. Rev. D* **88**, no. 5, 054509 (2013) Erratum: [*Phys. Rev. D* **88**, no. 7, 079901 (2013)] doi:10.1103/PhysRevD.88.079901, 10.1103/PhysRevD.88.054509 [arXiv:1306.2384 [hep-lat]].
- [132] J. A. Bailey *et al.*, *Phys. Rev. D* **93**, no. 2, 025026 (2016) doi:10.1103/PhysRevD.93.025026 [arXiv:1509.06235 [hep-lat]].
- [133] M. Beylich, G. Buchalla and T. Feldmann, *Eur. Phys. J. C* **71**, 1635 (2011) doi:10.1140/epjc/s10052-011-1635-0 [arXiv:1101.5118 [hep-ph]].
- [134] R. R. Horgan, Z. Liu, S. Meinel and M. Wingate, *Phys. Rev. D* **89**, no. 9, 094501 (2014) doi:10.1103/PhysRevD.89.094501 [arXiv:1310.3722 [hep-lat]].
- [135] R. R. Horgan, Z. Liu, S. Meinel and M. Wingate, *PoS LATTICE 2014*, 372 (2015) [arXiv:1501.00367 [hep-lat]].
- [136] A. Bharucha, D. M. Straub and R. Zwicky, *JHEP* **1608**, 098 (2016) doi:10.1007/JHEP08(2016)098 [arXiv:1503.05534 [hep-ph]].
- [137] D. Becirevic and E. Schneider, *Nucl. Phys. B* **854**, 321 (2012) doi:10.1016/j.nuclphysb.2011.09.004 [arXiv:1106.3283 [hep-ph]].
- [138] A. Ilakovac and A. Pilaftsis, *Nucl. Phys. B* **437**, 491 (1995) doi:10.1016/0550-3213(94)00567-X [hep-ph/9403398].
- [139] A. M. Baldini *et al.*, arXiv:1301.7225 [physics.ins-det].
- [140] C. Dohmen *et al.* [SINDRUM II Collaboration], *Phys. Lett. B* **317**, 631 (1993). doi:10.1016/0370-2693(93)91383-X
- [141] A. Alekou *et al.*, arXiv:1310.0804 [physics.acc-ph].
- [142] W. H. Bertl *et al.* [SINDRUM II Collaboration], *Eur. Phys. J. C* **47**, 337 (2006). doi:10.1140/epjc/s2006-02582-x
- [143] Y. Kuno [COMET Collaboration], *PTEP* **2013**, 022C01 (2013). doi:10.1093/ptep/pts089
- [144] A. M. Baldini *et al.* [MEG Collaboration], *Eur. Phys. J. C* **76**, no. 8, 434 (2016) doi:10.1140/epjc/s10052-016-4271-x [arXiv:1605.05081 [hep-ex]].

- [145] E. Bertuzzo, Y. F. Perez G., O. Sumensari and R. Zukanovich Funchal, JHEP **1601**, 018 (2016) doi:10.1007/JHEP01(2016)018 [arXiv:1510.04284 [hep-ph]].
- [146] P. A. N. Machado, Y. F. Perez, O. Sumensari, Z. Tabrizi and R. Z. Funchal, JHEP **1512**, 160 (2015) doi:10.1007/JHEP12(2015)160 [arXiv:1507.07550 [hep-ph]].
- [147] A. Abada, D. Bečirević, M. Lucente and O. Sumensari, Phys. Rev. D **91**, no. 11, 113013 (2015) doi:10.1103/PhysRevD.91.113013 [arXiv:1503.04159 [hep-ph]].
- [148] A. Abada, D. Bečirević, O. Sumensari, C. Weiland and R. Zukanovich Funchal, Phys. Rev. D **95**, no. 7, 075023 (2017) doi:10.1103/PhysRevD.95.075023 [arXiv:1612.04737 [hep-ph]].
- [149] R. Aaij *et al.* [LHCb Collaboration], JHEP **1610**, 030 (2016) doi:10.1007/JHEP10(2016)030 [arXiv:1608.01484 [hep-ex]].
- [150] A. Abada, A. M. Teixeira, A. Vicente and C. Weiland, JHEP **1402**, 091 (2014) doi:10.1007/JHEP02(2014)091 [arXiv:1311.2830 [hep-ph]].
- [151] A. Atre, T. Han, S. Pascoli and B. Zhang, JHEP **0905**, 030 (2009) doi:10.1088/1126-6708/2009/05/030 [arXiv:0901.3589 [hep-ph]].
- [152] U. Bellgardt *et al.* [SINDRUM Collaboration], Nucl. Phys. B **299**, 1 (1988). doi:10.1016/0550-3213(88)90462-2
- [153] S. L. Glashow, D. Guadagnoli and K. Lane, Phys. Rev. Lett. **114**, 091801 (2015) doi:10.1103/PhysRevLett.114.091801 [arXiv:1411.0565 [hep-ph]].
- [154] D. Guadagnoli and K. Lane, Phys. Lett. B **751**, 54 (2015) doi:10.1016/j.physletb.2015.10.010 [arXiv:1507.01412 [hep-ph]].
- [155] D. Bečirević, N. Košnik, O. Sumensari and R. Zukanovich Funchal, JHEP **1611**, 035 (2016) doi:10.1007/JHEP11(2016)035 [arXiv:1608.07583 [hep-ph]].
- [156] J. Gratx, M. Hopfer and R. Zwicky, Phys. Rev. D **93**, no. 5, 054008 (2016) doi:10.1103/PhysRevD.93.054008 [arXiv:1506.03970 [hep-ph]].
- [157] R. Aaij *et al.* [LHCb Collaboration], JHEP **1602**, 104 (2016) doi:10.1007/JHEP02(2016)104 [arXiv:1512.04442 [hep-ex]].
- [158] F. Kruger, L. M. Sehgal, N. Sinha and R. Sinha, Phys. Rev. D **61**, 114028 (2000) Erratum: [Phys. Rev. D **63**, 019901 (2001)] doi:10.1103/PhysRevD.61.114028, 10.1103/PhysRevD.63.019901 [hep-ph/9907386].
- [159] P. Ball and R. Zwicky, Phys. Rev. D **71**, 014029 (2005) doi:10.1103/PhysRevD.71.014029 [hep-ph/0412079].
- [160] I. F. Ginzburg and M. Krawczyk, Phys. Rev. D **72**, 115013 (2005) doi:10.1103/PhysRevD.72.115013 [hep-ph/0408011].
- [161] E. Ma, Phys. Rev. D **73**, 077301 (2006) doi:10.1103/PhysRevD.73.077301 [hep-ph/0601225].
- [162] R. Barbieri, L. J. Hall and V. S. Rychkov, Phys. Rev. D **74**, 015007 (2006) doi:10.1103/PhysRevD.74.015007 [hep-ph/0603188].

- [163] S. L. Glashow and S. Weinberg, *Phys. Rev. D* **15**, 1958 (1977). doi:10.1103/PhysRevD.15.1958
- [164] E. A. Paschos, *Phys. Rev. D* **15**, 1966 (1977). doi:10.1103/PhysRevD.15.1966
- [165] A. Pich and P. Tuzon, *Phys. Rev. D* **80**, 091702 (2009) doi:10.1103/PhysRevD.80.091702 [arXiv:0908.1554 [hep-ph]].
- [166] M. Jung, A. Pich and P. Tuzon, *JHEP* **1011**, 003 (2010) doi:10.1007/JHEP11(2010)003 [arXiv:1006.0470 [hep-ph]].
- [167] J. F. Gunion and H. E. Haber, *Phys. Rev. D* **67**, 075019 (2003) doi:10.1103/PhysRevD.67.075019 [hep-ph/0207010].
- [168] A. Barroso, P. M. Ferreira, I. P. Ivanov and R. Santos, *JHEP* **1306**, 045 (2013) doi:10.1007/JHEP06(2013)045 [arXiv:1303.5098 [hep-ph]].
- [169] B. W. Lee, C. Quigg and H. B. Thacker, *Phys. Rev. Lett.* **38**, 883 (1977). doi:10.1103/PhysRevLett.38.883
- [170] S. Kanemura, T. Kubota and E. Takasugi, *Phys. Lett. B* **313**, 155 (1993) doi:10.1016/0370-2693(93)91205-2 [hep-ph/9303263].
- [171] B. Świeżewska, *Phys. Rev. D* **88**, no. 5, 055027 (2013) Erratum: [*Phys. Rev. D* **88**, no. 11, 119903 (2013)] doi:10.1103/PhysRevD.88.055027, 10.1103/PhysRevD.88.119903 [arXiv:1209.5725 [hep-ph]].
- [172] T. Corbett, O. J. P. Eboli, D. Goncalves, J. Gonzalez-Fraile, T. Plehn and M. Rauch, *JHEP* **1508**, 156 (2015) doi:10.1007/JHEP08(2015)156 [arXiv:1505.05516 [hep-ph]].
- [173] D. Bečirević, E. Bertuzzo, O. Sumensari and R. Zukanovich Funchal, *Phys. Lett. B* **757**, 261 (2016) doi:10.1016/j.physletb.2016.03.073 [arXiv:1512.05623 [hep-ph]].
- [174] R. Barbieri, L. J. Hall, Y. Nomura and V. S. Rychkov, *Phys. Rev. D* **75**, 035007 (2007) doi:10.1103/PhysRevD.75.035007 [hep-ph/0607332].
- [175] M. Baak *et al.* [Gfitter Group], *Eur. Phys. J. C* **74**, 3046 (2014) doi:10.1140/epjc/s10052-014-3046-5 [arXiv:1407.3792 [hep-ph]].
- [176] V. Cacchio, D. Chowdhury, O. Eberhardt and C. W. Murphy, *JHEP* **1611**, 026 (2016) doi:10.1007/JHEP11(2016)026 [arXiv:1609.01290 [hep-ph]].
- [177] D. Chowdhury and O. Eberhardt, *JHEP* **1511**, 052 (2015) doi:10.1007/JHEP11(2015)052 [arXiv:1503.08216 [hep-ph]].
- [178] O. Eberhardt, U. Nierste and M. Wiebusch, *JHEP* **1307**, 118 (2013) doi:10.1007/JHEP07(2013)118 [arXiv:1305.1649 [hep-ph]].
- [179] B. Dumont, J. F. Gunion, Y. Jiang and S. Kraml, *Phys. Rev. D* **90**, 035021 (2014) doi:10.1103/PhysRevD.90.035021 [arXiv:1405.3584 [hep-ph]].
- [180] A. Celis, M. Jung, X. Q. Li and A. Pich, *JHEP* **1301**, 054 (2013) doi:10.1007/JHEP01(2013)054 [arXiv:1210.8443 [hep-ph]].

- 
- [181] M. Misiak and M. Steinhauser, *Eur. Phys. J. C* **77**, no. 3, 201 (2017) doi:10.1140/epjc/s10052-017-4776-y [arXiv:1702.04571 [hep-ph]].
- [182] X. Q. Li, J. Lu and A. Pich, *JHEP* **1406**, 022 (2014) doi:10.1007/JHEP06(2014)022 [arXiv:1404.5865 [hep-ph]].
- [183] C. Bobeth, M. Misiak and J. Urban, *Nucl. Phys. B* **574**, 291 (2000) doi:10.1016/S0550-3213(00)00007-9 [hep-ph/9910220].
- [184] G. Passarino and M. J. G. Veltman, *Nucl. Phys. B* **160**, 151 (1979). doi:10.1016/0550-3213(79)90234-7
- [185] V. Shtabovenko, R. Mertig and F. Orellana, *Comput. Phys. Commun.* **207**, 432 (2016) doi:10.1016/j.cpc.2016.06.008 [arXiv:1601.01167 [hep-ph]].
- [186] P. Arnan, D. Bečirević, F. Mescia and O. Sumensari, arXiv:1703.03426 [hep-ph].
- [187] C. Bobeth, A. J. Buras and T. Ewerth, *Nucl. Phys. B* **713**, 522 (2005) doi:10.1016/j.nuclphysb.2005.02.011 [hep-ph/0409293].
- [188] S. Bertolini, F. Borzumati, A. Masiero and G. Ridolfi, *Nucl. Phys. B* **353**, 591 (1991). doi:10.1016/0550-3213(91)90320-W
- [189] M. Ciuchini, G. Degrassi, P. Gambino and G. F. Giudice, *Nucl. Phys. B* **527**, 21 (1998) doi:10.1016/S0550-3213(98)00244-2 [hep-ph/9710335].
- [190] G. Degrassi, P. Gambino and P. Slavich, *Phys. Lett. B* **635**, 335 (2006) doi:10.1016/j.physletb.2006.02.067 [hep-ph/0601135].
- [191] T. Hermann, M. Misiak and M. Steinhauser, *JHEP* **1211**, 036 (2012) doi:10.1007/JHEP11(2012)036 [arXiv:1208.2788 [hep-ph]].
- [192] P. H. Chankowski and L. Slawianowska, *Phys. Rev. D* **63**, 054012 (2001) doi:10.1103/PhysRevD.63.054012 [hep-ph/0008046].
- [193] M. Misiak *et al.*, *Phys. Rev. Lett.* **114**, no. 22, 221801 (2015) doi:10.1103/PhysRevLett.114.221801 [arXiv:1503.01789 [hep-ph]].
- [194] J. P. Lees *et al.* [BaBar Collaboration], *Phys. Rev. D* **88**, no. 7, 071102 (2013) doi:10.1103/PhysRevD.88.071102 [arXiv:1210.5669 [hep-ex]].
- [195] J. P. Lees *et al.* [BaBar Collaboration], *Phys. Rev. D* **87**, no. 3, 031102 (2013) Erratum: [*Phys. Rev. D* **87**, no. 5, 059903 (2013)] doi:10.1103/PhysRevD.87.031102, 10.1103/PhysRevD.87.059903 [arXiv:1210.0287 [hep-ex]].
- [196] J. P. Lees *et al.* [BaBar Collaboration], *Phys. Rev. Lett.* **107**, 221803 (2011) doi:10.1103/PhysRevLett.107.221803 [arXiv:1108.3549 [hep-ex]].
- [197] A. Denner, S. Heinemeyer, I. Puljak, D. Rebuszi and M. Spira, *Eur. Phys. J. C* **71**, 1753 (2011) doi:10.1140/epjc/s10052-011-1753-8 [arXiv:1107.5909 [hep-ph]].
- [198] G. Aad *et al.* [ATLAS and CMS Collaborations], *JHEP* **1608**, 045 (2016) doi:10.1007/JHEP08(2016)045 [arXiv:1606.02266 [hep-ex]].

- [199] S. Kanemura, Y. Okada, E. Senaha and C.-P. Yuan, Phys. Rev. D **70**, 115002 (2004) doi:10.1103/PhysRevD.70.115002 [hep-ph/0408364].
- [200] G. T. Bodwin, F. Petriello, S. Stoynev and M. Velasco, Phys. Rev. D **88**, no. 5, 053003 (2013) doi:10.1103/PhysRevD.88.053003 [arXiv:1306.5770 [hep-ph]].
- [201] D. N. Gao, Phys. Lett. B **737**, 366 (2014) doi:10.1016/j.physletb.2014.09.019 [arXiv:1406.7102 [hep-ph]].
- [202] S. Alte, M. König and M. Neubert, JHEP **1612**, 037 (2016) doi:10.1007/JHEP12(2016)037 [arXiv:1609.06310 [hep-ph]].
- [203] P. Colangelo, F. De Fazio and P. Santorelli, Phys. Lett. B **760**, 335 (2016) doi:10.1016/j.physletb.2016.07.002 [arXiv:1602.01372 [hep-ph]].
- [204] D. Bečirević, B. Melić, M. Patra and O. Sumensari, arXiv:1705.01112 [hep-ph].
- [205] D. Bečirević, G. Duplančić, B. Klajn, B. Melić and F. Sanfilippo, Nucl. Phys. B **883**, 306 (2014) doi:10.1016/j.nuclphysb.2014.03.024 [arXiv:1312.2858 [hep-ph]].
- [206] C. McNeile, C. T. H. Davies, E. Follana, K. Hornbostel and G. P. Lepage, Phys. Rev. D **86**, 074503 (2012) doi:10.1103/PhysRevD.86.074503 [arXiv:1207.0994 [hep-lat]].
- [207] S. Godfrey and K. Moats, Phys. Rev. D **92**, no. 5, 054034 (2015) doi:10.1103/PhysRevD.92.054034 [arXiv:1507.00024 [hep-ph]].
- [208] L. Bergstrom, Z. Phys. C **14**, 129 (1982). doi:10.1007/BF01495033
- [209] Y. Jia and W. L. Sang, JHEP **0910**, 090 (2009) doi:10.1088/1126-6708/2009/10/090 [arXiv:0906.4782 [hep-ph]].
- [210] B. Aubert *et al.* [BaBar Collaboration], Phys. Rev. Lett. **103**, 181801 (2009) doi:10.1103/PhysRevLett.103.181801 [arXiv:0906.2219 [hep-ex]].
- [211] B. Aubert *et al.* [BaBar Collaboration], Phys. Rev. Lett. **103**, 081803 (2009) doi:10.1103/PhysRevLett.103.081803 [arXiv:0905.4539 [hep-ex]].
- [212] M. A. Sanchis-Lozano, Mod. Phys. Lett. A **17**, 2265 (2002) doi:10.1142/S0217732302008897 [hep-ph/0206156].
- [213] M. A. Sanchis-Lozano, Nucl. Phys. Proc. Suppl. **115**, 374 (2003) doi:10.1016/S0920-5632(02)02022-4 [hep-ph/0210364].
- [214] M. A. Sanchis-Lozano, Int. J. Mod. Phys. A **19**, 2183 (2004) doi:10.1142/S0217751X04018117 [hep-ph/0307313].
- [215] E. Fullana and M. A. Sanchis-Lozano, Phys. Lett. B **653**, 67 (2007) doi:10.1016/j.physletb.2007.06.078 [hep-ph/0702190].
- [216] W. Buchmuller, R. Ruckl and D. Wyler, Phys. Lett. B **191**, 442 (1987) Erratum: [Phys. Lett. B **448**, 320 (1999)]. doi:10.1016/S0370-2693(99)00014-3, 10.1016/0370-2693(87)90637-X
- [217] H. Georgi and S. L. Glashow, Phys. Rev. Lett. **32**, 438 (1974). doi:10.1103/PhysRevLett.32.438

- [218] J. C. Pati and A. Salam, Phys. Rev. D **10**, 275 (1974) Erratum: [Phys. Rev. D **11**, 703 (1975)]. doi:10.1103/PhysRevD.10.275, 10.1103/PhysRevD.11.703.2
- [219] L. F. Abbott and E. Farhi, Phys. Lett. **101B**, 69 (1981). doi:10.1016/0370-2693(81)90492-5
- [220] B. Schrempp and F. Schrempp, Phys. Lett. **153B**, 101 (1985). doi:10.1016/0370-2693(85)91450-9
- [221] J. Wudka, Phys. Lett. **167B**, 337 (1986). doi:10.1016/0370-2693(86)90356-4
- [222] I. Doršner, S. Fajfer and N. Košnik, Eur. Phys. J. C **77**, no. 6, 417 (2017) doi:10.1140/epjc/s10052-017-4987-2 [arXiv:1701.08322 [hep-ph]].
- [223] J. L. Hewett and T. G. Rizzo, Phys. Rev. D **36**, 3367 (1987). doi:10.1103/PhysRevD.36.3367
- [224] I. Doršner, S. Fajfer, N. Košnik and I. Nišandžić, JHEP **1311**, 084 (2013) doi:10.1007/JHEP11(2013)084 [arXiv:1306.6493 [hep-ph]].
- [225] I. Doršner, S. Fajfer, J. F. Kamenik and N. Kosnik, Phys. Lett. B **682**, 67 (2009) doi:10.1016/j.physletb.2009.10.087 [arXiv:0906.5585 [hep-ph]].
- [226] N. Kosnik, Phys. Rev. D **86**, 055004 (2012) doi:10.1103/PhysRevD.86.055004 [arXiv:1206.2970 [hep-ph]].
- [227] H. Fritzsch and P. Minkowski, Annals Phys. **93**, 193 (1975). doi:10.1016/0003-4916(75)90211-0
- [228] H. Georgi, AIP Conf. Proc. **23**, 575 (1975). doi:10.1063/1.2947450
- [229] P. Cox, A. Kusenko, O. Sumensari and T. T. Yanagida, JHEP **1703**, 035 (2017) doi:10.1007/JHEP03(2017)035 [arXiv:1612.03923 [hep-ph]].
- [230] R. Slansky, Phys. Rept. **79**, 1 (1981). doi:10.1016/0370-1573(81)90092-2
- [231] J. R. Ellis and M. K. Gaillard, Phys. Lett. **88B**, 315 (1979). doi:10.1016/0370-2693(79)90476-3
- [232] H. Georgi and C. Jarlskog, Phys. Lett. **86B**, 297 (1979). doi:10.1016/0370-2693(79)90842-6
- [233] H. Murayama and T. Yanagida, Mod. Phys. Lett. A **7**, 147 (1992). doi:10.1142/S0217732392000070
- [234] A. Giveon, L. J. Hall and U. Sarid, Phys. Lett. B **271**, 138 (1991). doi:10.1016/0370-2693(91)91289-8
- [235] I. Doršner and P. Fileviez Perez, Nucl. Phys. B **723**, 53 (2005) doi:10.1016/j.nuclphysb.2005.06.016 [hep-ph/0504276].
- [236] B. Bajc and G. Senjanovic, JHEP **0708**, 014 (2007) doi:10.1088/1126-6708/2007/08/014 [hep-ph/0612029].
- [237] P. Fileviez Perez and C. Murgui, Phys. Rev. D **94**, no. 7, 075014 (2016) doi:10.1103/PhysRevD.94.075014 [arXiv:1604.03377 [hep-ph]].

- [238] H. Nishino *et al.* [Super-Kamiokande Collaboration], Phys. Rev. D **85**, 112001 (2012) doi:10.1103/PhysRevD.85.112001 [arXiv:1203.4030 [hep-ex]].
- [239] S. N. Ahmed *et al.* [SNO Collaboration], Phys. Rev. Lett. **92**, 102004 (2004) doi:10.1103/PhysRevLett.92.102004 [hep-ex/0310030].
- [240] C. Bachas, C. Fabre and T. Yanagida, Phys. Lett. B **370**, 49 (1996) doi:10.1016/0370-2693(95)01561-2 [hep-th/9510094].
- [241] H. Murayama, Y. Okada and T. Yanagida, Prog. Theor. Phys. **88**, 791 (1992). doi:10.1143/PTP.88.791
- [242] M. E. Machacek and M. T. Vaughn, Nucl. Phys. B **222**, 83 (1983). doi:10.1016/0550-3213(83)90610-7
- [243] K. Abe *et al.*, arXiv:1109.3262 [hep-ex].
- [244] J. M. Arnold, B. Fornal and M. B. Wise, Phys. Rev. D **87**, 075004 (2013) doi:10.1103/PhysRevD.87.075004 [arXiv:1212.4556 [hep-ph]].
- [245] P. Fileviez Perez, Phys. Lett. B **595**, 476 (2004) doi:10.1016/j.physletb.2004.06.061 [hep-ph/0403286].
- [246] Y. Aoki, E. Shintani and A. Soni, Phys. Rev. D **89**, no. 1, 014505 (2014) doi:10.1103/PhysRevD.89.014505 [arXiv:1304.7424 [hep-lat]].
- [247] The ATLAS collaboration [ATLAS Collaboration], ATLAS-CONF-2016-084.
- [248] H. Nishino *et al.* [Super-Kamiokande Collaboration], Phys. Rev. D **85**, 112001 (2012) doi:10.1103/PhysRevD.85.112001 [arXiv:1203.4030 [hep-ex]].
- [249] I. Dorsner and P. Fileviez Perez, Phys. Lett. B **625**, 88 (2005) doi:10.1016/j.physletb.2005.08.039 [hep-ph/0410198].
- [250] C. D. Froggatt, R. G. Moorhouse and I. G. Knowles, Phys. Rev. D **45**, 2471 (1992). doi:10.1103/PhysRevD.45.2471
- [251] E. Keith and E. Ma, Phys. Rev. Lett. **79**, 4318 (1997) doi:10.1103/PhysRevLett.79.4318 [hep-ph/9707214].
- [252] R. Aaij *et al.* [LHCb Collaboration], Phys. Lett. B **724**, 203 (2013) doi:10.1016/j.physletb.2013.06.010 [arXiv:1304.6365 [hep-ex]].
- [253] R. Aaij *et al.* [LHCb Collaboration], Phys. Lett. B **725**, 15 (2013) doi:10.1016/j.physletb.2013.06.037 [arXiv:1305.5059 [hep-ex]].
- [254] M. Bauer and M. Neubert, Phys. Rev. Lett. **116**, no. 14, 141802 (2016) doi:10.1103/PhysRevLett.116.141802 [arXiv:1511.01900 [hep-ph]].
- [255] D. Das, C. Hati, G. Kumar and N. Mahajan, Phys. Rev. D **94**, 055034 (2016) doi:10.1103/PhysRevD.94.055034 [arXiv:1605.06313 [hep-ph]].
- [256] M. Aaboud *et al.* [ATLAS Collaboration], New J. Phys. **18**, no. 9, 093016 (2016) doi:10.1088/1367-2630/18/9/093016 [arXiv:1605.06035 [hep-ex]].

- [257] CMS Collaboration [CMS Collaboration], CMS-PAS-EXO-16-043.
- [258] CMS Collaboration [CMS Collaboration], CMS-PAS-EXO-16-007.
- [259] V. Khachatryan *et al.* [CMS Collaboration], JHEP **1703**, 077 (2017) doi:10.1007/JHEP03(2017)077 [arXiv:1612.01190 [hep-ex]].
- [260] CMS Collaboration [CMS Collaboration], CMS-PAS-EXO-16-023.
- [261] G. Aad *et al.* [ATLAS Collaboration], Eur. Phys. J. C **76**, no. 1, 5 (2016) doi:10.1140/epjc/s10052-015-3823-9 [arXiv:1508.04735 [hep-ex]].
- [262] V. Khachatryan *et al.* [CMS Collaboration], JHEP **1507**, 042 (2015) Erratum: [JHEP **1611**, 056 (2016)] doi:10.1007/JHEP11(2016)056, 10.1007/JHEP07(2015)042 [arXiv:1503.09049 [hep-ex]].
- [263] D. A. Faroughy, A. Greljo and J. F. Kamenik, Phys. Lett. B **764**, 126 (2017) doi:10.1016/j.physletb.2016.11.011 [arXiv:1609.07138 [hep-ph]].
- [264] A. Greljo and D. Marzocca, arXiv:1704.09015 [hep-ph].
- [265] A. Pich, Prog. Part. Nucl. Phys. **75**, 41 (2014) doi:10.1016/j.ppnp.2013.11.002 [arXiv:1310.7922 [hep-ph]].
- [266] M. Finkemeier, Phys. Lett. B **387**, 391 (1996) doi:10.1016/0370-2693(96)01030-1 [hep-ph/9505434].
- [267] V. Cirigliano and I. Rosell, Phys. Rev. Lett. **99**, 231801 (2007) doi:10.1103/PhysRevLett.99.231801 [arXiv:0707.3439 [hep-ph]].
- [268] G. Hiller and F. Kruger, Phys. Rev. D **69**, 074020 (2004) doi:10.1103/PhysRevD.69.074020 [hep-ph/0310219].
- [269] G. D'Amico, M. Nardecchia, P. Panci, F. Sannino, A. Strumia, R. Torre and A. Urbano, arXiv:1704.05438 [hep-ph].
- [270] G. Wormser, FPCP Conference, June 5, 2017;  
[https://indico.cern.ch/event/586719/contributions/2531261/attachments/1470695/2275578/2\\_fpcp\\_talk\\_wormser.pdf](https://indico.cern.ch/event/586719/contributions/2531261/attachments/1470695/2275578/2_fpcp_talk_wormser.pdf)
- [271] W. Altmannshofer, P. Stangl and D. M. Straub, arXiv:1704.05435 [hep-ph].
- [272] B. Capdevila, A. Crivellin, S. Descotes-Genon, J. Matias and J. Virto, arXiv:1704.05340 [hep-ph].
- [273] J. Matias, F. Mescia, M. Ramon and J. Virto, JHEP **1204**, 104 (2012) doi:10.1007/JHEP04(2012)104 [arXiv:1202.4266 [hep-ph]].
- [274] S. Descotes-Genon, J. Matias, M. Ramon and J. Virto, JHEP **1301**, 048 (2013) doi:10.1007/JHEP01(2013)048 [arXiv:1207.2753 [hep-ph]].
- [275] R. Aaij *et al.* [LHCb Collaboration], Phys. Rev. Lett. **111**, 191801 (2013) doi:10.1103/PhysRevLett.111.191801 [arXiv:1308.1707 [hep-ex]].
- [276] S. Descotes-Genon, L. Hofer, J. Matias and J. Virto, JHEP **1606**, 092 (2016) doi:10.1007/JHEP06(2016)092 [arXiv:1510.04239 [hep-ph]].

- [277] A. Abdesselam *et al.* [Belle Collaboration], arXiv:1604.04042 [hep-ex].
- [278] A. Khodjamirian, T. Mannel, A. A. Pivovarov and Y.-M. Wang, JHEP **1009**, 089 (2010) doi:10.1007/JHEP09(2010)089 [arXiv:1006.4945 [hep-ph]].
- [279] W. Altmannshofer, S. Gori, M. Pospelov and I. Yavin, Phys. Rev. D **89**, 095033 (2014) doi:10.1103/PhysRevD.89.095033 [arXiv:1403.1269 [hep-ph]].
- [280] W. Altmannshofer and I. Yavin, Phys. Rev. D **92**, no. 7, 075022 (2015) doi:10.1103/PhysRevD.92.075022 [arXiv:1508.07009 [hep-ph]].
- [281] W. Altmannshofer, M. Carena and A. Crivellin, Phys. Rev. D **94**, no. 9, 095026 (2016) doi:10.1103/PhysRevD.94.095026 [arXiv:1604.08221 [hep-ph]].
- [282] W. Altmannshofer, S. Gori, S. Profumo and F. S. Queiroz, JHEP **1612**, 106 (2016) doi:10.1007/JHEP12(2016)106 [arXiv:1609.04026 [hep-ph]].
- [283] R. Alonso, P. Cox, C. Han and T. T. Yanagida, arXiv:1705.03858 [hep-ph].
- [284] C. Bonilla, T. Modak, R. Srivastava and J. W. F. Valle, arXiv:1705.00915 [hep-ph].
- [285] A. Celis, J. Fuentes-Martin, M. Jung and H. Serodio, Phys. Rev. D **92**, no. 1, 015007 (2015) doi:10.1103/PhysRevD.92.015007 [arXiv:1505.03079 [hep-ph]].
- [286] D. Aristizabal Sierra, F. Staub and A. Vicente, Phys. Rev. D **92**, no. 1, 015001 (2015) doi:10.1103/PhysRevD.92.015001 [arXiv:1503.06077 [hep-ph]].
- [287] G. Bélanger, C. Delaunay and S. Westhoff, Phys. Rev. D **92**, 055021 (2015) doi:10.1103/PhysRevD.92.055021 [arXiv:1507.06660 [hep-ph]].
- [288] R. Gauld, F. Goertz and U. Haisch, JHEP **1401**, 069 (2014) doi:10.1007/JHEP01(2014)069 [arXiv:1310.1082 [hep-ph]].
- [289] A. J. Buras, F. De Fazio and J. Girrbach, JHEP **1402**, 112 (2014) doi:10.1007/JHEP02(2014)112 [arXiv:1311.6729 [hep-ph]].
- [290] S. M. Boucenna, A. Celis, J. Fuentes-Martin, A. Vicente and J. Virto, Phys. Lett. B **760**, 214 (2016) doi:10.1016/j.physletb.2016.06.067 [arXiv:1604.03088 [hep-ph]].
- [291] R. Alonso, P. Cox, C. Han and T. T. Yanagida, arXiv:1704.08158 [hep-ph].
- [292] J. M. Cline and J. Martin Camalich, arXiv:1706.08510 [hep-ph].
- [293] A. Crivellin, J. Fuentes-Martin, A. Greljo and G. Isidori, Phys. Lett. B **766**, 77 (2017) doi:10.1016/j.physletb.2016.12.057 [arXiv:1611.02703 [hep-ph]].
- [294] J. F. Kamenik, Y. Soreq and J. Zupan, arXiv:1704.06005 [hep-ph].
- [295] S. Fajfer and N. Košnik, Phys. Lett. B **755**, 270 (2016) doi:10.1016/j.physletb.2016.02.018 [arXiv:1511.06024 [hep-ph]].
- [296] R. Barbieri, G. Isidori, A. Pattori and F. Senia, Eur. Phys. J. C **76**, no. 2, 67 (2016) doi:10.1140/epjc/s10052-016-3905-3 [arXiv:1512.01560 [hep-ph]].
- [297] C. Biggio, M. Bordone, L. Di Luzio and G. Ridolfi, JHEP **1610**, 002 (2016) doi:10.1007/JHEP10(2016)002 [arXiv:1607.07621 [hep-ph]].

- [298] R. Barbieri, C. W. Murphy and F. Senia, *Eur. Phys. J. C* **77**, no. 1, 8 (2017) doi:10.1140/epjc/s10052-016-4578-7 [arXiv:1611.04930 [hep-ph]].
- [299] A. Crivellin, D. Müller and T. Ota, arXiv:1703.09226 [hep-ph].
- [300] G. Hiller and I. Nisandzic, arXiv:1704.05444 [hep-ph].
- [301] I. Doršner, S. Fajfer, D. A. Faroughy and N. Košnik, arXiv:1706.07779 [hep-ph].
- [302] B. Gripaios, M. Nardecchia and S. A. Renner, *JHEP* **1606**, 083 (2016) doi:10.1007/JHEP06(2016)083 [arXiv:1509.05020 [hep-ph]].
- [303] P. Arnan, L. Hofer, F. Mescia and A. Crivellin, *JHEP* **1704**, 043 (2017) doi:10.1007/JHEP04(2017)043 [arXiv:1608.07832 [hep-ph]].
- [304] F. Sala and D. M. Straub, arXiv:1704.06188 [hep-ph].
- [305] E. Megias, G. Panico, O. Pujolas and M. Quiros, *JHEP* **1609**, 118 (2016) doi:10.1007/JHEP09(2016)118 [arXiv:1608.02362 [hep-ph]].
- [306] I. Garcia Garcia, *JHEP* **1703**, 040 (2017) doi:10.1007/JHEP03(2017)040 [arXiv:1611.03507 [hep-ph]].
- [307] C. Niehoff, P. Stangl and D. M. Straub, *Phys. Lett. B* **747**, 182 (2015) doi:10.1016/j.physletb.2015.05.063 [arXiv:1503.03865 [hep-ph]].
- [308] A. Carmona and F. Goertz, *Phys. Rev. Lett.* **116**, no. 25, 251801 (2016) doi:10.1103/PhysRevLett.116.251801 [arXiv:1510.07658 [hep-ph]].
- [309] Y. Cai, J. Gargalionis, M. A. Schmidt and R. R. Volkas, arXiv:1704.05849 [hep-ph].
- [310] K. A. Olive *et al.* [Particle Data Group], *Chin. Phys. C* **38**, 090001 (2014). doi:10.1088/1674-1137/38/9/090001
- [311] J. P. Lees *et al.* [BaBar Collaboration], *Phys. Rev. D* **87**, no. 11, 112005 (2013) doi:10.1103/PhysRevD.87.112005 [arXiv:1303.7465 [hep-ex]].
- [312] A. J. Buras, J. Girrbach-Noe, C. Niehoff and D. M. Straub, *JHEP* **1502**, 184 (2015) doi:10.1007/JHEP02(2015)184 [arXiv:1409.4557 [hep-ph]].
- [313] W. Altmannshofer, A. J. Buras, D. M. Straub and M. Wick, *JHEP* **0904**, 022 (2009) doi:10.1088/1126-6708/2009/04/022 [arXiv:0902.0160 [hep-ph]].
- [314] R. Glattauer *et al.* [Belle Collaboration], *Phys. Rev. D* **93**, no. 3, 032006 (2016) doi:10.1103/PhysRevD.93.032006 [arXiv:1510.03657 [hep-ex]].
- [315] A. Abdesselam *et al.* [Belle Collaboration], arXiv:1702.01521 [hep-ex].
- [316] A. Greljo, G. Isidori and D. Marzocca, *JHEP* **1507**, 142 (2015) doi:10.1007/JHEP07(2015)142 [arXiv:1506.01705 [hep-ph]].
- [317] B. Aubert *et al.* [BaBar Collaboration], *Phys. Rev. Lett.* **104**, 021802 (2010) doi:10.1103/PhysRevLett.104.021802 [arXiv:0908.2381 [hep-ex]].
- [318] Y. Sakaki, M. Tanaka, A. Tayduganov and R. Watanabe, *Phys. Rev. D* **88**, no. 9, 094012 (2013) doi:10.1103/PhysRevD.88.094012 [arXiv:1309.0301 [hep-ph]].

- [319] D. Bečirević and O. Sumensari, JHEP **1708** (2017) 104 doi:10.1007/JHEP08(2017)104 [arXiv:1704.05835 [hep-ph]].
- [320] L. Lavoura, Eur. Phys. J. C **29**, 191 (2003) doi:10.1140/epjc/s2003-01212-7 [hep-ph/0302221].
- [321] A. Nyffeler, Nuovo Cim. C **037**, no. 02, 173 (2014) [Int. J. Mod. Phys. Conf. Ser. **35**, 1460456 (2014)] doi:10.1393/ncc/i2014-11752-0, 10.1142/S2010194514604566 [arXiv:1312.4804 [hep-ph]].
- [322] E. Coluccio Leskow, G. D'Ambrosio, A. Crivellin and D. Müller, Phys. Rev. D **95**, no. 5, 055018 (2017) doi:10.1103/PhysRevD.95.055018 [arXiv:1612.06858 [hep-ph]].
- [323] T. A. Aaltonen *et al.* [CDF Collaboration], Phys. Rev. D **89**, no. 9, 091101 (2014) doi:10.1103/PhysRevD.89.091101 [arXiv:1402.6728 [hep-ex]].
- [324] B. Grinstein and A. Kobach, Phys. Lett. B **771**, 359 (2017) doi:10.1016/j.physletb.2017.05.078 [arXiv:1703.08170 [hep-ph]].
- [325] D. Bigi, P. Gambino and S. Schacht, Phys. Lett. B **769**, 441 (2017) doi:10.1016/j.physletb.2017.04.022 [arXiv:1703.06124 [hep-ph]].
- [326] I. Caprini and M. Neubert, Phys. Lett. B **380**, 376 (1996) doi:10.1016/0370-2693(96)00509-6 [hep-ph/9603414].
- [327] I. Caprini, L. Lellouch and M. Neubert, Nucl. Phys. B **530**, 153 (1998) doi:10.1016/S0550-3213(98)00350-2 [hep-ph/9712417].
- [328] W. Dungen *et al.* [Belle Collaboration], Phys. Rev. D **82**, 112007 (2010) doi:10.1103/PhysRevD.82.112007 [arXiv:1010.5620 [hep-ex]].
- [329] A. F. Falk and M. Neubert, Phys. Rev. D **47**, 2965 (1993) doi:10.1103/PhysRevD.47.2965 [hep-ph/9209268].
- [330] M. Neubert, Phys. Rev. D **46**, 2212 (1992). doi:10.1103/PhysRevD.46.2212
- [331] C. G. Boyd, B. Grinstein and R. F. Lebed, Phys. Rev. D **56**, 6895 (1997) doi:10.1103/PhysRevD.56.6895 [hep-ph/9705252].
- [332] F. U. Bernlochner, Z. Ligeti, M. Papucci and D. J. Robinson, Phys. Rev. D **95**, no. 11, 115008 (2017) doi:10.1103/PhysRevD.95.115008 [arXiv:1703.05330 [hep-ph]].
- [333] D. Guadagnoli, Mod. Phys. Lett. A **32**, no. 7, 1730006 (2017) doi:10.1142/S0217732317300063 [arXiv:1703.02804 [hep-ph]].
- [334] B. Bhattacharya, A. Datta, D. London and S. Shivashankara, Phys. Lett. B **742**, 370 (2015) doi:10.1016/j.physletb.2015.02.011 [arXiv:1412.7164 [hep-ph]].
- [335] R. Alonso, B. Grinstein and J. Martin Camalich, JHEP **1510**, 184 (2015) doi:10.1007/JHEP10(2015)184 [arXiv:1505.05164 [hep-ph]].
- [336] L. Calibbi, A. Crivellin and T. Ota, Phys. Rev. Lett. **115**, 181801 (2015) doi:10.1103/PhysRevLett.115.181801 [arXiv:1506.02661 [hep-ph]].

- [337] F. Feruglio, P. Paradisi and A. Pattori, Phys. Rev. Lett. **118**, no. 1, 011801 (2017) doi:10.1103/PhysRevLett.118.011801 [arXiv:1606.00524 [hep-ph]].
- [338] L. Di Luzio and M. Nardecchia, arXiv:1706.01868 [hep-ph].
- [339] M. Bordone, G. Isidori and S. Trifinopoulos, arXiv:1702.07238 [hep-ph].
- [340] A. Crivellin, C. Greub and A. Kokulu, Phys. Rev. D **86**, 054014 (2012) doi:10.1103/PhysRevD.86.054014 [arXiv:1206.2634 [hep-ph]].
- [341] X. Q. Li, Y. D. Yang and X. Zhang, JHEP **1608**, 054 (2016) doi:10.1007/JHEP08(2016)054 [arXiv:1605.09308 [hep-ph]].
- [342] R. Alonso, B. Grinstein and J. Martin Camalich, Phys. Rev. Lett. **118**, no. 8, 081802 (2017) doi:10.1103/PhysRevLett.118.081802 [arXiv:1611.06676 [hep-ph]].
- [343] A. Celis, M. Jung, X. Q. Li and A. Pich, Phys. Lett. B **771**, 168 (2017) doi:10.1016/j.physletb.2017.05.037 [arXiv:1612.07757 [hep-ph]].
- [344] D. Buttazzo, A. Greljo, G. Isidori and D. Marzocca, arXiv:1706.07808 [hep-ph].
- [345] D. Bečirević, S. Fajfer, N. Košnik and O. Sumensari, Phys. Rev. D **94**, no. 11, 115021 (2016) doi:10.1103/PhysRevD.94.115021 [arXiv:1608.08501 [hep-ph]].
- [346] N. Carrasco *et al.* [ETM Collaboration], JHEP **1403**, 016 (2014) doi:10.1007/JHEP03(2014)016 [arXiv:1308.1851 [hep-lat]].
- [347] G. C. Donald *et al.* [HPQCD Collaboration], Phys. Rev. D **90**, no. 7, 074506 (2014) doi:10.1103/PhysRevD.90.074506 [arXiv:1311.6669 [hep-lat]].
- [348] J. Brod, M. Gorbahn and E. Stamou, Phys. Rev. D **83**, 034030 (2011) doi:10.1103/PhysRevD.83.034030 [arXiv:1009.0947 [hep-ph]].
- [349] M. Atoui, V. Morénas, D. Bečirevic and F. Sanfilippo, Eur. Phys. J. C **74**, no. 5, 2861 (2014) doi:10.1140/epjc/s10052-014-2861-z [arXiv:1310.5238 [hep-lat]].
- [350] W. Love *et al.* [CLEO Collaboration], Phys. Rev. Lett. **101**, 201601 (2008) doi:10.1103/PhysRevLett.101.201601 [arXiv:0807.2695 [hep-ex]].
- [351] D. Melikhov and B. Stech, Phys. Rev. D **62**, 014006 (2000) doi:10.1103/PhysRevD.62.014006 [hep-ph/0001113].
- [352] R. Aaij *et al.* [LHCb Collaboration], Phys. Rev. Lett. **118**, no. 25, 251802 (2017) doi:10.1103/PhysRevLett.118.251802 [arXiv:1703.02508 [hep-ex]].
- [353] G. W. Bennett *et al.* [Muon g-2 Collaboration], Phys. Rev. D **73**, 072003 (2006) doi:10.1103/PhysRevD.73.072003 [hep-ex/0602035].

# Résumé en Français

Le modèle Standard (MS) de la physique des particules est une théorie de jauge quantique qui décrit avec élégance et précision les interactions des particules subatomiques. Ses prédictions théoriques ont été testées dans les accélérateurs de particules à basses et hautes énergies, en montrant un excellent accord avec les données expérimentales. En particulier, la découverte au LHC de la dernière particule manquante dans son spectre, le boson de Higgs, représente une de ses plus importantes prouesses et corrobore six décennies de succès phénoménologiques persistents [1, 2].

Néanmoins, le MS ne peut pas être la théorie ultime de la nature. Premièrement, le MS n'incorpore pas les interactions gravitationnelles, bien que les effets quantiques de la gravité deviennent importants seulement à des échelles d'énergie pratiquement inaccessibles, près de l'échelle de Planck. En outre, les neutrinos sont des particules sans masses dans le MS, ce qui contredit les observations expérimentales selon lesquelles les neutrinos sont massifs et oscillent entre différents saveurs. Il existe aussi un nombre croissant d'évidences d'origine astrophysique et cosmologique, basées sur le modèle standard cosmologique et sur la relativité générale, qui suggèrent qu'une partie substantielle de la matière dans l'univers n'est pas barionique, ni chargée par les interactions électromagnétiques. Si on suppose la validité de ces théories aux larges échelles, on en déduit que la physique des particules doit proposer des nouvelles particules qui interagissent par des moyens non décrits par le MS de la physique des particules pour expliquer ces phénomènes.

En plus des observations expérimentales évoquées ci-dessus qui ne peuvent pas être décrites par le MS, il existe aussi plusieurs problèmes conceptuels qui ne peuvent être entièrement compris sans postuler l'existence de la physique au-delà du MS. Alors que le secteur de jauge du MS est étonnamment simple et prédictif, notre compréhension actuelle de la saveur est très insatisfaisante. Les fermions sont organisés en trois copies identiques qui se distinguent uniquement par leurs interactions de Yukawa. Contrairement au secteur de jauge, le secteur de Yukawa est peu contraint par des symétries. Par conséquent, de nombreux paramètres (masses des fermions et paramètres de mélange) doivent être déterminés en confrontant les prédictions théoriques avec les mesures expérimentales. En particulier, les mesures des masses fermioniques ont montré une frappante hiérarchie de valeurs, comme montre la Fig. B.1. De même, une structure très hiérarchique a été observée pour les éléments de la matrice de Cabibbo-Kobayashi-Maskawa (CKM) qui devient manifeste dans la paramétrisation de Wolfenstein, à savoir, [66]

$$V_{\text{CKM}} = \begin{pmatrix} 1 - \frac{\lambda^2}{2} & \lambda & A \lambda^3(\rho - i\eta) \\ -\lambda & 1 - \frac{\lambda^2}{2} & A \lambda^2 \\ A \lambda^3(1 - \rho - i\eta) & -A \lambda^2 & 1 \end{pmatrix} + \mathcal{O}(\lambda^4), \quad (\text{B.21})$$

où  $A$ ,  $\rho$  et  $\eta$  sont des nombres réels d'ordre  $\mathcal{O}(1)$ .<sup>2</sup> Ces motifs hiérarchiques suggèrent

---

<sup>2</sup>Les études actuelles des observables de la physique de la saveur nous ont permis de déterminer  $\rho =$

l'existence des symétries sous-jacentes au MS qui restent à être dévoilées. Le manque de compréhension de la structure de saveur du MS est connu comme le problème de la saveur. De plus, les corrections quantiques à la masse du boson de Higgs ont des divergences quadratiques, elles sont ainsi paradoxalement sensibles aux détails de la théorie ultraviolette qui complète le MS. Ce problème est connu sous le nom de problème de hiérarchie et constitue la principale motivation pour rechercher les effets de la nouvelle physique (NP) à l'échelle du TeV.

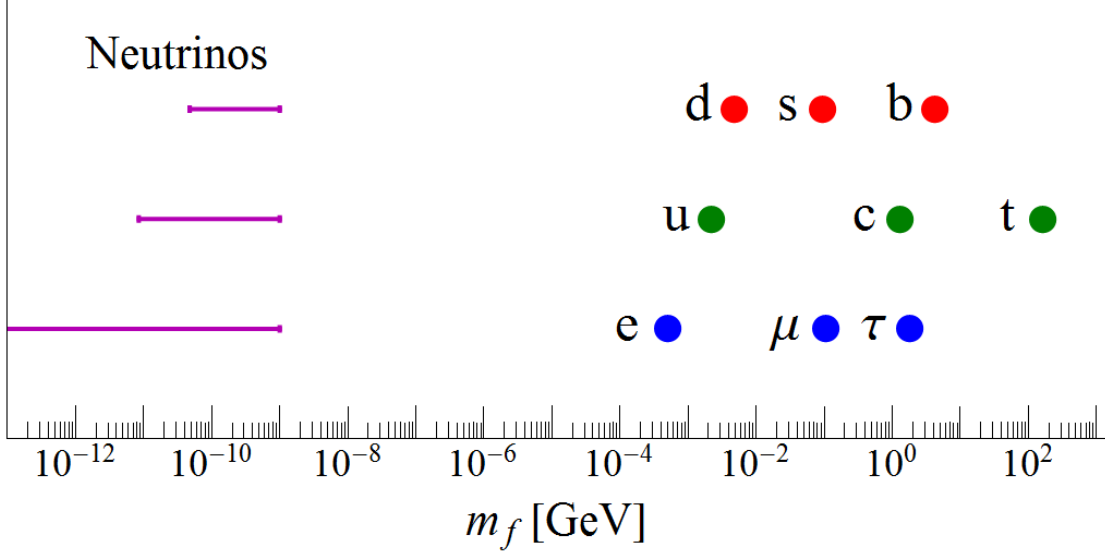


**Figure B.1:** Masses des fermions déterminés par la comparaison entre la théorie et l'expérience. Nous prenons les masses de quarks dans le schéma  $\overline{MS}$  à l'échelle  $\mu = 2$  GeV pour les quarks légers et à  $\mu = m_q$  pour  $q = c, b, t$  [22].

Tous les problèmes décrits ci-dessus requièrent l'existence de la physique au-delà du SM, et de nombreuses propositions ont été faites au cours des dernières décennies pour résoudre chacun de ces problèmes. En particulier, la simplicité et la beauté ont été les principaux guides dans la quête de la NP. Cependant, malgré l'intense effort théorique, à l'heure actuelle il n'existe pas de préférence théorique pour un scénario spécifique de la physique au-delà du SM. Il devient donc nécessaire d'utiliser les expériences modernes pour choisir parmi les différentes options de scénarios de la NP. La recherche des effets de la NP peut se faire par deux approches complémentaires : la recherche directe de nouvelles particules dans des accélérateurs à très hautes énergies, et la recherche indirecte des effets de la NP dans les observables à basses énergies. La dernière approche a constitué l'objet principal d'étude de cette thèse.

Les résultats des recherches indirectes, et plus particulièrement ceux de la physique de la saveur, ont été largement utilisés dans le passé pour sonder les hautes échelles d'énergie à travers des expériences à basse énergie. Un exemple notable est la première observation du mélange des mésons  $B^0 - \overline{B}^0$  [3], qui a indiqué que le quark top devrait être beaucoup plus lourd que les autres fermions du MS avant sa découverte au Tevatron [4, 5]. En outre, les observables de la physique des saveurs fournissent des informations très utiles sur la physique au-delà du SM. Un exemple remarquable est le paramètre de mélange  $\epsilon_K$  pour les mésons  $K^0 - \overline{K}^0$  qui, après la comparaison des prédictions théoriques du MS avec les mesures expérimentales, nous permet d'établir une limite inférieure d'environ  $10^8$  GeV pour l'échelle de la NP – sous l'hypothèse de couplages d'ordre  $\mathcal{O}(1)$  universels [6]. En

0.157(14),  $\eta = 0.352(11)$ ,  $A = 0.833(12)$  e  $\lambda = 0.22497(69)$  [64].

particulier, cela signifie que les modèles de la NP avec des particules aux alentours de l'échelle du TeV, comme le problème de la hiérarchie suggère, doivent avoir une structure non-triviale de la saveur. En ce qui concerne les recherches de la NP, on s'appuie sur des approches génériques avec le moins d'hypothèses possibles. Les théories des champs effectifs (EFT) sont l'approche la plus efficace à cet égard, car elles fournissent une description générale de la physique des basses énergies sans avoir à postuler ce qui se passe à des échelles d'énergie arbitrairement élevées. Une autre approche complémentaire consiste à considérer des extensions minimales et pragmatiques du SM, de préférence génériques, qui nous permettent d'utiliser les informations issues des observables de la saveur pour guider les recherches directes de nouvelles résonances à hautes énergies. Un tel exemple est celui des modèles aux deux doublets de Higgs (2HDM), aussi intégrés dans diverses extensions super-symétriques (ou non) du MS [7]. Une autre possibilité qui a gagné en popularité ces dernières années est de considérer les différents bosons leptoquark (LQ), qui peuvent apparaître dans les scénarios de grande unification et dans les modèles composites de Higgs, parmi d'autres scénarios de la NP [8].

Dans cette thèse, nous avons extrait l'information de la nouvelle physique à travers les observables de la physique de la saveur. Les expériences en cours à NA62, BES-III et LHCb nous ont fourni un riche ensemble de données pour tester les différents scénarios de la NP et pour guider l'effort théorique vers une théorie de la saveur au-delà du MS. Les informations extraites de ces données seront corroborées/complétées par les expériences futures, à savoir, Belle-II, KOTO, TREK,  $(g - 2)_\mu$  et Mu2E, en produisant un scénario très prolifique pour la physique de la saveur. Pour interpréter ces résultats, nous avons formulé des théories efficaces des champs qui ont été mises en correspondance avec les modèles minimaux de la NP motivés par les récentes découvertes expérimentales. La première partie de cette thèse est consacrée au boson de Higgs, la dernière particule prédite par le MS à être observée expérimentalement. Alors que les couplages du boson de Higgs mesurés au LHC permettent toujours des larges déviations des prédictions du MS, les recherches directes n'ont pas encore exclu la possibilité de l'existence d'autres particules légères dans le spectre. Dans la première partie de cette thèse, nous nous sommes concentrés sur les 2HDM, et nous avons exploré les leçons qui peuvent être tirées des contraintes théoriques et phénoménologiques sur ces modèles. Les masses et couplages des particules scalaires permises par notre analyse basée sur les contraintes génériques ont été confrontées avec les observables de la physique de la saveur. A cette fin, nous avons calculé l'ensemble complet de coefficients de Wilson contribuant aux désintégrations des mésons pertinentes au niveau de l'arbre et au niveau des boucles. Ces résultats ont été confrontés avec les résultats expérimentaux pour dériver des contraintes sur le spectre des 2HDM. Une attention particulière a été accordée aux modes exclusifs de la désintégration  $b \rightarrow s\ell^+\ell^-$  en raison du grand effort expérimental consacré à l'étude de ces observables au LHCb. Parmi les scénarios que nous considérons, la possibilité intrigante qu'un Higgs CP-impair léger ( $m_A \lesssim 125$  GeV) soit présent dans le spectre a été explorée. Une telle particule serait la bienvenue en tant que médiateur entre le MS et le secteur sombre. Cela provient du fait que le portail pseudoscalaire peut échapper aux sévères contraintes provenant de l'absence de signal dans les expériences de détections directe de la matière noire [9, 10]. Nous avons montré que ce scénario est parfaitement plausible à la lumière des contraintes théoriques et expérimentales actuelles, et nous avons discuté des stratégies pour rechercher cette particule dans les désintégrations exclusives de Higgs et dans les modes de désintégration de quarkonia.

La seconde partie de cette thèse a été consacrée aux signes de violation de l'universalité de la saveur leptonique (LFU) dans les désintégrations semileptoniques des mésons  $B$ . Plus

précisément, la mesure par LHCb de [11]

$$R_K = \frac{\mathcal{B}(B \rightarrow K \mu^+ \mu^-)}{\mathcal{B}(B \rightarrow K e^+ e^-)} \Big|_{q^2 \in [1,6] \text{ GeV}^2}, \quad (\text{B.22})$$

et plus récemment de [12]

$$R_{K^*} = \frac{\mathcal{B}(B \rightarrow K^* \mu^+ \mu^-)}{\mathcal{B}(B \rightarrow K^* e^+ e^-)} \Big|_{q^2 \in [q_{\min}^2, q_{\max}^2]}, \quad (\text{B.23})$$

dans différentes régions de moment leptonique carré  $q^2$  étaient significativement plus basses que prévu par le MS [13]. Ces observables sont presque exempts d'incertitudes théoriques puisque les incertitudes hadroniques s'annulent dans le rapport. Tandis que ces résultats doivent encore être confirmés par une expérience indépendante (à savoir, Belle-II), ils ont déclenché une activité théorique intense pour comprendre les possibles origines de ces écarts. Dans les scénarios 2HDM discutés ci-dessus, la violation de LFU est négligeable, qui suggère que d'autres contributions bosoniques soient nécessaires pour expliquer ces effets. Pour ce faire, nous considérons les scénarios postulant l'existence de divers états LQ à basses énergies. Alors que ces particules sont souvent considérées comme exotiques dans les recherches directes au LHC, elles offrent l'un des candidats les plus proéminents pour expliquer les effets de la violation de la LFU. Dans cette thèse, nous avons examiné les explications de  $R_{K^{(*)}}^{\text{exp}} < R_{K^{(*)}}^{\text{SM}}$  à travers les états LQ et nous avons exploré les implications de ces scénarios pour les expériences actuelles et futures. En particulier, nous avons montré qu'un scénario très populaire dans la littérature n'est pas viable, et nous avons proposé un nouveau mécanisme LQ pour expliquer  $R_{K^{(*)}}^{\text{exp}} < R_{K^{(*)}}^{\text{SM}}$  à travers les boucles. Parmi les prédictions de ces modèles, nous soulignerons l'importance des désintégrations avec la violation de la saveur leptonique (LFV), car elles offrent une alternative très propre qui permet de tester la plupart des scénarios de nouvelle physique proposés.

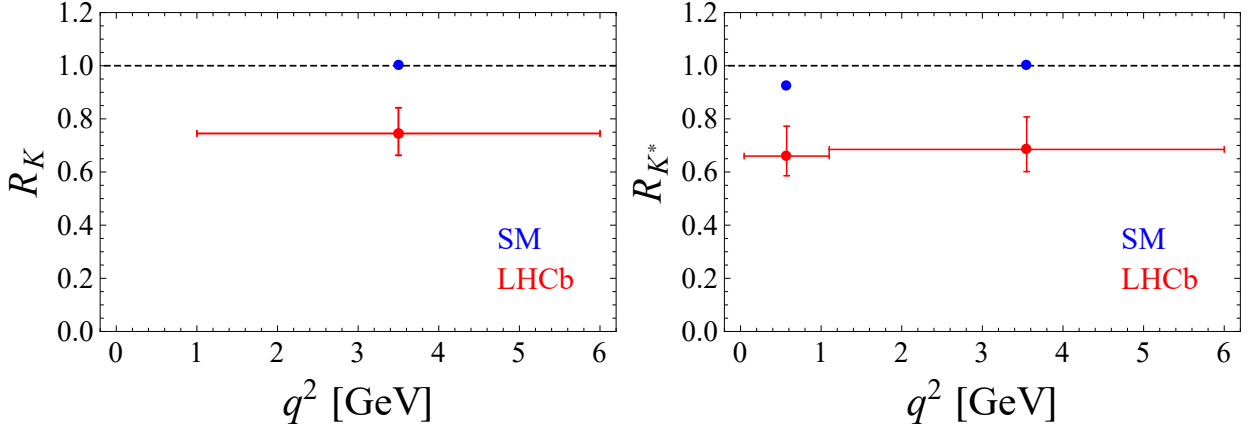


**Figure B.2:** Résultats expérimentaux pour  $R_K$  et  $R_{K^*}$  obtenus par LHCb [11, 12].

Une autre évidence intrigante de violation de la LFU a été observée dans les processus médiés par le courant chargé [14], où il a été constaté que

$$R_{D^{(*)}} = \frac{\mathcal{B}(B \rightarrow D^{(*)} \tau \nu)}{\mathcal{B}(B \rightarrow D^{(*)} l \nu)}, \quad (\text{B.24})$$

avec  $l = e, \mu$ , sont plus élevés que prévu dans le MS [15–17]. La possibilité que les anomalies  $b \rightarrow s$  et  $b \rightarrow c$  soient générées par le même mécanisme, peut-être liée aux effets de la brisure

de la saveur au-delà du MS, a suscité beaucoup d'intérêt dans la communauté théorique. Il faut cependant être prudent, car la prédiction de  $R_{D^*}$  nécessite encore de l'évaluation de l'ensemble des facteurs de forme  $B \rightarrow D^*$  qui ne sont toujours pas disponibles par les calculs basés sur les premiers principe. Dans cette thèse, après un examen critique du statut des prédictions MS de  $R_{D^{(*)}}$ , nous avons discuté des modèles qui ont été proposés pour expliquer simultanément l'ensemble des observables qui brisent la LFU. En particulier, nous avons proposé un modèle LQ minimal qui nous permet d'expliquer certains de ces écarts.

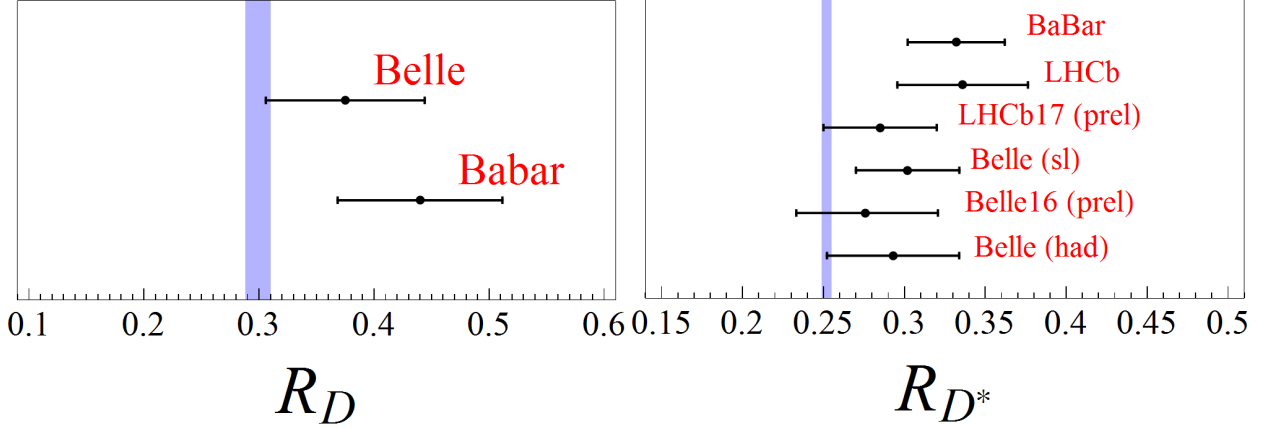


**Figure B.3:** Résultats expérimentaux pour  $R_D$  and  $R_{D^*}$  obtenus par LHCb [74, 270], BaBar [72] et Belle [73, 75, 76], ainsi que les prédictions du MS pour ces observables [14, 17].

Il est clair que les solutions aux problèmes abordés dans cette thèse restent un travail en cours. Tout d'abord, nous ne savons pas encore si le boson scalaire observé au LHC est celui prédit par le SM. La réponse à cette question nécessitera un effort combiné de recherches expérimentales directes et indirectes. En outre, tandis ce que les nouveaux résultats de LHCb sur  $R_{K^{(*)}}$  et  $R_{D^{(*)}}$  et la détermination de Belle-II des mêmes observables sont encore attendus, le problème de la LFUV reste une question ouverte. Il faut aussi garder à l'esprit que le moment magnétique anormal  $(g - 2)_\mu$  présente un écart d'environ  $3.6\sigma$  par rapport au MS [353]. Cet écart sera bientôt confirmé ou réfuté par l'effort conjoint des groupes expérimentaux au Fermilab et de la communauté de QCD sur réseau, qui travaillent pour réduire les incertitudes expérimentales et théoriques pour cet observable. Proposer un scénario minimal nous permettant d'expliquer simultanément les écarts observés tout en respectant la pléthore de contraintes directes et indirectes est une tâche très difficile pour laquelle aucune solution convaincante n'a pas encore émergé. De plus, il n'est pas clair si le motif observé pour ces écarts serait une manifestation de la brisure de la saveur au-delà du MS, ou d'un autre mécanisme de NP possiblement lié à l'un des problèmes du MS.

Nous espérons que les réponses aux questions mentionnées ci-dessus seront bientôt fournies par l'effort collectif des expériences de physique des saveurs à NA62, BES-III et LHCb avec les futures à Belle-II, KOTO, TREK,  $(g - 2)_\mu$  et Mu2E qui nous fourniront une quantité de données sans précédent. La combinaison de ces résultats avec ceux des recherches directes effectuées au LHC servira de guide pour l'effort théorique vers une meilleure compréhension du mécanisme de violation de la saveur au-delà du MS et aidera peut-être à résoudre certains des problèmes de longue date en physique théorique.

**Titre :** Recherche de la nouvelle physique à travers les observables de la physique de la saveur

**Mots clés :** changement de la saveur, B meson, désintégration semileptonique, théorie effective des champs, Higgs, leptoquark.

**Résumé :** La recherche indirecte des effets de la physique au-delà du Modèle Standard à travers les processus de la saveur est complémentaire aux efforts au LHC pour observer directement la nouvelle physique. Dans cette thèse nous discutons plusieurs scénarios au-delà du Modèle Standard (a) en utilisant une approche basée sur les théories de champs effective et (b) en considérant des extensions explicites du Modèle Standard, à savoir les modèles à deux doublets de Higgs et les scénarios postulant l'existence des bosons leptoquarks scalaires à basse énergie.

En particulier, nous discutons le phénomène de la brisure de l'universalité des couplages leptoniques dans les désintégrations basées sur les transitions  $b \rightarrow s\mu\mu$  and  $b \rightarrow c\tau\nu$ , et la possibilité de chercher les signatures de la violation de la saveur leptonique à travers les modes de désintégration similaires. Une proposition pour tester la présence d'un boson pseudoscalaire léger à travers les désintégrations des quarkonia est aussi présentée.

**Title :** Search of new physics through flavor physics observables

**Keywords :** flavor changing, B meson, semileptonic decay, effective field theory, Higgs particle, leptoquark.

**Abstract :** Indirect searches of physics beyond the Standard Model through flavor physics processes at low energies are complementary to the ongoing efforts at the LHC to observe the New Physics phenomena directly. In this thesis we discuss several scenarios of physics beyond the Standard Model by (a) reusing the effective field theory approach and (b) by considering explicit extensions of the Standard Model, namely the two-Higgs doublet models and the scenarios involving the low energy scalar leptoquark states.

Particular emphasis is devoted to the issue of the lepton flavor universality violation in the exclusive decays based on  $b \rightarrow s\mu\mu$  and  $b \rightarrow c\tau\nu$ , and to the possibility of searching for signs of lepton flavor violation through similar decay modes. A proposal for testing the presence of the light CP-odd Higgs through quarkonia decays is also made.

